Interfacial Adsorption of Proteins: A Neutron Reflectivity Study

A thesis submitted for the degree of Doctor of Philosophy



By

Edward Latter

Balliol College

Trinity Term 2012

Abstract

Protein adsorption at the solid/liquid interface is of wide ranging importance in many different areas of science such as biomaterial design, the fate of nanoparticles and in the food industry. As a result, many studies have been undertaken with varying foci but there still remains a lack of agreement between many working in this field and fundamental questions regarding the adsorption of proteins at the solid/liquid interface.

Neutron reflectivity is a powerful technique for probing the properties of adsorbed layers at interfaces due to its high structural resolution and the possibility of using isotopic substitution to distinguish between components of a mixture. In this work, neutron reflectivity has been used as the primary technique for the investigation of proteins adsorbed sequentially or from a binary mixture.

Initially, the adsorption of four proteins (carbonic anhydrase II, lysozyme, human serum albumin and maltose binding protein) onto a clean silica surface was investigated which revealed the importance of electrostatic interactions and entropic contributions to the driving forces for adsorption. Most of the adsorbed layers were described by a 2-layer model with a thinner, denser layer adjacent to the surface and a thick, diffuse layer extending into the bulk solution. The presence of impurities is also shown to have a significant impact on the adsorption of HSA. A study of the HSA/myristic acid system shows that the presence of small amphiphiles can inhibit HSA adsorption and also remove a pre-adsorbed layer.

A comparison was made between the protonated and deuterated forms of two proteins, HSA & MBP, showing the deuterated proteins to have a higher affinity for the surface with adsorption occurring in a 3:1 ratio when from a 1:1 mixture. Likewise, d-MBP displaced h-MBP more readily than *vice versa* in an investigation into the effect of incubation time on the properties of the protein layer. The extent of desorption into protein free buffer is not affected by incubation time but the extent to which d-MBP was displaced by h-MBP showed a clear trend of decreased exchange with increasing incubation time indicating an active exchange process was occurring. This was also observed to a lesser extent for the sequential adsorption of binary protein systems, HSA & LYS and HSA & MBP.

When investigating binary protein mixtures the higher propensity for deuterated proteins to adsorb is observed. LYS dominates when adsorbed from a mixture with h-HSA but from a d-HSA & LYS mix both proteins were adsorbed. The

marked difference between the adsorption characteristics of perdeuterated proteins and their protonated counterparts provides a good case study for testing the neutron reflectivity technique when investigating systems with more than one component. This thesis assesses the limitations of the methodology of contrast variation for investigating mixtures as well as using different solvent contrasts.

A comparison of neutron reflectivity and dual polarisation interferometry (DPI) shows that the two techniques are similar and any small differences can be attributed to the small change in surface chemistry. This comparison also highlights the advantages of DPI; high throughput of samples and detailed information but the restriction to using a 1-layer model limits its use.

Acknowledgements

First and foremost my thanks must go to my supervisors Bob Thomas and Jeff Penfold for all their help, guidance and advise over the course of my DPhil studies. I have very much enjoyed working with both of them and they have been an invaluable source of knowledge on all topics from the finer points of neutron reflectivity to restaurant recommendations in Grenoble and cricket. The rest of the Thomas group have made the PTCL a good place to spend the days and I'd like to thank them for their help in the lab when required and jovial conversations in the office and at our infrequent group dinners. In particular thanks to Ye, Minglei, Rob, Peixun and Mauro- time for tea anyone?

This work could not have been completed without the input of the instrument scientists at ISIS and the ILL. Thanks to Phil Taylor for all his help on SURF and with the DPI experiments, to John Webster for his instruction when using INTER and to Richard Campbell and Hanna Wacklin for their help running experiments on D17.

Life is not all about work and it would be remiss of me not to include those with whom I've shared good times. To Tom I owe a huge debt of gratitude for introducing me to some excellent music and being a great friend- understanding, supportive, occasionally humorous and a competent sous chef. Thanks also to my other housemates; Sarah for many good times shared over a drink (or ten) and her contagious effervescent personality and to Anne for putting up with my bad habits some of the time. Thanks also to Tom, Kirsten, Liz, Andy, T-Pain and the Osney Raiders. The members of Balliol MCR have also played a significant part in my time in Oxford and I will take with me many fond memories of afternoons spent on the cricket pitch or playing 5-a-side football and evenings in the Megaron throwing some arrows or putting the world to rights with a fine single malt.

Last but by no means least thanks to my family. We have travelled an oft-rocky road together but you have all been endlessly encouraging and supportive and I couldn't have done it without you.

Contents

1 Introduction **1**

1.1 Protein structure and properties . . . 2
1.1.1 Human Serum Albumin . . . 3
1.1.2 Lysozyme . . . 3
1.1.3 Maltose Binding Protein . . . 3
1.1.4 Carbonic Anhydrase II . . . 4
1.2 Factors effecting adsorption at the solid/liquid interface . . . 4
1.2.1 Protein properties . . . 6
1.2.2 Solution conditions . . . 8
1.2.3 Effect of deuteration . . . 10
1.2.4 Surface properties . . . 12
1.3 The adsorbed protein: orientation and post adsorption changes . . . 15
1.4 Theoretical models of protein adsorption . . . 18
1.4.1 Kinetic models . . . 18
1.4.2 Thermodynamic models . . . 20
1.5 Protein exchange . . . 21
1.5.1 Sequential adsorption . . . 22
1.5.2 Competitive adsorption . . . 23
1.6 Aims of this work . . . 24
References . . . 27

2 Methods and Materials **38**

2.1 Neutron Reflectivity . . . 38
2.1.1 Introduction . . . 38
2.1.2 Theory of neutron reflection . . . 39
2.1.3 Calculating the scattering length densities of proteins . . . 46
2.1.4 Neutron sources and instrumentation . . . 47
2.1.5 Solid/Liquid reflectivity measurements . . . 49
2.1.6 Data analysis . . . 51
2.2 Dual Polarisation Interferometry . . . 54
2.2.1 Operating principles . . . 54
2.2.2 Method . . . 56
2.2.3 Data analysis . . . 58

2.3 Materials . . . 58
References . . . 60

3 Results: Adsorption of single protein solutions 63
3.1 Carbonic Anhydrase II . . . 64
3.2 Lysozyme . . . 68
3.2.1 Desorption of LYS . . . 72
3.3 Human Serum Albumin . . . 75
3.3.1 h-HSA in D_2O, CM5 and H_2O . . . 76
3.3.2 d-HSA in D_2O, CM5 and H_2O . . . 81
3.3.3 Mixture of d- and h-HSA in D_2O and H_2O . . . 85
3.4 Maltose Binding Protein . . . 87
3.4.1 h-MBP in H_2O, CM3.6 and CMSi . . . 88
3.4.2 d-MBP in H_2O and CMSi . . . 93
3.4.3 Mixture of h- and d-MBP in CMSi . . . 100
3.4.4 Effect of incubation time on the desorption of d-MBP . . . 104
3.4.5 Self exchange . . . 105
3.5 Discussion . . . 114
3.5.1 Comparison of different protonated proteins . . . 114
3.5.2 Comparison of protonated and deuterated proteins . . . 115
References . . . 117

4 Results: Sequential adsorption of proteins 121
4.1 Adsorption onto a pre-adsorbed HSA layer . . . 122
4.1.1 CA II . . . 122
4.1.2 LYS . . . 124
4.1.3 MBP . . . 135
4.2 Adsorption of HSA onto a pre-adsorbed protein layer . . . 142
4.2.1 CA II . . . 143
4.2.2 LYS . . . 144
4.2.3 MBP . . . 150
4.3 Discussion . . . 158
References . . . 165

5 Results: Adsorption of binary protein mixtures 168
5.1 HSA and CA II . . . 169
5.2 HSA and LYS . . . 171
5.3 HSA and MBP . . . 176
5.4 Discussion . . . 180
References . . . 182

6 Results: Effect of fatty acids on the adsorption of HSA **184**
6.1 Introduction . . . 184
6.2 Sample preparation . . . 185
6.3 Adsorption from a mixture . . . 185
6.4 Sequential adsorption . . . 187
References . . . 190

7 Dual Polarisation Interferometry results **191**
7.1 Introduction . . . 191
7.2 Results . . . 192
7.2.1 LYS adsorption . . . 192
7.2.2 HSA adsorption . . . 193
7.3 Discussion . . . 194
7.3.1 Comparison of DPI with other techniques . . . 195
References . . . 198

8 Conclusions **200**

Appendices **204**

A LYS neutron reflectivity data **204**

B HSA neutron reflectivity data **207**
B.1 h-HSA . . . 207
B.2 d-HSA . . . 217

C MBP neutron reflectivity data **219**
C.1 Desorption of d-MBP . . . 219
C.2 Self exchange of MBP . . . 223

Chapter 1

Introduction

Protein adsorption on solid surfaces is of importance in numerous scientific areas including fouling in the food industry[1], biomaterials design[2], biosensors[3], bioseparation units[4] and the fate of nanoparticles[5]. In short, any time a solid substrate comes into contact with a biological milieu, the surface will, most likely, be covered in proteins. Unlike small molecules, which behave like rigid particles with certain adsorption and desorption probabilities, the wide ranging and complex nature of protein structures and composition lead to far more possibilities such as structural rearrangements or aggregation. Both of these processes are affected by the timescales of interest. The surface may be covered in a protein layer in a matter of seconds but the structural rearrangements may take place over several hours or even days. The issue is complicated further when considering mixtures of proteins as the protein-protein interactions must also be considered.

Due to the wide range of importance and the complexity of the problem, there exists a vast literature under the umbrella of "protein adsorption" and as noted by Erwin Vogler in a recent opinion article on this topic *"anyone closely examining the literature in its entirety will be struck by a lack of consensus so extreme that nearly no general conclusions can be extracted."*[6]. With this in mind, this chapter will aim to outline the basis for the complexity and provide examples of some of the main works in this area. The focus will be on the aspects of most relevance to this thesis namely, the driving forces for adsorption at the solid/liquid interface, the relevant timescales and adsorption of two or more proteins either from a mixture or sequentially.

The details of human serum albumin (HSA), lysozyme (LYS), maltose binding protein (MBP) and carbonic anhydrase II (CA II) will be highlighted as these are

the proteins of interest in this thesis. As will be discussed, all four of these proteins have well known structures and properties making them very useful as model protein systems.

1.1 Protein structure and properties

The fundamental building block for all proteins is the amino acid, a molecule consisting of an amine group, a carboxylic acid group and a side chain that differs for each amino acid. In total there are 20 common, naturally occurring amino acids and these can polymerise to form a polypeptide chain. The sequence in which they occur in a protein is called the primary structure and is unique for each protein.

One of the most fascinating aspects of polypeptide chains, as opposed to most other polymeric species, is their propensity to form into particular structures such as α-helices, β-sheets and β-turns; a process driven by a number of non-covalent interactions such as hydrogen bonding, ionic interactions, Van Der Waals forces, and hydrophobic packing. These features make up the secondary structure of the protein.

The folding of the α-helices, β-sheets and turns into a 3D, globular structure is driven by non-specific hydrophobic interactions which aim to minimise the interaction of solvent water molecules with hydrophobic amino acid side chains. This so-called tertiary structure is held together by salt bridges, hydrogen bonds and disulfide bonds and this specific 3D structure is ultimately responsible for carrying out the biological function of the protein. Some proteins exhibit almost no tertiary structure and are often referred to as "random coil" proteins. Others, such as LYS, HSA, CA II and MBP, fold into globular structures with varying degrees of rigidity and rotational freedom for the polypeptide backbone. A more loosely bound tertiary structure allows for more conformational changes either due to varying solution conditions or adsorption at an interface.

Some proteins may also exhibit quaternary structure whereby they each act as a subunit to form a larger assembly or include other non-peptide entities such as metal ions, oligosaccharides (glycoproteins) or phosphates.

1.1.1 Human Serum Albumin

HSA is the most abundant protein in human plasma ($\sim$ 0.6 mM) and can also be found in bodily tissues and secretions. It consists of 585 amino acid residues, has a molecular weight of 66.5 kDa and an isoelectric point[1] (IEP) of 4.7. The protein's secondary structure consists of 67 % α-helices with no β-sheets. Its main functions are to regulate osmotic pressure and the transport of ligands such as fatty and amino acids. A detailed crystal structure was first determined by He and Carter[7] which shows that the molecule consists of three well defined domains (labelled I-III) each of which is comprised of two sub-domains (A and B). When crystalline it is roughly heart shaped and can be approximated to an equilateral triangle with sides of 80 Å and depth of 30 Å. A total of 17 intra-subdomain disulphide bridges help to stabilise the domain structure but the lack of any inter-subdomain bridges allows for some flexibility and the protein undergoes conformational changes as a result of changing pH[8, 9]. The fatty acid binding sites are each slightly different but all comprise a hydrophobic pocket capped at one end with basic or polar side chains [10].

1.1.2 Lysozyme

LYS is an enzyme that is present in egg white, tears and other secretions. It was discovered by Fleming in 1922 and is responsible for breaking down the polysaccharide walls of bacteria, especially Gram-positive bacteria. It consists of 129 amino acid residues, has a molecular weight of 14.3 kDa and an IEP of 11.16[11]. The first determination of its crystal structure was by Phillips in 1965[12] which revealed it to be ellipsoidal with a prominent cleft and dimensions of $30 \times 30 \times 45$ Å^3. Its secondary structure consists of $\sim$34% α-helices and $\sim$35% β-sheets [13]. Four disulfide bridges and tight folding mean that the polypeptide backbone has very little rotational freedom and the structure is relatively rigid when compared to other proteins.

1.1.3 Maltose Binding Protein

MBP is one of a family of periplasmic binding proteins in Gram-negative bacteria that recognize small molecules with high affinity. Its molecular weight is 40.5 kDa and it has an IEP of 5.2[14]. The structure of MBP has been well characterised by

[1] The isoelectric point is defined as the pH at which a protein or surface carries no net electical charge.

Spurlino et al.[15] and Choy et al. [16]; it is approximately ellipsoidal in shape with dimensions of $30 \times 40 \times 65$ Å^3 and consists of two globular domains with a deep grove between them where the maltose binding site is located. It consists of 40% α-helix and 20% β-sheets with the principle folding pattern being alternating β-sheets and α-helices[17]. Binding of maltose induces a major conformational change [18]. The importance of understanding transport systems has led to a lot of biochemical interest and the high affinity binding has resulted in applications in protein purification. There are, however, relatively few studies of the adsorption of MBP to solid surfaces which makes this an ideal protein for use in this particular study as a comparison to the better documented HSA and LYS.

1.1.4 Carbonic Anhydrase II

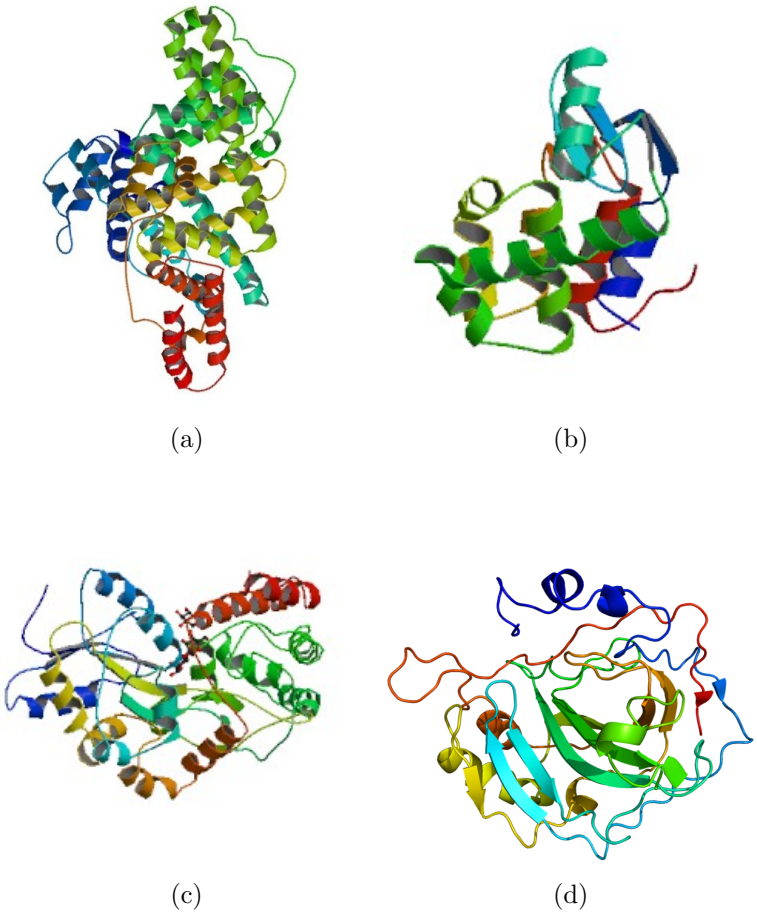
CA II is one of seven genetically distinct forms of human α-carbonic anhydrases and its function is to catalyse the reversible hydration of carbon dioxide ($CO_2 + H_2O \rightleftharpoons HCO_3^- + H^+$). It comprises a single polypeptide chain of 230 amino acid residues and a zinc ion [19]. Its total molecular weight is 29.3 kDa[20] and it has an IEP of 7.4 [21]. The three-dimensional structure of HCAII is known from crystallographic studies[22]. The molecule has an ellipsoidal shape with dimensions of $50 \times 40 \times 40$ Å^3 and a deep active site cavity containing the zinc ion. The zinc ion is chelated by three histidine residues and one water molecule with a close to tetrahedral co-ordination geometry.

1.2 Factors effecting adsorption at the solid/liquid interface

Whatever the mechanism of adsorption, at constant temperature and pressure, adsorption proceeds spontaneously if the Gibbs free energy of the system upon adsorption, ΔG_{ads}, is negative.

$$\Delta G_{ads} = \Delta H_{ads} - T\Delta S_{ads} < 0 \tag{1.1}$$

where ΔH_{ads} and ΔS_{ads} are the enthalpy and entropy changes upon adsorption. Thus it is necessary to consider both the enthalpic and entropic contributions when interpreting protein adsorption data or devising theoretical models. Even for the



(a) (b)

(c) (d)

Figure 1.1: Ribbon representations of the structures of (a) HSA[23], (b) LYS[24], (c) MBP (shown with bound oligosaccharide)[25] and (d) CA II (from[26], a PDB[2] rendering based on [27]).

same protein, the enthalpy of adsorption can be endothermic onto one surface but exothermic on another e.g HSA onto silica[28] and polymer nanoparticles[29]. The major enthalpic contributions come from hydrogen bonds, van der Waals forces and Coulombic forces whereas the increase in entropy upon adsorption arises from the dehydration of the interface and changes to the structural freedom of the polypeptide chain.

The process of protein adsorption can be thought of in simple terms as being comprised of two steps; transport from the bulk to the surface and attachment to the surface. Once adsorbed, the protein may undergo post-adsorption rearrangements, desorb back into the bulk or be actively exchanged for another protein. These

[2]The Protein Data Bank (PDB) is a repository for the 3D structural data of large biological molecules.

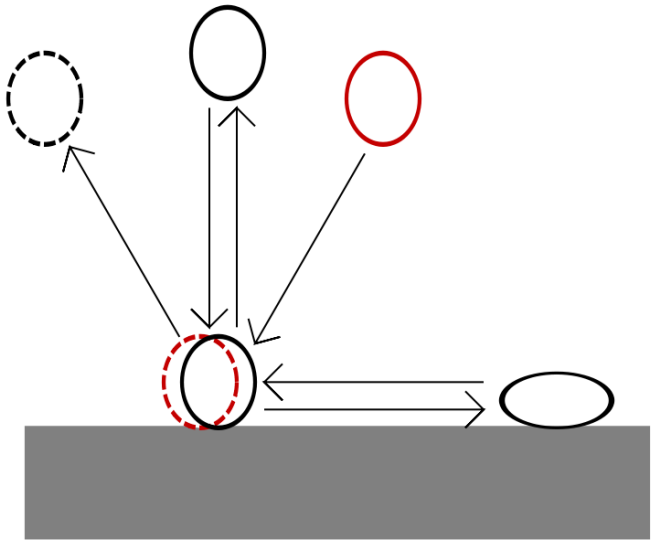


Figure 1.2: A schematic representation of the adsorption process and possible post-adsorption fates

possible fates are shown schematically in figure (1.2). The details of each of these stages will alter greatly depending on the system of interest which is a combination of the properties of the protein, the surface and the bulk solution.

1.2.1 Protein properties

The diversity of proteins that occur in the natural world make simple hypotheses regarding their adsorption behaviour difficult and each can be thought of as having a "unique molecular personality"[30]. However, it is possible to deduce the effects of some protein properties by classifications based on proteins that exhibit similar properties like size, hydrophobic/hydrophilic, electric charge or the degree of structural flexibility.

In the absence of convection, the transfer of proteins is a stochastic process and the flux, J, towards the surface is given by[31]

$$J = (c_b - c_s)\left(\frac{D}{\pi t}\right)^{1/2} \tag{1.2}$$

where c_b and c_s are the bulk and surface concentrations, t is the incubation time and, D the diffusion coefficient (for a spherical particle) is given by

$$D = \frac{kT}{6\pi\eta R} \tag{1.3}$$

where k is the Boltzmann constant, T is the absolute temperature, η is the viscosity and R is the radius of a spherical particle.

Although the accurate determination of diffusion coefficients for proteins is far from trivial due to irregular geometries and the effect of hydration spheres[32] the Stokes-Einstein equation (1.3) is a useful model for semi-quantative comparisons and it is a good assumption that smaller proteins will reach the surface faster than larger ones. An increase in the temperature will also result in an increased rate of diffusion.

Larger proteins, however, will typically have a greater contact area with the surface and will displace more solvent molecules which is entropically more favourable and a major driving force for protein adsorption. The consequences of these differences with respect to adsorption from mixtures will be discussed in more detail in section (1.5.2).

As well as differences in size, proteins exhibit a variety of structural stability and are often classed as either "soft" e.g. immunoglobulin, HSA or "hard" e.g. α-chymotrypsin, LYS. Denaturing and associated spreading on surfaces is more likely for "soft" rather than "hard" proteins [33, 34] and results in them being bound more strongly to the surface due to more individual points of contact between amino acids and the surface.

Of the 20 amino acids, eight have hydrophobic side chains. One of the main driving forces for protein folding is to bury as many of these within the core of the protein in order to minimise their interaction with solvent water molecules [35] but the water accessible fraction of the protein that is non-polar may, in some cases, be as high as 40-50 %[36]. Despite differences in the hydrophobicity of proteins and the importance of dehydration as a driving force for adsorption the effect has not been subject to specific study due to difficulties in both accurate quantification[37] and isolating its influence. The use of mutant variants[38], truncated forms[39] or additions of hydrophobic moieties will most likely cause other changes to the protein, such as structural stability or charge, and so mask any changes in hydrophobicity. It is more common to alter the hydrophobicity of the substrate (see section 1.2.4) in order to probe the effects of hydrophobic forces.

The majority of a protein's surface will be made up of amino acids with charged

or ionizable side chains. This results in the exterior of the protein being charged. The net charge is a function of the pH of the solution and the amino acid composition on the protein exterior. When considering single protein systems it is well accepted that protein adsorption is greatest when the pH is equal to the IEP of the protein[40, 41, 42, 43, 44] because of the reduced degree of lateral electrostatic repulsion.

Even when pH= IEP and the net charge is zero there will still be regions of positive and negative charge as the surface of proteins does not have an even distribution of charged amino acids. Hence, it is also necessary to consider the charge distribution. For example, Forciniti and Hamilton[45] suggest that the adsorption of negatively charged HSA onto negatively charged quartz takes place via its positively charged tip. Likewise, an overshoot of the adsorption kinetics of β-lactoglobulin onto a mica surface has been interpreted by Rabe et al.[46] as a transition from an irreversibly bound orientation that maximises favourable surface-protein electrostatic interactions to a reversible state where lateral repulsions are reduced. This is made possible by the protein's non-uniform charge distribution. Using fluorescence probes attached to different areas of the surface of carbonic anhydrase II, Karlsson and Carlsson[47] have shown that the orientation is strongly pH dependent and that adsorption to the negatively charged silica nanoparticles occurs via positively charged regions of the proteins surface.

1.2.2 Solution conditions

The solution conditions of interest when considering protein adsorption will largely have an effect on the electrostatic driving forces, and thus the enthalpy of adsorption. As mentioned in the previous section, the electrostatic state of the protein varies with the pH of the solution. The effect of pH on the adsorption of LYS[48] and bovine serum albumin[40] on silica both show that the degree of lateral repulsion between adsorbed proteins is of more importance when determining the adsorbed amount than the electrostatic forces between the surface and the protein (the charge on the silica surface remains constant over the pH range of interest in these studies). In the case of LYS adsorption the increasing lateral repulsion at pH 4 compared with pH 7 induces a reorientation of the adsorbed molecules from side-on to a more tilted orientation[49].

Another route to screening the lateral repulsion is an increase in the ionic

strength of the solution. The ionic strength of an electrolyte solution, $I = \frac{1}{2}\sum_{i=1}^{n} c_i z_i^2$, is determined by the molar concentration, c_i, and charge number, z_i of the ions present. The Debye screening length, κ^{-1}, is a measure of the separation distance over which charges interact[50]

$$\kappa^{-1} = \left(\frac{\epsilon_r \epsilon_0 k_B T}{2 N_A e^2 I}\right)^{1/2} \tag{1.4}$$

where ϵ_r and ϵ_0 are the vacuum and relative permittivity respectively. An increase in the electrolyte concentration hampers the adsorption of charged proteins to oppositely charged substrates by reducing the attractive forces whereas adsorption to like-charged substrates is enhanced[51]. This will impact both the kinetics of the adsorption process, the structure of the adsorbed layer and adsorbed amount[52, 53]. Moreover, conditions of high ionic strength will increase the tendency of proteins to aggregate in solution as the longer range and attractive van der Waal's forces dominate over repulsive, shorter range electrostatic repulsion (Derjaguin-Landau-Verwey-Overbeek theory[50]). Using AFM to probe the strength of interaction between mica surfaces and fibrinogen coated silica particles, Tsapikouni et al. showed that when the salt concentration of the phosphate buffered saline (PBS) is 150 mM there exists an attractive force between the like charged surfaces as the electrostatic repulsion is restricted in the range where van der Waals attractions are becoming dominant. This was not observed at 15 mM where the repulsive electrostatic forces are not screened nor at 500 mM when the hydration forces and the compact molecular conformation become crucial, restricting adsorption.[54].

As well as the ionic strength, the specific ions present can also impact on the protein adsorption. It has been suggested that the effect of different ions correlates with the ability to stabilise the native conformation of proteins which would influence their adsorption tendency[55]. Wendorf et al.[56] have attributed the amount of adsorbed protein at a hydrophilic surface following a salt series being primarily influenced by changes in hydrophobic interactions between the surface and protein resulting from differences in water structure arising from the presence of the electrolytes. PBS is the most commonly used buffer at physiological pH and Wei et al.[57] have carried out a comparison with Tris-HCl buffer. They concluded that phosphate ions adsorb competitively with the proteins and this depresses the initial adsorption.

Another factor of interest in this work is the effect of different ratios of H_2O to D_2O as changing this ratio is routinely used in neutron reflectivity to avoid the possibility of finding a non-unique solution. It is assumed that the systems of interest are not changed significantly when altering the solvent. This is a good assumption when considering small surfactants but its impact on protein adsorption has yet to be investigated. The role of water is a significant driver of protein adsorption and ignoring its influence runs the risk of completely misunderstanding a fundamental aspect of protein adsorption[6]. This, combined with the well known kinetic isotope effect discussed in section 1.2.3 suggests that the changing the ratio of H_2O to D_2O is likely to impact on the adsorption process.

1.2.3 Effect of deuteration

The difference in mass of hydrogen and deuterium has long been noted as of importance in physical chemistry and is usually concerned with the rate of cleavage of covalent bonds to hydrogen. This kinetic isotope effect has also has been exploited by organic chemists to direct organic mechanisms in small molecules since the 1950s[58, 59]. Perdueterated proteins are obtained by growing simple organisms, such as bacteria or yeasts, in fully deuterated media. The biochemical implications of deuteration have been looked at since the early 1960s[60, 61] and more recently, used in determination of enzymatic mechanisms[62]. As characterisation techniques have become more advanced so has the level of detail available and the exchange process had been used widely.

Monitoring H/D exchange and specific deuteration of proteins and peptides is now a well established method in NMR and neutron diffraction studies. This is based on the assumption that the protonated and deuterated forms have the same structure. Many studies agree with this assumption, for example for *Staphylococcal nuclease*[63], as does anecdotal evidence suggesting that the deuterated forms crystallise under similar conditions to protonated proteins (if they do indeed crystallise)[64]. The fine tuning of the folding process to determine a protein's native structure has occurred over millions of years due to natural selection[65] and could plausibly be disrupted by the exchange of ^1H for ^2H although there is little evidence to support this hypothesis. Yokogaki et al. provide a notable exception[66] with evidence of misfolding and even if a protein is not markedly different from its protonated counterpart both the global unfolding equilibrium and the activation barriers for

transient local unfolding fluctuations are reduced on perdeuteration[67].

On an individual bond the change in free energy is small but the cumulative effect of many such interactions when considering macromolecules could be considerable. Any change in the folding and structure of the protein will impact on the surface characteristics of the protein and hence the adsorption process. As with all protein systems the underlying complexity and variability makes the process of drawing general conclusions fraught with danger but some trends do emerge when the whole literature is considered. Some recent studies have started to cast a shadow of doubt on the assumption that H/D exchange does not significantly effect the structure and function of the protein. For example, a comparison of h- and d-haloalkane dehaloagenase showed similar conformations but with slightly altered surface regions and active sites of the enzyme due to different packing environments[68]. Other studies have shown that deuteration reduces the thermal stability but does not necessarily involve any structural difference[69, 70]. Likewise, enzymatic activity due to deuteration can be unchanged[71] or even increased compared to the protonated form[67]. It is most likely that the H-bonding network is disrupted, which has been proposed as a mechanism for altering the α-helix formation in a smaller polypeptide[72]. A more detailed thermodynamic treatment by Shi et al. has shown that the contribution of amide related H-bonds to the stability is greater in α-helical regions than β-sheets[73].

Generally, these studies focus on the biochemical nature of the proteins but a closer investigation of the physiochemical properties by Brockwell et al.[67] conclude that even if proteins show similar biochemical properties they could be very different from a physicochemical view point and they provide anecdotal evidence, such as the propensity for solutions of deuterated proteins to precipitate more readily when stored to support this argument. More direct evidence using gel filtration[71] and static light scattering[67] have both shown that deuteration of the proteins leads to increased dimerisation (for glutathione S-transferase) or the formation of a collection of many other species of oligomers (for the enzyme I^{Ntr}). This should not be a surprising result given that some proteins known to form dimers or oligomers when in solution, such as insulin and β-lactoglobulin, do so via a shared β-sheet structure where H-bonding is important[74]. This increased H-bonding strength for deuterated proteins and other factors involved in bulk association are likely to be similar to those for adsorption, particularly in the case of multilayer formation.

As well as the underlying structure of the polypeptide backbone it is also nec-

essary to consider the effect of changing the solvent composition with varying ratio of H_2O:D_2O as the labile hydrogens on the protein will exchange for the solvent hydrogens. On a macroscopic level, D_2O is often considered to be a worse solvent than H_2O and it therefore attempts to reduce the surface area of contact[75]. This exchange of ^1H for ^2H increases the rigidity of the native structure[75, 70, 76] which is in contrast to the previously mentioned studies showing that non-labile H exchange decreases the thermal stability. The effect of the solvent change is consistent with a solvation effect[75] whereas the isotope change in the backbone will more likely have an influence on the internal hydrogen bonding network which confers the internal segmental rigidity.

A detailed examination of some unanswered questions regarding the reasons behind these changes are beyond the scope of this thesis but a comparison of the adsorption characteristics will be made of the protonated and deuterated forms of two proteins, HSA and MBP. An investigation into the effect of perdeuteration on the adsorption of proteins has not previously been carried out using proteins but deuterated polymers have been shown to have a higher affinity for the surface [77, 78]. Similarly, adsorption of the same proteins will be compared when under a range of H_2O:D_2O ratios. This is a common technique when using neutron reflectivity known as contrast variation and is discussed in more detail in chapter 2.

1.2.4 Surface properties

In experimental studies of protein adsorption the choice of substrate typically reflects the context of the project and several important parameters, such as charge, polarity and morphology, need to be considered. The choice of surface must also fit in to certain restrictions imposed by the experimental technique used; surface plasmon resonance (SPR) and the quartz crystal microbalance (QCM), for example, require an electrically conducting substrate. Although, there are many unmodified surfaces that have been used for protein adsorption studies e.g. mica, glass and metal oxides, surface modifications are often used as a route to tuning the desired properties of the surface. For a substrate that has exposed hydroxyl groups e.g. silica, the use of chlorosilanes or ethoxy silanes can be used. The exposure of noble metal substrates e.g. gold, to alkanethiols is commonly used to produce self assembled monolayers (SAMs). Other methods for surface functionalisation include polymer coating and Langmuir-Blodgett films. In each case the end goal is to tune the properties of the

surface to give the desired conditions.

One main focus has been on the hydrophobicity of the surface. Hydrophobic interactions are a major driving force for adsorption and account for adsorption when protein-surface interactions result in a net electrostatic repulsion. The general experimental trend is that proteins have a higher affinity for hydrophobic surfaces over hydrophilic ones. In a study of different copolymer nanoparticles by Lindman et al.[29] using isothermal calorimetry it was shown that enthalpy change upon HSA adsorption onto the most hydrophobic particles was up to nearly six times greater than onto the most hydrophilic, with the effect being most pronounced on the smaller particles. Likewise, Koehler et al.[79] report that the adhesion force for LYS adsorbing at pH 6.6 is 30 times greater onto a hydrophobic vs hydrophilic surface. Glycoproteins are a notable exception to this due to their hydrophobic domains are buried inside a shell of glycans[80].

To gain an overview of the effect of surface hydrophobicity, Su et al. and Lu et al. have studied LYS adsorption on three surfaces with different contact angles; silica[81] ($\theta_c = ca.0^o$), $C_{15}OH$ attached via silane chemistry[82] ($\theta_c = 52^o$) and a monolayer of octadecyl trichlorosilane[83] (OTS, $\theta_c = ca.110^o$). The full reversibility of pH cycling was only apparent on the most hydrophilic surface and the change in hydrophobicity had an effect on the structure of the adsorbed layer. On the OTS surface, a 2-layer model showed a dense layer adjacent to the surface (thickness of 12-15 Å and volume fraction of 0.85) and then a diffuse, 50 Å layer extending into the solution. The increased strength of binding to more hydrophobic surfaces is a result of the unfolding of the globular framework to expose the inner core of hydrophobic amino acids which can then interact favourably with the sorbent surface.

The electrostatic forces are a combination of protein-surface and protein-protein interactions and the electric properties of the solvent. The last two of these have already been discussed in sections (1.2.2) and (1.2.1). In the presence of a charged surface there will be an equivalent excess of counterions to maintain charge neutrality. The distribution of these is a combination of coulombic forces and entropic considerations. For small surface potentials ($\leq$ 25 mV), the potential profile is given by Gouy-Chapman theory as[50]

$$\Phi(x) = \Phi_0(x)exp(-\kappa x) \tag{1.5}$$

where Φ is the normalised potential Φ_0 is the potential at the surface and κ is the

Debye length as given in equation (1.4). To account for the finite size of ions, a common extension of this model is to introduce a Stern layer whereby the potential adjacent to the surface drops off linearly before the region of exponential decay. When a charged protein approaches a charged surface closer than the Debye screening length it will experience either a repulsive (if like charged such as HSA-silica at pH>4.7) or attractive force (e.g. LYS-silica at pH 3-11) which provides a driving force for adsorption of the protein. In some cases, this is thought to be the major driving force for adsorption and adsorbed amounts have been shown to correlate with increasing surface charge density of unmodified metal oxide surfaces[84], hydroxyapatite[85], polymeric nanoparticles[86] and grafted polymer brushes[87]. Bremer et al. have developed a model based on an electrostatic double-layer and show good agreement with experimental data for IgG adsorbing onto bare and modified silica[41]. Recently, a new description of the close surface region has been proposed for protein solutions by Vogler and his group[88, 89, 6] and is starting to gain some support[90]. They postulate the existence of an interphase region near to the surface where the protein concentration can be orders of magnitude higher than in solution and where a more ordered matrix structure of interacting proteins can be formed.

Seemingly small changes to the nature of the surface can have a large influence on the adsorption. Lu et al.[91] compared the adsorption of LYS under identical solution conditions but using two different experimental methods, neutron reflectivity and dual polarisation interferometry (DPI). For the neutron reflectivity studies a silica surface was used and the DPI chip is similarly silica based but with the inclusion of a small fraction of nitrogen. The DPI results reported both a thinner layer and lower adsorbed amount compared with the neutron reflectivity experiments. This was attributed to the differences in the chemical composition of the surfaces as both carry a comparable negative charge and degree of hydrophilicity. It is possible that this could be due to specific interactions between the surface and the protein whereby the chemistry of the surface on a molecular scale is of importance. This kind of specific interaction has been reported to account for higher than expected adhesion energies of Mefp-1 protein onto a polyethersulfone surface due to a $\pi - \pi$ interaction between groups on the protein and aromatic moieties on the polymer[92].

As well as the physicochemical properties of the surface, it is important not to disregard the purely physical features that may also affect the adsorption. The roughness of the interface will have a two fold impact; first, it is likely to directly impact on the adsorption process. Cuppett et al. have shown that the presence of

polishing marks on silica impacts on the adsorption of LYS in terms of where the protein binds and also the strength of attachment to the surface[93]. A higher degree of roughness has been shown to increase the surface excess on metal oxide surfaces with the effect more pronounced for Fibrinogen than BSA [94]. Wehmeyer et al.[95] have also attributed the higher than predicted surface excess of BSA onto TiO_2 surfaces as being due to the nanoscale topography in their experiments. The second influence occurs during the analysis of the experimental data where the starting assumption is often of a smooth interface. To account for the roughness it is necessary for both the technique to have the required sensitivity in its measurements and also for this to be accounted for during the analysis of the data e.g in ellipsometry[96] and neutron reflectivity[97].

1.3 The adsorbed protein: orientation and post adsorption changes

In the above section the major driving forces for the adsorption process have been discussed. Now we will turn our attention to the state of the adsorbed protein molecules and post-adsorption changes that occur.

Proteins are typically not spherical but exhibit a wide range of shapes; ellipsoids and rod-like shapes are quite common and some important classes of proteins have more complex geometries such as the Y-shaped immunoglobulins or heart shaped serum albumins. When in solution they rotate freely but upon attachment to a surface this rotational freedom is restricted. This loss of entropy is compensated for by a stronger attachment to the surface either via favourable electrostatic, van der Waals or hydrophobic interactions between the protein and the surface. Thus, proteins tend to adopt a certain orientation when adsorbed that corresponds to a free energy minimum. The orientation of the adsorbed protein determines the regions that are exposed to the bulk solution which is of particular interest with regards to the biological activity of the protein if this is associated with a certain part of the molecule. For example, the adsorbed mouse monoclonal antibody onto a silica surface has a side on orientation and this in itself does not hinder antigen binding, which is high when at low surface coverages of the IgG, but binding is reduced as the surface excess increases due to steric hindrance from neighbouring antibodies[98]. This example also illustrates that care has to be taken when de-

ducing orientation from binding studies alone as factors such as steric hindrance, conformational changes resulting in loss of activity (or possibly the exposure of novel epitopes that are not exposed when in solution but may bind the ligand/antigen[5]) and non-specific binding may also occur. Lee and Belfort[99] noted an increase in the activity of RNase A from 16% of solution activity after 1 hour up to 78 % after 24 hours which was interpreted as being due to a reorientation of the protein on the mica surface.

The orientation of a protein is most usually inferred from comparisons of the layer thickness and the known dimensions of the protein in the bulk solution. In this instance, it is assumed that the gross morphology of the protein is stable with respect to the timescale of the measurements. Adsorbed layer thicknesses that do not equal the dimensions of the protein can be attributed to different phenonemna. A smaller adsorbed thickness than bulk dimensions indicates fast spreading or denaturation on the surface. This spreading will be faster and more extensive on a hydrophobic surface with some results suggesting that a protein footprint can be increased up to five times the initial adsorption in only a few hours[100]. Intermediate dimensions can be interpreted as the protein forming some slanted orientation or a mix of side-on and end-on conformations. An adsorbed thickness greater than the solution dimensions is a good indication of multilayer formation. In these scenarios, any experimental technique which allows for models of multiple layers to be fitted or some estimation of the layer roughness e.g. X-ray or neutron reflectometry, is highly advantageous as this will allow for distinctions to be made between possible modes of mixed orientation, multilayer formation and denaturation.

As well as the use of more complex models to be distinguished, it is also possible to infer some structural details of the adsorbed layer by comparison at different time points. For example, if we consider an ellipsoidal protein of dimensions a x a x b, a gradual change in layer thickness from a to b suggests that as the adsorption continues and the packing density increases this induces a re-orientation of the molecule on the surface. However, if there is a more sudden change from a to $2a$ (with the second layer being more diffuse) then this is more distinctive of the formation of a second layer of side-on orientation on top of the first.

As well as a preferred orientation of the adsorbed protein associated with an initial minimum in the free energy of the adsorption process, conformational change can subsequently occur to reduce the free energy of the system. Structural rearrangements, driven by favourable surface-protein interactions occur. This results

in a change to the protein's secondary and tertiary structure. The subsequent loss of ordered structure within the molecule results in a favourable entropy gain, as does the release of solvent and counter-ions from the surface as they are displaced by the increasing number of protein attachment points. Over time, these changes will manifest themselves in macroscopically observable effects such as a change in reduction in α-helical and β-structure content or an increase in the proportion of irreversibly adsorbed protein. Some attempts have even been made to quantify the rate of spreading with results showing that Fibrinogen generally spreads faster than HSA and for both, spreading is faster and more extensive when on a hydrophobic surface[100, 101]. The likelihood and extent of conformational changes is often linked to the proteins structural stability in solution and proteins are often classed in this manner as either "hard" or "soft" which can be a useful concept when trying to make generalisations about protein adsorption. The slow nature of the conformational changes has been suggested as a mechanism for the increased irreversibility of adsorbed BSA and β-lactoglobulin with respect to displacement when incubation times of 1 and 4 hours are compared[102].

Direct information about structural changes can be obtained from techniques such as ATR-FTIR and circular dichroism (CD) although these techniques have less use with respect to quantifying the morphology of the adsorbed layer. The increased strength of attachment to the surface will result in slower desorption kinetics as the incubation time increases. By using a simple kinetic model it is possible to determine the transition rates between different states of the protein ranging from the easily desorbed to those that are irreversibly bound. Experimentally, this can be observed using many techniques that follow the adsorbed amount over time and allowing the running buffer to replace the bulk solution after varying incubation times e.g. dual polarisation interferometry (DPI) and ellipsometry. Given recent advances in technology, it is also now a possibility that neutron reflectivity will be able to monitor these changes on an appropriate timescale and, at the same time, monitor the structural changes that are occurring (this will be discussed more in section 1.6 and in subsequent chapters of this thesis).

The change in orientation and structure does not necessarily result in an irreversibly bound state. It is possible that a modified protein may be exchanged or desorb from the surface and the desorbed protein has been shown to have the same secondary structure and thermal stability as the proteins in bulk solution[103].

As well as changes to the adsorbed proteins when in place, it has also been

observed in several systems that lateral diffusion can occur over distances that are orders of magnitude greater than the length of the protein molecule[104]. The lateral movement of proteins in lipid bilayers can be explained in terms of a protein in a viscous liquid but diffusion of a protein adsorbed at a solid/liquid interface is a different entity. This requires the motion of many physisorbed segments and as a simplistic analogy it can be thought of in similar terms to the motion of a crawling worm; at any instant some parts of the protein are attached but a few segments that detach and then reattach at a different site allow for movement of the protein. A more detailed description of the diffusion process is beyond the scope of this thesis but it is mentioned in passing as for the sake of completeness when concerning the interesting and complex phenomena involved in protein adsorption.

1.4 Theoretical models of protein adsorption

Mathematical models can largely be divided into two categories; a description of the adsorption kinetics or a thermodynamic description that aims to predict the equilibrium structure of the adsorbed layer. Experimental data of protein adsorption provides a macroscopic picture of the properties of the adsorbed layer whereas mathematical models offer a route to ascertain more mechanistic detail of the adsorption process. An agreement, or otherwise, with experimental data can be seen as a validation of the model but this also implies that the models are somewhat restricted to experimental limits within which their hypotheses can be tested[52].

1.4.1 Kinetic models

Mathematical descriptions of the adsorption/desorption kinetics are most commonly given in the form of rate equations and are often based on extending models that have been derived for less complex systems. Probably the most widely recognized is the Langmuir adsorption model

$$\frac{d\Theta}{dt} = k_{on}N(1-\Theta) - k_{off}N\Theta \tag{1.6}$$

where k_{on} and k_{off} are the adsorption and desorption rate constants respectively, N is the total number of adsorption sites and Θ is the number of occupied sites.

This is a good basis from which to start but, given the assumptions on which it is based, it is far too simplistic to accurately model the complex nature of protein

adsorption and quantative conclusions drawn from it are essentially nugatory. To account for the protein's ability to occupy more than one surface site it is possible to use a function that describes the available surface area, $\Phi(\theta)$, in the random sequential adsorption (RSA) model[105]. In its simplest form this model assumes irreversible adsorption and predicts a 'jamming limit' when surface coverage is $\sim 55\%$. The main limitation of this model is that it is hard to include detailed molecular information of the proteins[106].

The most common methodology when extending known models is to account for different states of proteins on the surface, such as side-on or end-on orientations[107], post-adsorption spreading[108] and clustering[109]. These models reflect the need to better resemble the commonly accepted empirical observations. The exact nature of the different states will vary depending on the author's interest and the range of parameters to which the models can be applied. In a review by Rabe et al.[52] the author suggests nine general mechanistic based models (including the Langmuir and RSA). Bearing in mind the complexity of protein adsorption it is likely that many different processes are occurring at any particular time but to include all of them in one theory would make this mathematical description very complex and not provide any real mechanistic insight whereas by focussing on different aspects of the adsorption process and tailoring the model appropriately, it is possible the draw legitimate conclusions from differing descriptive models.

To account for the experimental observation that some proteins adsorb irreversibly, a 'two-states model' was developed by McGuire et al.[110] whereby proteins could either adsorb in the two states or adsorb initially in the reversible state and then subsequently undergo a transition to the irreversible state. The 'transition model' was then extended further by Szollosi et al.[108] to include more than two states. Each state, i, is characterised by a binding energy to the surface, ε_i, and a footprint size, l_i, and the states are separated by a potential barrier, as shown in figure (1.3). This model has the advantage of being able to follow the exchange of unlabelled for labelled proteins which, the authors argue, is only possible when in the context of a reversible model which allows for multiple states. They propose a mechanism of exchange whereby the adsorption of an incoming protein induces the pre-adsorbed protein to be "ratcheted" up to smaller footprints before being expelled. This results in a higher rate of removal of the pre-adsorbed protein when compared to the scenario of desorption into protein-free buffer.

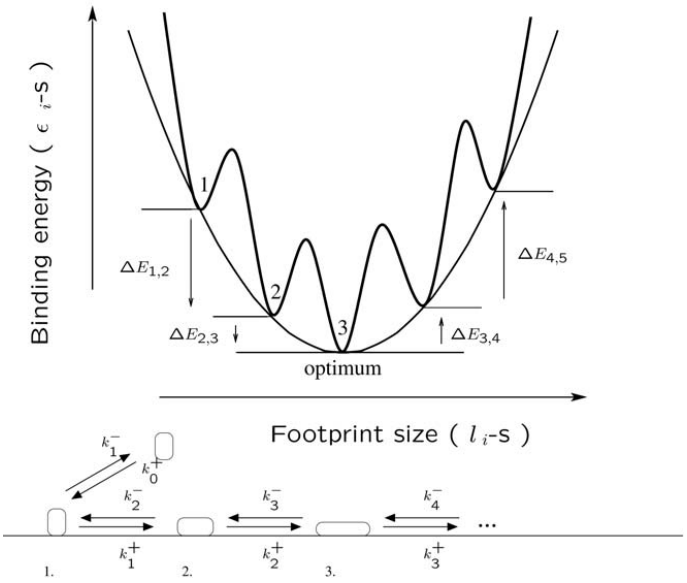


Figure 1.3: Binding energies of different footprint sizes. Figure reproduced from [108].

1.4.2 Thermodynamic models

Thermodynamic models are more extensively made for the air/liquid interface due to the ability to experimentally determine the thermodynamical parameter of surface tension (or surface pressure). Quantifying the thermodynamic parameters at the solid/liquid interface is more difficult but techniques such as isothermal calorimetry[29] or flow microcalorimetry[111] can provide some information on the enthalpies of the adsorption.

Detailed atomistic approaches for adsorption of even single protein molecules are currently not feasible due to the timescale of the adsorption process far out stripping the computational capabilities. Mathematical models therefore are most often based on calculating the free energy of the system either from a macroscopic or molecular viewpoint. Vogler[6] suggests that the overall free energy can be subdivided into three due to the different contributions from the hydrophobic effect, surface dehydration and interactions (protein-protein and protein-surface); $\Delta G^o_{ads} = \Delta G^o_{hydrophobic} + \Delta G^o_{dehydration} + \Delta G^o_{interaction}$. A molecular theory approach aiming to help bridge the gap between atomistic and macroscopic models by Fang and Szleifer[106, 53] starts with a molecular description of a bulk system at equilibrium which is brought into contact with a surface. The time evolution of the distribution of the proteins is then calculated with a diffusion-like equation with a

chemical potential difference being the driving force. This model provides a route for explaining both kinetic features and the longer time scale equilibrium properties of the adsorbed layer and has been applied successfully to some simple systems[106]. The main limitation of applying this theory is that it requires the input of the possible conformations of the protein and rate of conformational transition which are very difficult quantities to obtain.

1.5 Protein exchange

It has been noted earlier that the adsorption of macromolecules such as proteins differs greatly from that of small amphiphiles such as surfactants. One main difference is the apparent irreversibility of protein adsorption when exposed to a buffer solution. Although each individual linkage between the protein and the surface is only of the order of kT, the numerous attachments result in a high activation energy for the desorption of the whole molecule which requires all of the linkages to be broken [112]. However, even after saturation of the surface has occurred proteins can still be removed from the surface due to interactions with other species in the bulk. The removal by different, small surfactants has been shown to varying extents depending on the nature of the surfactant and the protein[113, 114]. Exchange of the adsorbed protein can also occur due to replacement by other proteins[115]. It is necessary at this stage to distinguish between competitive adsorption and sequential adsorption. In the case of competitive adsorption i.e. from a mix of proteins in the bulk solution, the adsorption process involves numerous interactions and is determined by many factors such as transport to the surface and processes at the interface. Sequential adsorption follows the stepwise procedure of initial adsorption of a single protein, a washing stage and then exposure to a different protein in the bulk solution.

A comparison of the two methods by Noh and Vogler[116] showed no difference in terms of adsorbed amounts when an incubation time of 1 hour was used in the sequential adsorption but, more commonly, it is expected that in sequential adsorption experiments the first protein has more time to form stronger bonds with the surface and thus, the final adsorpbed layer will differ from competitive adosprion. This has been shown by Lassen and Malmsten[117] on polymer surfaces. When adsorbed from a bulk mixture with HSA, Fibrinogen and IgG dominated the layer but in sequential studies they could not displace the pre-adsorbed HSA. The two experimental strategies will now be considered individually.

1.5.1 Sequential adsorption

The main aims of sequential adsorption experiments can be considered to probe two aspects of protein adsorption. Firstly, when considering the same two proteins the extent of exchange with respect to the incubation time of the first can be seen as an indirect measure of the post-adsorption changes occurring to the adsorbed protein. Less extensive exchange after a longer incubation time is indicative of a stronger attachment to the surface. For example, Nasir and McGuire[102] have observed that β-casein can completely remove BSA and β-lactoglobulin from a surface when the incubation time, t_{inc}, is 1 hour but only partial exchange occurs when t_{inc}=4 hours which was not observed for α-lactalbumin. This is in good agreement with Wertz and Santore who showed that an increased incubation time for BSA dramatically reduced Fibrinogen adhesion[100].

Secondly, an experimental protocol where the second protein is changed offers a chance to probe how different proteins interact and another measure of their relative surface activities. This can be seen as either increased exchange of the incumbent protein or varying degrees of adsorption onto the pre-adsorbed layer which will alter the "seen" surface. From a technical view point it is very difficult to distinguish between the displacement of a protein and adsorption onto the layer although some conclusions regarding the nature of the final layer can be drawn when compared to single protein studies using techniques with a high degree of structural resolution. One such study on Fibrinogen and HSA adsorption using neutron reflectivity has shown a mixture of multilayer formation (and subsequent removal), displacement at the surface and the incoming protein filling in gaps in the pre-adsorbed layer[45].

The extent to which the first protein blocks the incoming one is also dependent on the nature of the surface. A more hydrophobic surface will encourage the protein to unfold more and thus be more resistant to exchange[117, 118] even for the same incubation time. However, it has also been suggested that it is the ability of the incoming protein to adsorb within a small available area that is of greater importance rather than the properties of the adsorbed layer. Podhipleux et al. have shown that wild type LYS displaces a less thermally stable variant even though the rate and extent of unfolding on the surface would be more extensive (and lead to a stronger binding to the surface) for the mutant variant [118].

1.5.2 Competitive adsorption

Essentially all biological and practical systems of interest will be composed of a mixture of proteins. In blood plasma, for example, more than 1000 proteins have been identified with individual concentrations spanning more than 10 orders of magnitude[6]. Most of the early work concerning protein mixtures has focussed on Fibrinogen and other blood proteins due to the importance of their adsorption in effecting the adhesion of blood cells and platelets[119]. The ideas developed have now been extended to a more universal way of thinking that when adsorption occurs from a mixture of proteins, it has been empirically observed that at short times the surface is initially covered with small, mobile proteins and as time progresses these are displaced by larger proteins or those with a higher affinity for the surface. This is a well known phenomena and has been named as the Vroman effect[120] in recognition of pioneering work in this field carried out by Vroman[121].

The sequence of adsorption is often found to follow that of the molecular weights[31, 122]. This is not universally observed and more research is needed to determine the importance of other factors involved. It also does not provide any useful information when considering the final structure of the adsorbed layer. A study carried out by Arai and Norde[123] of four proteins with similar molecular weights (LYS, ribonuclease, myoglobin and α-lactalbumin) suggest that the adsorption is largely governed by electrostatics with superimposed effects of surface hydrophobicity and structural rearrangements when comparing proteins of similar structural flexibility. The low structural stability of a flexible protein (α-lactalbumin) can override these factors to dominate in a competitive scenario. This has also been shown to be the case when the adsorption of wild type LYS is in competition with two mutant variants and in instances in which exchange reactions between adsorbed protein and protein in the bulk occur, they occur such that more stable variants are removed from the surface by less stable variants[38]. This is in direct contrast to the sequential adsorption experiments mentioned in the previous section [118] and illustrates both the complexity of the protein adsorption problem and the discourse existing in the literature.

1.6 Aims of this work

As with any project or body of work where new ground is attempting to be broken the final conclusions may not fit well with the original imaginings of the researches and may uncover new questions rather than the answers sought at the outset. To an extent, so it has proved with this work. The initial experimental aims were based on the effect of nanoparticles on the nucleation protein β-2 microglobulin[124]. It was hoped to be able to study the timescales of self-exchange of the protonated and perdeuterated forms of this protein using neutron reflectivity but, due to various reasons, producing the required amounts of the protein required for the experiments proved the undoing of this aim. However, in the ensuing time it appeared that exploring model systems of well characterised proteins would also be of benefit in answering some questions and laying the groundwork for future investigations using perdeuterated proteins.

Thus the initial aim was to characterise the adsorption of single protein solutions of CA II, HSA, LYS and MBP and also look for any time evolution of the neutron reflectivity profiles and hence direct evidence for changes in the gross morphology of the adsorbed layer. Using neutron reflectivity for protein adsorption studies at the solid/liquid interface has shown that high structural resolution is possible but has previously mostly been reported for the equilibrium (or steady state) adsorbed layer i.e. after the reflectivity profile has stopped changing. Recent improvements in the instrumentation and neutron sources have allowed for reflectivity profiles to be recorded in less time than in previous work which has in turn allowed for a more detailed investigation of the longer timescale changes that are thought to occur in protein adsorption.

With the combined aim of looking for indirect evidence, i.e. propensity for exchange, of changes over time and testing the hypothesis that neutron reflectivity can be usefully applied to two-component systems without the need for extensive deuteration, sequential adsorption experiments were carried out with a variety of incubation times of the pre-adsorbed protein. The experimental findings showed that with only protonated proteins some useful information can be gained but the similarity of the scattering length densities limits the effectiveness and range of these experiments. However, these results proved to be a good enough basis for proposals through which we obtained enough perdeuterated proteins (d-MBP and d-HSA) from the Institut Laue-Langevin deuteration lab in Grenoble, France. These were

used to perform both the self-exchange experiments (with MBP) and repeat the HSA-LYS sequential adsorption experiments with d-HSA.

The use of perdeuterated proteins fulfills two roles; firstly, by use of contrast variation the aim was to provide a detailed structural picture of the adsorbed layer with respect to distinguishing between protein exchange and further adsorption, to comment on the timescales of these changes and look at adsorption from binary protein mixtures. In so doing questions arose concerning the effect of the deuteration and isotope effects that might influence the adsorption. It is generally assumed when using perdeuterated species for adsorption studies, for example with surfactants, that the effect of deuteration is not overly significant and this was our working hypothesis at the start of the analysis. However, it became clear that this was not the case for proteins and a marked difference between the protonated and deuterated proteins emerged. The experiments run with perdeuterated proteins should be viewed in terms of a very good test case for the limitations of using neutron reflectivity in this way and the need to continually question the underlying assumptions of the technique and analysis. These experiment could also be used as the basis for probing some of the underlying driving factors for protein adsorption and one aim of this work is to comment on the possible experimental methodology that should be applied to future studies of protonated and deuterated proteins. On the one hand they could be considered as the same protein and self-exchange processes can be explored, analogous to radiolabelling or fluorescent labelling techniques. Alternatively the results should be viewed more in the terms of similar proteins with slightly altered properties, following the path of the use of mutant variants with slightly altered primary amino acid sequences to alter their properties. In both cases more work is required to determine the effect of the deuteration both on the protein properties and on the adsorption process.

In summary, the aims of this work have turned out to be two pronged; an investigation into the properties of the protein systems of interest and an assessment of the neutron reflectivity technique for protein adsorption studies. Chapters 3, 4 and 5 of this thesis are ordered in terms of the protein systems; single protein followed by sequential adsorption then mixtures. Comments concerning the isotope effects are a running theme throughout and are discussed in the most appropriate context. Chapter 6 provides a slight aside regarding the effect of other components on HSA adsorption and should be viewed in the context of HSA adsorption discussed in Chapter 3.

A logical extension of the assessment of neutron reflectivity as a technique was to compare it to another available technique, dual polarisation interferometry (DPI) and this is explored in Chapter 7. It was also the aim of using this technique to look at any shorter timescale phenomena that could be occurring. However, it should also be noted that this technique provides no route for distinguishing between different proteins or the same structural detail as neutron reflectivity and thus its use is perhaps somewhat limited when considering adsorption of protein mixtures.

References

[1] T. Merian and J. M. Goddard, "Advances in nonfouling materials: Perspectives for the food industry," *Journal of Agricultural and Food Chemistry*, vol. 60, no. 12, pp. 2943–2957, 2012.

[2] E. A. Vogler, "The Goldilocks surface," *Biomaterials*, vol. 32, no. 28, pp. 6670 – 6675, 2011.

[3] C. R. Taitt, G. P. Anderson, and F. S. Ligler, "Evanescent wave fluorescence biosensors," *Biosensors and Bioelectronics*, vol. 20, no. 12, pp. 2470 – 2487, 2005. 20th Anniversary of Biosensors and Bioelectronics.

[4] T. J. Su, J. R. Lu, Z. F. Cui, R. K. Thomas, and R. K. Heenan, "Application of small angle neutron scattering to the in situ study of protein fouling on ceramic membranes," *Langmuir*, vol. 14, no. 19, pp. 5517–5520, 1998.

[5] I. Lynch, T. Cedervall, M. Lundqvist, C. Cabeleiro-Lago, S. Linse, and K. A. Dawson, "The nanoparticle-protein complex as a biological entity; a complex fluids and surface science challenge for the 21st century.," *Advances in Colloid and Interface Science*, vol. 134-135, pp. 167–174, 2007.

[6] E. A. Vogler, "Protein adsorption in three dimensions," *Biomaterials*, vol. 33, pp. 1201–1237, 2012.

[7] X. M. He and D. C. Carter, "Atomic structure and chemistry of human serum albumin," *Nature*, vol. 358, pp. 209–215, 1992.

[8] J. R. Olivieiri and A. F. Craievich, "The subdomain structure of human serum albumin in solution under different pH conditions studied by small angle X-ray scattering," *European Biophysics Journal*, vol. 24, pp. 77–84, 1995.

[9] O. J. Bos, J. F. Labro, M. J. Fischer, J. Wilting, and L. H. Janssen, "The molecular mechanism of the neutral-to-base transition of human serum albumin. Acid/base titration and proton nuclear magnetic resonance studies on a large peptic and a large tryptic fragment of albumin.," *Journal of Biological Chemistry*, vol. 264, no. 2, pp. 953–959, 1989.

[10] S. Curry, P. Brick, and N. P. Franks, "Fatty acid binding to human serum albumin: new insights from crystallographic studies," *Biochimica et Biophysica Acta*, vol. 1441, pp. 131–140, 1999.

[11] D. E. Kuehner, J. Engmann, F. Fergg, M. Wernick, H. W. Blanch, and J. M. Prausnitz, "Lysozyme net charge and ion binding in concentrated aqueous electrolyte solutions," *The Journal of Physical Chemistry B*, vol. 103, no. 8, pp. 1368–1374, 1999.

[12] C. C. F. Blake, D. F. Koenig, G. A. Mair, A. C. T. North, D. C. Phillips, and V. R. Sarma, "Structure of hen egg-white lysozyme: A three-dimensional fourier synthesis at 2 Å resolution," *Nature*, vol. 206, pp. 757–761, 1965.

[13] Y. Efimova, *Proteins at Surfaces*. PhD thesis, Technische Staatsuniversiteit van Sint-Petersburg, 2006.

[14] S. Raghava, S. Aquil, S. Bhattacharyya, R. Varadarajan, and M. N. Gupta, "Strategy for purifying maltose binding protein fusion proteins by affinity precipitation," *Journal of Chromatography A*, vol. 1194, no. 1, pp. 90 – 95, 2008. 27th International Symposium on the Separation of Proteins, Peptides & Polynucleotides.

[15] J. C. Spurlino, G.-Y. LuSI, and F. A. Quiocho, "The 2.3-Å resolution structure of the maltose- or maltodextrin binding protein, a primary receptor of bacterial active transport and chemotaxis," *The Journal of Biological Chemistry*, vol. 266, pp. 5202–5219, 1991.

[16] W.-Y. Choy, M. Tollinger, G. A. Mueller, and L. E.Kay, "Direct structure refinement of high molecular weight proteins against residual dipolar couplings and carbonyl chemical shift changes upon alignment: an application to maltose binding protein," *Journal of Biomolecular NMR*, vol. 21, pp. 31–40, 2001.

[17] J. C. Spurlino, *The three-dimensional structure of the D-maltose-binding protein from Escherichia coli*. PhD thesis, Rice University, 1988.

[18] A. J. Sharff, L. E. Rodseth, J. C. Spurlino, and F. A. Quiocho, "Crystallographic evidence of a large ligand-induced hinge-twist motion between the two domains of the maltodextrin binding protein involved in active transport and chemotaxis," *Biochemistry*, vol. 31, pp. 10657–10663, 1992.

[19] K. Hakansson, M. Carlsson, L. Svensson, and A. Liljas, "Structure of native and apo carbonic anhydrase II and structure of some of its anion-ligand complexes.," *Journal of Molecular Biology*, vol. 227(4), pp. 1192–1204, 1992.

[20] R. Recacha, M. J. Costanzo, B. E. Maryanoff, and D. Chattopadhyay, "Crystal structure of human carbonic anhydrase II complexed with an anti-convulsant sugar sulphamate," *Biochem. J.*, vol. 361, pp. 437–441, 2002.

[21] K. Kishida and N. Ochi, "Evidence for the existence of two carbonic anhydrase isozymes in rabbit ciliary body," *Experientia*, vol. 36, pp. 42–43, 1980.

[22] A. Liljas, K. K. Kannan, P.-C. Bergsten, I. Waara, K. Fridborh, B. Strandberg, U. Carlbom, L. Jarup, S. Lovgren, and M. Petef, "Crystal structure of human carbonic anhydrase C," *nature new biology*, vol. 235, pp. 131–137, 1972.

[23] S. Sugio, A. Kashima, S. Mochizuki, M. Noda, and K. Kobayashi, "Crystal structure of human serum albumin at 2.5 Å resolution," *Protein Engineering*, vol. 12, pp. 439–446, 1999.

[24] D. Rose, J. Phipps, J. Michniewicz, G. Birnbaum, F. Ahmed, A. Muir, W. Anderson, and S. Narang, "Crystal structure of T4-lysozyme generated from synthetic coding DNA expressed in Escherichia coli.," *Protein Engineering*, vol. 2, pp. 277–282, 1988.

[25] F. Quiocho, J. Spurlino, and L. Rodseth, "Extensive features of tight oligosaccharide binding revealed in high-resolution structures of the maltodextrin transport/chemosensory receptor.," *Structure*, vol. 5, pp. 997–1015, 1997.

[26] en.wikipedia.org/wiki/Carbonic_anhydrase_II.

[27] S. K. Nair, T. L. Calderone, D. W. Christianson, and C. A. Fierke, "Altering the mouth of a hydrophobic pocket. Structure and kinetics of human carbonic anhydrase II mutants at residue Val-121.," *Journal of Biological Chemistry*, vol. 266, no. 26, pp. 17320–17325, 1991.

[28] G. A. Kulikova, I. V. Ryabinina, S. S. Guseynov, and E. V. Parfenyuk, "Calometric study of adsorption of human serum albumin onto silica particles," *Thermochemica Acta*, vol. 503-504, pp. 65–69, 2010.

[29] S. Lindman, I. Lynch, E. Thulin, H. Nilsson, K. A. Dawson, and S. Linse, "Systematic investigation of the thermodynamics of HSA adsorption to N-iso-Propylacrylamide/ N-tert-Butylacrylamide compolymer nanoparticles. Effects of particle size and hydrophobicity," *Nano Letters*, vol. 7 (4), pp. 914–920, 2007.

[30] J. D. Andrade, V. Hlady, and A. P. Wei, "Adsorption of complex proteins at interfaces," *Pure and Applied Chemistry*, vol. 64, pp. 1777–1781, 1992.

[31] W. Norde, *Physical Chemistry of Biological Interfaces*, ch. 4. Proteins at Solid Surfaces, pp. 115–135. Marcel Dekker, Inc., 2000.

[32] M. T. Tyn and T. W. Gusek, "Prediction of diffusion coefficients of proteins," *Biotechnology and Bioengineering*, vol. 35, no. 4, pp. 327–338, 1990.

[33] C. A. Haynes and W. Norde, "Structures and stabilities of adsorbed proteins," *Journal of Colloid and Interface Science*, vol. 169, no. 2, pp. 313 – 328, 1995.

[34] K. Nakanishi, T. Sakiyama, and K. Imamura, "On the adsorption of proteins on solid surfaces, a common but very complicated phenomenon," *Journal of Bioscience and Bioengineering*, vol. 91, no. 3, pp. 233 – 244, 2001.

[35] L. Lins and R. Brasseur, "The hydrophobic effect in protein folding," *The FASEB Journal*, vol. 9, no. 7, pp. 535–540, 1995.

[36] B. Lee and F. Richards, "The interpretation of protein structures: Estimation of static accessibility," *Journal of Molecular Biology*, vol. 55, no. 3, pp. 379 – 400, IN3–IN4, 1971.

[37] C. A. Haynes and W. Norde, "Globular proteins at solid/liquid interface," *Colloids and Surface B: Biointerfaces*, vol. 2, pp. 517–566, 1994.

[38] W.-K. Lee, J. McGuire, and M. K. Bothwell, "Competitive adsorption of bacteriophage T4 lysozyme stability variants at hydrophilic glass surfaces," *Journal of Colloid and Interface Science*, vol. 269, pp. 251–254, 2004.

[39] P. Billsten, P.-O. Freskard, U. Carlsson, B.-H. Jonsson, and H. Elwing, "Adsorption to silica nanoparticles of human carbonic anhydrase II and truncated forms induced a molten-globule-like structure," *Federation of European Biochemical Sciences*, vol. 402, pp. 67–72, 1997.

[40] T. J. Su, J. R. Lu, R. K. Thomas, and Z. F. Cui, "Effect of pH on the adsorption of bovine serum albumin at the silica/water interface studied by neutron reflection," *The Journal of Physical Chemistry B*, vol. 103 (18), pp. 3727–3736, 1999.

[41] M. G. Bremer, J. Duval, W. Norde, and J. Lyklema, "Electrostatic interactions between immunoglobulin (IgG) molecules and a charged sorbent," *Colloids and Surfaces A: Physicochemical and Engineering Aspects*, vol. 250, no. 1-3, pp. 29 – 42, 2004. In honour of the 250th volume of Colloid and Surfaces A and the 25th Anniversary of the International Association of Colloid and Interface Scientists (IACIS).

[42] S. Demanche, J.-P. Chapel, L. J. Monrozier, and H. Quiquampoix, "Dissimilar pH-dependent adsorption features of bovine serum albumin and α-chymotrypsin on mica probed by AFM," *Colloids and Surfaces B: Biointerfaces*, vol. 70, no. 2, pp. 226 – 231, 2009.

[43] F. Hook, M. Rodahl, B. Kasemo, and P. Brzezinski, "Structural changes in haemoglobin during adsorption to solid surfaces: Effects of pH, ionic strength, and ligand binding," *PNAS*, vol. 95, pp. 12271–12276, 1998.

[44] R. Maheshwari and A. Dhathathreyan, "Mucin at solution/air and solid/solution interfaces," *Journal of Colloid and Interface Science*, vol. 293, no. 2, pp. 263 – 269, 2006.

[45] D. Forciniti and W. A. Hamilton, "Surface enrichment of proteins at quartz/water interfaces: A neutron reflectivity study," *Journal of Colloid and Interface Science*, vol. 285, pp. 458–468, 2005.

[46] M. Rabe, D. Verdes, M. Rankl, G. R. J. Artus, and S. Seeger, "A comprehensive study of concepts and phenomena of the nonspecific adsorption of β-lactoglobulin," *ChemPhysChem*, vol. 8, no. 6, pp. 862–872, 2007.

[47] M. Karlsson and U. Carlsson, "Protein adsorption orientation in the light of fluorescent probes: Mapping of the interaction between site-diectly labeled human carbonic anhydrase II and silica nanoparticles," *Biophysical Journal*, vol. 88, pp. 3536–3544, 2005.

[48] T. J. Su, J. R. Lu, R. K. Thomas, Z. F. Cui, and J. Penfold, "The effect of solution pH on the structure of lysozyme layers adsorbed at the silica-water interface studied by neutron reflection," *Langmuir*, vol. 14, pp. 438–445, 1998.

[49] J. R. Lu, X. Zhao, and M. Yaseen, "Protein adsorption studied by neutron reflection," *Current Opinion in Colloid & Interface Science*, vol. 12, pp. 9–16, 2007.

[50] J. Israelachvili, *Intermolecular and surface forces, 2nd Edition.* Academic Press, London, 1992.

[51] K. L. Jones and C. R. O'Melia, "Protein and humic acid adsorption onto hydrophilic membrane surfaces: Effects of pH and ionic strength," *Journal of Membrane Science*, vol. 165, no. 1, pp. 31 – 46, 2000.

[52] M. Rabe, D. Verdes, and S. Seeger, "Understanding protein adsorption phenomena at solid surfaces," *Advances in Colloid and Interface Science*, vol. 162, pp. 87–106, 2011.

[53] F. Fang and I. Szleifer, "Competitive adsorption in model charged protein mixtures: Equilibrium isotherms and kinetics behavior," *The Journal of Chemical Physics*, vol. 119, pp. 1053–1065, 2003.

[54] T. S. Tsapikouni, S. Allen, and Y. F. Missirlis, "Measurement of interaction forces between fibrinogen coated probes and mica surface with the atomic force microscope: The pH and ionic strength effect," *Biointerphases*, vol. 3(1), pp. 1–8, 2008.

[55] M. G. Cacace, E. M. Landau, and J. J. Ramsden, "The Hofmeister series: salt and solvent effects on interfacial phenomena," *Quarterly Reviews of Biophysics*, vol. 30, no. 03, pp. 241–277, 1997.

[56] J. R. Wendorf, C. J. Radke, and H. W. Blanch, "The role of electrolytes on protein adsorption at a hydrophlic solid-water interface," *Colloids and Surfaces B: Biointerfaces*, vol. 75, pp. 100–106, 2010.

[57] T. Wei, S. Kaewtathip, and K. Shing, "Buffer effect on protein adsorption at liquid/solid interface," *The Journal of Physical Chemistry C*, vol. 113, no. 6, pp. 2053–2062, 2009.

[58] K. B. Wiberg and L. H. Slaugh, "The deuterium isotope effect in the side chain halogenation of toluene," *Journal of the American Chemical Society*, vol. 80, no. 12, pp. 3033–3039, 1958.

[59] C. Hennig, R. B. Oswald, and S. Schmatz, "Secondary kinetic isotope effect in nucleophilic substitution: A quantum-mechanical approach," *The Journal of Physical Chemistry A*, vol. 110, no. 9, pp. 3071–3079, 2006. PMID: 16509628.

[60] J. J. Katz, "Chemical and biological studies with deuterium," *American Scientist*, vol. 48, no. 4, pp. 544–580, 1960.

[61] J. J. Katz, H. L. Crespi, and A. J. Finkel, "Isotope effects in fully deuterated hexoses, proteins an nucleic acids," *Pure and Applied Chemistry*, vol. 8, pp. 471–481, 1964.

[62] W. W. Cleland, "The use of isotope effects to determine enzyme mechanisms," *Journal of Biological Chemistry*, vol. 278, no. 52, pp. 51975–51984, 2003.

[63] T. R. Gamble, K. R. Clauser, and A. A. Kossiakoff, "The production and X-ray structure determination of perdeuterated Staphylococcal nuclease," *Biophysical Chemistry*, vol. 53, pp. 15–26, 1994.

[64] T. Forsyth (private communication).

[65] P. Echenique, "Introduction to protein folding for physicists," *Contemporary Physics*, vol. 48, no. 2, pp. 81–108, 2007.

[66] S. Yokogaki, K. Unno, N. Oku, and S. Okada, "Chaperonin-repairable subtle incompleteness of protein assembly induced by a substitution of hydrogen with deuterium: Effect of GroE on deuterated ribulose 1,5-bisphosphate carboxylase," *Plant and Cell Physiology*, vol. 36, no. 3, pp. 419–423, 1995.

[67] D. Brockwell, L. Yu, S. Cooper, S. Mccleland, A. Cooper, D. Attwood, S. J. Gaskell, and J. Barber, "Physicochemical consequences of the perdeuteriation of glutathione S-transferase from S. japonicum," *Protein Science*, vol. 10(3), pp. 572–580, 2001.

[68] X. Liu, B. L. Hanson, P. Langan, and R. E. Viola, "The effect of deuteration on protein structure: a high-resolution comparison of hydrogenous and perdeuterated haloalkane dehalogenase," *Acta Crystallographica Section D*, vol. 63, pp. 1000–1008, Sep 2007.

[69] F. Meilleur, J. Contzen, D. Myles, and C. Jung, "Structural stability and dynamics of hydrogenated and perdeuterated cytochrome P450cam (CYP101)," *Biochemistry*, vol. 43, pp. 8744–8753, 2004.

[70] A. Hattori, H. L. Crespi, and J. J. Katz, "Effect of side-chain deuteration on protein stability," *Biochemistry*, vol. 4, no. 7, pp. 1213–1225, 1965.

[71] G. Piszczek, J. C. Lee, N. Tjandra, C.-R. Lee, Y.-J. Seok, R. L. Levine, and A. Peterkofsky, "Deuteration of Escherichia coli enzyme INtr alters its stability," *Archives of Biochemistry and Biophysics*, vol. 507, pp. 332–342, 2011.

[72] S. R. Dennison, T. Hau, S. Dante, K. Brandenburg, F. Harris, and D. A. Phoenix, "Deuteration can affect the conformational behaviour of amphiphilic alpha-helical structures," *Biophysical Chemistry*, vol. 119, no. 2, pp. 115 – 120, 2006.

[73] Z. Shi, B. A. Krantz, N. Kallenbach, and T. R. Sosnick, "Contribution of hydrogen bonding to protein stability estimated from isotope effects," *Biochemistry*, vol. 41, no. 7, pp. 2120–2129, 2002. PMID: 11841202.

[74] T. Nylander, *Surfactant Science Series Volume 110: Biopolymers at Interfaces (2nd ed.)*, ch. 10. Protein Adsorption in Relation to Solution Association and Aggregation, pp. 259–294. Marcel Dekker, Inc., 2003.

[75] P. Cioni and G. B. Strambini, "Effect of heavy water on protein flexibility," *Biophysical Journal*, vol. 82, pp. 3246–3253, 2002.

[76] L. Fu, S. Villette, S. Petoud, F. Fernandez-Alonso, and M.-L. Saboungi, "H/D isotope effects in protein thermal denaturation: The case of bovine serum albumin," *The Journal of Physical Chemistry B*, vol. 115, no. 8, pp. 1881–1888, 2011.

[77] D. J. Kuzmenka and S. Granick, "Kinetics of polymer adsorption measured in situ at the solidliquid interface: Utility of the infrared total internal reflection method," *Colloids and Surfaces*, vol. 31, pp. 105 – 116, 1988. Proceedings of an International Conference.

[78] D. C. Leonhardt, H. E. Johnson, and S. Granick, "Adsorption isotope effect for protio- and deuteropolystyrene at a single solid surface," *Macromolecules*, vol. 23, no. 2, pp. 685–687, 1990.

[79] J. A. Koehler, M. Ulbricht, and G. Belfort, "Intermolecular forces between a protein and a hydrophilic modified polysulfone film with relevance to filtration," *Langmuir*, vol. 16, no. 26, pp. 10419–10427, 2000.

[80] J. McColl, G. E. Yakubov, and J. J. Ramsden, "Complex desorption of mucin from silica," *Langmuir*, vol. 23, no. 13, pp. 7096–7100, 2007.

[81] T. J. Su, J. R. Lu, R. K. Thomas, Z. F. Cui, and J. Penfold, "The adsorption of lysozyme at the silica-water interface: A neutron reflection study," *Journal of Colloid and Interface Science*, vol. 203, pp. 419–429, 1998.

[82] T. J. Su, R. J. Green, Y. Wang, E. F. Murphy, J. R. Lu, R. Ivkov, and S. K. Satija, "Adsorption of lysozyme onto the silicon oxide surface chemically grafted with a monolayer of pentadecyl-1-ol," *Langmuir*, vol. 16, no. 11, pp. 4999–5007, 2000.

[83] J. R. Lu, T. J. Su, P. N. Thirttle, R. K. Thomas, A. R. Rennie, and R. Cubitt, "The denaturation of lysozyme layers adsorbed at the hydrophobic solid/liquid surface studied by neutron reflection," *Journal of Colloid and Interface Science*, vol. 206, pp. 212–223, 1998.

[84] S. Fukuzaki, H. Urano, and K. Nagata, "Adsorption of bovine serum albumin onto metal oxide surfaces," *Journal of Fermentation and Bioengineering*, vol. 81, no. 2, pp. 163 – 167, 1996.

[85] G. Yin, Z. Liu, J. Zhan, F. Ding, and N. Yuan, "Impacts of the surface charge property on protein adsorption on hydroxyapatite," *Chemical Engineering Journal*, vol. 87, no. 2, pp. 181 – 186, 2002.

[86] A. Gessner, A. Lieske, B. R. Paulke, and R. H. Mller, "Influence of surface charge density on protein adsorption on polymeric nanoparticles: analysis by two-dimensional electrophoresis," *European Journal of Pharmaceutics and Biopharmaceutics*, vol. 54, no. 2, pp. 165 – 170, 2002.

[87] K. Kato, S. Sano, and Y. Ikada, "Protein adsorption onto ionic surfaces," *Colloids and Surfaces B: Biointerfaces*, vol. 4, no. 4, pp. 221 – 230, 1995.

[88] N. Barnthip, P. Parhi, A. Golas, and E. A. Vogler, "Volumetric interpretation of protein adsorption: Kinetics of protein-adsorption competition from binary solution," *Biomaterials*, vol. 30, no. 33, pp. 6495 – 6513, 2009.

[89] N. Barnthip, H. Noh, E. Leibner, and E. A. Vogler, "Volumetric interpretation of protein adsorption: Kinetic consequences of a slowly-concentrating interphase," *Biomaterials*, vol. 29, no. 21, pp. 3062 – 3074, 2008.

[90] M. Holmberg and X. Hou, "Fibrinogen adsorption on blocked surface of albumin," *Colloids and Surfaces B: Biointerfaces*, vol. 84, no. 1, pp. 71 – 75, 2011.

[91] J. R. Lu, M. J. Swann, L. L. Peel, and N. J. Freeman, "Lysozyme adsorption studies at the silica/water interface using dual polarisation interferometry," *Langmuir*, vol. 20, pp. 1827–1832, 2004.

[92] B. P. Frank and G. Belfort, "Atomic force microscopy for low-adhesion surfaces: Thermodynamic criteria, critical surface tension, and intermolecular forces," *Langmuir*, vol. 17, no. 6, pp. 1905–1912, 2001.

[93] C. M. Cuppett, L. J. Doneski, and M. J. Wirth, "Irreversible adsorption of lysozyme to polishing marks on silica," *Langmuir*, vol. 16, no. 18, pp. 7279–7284, 2000.

[94] K. Rechendorff, M. B. Hovgaard, M. Foss, V. P. Zhdanov, and F. Besenbacher, "Enhancement of protein adsorption induced by surface roughness," *Langmuir*, vol. 22, no. 26, pp. 10885–10888, 2006.

[95] J. L. Wehmeyer, R. Synowicki, R. Bizios, and C. D. Garcia, "Dynamic adsorption of albumin on nanostructured TiO_2 thin films," *Materials Science and Engineering C*, vol. 30, pp. 277–282, 2010.

[96] T. E. Jenkins, "Multiple-angle-of-incidence ellipsometry," *Journal of Physics D: Applied Physics*, vol. 32, pp. R45–R56, 1999.

[97] M. Born and E. Wolf, *Principles of Optics*. Pergammon: Oxford, 1970.

[98] H. Xu, J. R. Lu, and D. E. Williams, "Effect of surface packing density of interfacially adsorbed monoclonal antibody on the binding of hormonal antigen human chorionic gonadotrophin," *Journal of Physical Chemistry B*, vol. 110, pp. 1907–1914, 2006.

[99] C. S. Lee and G. Belfort, "Changing activity of ribonuclease A during adsorption: A molecular explanation," *Proceedings of the National Academy of Sciences*, vol. 86, no. 21, pp. 8392–8396, 1989.

[100] C. F. Wertz and M. M. Santore, "Adsorption and relaxation kinetics of albumin and fibrinogen on hydrophobic surfaces: Single-species and competitive behavior," *Langmuir*, vol. 15, no. 26, pp. 8884–8894, 1999.

[101] C. F. Wertz and M. M. Santore, "Effect of surface hydrophobicity on adsorption and relaxation kinetics of albumin and fibrinogen: Single-species and competitive behavior," *Langmuir*, vol. 17, no. 10, pp. 3006–3016, 2001.

[102] A. Nasir and J. McGuire, "Sequential and competitive adsorption of bovine serum albumin and β-lactoglobulin, and their resistance to exchange with α-lactalbumin and β-casein," *Food Hydrocolloids*, vol. 12, no. 1, pp. 95 – 103, 1998.

[103] C. E. Giacomelli and W. Norde, "The adsorption-desorption cycle. Reversibility of the BSA-silica system," *Journal of Colloid and Interface Science*, vol. 233, no. 2, pp. 234 – 240, 2001.

[104] R. D. Tilton, *Surfactant Science Series Volume 110: Biopolymers at Interfaces (2nd ed.)*, ch. 9. Mobility of Biomolecules at Interfaces, pp. 221–257. Marcel Dekker, Inc., 2003.

[105] J. Talbot, G. Tarjus, P. R. V. Taessel, and P. Viot, "From car parking to protein adsorption: An overview of sequential adsorption processes," *Colloids and Surfaces A: Physicochemical and Engineering Aspects*, vol. 165, pp. 287–324, 2000.

[106] F. Fang and I. Szleifer, "Kinetics and thermodynamics of protein adsorption: A generalized molecular theoretical approach," *Biophysical Journal*, vol. 80, no. 6, pp. 2568 – 2589, 2001.

[107] C. F. Wertz and M. M. Santore, "Adsorption and reorientation kinetics of lysozyme on hydrophobic surfaces," *Langmuir*, vol. 18, pp. 1190–1199, 2002.

[108] G. Szollosi, I. Derenyi, and J. Voros, "Reversible mesoscopic model of protein adsorption: From equilibrium to dynamics," *Physica A*, vol. 343, pp. 359–375, 2004.

[109] A. P. Minton, "Effects of excluded surface area and adsorbate clustering on surface adsorption of proteins. II. Kinetic models," *Biophysical Journal*, vol. 80(4), pp. 1641–1648, 2001.

[110] J. McGuire, M. C. Wahlgren, and T. Arnebrant, "Structural stability effects on the adsorption and dodecyltrimethylammonium bromide-mediated elutability of bacteriophage T4 lysozyme at silica surfaces," *Journal of Colloid and Interface Science*, vol. 170, no. 1, pp. 182 – 192, 1995.

[111] K. Kandori, K. Murata, and T. Ishikawa, "Microcalorimetric study of protein adsorption onto calcium hydroxyapatites," *Langmuir*, vol. 23, no. 4, pp. 2064–2070, 2007.

[112] D. Sarkar and D. Chattoraj, "Activation parameters for kinetics of protein adsorption at silica-water interface," *Journal of Colloid and Interface Science*, vol. 157, no. 1, pp. 219 – 226, 1993.

[113] R. J. Green, T. J. Su, J. R. Lu, and J. Penfold, "The interaction between SDS and lysozyme at the hydrophilic solid-water interface," *Journal of Physical Chemistry B*, vol. 105, p. 1594, 2001.

[114] S. J. McClellan and E. I. Franses, "Mechanisms of competitive adsorption of albumin and sodium myristate at the silicon oxide/aqueous interface," *Langmuir*, vol. 21, pp. 10148–10153, 2005.

[115] V. Ball, P. Schaaf, and J.-C. Voegel, *Surfactant Science Series Volume 110: Biopolymers at Interfaces (2nd ed.)*, ch. 11. Mechanisms of Interfacial Excahnge Phenomena for Proteins Adsorbed at Solid-Liquid Interfaces, pp. 295–320. Marcel Dekker, Inc., 2003.

[116] H. Noh and E. A. Vogler, "Volumetric interpretation of protein adsorption: Competition from mixtures and the Vroman effect," *Biomaterials*, vol. 28, pp. 405–422, 2007.

[117] B. Lassen and M. Malmsten, "Competitive protein adsorption at plasma polymer surfaces," *Journal of Colloid and Interface Science*, vol. 186, no. 1, pp. 9 – 16, 1997.

[118] N. Podhipleux, J. McGuire, M. Bothwell, and T. Horbett, "Sequential adsorption of bacteriophage T4 lysozyme stability variants at solidwater interfaces," *Colloids and Surfaces B: Biointerfaces*, vol. 27, no. 4, pp. 277 – 285, 2003.

[119] S. M. Slack and T. A. Horbett, *Proteins at Interfaces II. Fundamentals and Applications*, ch. 8. The Vroman Effect: A Critical Review, pp. 112–128. American Chemical Society, Washington DC, 1995.

[120] L. Vroman, "Effect of adsorbed proteins on the wettability of hydrophilic and hydrophobic solids," *Nature*, vol. 196, pp. 476–477, 1962.

[121] L. Vroman, "Finding seconds count after contact with blood (and that is all i did)," *Colloids and Surfaces B: Biointerfaces*, vol. 62, no. 1, pp. 1 – 4, 2008.

[122] L. Vroman and A. L. Adams, "Adsorption of proteins out of plasma and solutions in narrow spaces," *Journal of Colloid and Interface Science*, vol. 111, no. 2, pp. 391 – 402, 1986.

[123] T. Arai and W. Norde, "The behavior of some model proteins at solid-liquid interfaces. 2. Sequential and competitive adsorption," *Colloids and Surfaces*, vol. 51, pp. 17–28, 1990.

[124] S. Linse, C. Cabaleiro-Lago, W.-F. Xue, I. Lynch, S. Lindman, E. Thulin, S. E. Radford, and K. A. Dawson, "Nucleation of protein fibrillation by nanoparticles," *Proceedings of the National Academy of Sciences*, vol. 104, no. 21, pp. 8691–8696, 2007.

Chapter 2

Methods and Materials

2.1 Neutron Reflectivity

2.1.1 Introduction

Reflection of neutrons from a surface was first observed by Fermi and Zinn in 1944 [1]. Until the early 1980s, however, the technique was primarily used to determine the neutron refractive indices of materials from the total critical angle of reflection. Since then the technique has developed from characterising simple interfaces to routine measurements of structure and composition of adsorbed layers such as surfactants [2, 3], polymers [4, 5], proteins [6, 7, 8] and lipid bilayers [9].

The underlying principle for neutron reflection is based on Newton's observations that the colour of a thin film illuminated by white light could be used to determine its thickness. Neutrons have an intrinsic advantage over light or laser sources in that the wavelength of neutrons is approximately two orders of magnitude smaller than visible light and is thus more sensitive to structural changes on a molecular level. A more appropriate comparison is with X-rays because of their comparable wavelengths but still differences occur which gives neutrons some advantages over X-rays. Isotopic substitution offers greater flexibility because neutrons interact with atomic nuclei (rather than electron density), attenuation of neutrons when penetrating a material is less than for X-rays meaning that they are more suited to the investigation of buried (solid/liquid, liquid/liquid) interfaces. They also do not damage delicate systems, such as many of those which are of biological importance.

Neutron reflectometry data can be analyzed by two main methods, the optical matrix method [10] (analogous with classical optics) and the kinematic scattering

approximation [11]. The kinematic approximation applies in the "weak scattering" limit, whereas the optical approach is the full dynamical treatment. In either case the spatial resolution is of the order of 1-3 Å.

The following sections will outline the theoretical basis for treating neutron reflectometry data with an emphasis on reflection from a solid/liquid interface.

2.1.2 Theory of neutron reflection

When a neutron is incident (i) on an interface between two media of different refractive indices (n_1 and n_2) there are four possible fates for this neutron: specular (sr) and off-specular (osr) reflection, non-coherent scattering (ncs) and transmission (t) i.e. refraction. These possibilities are shown in Figure (2.1) below.

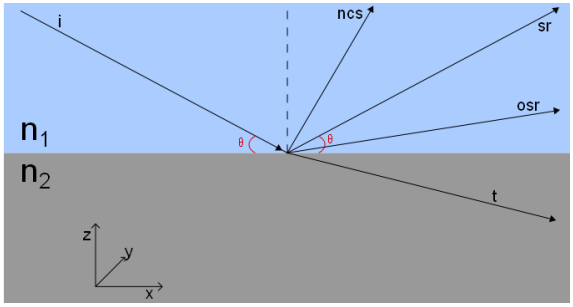


Figure 2.1: Possible fates of a neutron impinging on a planar surface.

The Schrödinger equation for an elastically scattered neutron is shown in equation (2.1). It is safe to assume that all scattering is elastic given that inelastic scattering is much weaker and therefore only makes up a small proportion of the total signal.

$$\frac{\hbar^2}{2m}\nabla^2\Psi(r) + V(r)\Psi(r) = E\Psi(r) \tag{2.1}$$

$\Psi(r)$ is the neutron wavefunction, E its energy, m its mass and $\hbar$ is Planck's constant divided by 2π. *V(r)* is the Fermi pseudo-potential which describes the interaction of a neutron at R with a single nucleus at r_i. Summing over all the individual interactions the total potential experienced by the neutron is given by equation (2.2) below.

$$V(r) = \frac{h^2}{2\pi m}\left\langle \sum_j b_j \delta(\vec{R} - \vec{r}_j) \right\rangle \tag{2.2}$$

The δ-function indicates that the potential is only non-zero when $\underline{R} = \underline{r}_j$. This is a result of the difference in size of the nuclei (10^{-15} m) compared with the wavelengths of thermal neutrons (10^{-10} m) and so the nuclei scatter like point objects. The constant b_j is the coherent scattering length of species j and is characteristic to each type of nucleus. The complexity of nuclei with respect to their make up of fundamental particles means that the scattering lengths can not be calculated and also they do not vary consistently with atomic weight, as for X-rays. Indeed, one of the great advantages of neutrons is that hydrogen and deuterium differ in their scattering lengths; $b_H = -3.74 \times 10^{-5}$Å and $b_D = 6.67 \times 10^{-5}$Å. This difference is exploited by using isotopic substitution which will be discussed in more detail later.

For any medium it is possible to define an average coherent scattering length density, ρ, using b_j and the number density of atomic species, n_j, present.

$$\rho = \sum_j b_j n_j \tag{2.3}$$

and from this the mean potential experienced by the neutron is calculated.

$$V(r) = \frac{h^2 \rho}{2\pi m} \tag{2.4}$$

Considering a planar neutron wave incident on a plane boundary of two media, as shown in figure (2.1), equation (2.4) shows that at an interface there is a change in the potential if their is a difference in scattering length densities of the media. Assuming that the two media are homogeneous with respect to nuclear density averaged over the xy-plane the potential change can only be a function of z and the only change in the neutron upon reflection occurs in the z-direction. Thus, the overall wavefunction can be expressed as

$$\Psi(r) = e^{ik_r} \rightarrow \Psi(x,z) = \Psi(x)\Psi(z) = e^{ik_x}\Psi(z) \tag{2.5}$$

where k_x is the wave vector that describes the propagation of the wave parallel to the interface and does not change in an elastic scattering event. Substituting the result of equation (2.5) into equation (2.1) gives:

$$\frac{\partial^2 \Psi}{\partial z^2} + {q_z}^2 \Psi(z) = 0 \tag{2.6}$$

where q_z is known as the momentum transfer vector given by:

$$q_z{}^2 = \frac{8\pi^2 m}{h^2}[E - V(z)] - k_x{}^2 \tag{2.7}$$

In the final solution of the Schrödinger equation consideration needs to be made to account for both the reflected and transmitted parts of the wave. Thus, the z-component of the wavefunction is expressed as a sum of plane waves; the incident, reflected and transmitted waves.

$$\Psi(z) = \left\{ \begin{array}{c} e^{iq_{1z}} + r_{12}e^{-iq_{1z}} \\ t_{12}e^{iq_{2z}} \end{array} \right\} \tag{2.8}$$

The subscripts 1 and 2 in equation (2.8) refer to which of the two media the neutron wave is in and r and t are the reflection and transmission coefficients respectively. These can be calculated by considering the boundary conditions i.e. both $\Psi(z)$ and $\frac{d\Psi(z)}{dz}$ must be continuous at the interface. Thus at $z = 0$ the solution to equation (2.8) is

$$1 + r_{12} = t_{12} \tag{2.9}$$

and for the derivative:

$$q_1 - q_1 r = q_2 t \tag{2.10}$$

Solving equations (2.9) and (2.10) simultaneously for r and t gives:

$$r_{12} = \frac{q_1 - q_2}{q_1 + q_2} \quad and \quad t_{12} = \frac{2q_1}{q_1 + q_2} \tag{2.11}$$

These are known as the Fresnel coefficients for a wave that is partially reflected and transmitted when incident on an interface between two uniform media. The reflectivity, R, has been shown to be

$$R = |r|^2 \leq 1 \tag{2.12}$$

From a practical view point the above expressions for the Fresnel coefficients are of limited use unless they can be related to some physical properties of the media in question. This can be done by considering the geometry of the different wave vectors before and after interaction of the wave with the surface. These are shown in figure (2.2).

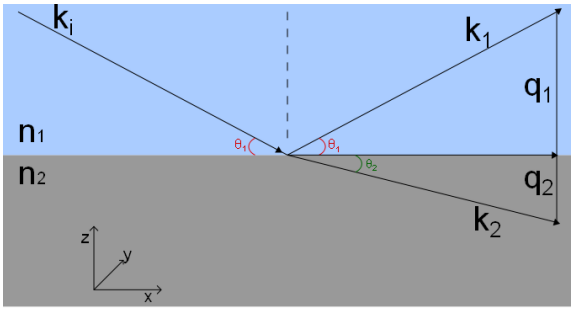


Figure 2.2: Geometry of the wave vectors involved in a reflection event.

The boundary conditions stipulate that for the resultant wave the in-plane components must be equal

$$k_1 \cos\theta_1 = k_2 \cos\theta_2 \tag{2.13}$$

and by analogy with light optics, the ratio of the neutron refractive indices between the two media is equal to the ratio of the wave vectors:

$$\frac{n_2}{n_1} = n_{12} = \frac{k_1}{k_2} \tag{2.14}$$

Combining equations (2.13) and (2.14) leads to Snell's law:

$$n_{12} = \frac{\cos\theta_1}{\cos\theta_2} \tag{2.15}$$

It can also be seen from figure (2.2) that

$$q_1 = k_1 \sin\theta_1 \quad and \quad q_2 = k_2 \sin\theta_2 \tag{2.16}$$

and by substituting the geometric relation $k_i^2 = k_x^2 + q_i^2$ into equation (2.7) it can be shown that

$$k_i^2 = \frac{8\pi^2 m}{h^2}(E - V_1) \tag{2.17}$$

Thus, equation (2.14) becomes

$$n_{12} = \frac{E - V_1}{E - V_2} \tag{2.18}$$

The de Broglie relation defines the energy as $E = h^2/2m\lambda^2$ and equation (2.4) gives an expression for the potential in terms of the scattering length density. By

combining these two expressions with equation (2.18) gives:

$$n_{12} = \frac{1-(\rho_2\lambda^2/\pi)}{1-(\rho_1\lambda^2/\pi)} = 1 - \frac{\lambda^2}{2\pi}(\rho_2 - \rho_1) \tag{2.19}$$

It is now possible to define a critical angle, θ_c, by noting that total reflection occurs when $\theta_2 = 0$ and then Snell's law gives

$$\cos\theta_c = 1 - \frac{\lambda^2}{2\pi}(\rho_2 - \rho_1) \tag{2.20}$$

In practice, the parameter that is of experimental interest is the total momentum transfer in the z-direction which equals $2k\sin\theta$. This also has a critical value, Q_c, below which total reflection occurs.

$$Q_c = \frac{4\pi\sin\theta_c}{\lambda} \tag{2.21}$$

The critical edge occurs at $Q_c = 0.0147$Å for a D_2O-silica interface which is of relevance in this thesis.

It is now necessary to extend the above approach to consider the case of a homogeneous monolayer adsorbed at an interface where there are now two changes in potential. At each interface the wave will be partially reflected and transmitted with the resultant reflected beam that is observed will be the sum of all the waves that propagate back into the initial media from all possible paths. This is shown in figure (2.3)

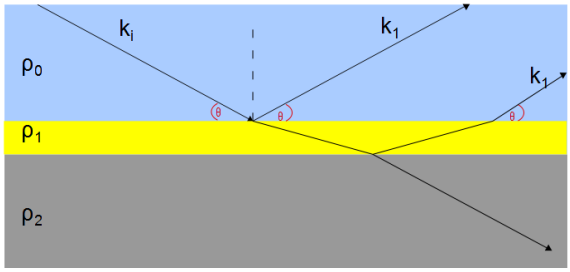


Figure 2.3: Some possible fates of a neutron beam incident on an adsorbed monolayer.

The total reflected amplitude, R, can be written in terms of the Fresnel coefficients, r_{ij} and t_{ij} [12]:

$$\mathbf{R} = r_{12} + t_{12}r_{23}t_{21}e^{2i\beta} + t_{12}r_{23}r_{21}r_{23}r_{21}e^{4i\beta} + \ldots \tag{2.22}$$

where β is the phase difference of a wave that has travelled through of layer with thickness τ:

$$\beta_i = \frac{2\pi}{\lambda} n_i \tau_i \sin\theta_i \tag{2.23}$$

Applying conservation of energy and noting that $r_{12} = -r_{21}$ and $t_{12}t_{21} = 1 - (r_{12})^2$, the series reduces to

$$\mathbf{R} = \frac{r_{12} + r_{23}e^{2i\beta}}{1 + r_{12}r_{23}e^{2i\beta}} \tag{2.24}$$

from which the reflectivity can be calculated exactly and is given by the squared modulus of the amplitude:

$$R = |\mathbf{R}|^2 = \frac{r_{12}^2 + r_{23}^2 + 2r_{12}r_{23}\cos 2\beta}{1 + (r_{12}r_{23})^2 + 2r_{12}r_{23}\cos 2\beta} \tag{2.25}$$

The maxima and minima in R will occur at values of $\cos 2\beta = \pm 1$ and the thickness of the layer can be estimated directly from the period of these so-called Kiessig fringes [13].

$$\tau = \frac{2\pi}{\Delta Q} \tag{2.26}$$

For a more complex system of many layers the optical matrix method is used. This method was initially developed by Born and Wolf [12] who took the approach of constructing a matrix for each layer which are assumed to be smooth and homogeneous. Abeles extended this theory by constructing a characteristic reflectivity amplitude matrix, $[M_{ij}]$, to describe each interface between two layers, i and j by considering the necessity for continuity of the wavefunction at each interface[14]. The matrix is given by

$$M_{ij} = \begin{pmatrix} e^{i\beta_i} & \tau_{ij}e^{i\beta_i} \\ \tau_{ij}e^{-i\beta_i} & e^{-i\beta_i} \end{pmatrix} \tag{2.27}$$

where r_{ij} is as defined in equation (2.11) and β in equation (2.23). For a series of n layers a total matrix describing the whole system, $[M_T]$, is produced by multiplication of the individual matrices describing each interface.

$$[M_T] = [M_{01}] \times [M_{12}] \times \cdots \times [M_{(n-1)n}] \times [M_{n(n+1)}] \tag{2.28}$$

This assumes that the subphase (layer $n+1$) is infinite such that there is no reflection arising from within it. The total reflectivity, R_f, is then given by

$$R_f = \frac{m_{21}m_{21}^*}{m_{11}m_{11}^*} \tag{2.29}$$

where m_{ij} is the element of the matrix $[M_T]$ and m_{ij}^* is its complex conjugate.

One of the assumptions of this analysis method is that all the layers are smooth and hence the interfaces are sharp. In practice, this is not a realistic assumption and so some effort is required to account for the interfacial roughness. The two types of interfacial roughness, namely lateral inhomogeneities and a diffuse interface, both have the same effect on the reflectivity profile when specular reflection is considered in that there is an increase in off-specular scattering and thus a higher background and a reduced intensity of the specular signal. Both can be modelled in the optical matrix by applying a Debye-Waller type smearing of the interface. The Fresnel reflectivity coefficient, r_{ij}, is replaced with r_{ij}^+ which is defined as

$$r_{ij}^+ = r_{ij}e^{-q_i q_j \sigma_{ij}^2} \tag{2.30}$$

The scattering length density profile is modelled as a Gaussian function where σ_{ij} is the standard deviation of this function i.e. the Gaussian width is descriptive of the length scale of the roughness .

When performing neutron reflectivity experiments the measurable parameter is the square of the amplitude and this causes the information regarding the phase of the wave to be lost. This loss of phase information has the effect that any solution using the optical matrix method is not unique i.e. a number of different scattering length density profiles give the same reflectivity profile. This problem is compounded by the limited range of accesible wave vector transfer in the experiments. As mentioned previously hydrogen and deuterium have different scattering lengths with respect to both sign and magnitude. This difference is taken advantage of in the technique known as contrast variation whereby taking measurements with varying ratios of H_2O to D_2O in the solvent provides more information about the system and thus greatly reduces the chance of an overall picture of the system being non-unique.

2.1.3 Calculating the scattering length densities of proteins

As can be seen from equation (2.3), in order to calculate the scattering length density of proteins it is necessary to know the number density of all the atoms present i.e the chemical composition and volume. The protein volume can be calculated from the known volumes of the amino acids [15] and the amino acid sequence of the protein of interest. The details of the protonated forms of the amino acids are given in table (2.1).

Residue	**Exchangeable H**	**b**/10^{-4} **Å**$^{-1}$	**mass/** $g\,mol^{-1}$	**volume/ Å**^{3}
Alanine	1	1.645	71	89
Arginine	6	3.466	156	173
Asparagine	3	3.456	115	114
Aspartate	1	3.845	114	111
Cysteine	2	2.88	103	108
SS-cysteine	1	3.254	102	108
Glutamic acid	1	3.373	128	148
Glycine	1	1.728	57	60
Histidine	1.5	4.959	137	153
Isoleucine	1	1.396	113	167
Leucine	1	1.396	113	167
Lysine	4	1.586	128	169
Methionine	1	1.764	131	163
Phenylalanine	1	4.139	147	190
Proline	0	2.227	97	113
Serine	2	2.225	87	89
Threonine	2	2.142	101	116
Tryptophan	2	6.035	186	228
Tyrosine	2	4.719	163	194
Valine	1	1.479	99	140

Table 2.1: Properties of amino acids.

When considering the final scattering length densities of proteins with a mixture of H and D it is necessary to consider two factors; the degree of deuteration of the polypeptide backbone and the exchange of H/D with the solvent. Given the large difference of scattering lengths of H and D and the large hydrogenous content of proteins it can be seen that perdeuteration of the proteins is highly advantageous as the two forms (herein referred to as h- and d-) will have markedly different scattering length densities as shown in Table (2.2).

Protein	**SLD in H_2O/10^{-6} Å^{-2}**	**SLD in D_2O/10^{-6} Å^{-2}**
h-HSA	1.76	3.03
d-HSA	6.11	7.38
h-MBP	1.75	2.96
d-MBP	6.2	7.41
LYS	2.03	3.60
CA II	1.81	3.08

Table 2.2: The scattering length densities of proteins used in this thesis in H_2O and D_2O

Within proteins there exist two types of hydrogen; labile and non-labile. It is assumed that when the protonated form is in H_2O (and perdeuterated forms in D_2O) all the hydrogens are H (or D). However, with all other permeations the number of labile hydrogens and the extent of exchange with the solvent must be taken into account in order to accurately calculate the scattering length density of the protein.

Labile hydrogens can be found on both the amine groups of polypeptide backbone and on the amino acid side chains. In the case of globular proteins the position of the hydrogens within the secondary structural framework is also of importance. Exposure to the solvent can be hindered by inclusion in α-helices and β-sheets or by hydrophobic encapsulation in the protein core [16]. The ease of exchange has been used as a measure of the degree of masking for portions of the protein and thus a useful means of probing the folding and unfolding probing pathways [16, 17]. More recently, Efimova et al. [18, 19] have presented a method for the theoretical calculation of the amount of labile H atoms from the amino acid sequence of the protein and the knowledge of its secondary structure. These studies applied positive electrospray ionization mass spectroscopy (ES^+I^-) to follow the H/D exchange and were focussed on the accurate calculation of the neutron scattering length densities of β-casein and lysozyme.

2.1.4 Neutron sources and instrumentation

Neutrons are produced in two different ways; in a nuclear reactor or by spallation. In reactor sources nuclear fission reactions are optimised for the production of continuous beam of thermal neutrons whereas in spallation source the neutrons are produced by collision of a high-energy charged particle into a heavy metal target e.g. tantalum. The work in this thesis was carried out on three different instruments;

D17 at the Institut Laue-Langevin (ILL) in Grenoble, France (a reactor source) and the reflectometers SURF and INTER at ISIS, Rutherford Appleton Laboratory in Didcot, UK (a spallation source). In both cases the neutrons produced are of shorter wavelength than is optimal for soft condensed matter studies. This is rectified by passing the neutrons through a moderator of cold (20-25 K) hydrogen or deuterium rich environment where multiple inelastic scattering events thermalise the neutrons to lower temperatures and longer wavelengths (approximately 0.5-15 Å for spallation sources and 2.2 to 19 Å for reactors depending on the instrument).

The measurable parameter in neutron reflectivity experiments is the variation of reflectivity, $R = I/I_0$, where I and I_0 are the intensities of the reflected and incident beams respectively, with Q_z, the wave vector transfer perpendicular to the interface which is given by

$$Q_z = \frac{4\pi \sin\theta}{\lambda} \tag{2.31}$$

This expression shows that Q-variation can be achieved by either varying the angle, θ, or the wavelength of the neutrons, λ. All three reflectometers used in this work are of the energy-dispersive (or time-of-flight, TOF) type in which the angle is kept constant and a range of wavelengths is incident on the sample. The time that the neutrons take to travel from source to sample and then sample to detector is then measured with shorter wavelengths arriving first which correspond to higher Q values. The wavelength range is determined by using a set of mechanical choppers and this determines the available Q-range. In order to record all Q values of interest (approx. 0.01 to 0.25 $Å^{-1}$) it is necessary to measure at two or three set angles. It should also be noted that there is a variation in neutron flux over the range of wavelengths which follows a Maxwell-Boltzman distribution of velocities.

Compared with fixed wavelength (monochromatic) reflectometers, measurements in the TOF-mode have the advantage of being able to be used for kinetic studies as each reflectivity profile can be considered to be a snapshot of the time evolution. This is assuming that the timescale of the process is of the same order as the neutron counting time. The counting time for monochromatic mode measurements is greater than for TOF modes due to the number of accurate positional adjustments required. Furthermore, any time dependent changes are averaged over the Q-range whereas the monochromatic mode would show Q-dependence due to measurement of increasing Q with increasing time.

The time taken for measurements in this thesis have depended on a number of factors. First, over the course of this work some improvements to the beam collimation on D17 have resulted in the time to take a reflectivity profile being reduced from approximately 2 hours down to 1 hour. Second, the building of a new target station at ISIS and a new reflectometer, INTER, has greatly improved the neutron flux as compared to that on SURF and thus reduced the run time at this facility.

The resolution in TOF reflectivity experiments is determined by both the angular spread and the ratio of pulse width, δt and TOF, t for each pulse :

$$\left(\frac{\delta q}{q}\right)^2 = \left(\frac{\delta\theta}{\theta}\right)^2 + \left(\frac{\delta t}{t}\right)^2 \tag{2.32}$$

This means that for a given pulse width the relative resolution is constant and defined by the angular divergence of the incoming beam but the actual resolution varies over the Q-range. The degree of change will depend on the experimental set up; the slit settings are usually changed to keep $\frac{\delta\theta}{\theta}$ constant to reduce the variation of the resolution.

2.1.5 Solid/Liquid reflectivity measurements

As mentioned in section (2.1.4) the measurements in this thesis were carried out on three different instruments. A photo of the cells used for all experiments at the solid/liquid interface is shown below in figure (2.4). This consists of an aluminium casing which holds a $5 \times 5 \times 1$ cm polished silicon block and a teflon trough with a sample volume of 3 ml. To allow for temperature regulation the Al casings of the separate cells are all connected via tubing through which water from a circulating water bath can flow to regulate the temperature.

The silicon blocks were cleaved on the (111) face and were supplied and polished by Crystan Ltd. To prepare the hydrophilic silica layer required the blocks were cleaned in a so-called Piranha solution which consists of a 1:5:4 ratio of H_2O_2, H_2O and H_2SO_4 for a minimum of 15 min at a temperature between 80 and 100°C. The blocks were then stored in ultra pure water before being put in the aluminium cells which were then filled with D_2O. Great care at this stage was taken to remove all air bubbles as this reduces the reflected intensity greatly and results in a poorly defined critical edge on the reflectivity profile.

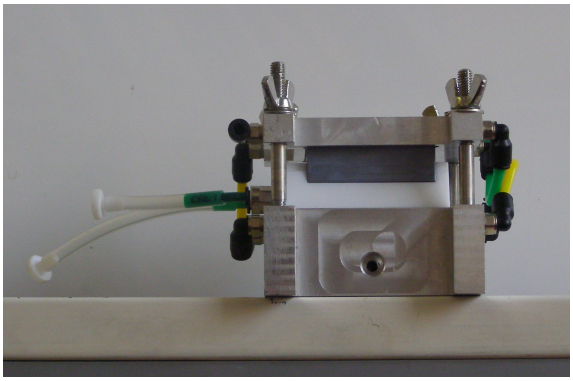


Figure 2.4: A photo of the cell used in the solid/liquid experiments.

The cells are mounted either on a custom made base plate when using SURF or INTER or attached to a mount when using D17. Both of these have been designed to hold four sample cells to allow for measurements of multiple samples. The set up for INTER is shown below in figure (2.5). Once the cells are *in situ* in the block house the first stage is to align the oxide surface such that the maxima of the specular ridge is being recorded. An approximate position is found using a laser that follows the same path as the neutrons. The alignment is then refined using the neutron beam by doing iterative scans over ranges of height and the rocking angle parallel to the direction of the neutron beam. Two runs at zero angle (one through the block and one through air) are required to account for any neutron losses when analysing the reflectivity data.

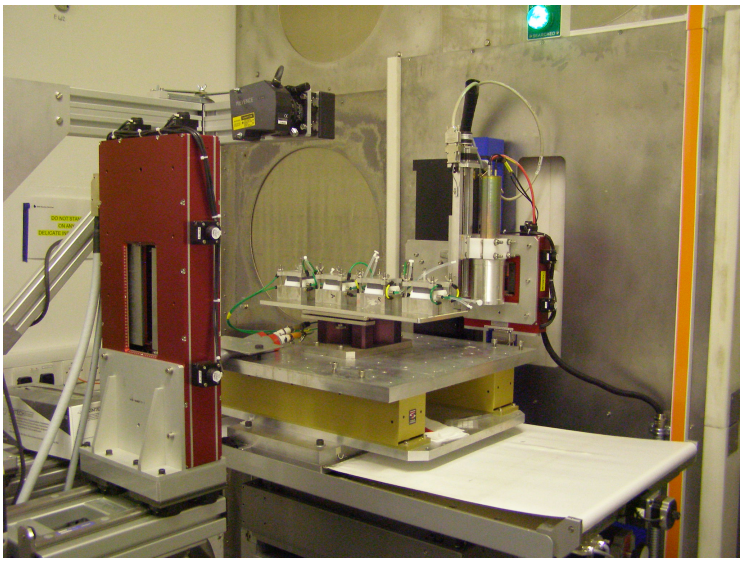


Figure 2.5: A photo of 4 cells in position on the instrument INTER.

Before any analysis is carried out it is also necessary to combine two or more reflectivity profiles taken at different incident angles and scale the magnitude of reflectivity to an abseloute scale. A run with D_2O is used to find the scale factor because below $Q = 0.014$ Å all neutrons are totally reflected and therefore, below this value, the critical edge, reflectivity is by definition unity. This scale factor, which is largely a function of surface quality and illuminated area, can then be used for reflectivity profiles of the same block but different solvents where no critical edge is observed. Reflectivity profiles taken at different incident angles can then be combined by scaling to the lower angle, provided there is sufficient overlap in the Q-ranges. This process increases the measurable Q-range and provides more information about the adsorbed layer.

To determine the roughness and thickness of the oxide layer two reflectivity profiles are taken, one with D_2O as the liquid medium and the other using contrast matched silicon (CMSi), which has the same scattering length density as silicon (2.07) in order to highlight the oxide layer which has a scattering length density of 3.4. If the protein adsorption experiments where to be carried out in a solvent contrast other than D_2O or CMSi then this solvent blank was also taken. This was used to determine an appropriate run time for this solvent, provide more information about the oxide layer and it could be used as a reference during the running of the experiments so changes in the reflectivity profile over time could be assessed qualitatively. The oxide layer was typically found to be 7-20 Å thick with a roughness of less than 5 Å deemed to be acceptable. The reflectivity profiles and fits for a typical characterisation of an oxide layer is shown below in figure (2.6). During the analysis of the protein adsorption data it is assumed that the adsorption of the protein does not effect the oxide layer, in particular with respect to the amount of incorporated solvent. The background scattering is also accounted for during the data analysis stage which is described in the next section.

2.1.6 Data analysis

The most common way to analyse reflectivity data is to compare measured profiles against ones generated from an optical matrix simulation and there are several programs that exist to do this. In this work the analysis was done using the Igor-Pro based Motofit[20] fitting program. Motofit calculates reflectivity profiles using the Abeles matrix method see equations (2.27, 2.28 and 2.29), when benchmarked

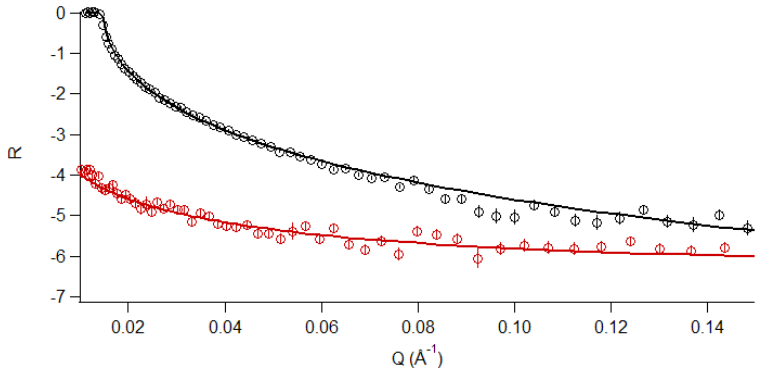


Figure 2.6: Reflectivity profiles and fits for the characterisation of the oxide layer in D_2O (black) and CMSi (red) at the silica-solution interface. The oxide layer shown has a thickness of 8 Å and roughness of 3 Å.

against other fitting programs has been shown to give identical results to the Parratt recursions relationship for specular reflection from a stratified medium[21].

Each reflectivity curve is described using a minimum of five experimental variables: the scale factor, background scattering level, roughness, solvent SLD and sub-phase (e.g. silicon) SLD. The addition of an adsorbed layer requires a further four variables: layer thickness, layer SLD, solvent percentage in layer and roughness. The overall SLD of the layer is a volume fraction weighted combination of the adsorbent and solvent SLDs. The software interface allows the user to enter a value for all of these parameters and can restrict the program to allowed ranges. This removes the problem of a mathematical solution being found that is physically unrealistic when there is prior knowledge of the system such as accurate SLDs of the adsorbing species.

The χ^2 value (described by equation (2.33 below) is a statistical measure of the agreement between the experimental data and the theoretical model. Another useful feature of the Motofit software is the ability to plot χ^2 values as a function of any given parameter or 2D plots showing combining the effect of two variables. Combining this with the manually entered restrictions allows the user to find (and produce optimised fits for) a number of plausible models from each reflectivity profile corresponding to localised minima in the χ^2 value. This is of use when comparing models taken at different times or water contrasts.

$$\chi^2 = \sum_{n=1}^{L} \frac{1}{L-p} \left(\frac{y_{n,obs} - y_{n,calc}}{y_{n,err}} \right)^2 \tag{2.33}$$

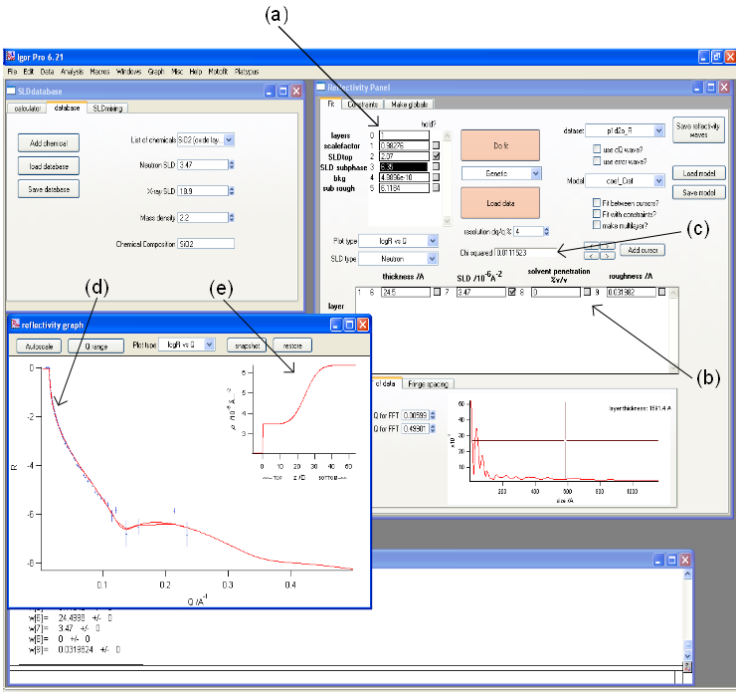


Figure 2.7: A screen shot of the Motofit software interface showing (a) experimental parameters, (b) adsorbed layer parameters, (c) χ^2 value, (d) reflectivity profile (red line= fit, blue data points= experimental data) and (e) the SLD profile.

where L is the number of measured data points, p the number of variables allowed to change during the fit procedure, y_{obs} (with a statistical error of y_{err}) and a corresponding theoretical value, y_{calc}.

This fitting process yields a layer model in terms of thickness, τ, and volume fraction of the solvent (and hence, volume fraction of the protein, ϕ). From this it is possible to calculate an adsorbed amount per unit area. The total volume occupied per unit area is given by

$$V = \sum_i \phi_i \tau \tag{2.34}$$

The number of molecules per unit area, Γ_m is then given by

$$\Gamma_m = \frac{V}{V_m} \tag{2.35}$$

where V_m is the volume of one molecule as calculated from the amino acid volumes in the same manner as for calculating the scattering length density of proteins described previously. Thus, overall the adsorbed amount per unit area, Γ, is given

by

$$\Gamma = \sum_i \phi_i \tau \times \frac{1}{V_m} \times m \tag{2.36}$$

where m is the mass of one molecule (M_r/N_A).

2.2 Dual Polarisation Interferometry

2.2.1 Operating principles

The fundamental basis for dual polarisation interferometry (DPI) is the same as that demonstrated in Young's double slit experiment [22]; coherent waves passing through two closely-spaced slits are observed to interfere with each other and produce a characteristic fringe pattern consisting of alternating regions of high and low intensity which correspond to constructive and destructive interference respectively. In the case of DPI, the slits are replicated by a four-layer dielectric stack of silicon oxynitride on a silicon wafer surface. The refractive index of the second and fourth layers is higher than that of the first and third thus, on introducing a collimated (or lightly focused) laser beam to the end face of the device a standing wave is set up and propagates through these waveguides. At the output, the waves from both waveguides are allowed to diffract into the far-field where they interfere with each other to form the characteristic interference pattern.

The majority of the propagating wave is confined to the core of the waveguides. However, a proportion of the wave decays exponentially into the cladding. This is known as the evanescent field. In the upper waveguide, two channels are etched into the cladding such that the one of the waveguide boundaries is now exposed and in contact with the analyte solution. Any changes to the refractive index of the so called sensing region above the boundary, such as adsorption of a protein film, will interact with the evanescent field and alter the propagation velocity of the wave through the waveguide. This, in turn, will then alter the position of the interference pattern in the far-field.

The phase position of a fringe, $\Delta\phi$ is given by

$$\Delta\phi = k_0 L \Delta n_s \tag{2.37}$$

where k_0 is the propagation constant, L is the path length, which is fixed, and Δn_s

is the effective change in the refractive index of the sensing waveguide. The relative phase position of the fringe pattern is monitored by performing a Fourier transformation that relates intensity to position. The measured change relates solely to the sensing waveguide since the effective refractive index of the reference waveguide is unchanged. Thus, the experimental data can be related to changes in the effective refractive index of the sensing waveguide.

In surface plasmon resonance (SPR) only the transverse magnetic (TM) polarisation mode of light is utilised. With only one optical stimulus only one unknown parameter, the optical mass, can be determined and it is not possible to differentiate between a thick, diffuse layer and a thin, dense layer. DPI, as its name suggests, makes use of both TM and the transverse electric (TE) modes by using a fast liquid crystal switch acting as a switchable half-wave plate and involves no mechanical realignment. Thus, two responses can be recorded alternately at a typical rate of 50 Hz [23]. The electric field vectors within the waveguide and at its boundaries differ depending on the polarisation mode of the light and the resulting evanescent field magnitude and profile differ for the two polarisations. The TE mode is more sensitive to changes near the surface as its evanescent field is more closely confined to the boundary.

Maxwell's equations of electromagnetism for a system of uniform multiple dielectric layers are used to determine the abseloute effective refractive index for both TM and TE modes. This gives the relationship between changes in the effective refractive index, Δn_s, of the waveguide in each mode and changes of thickness of the observed layer, t_{ad}.

$$\Delta n_s = \left(\frac{\partial n_s}{\partial t_{ad}}\right) \Delta t_{ad} + \left(\frac{\partial n_s}{\partial n_c}\right) \Delta n_c \tag{2.38}$$

If only the TM mode is considered, changes to the adsorbed layer will result in a change to the effective refractive index and there is a range of thickness and refractive index values that satisfy the observed interference fringe movement. However, solutions to the Maxwell equations for the TE mode will also produce a range of refractive index and thickness values and, due to the different properties of the evanescent field, this range will not be the same as for the TM mode. When the two series of computed values are overlayed it can be seen that there is a single point of intersection i.e. there is only one layer condition that can give rise to the observed TE and TM responses and the thickness and refractive index of the adsorbed layer

can be resolved. Since the refractive index of protein solutions is a linear function of concentration over a wide range of concentrations, the surface coverage can be calculated using de Feijter's formula [24]:

$$\Gamma = \frac{n_{ad} - n_c}{dn_{ad} \backslash dn_c} t_{ad} \tag{2.39}$$

where n_{ad} is the refractive index of the adsorbed layer, n_c is the refractive inde of the running buffer, C is the concentration, Γ is the surface coverage and $dn_{ad} \backslash dn_c$ is the refractive index increment, taken to be 0.18 ml/g for proteins [25].

2.2.2 Method

The instrument used for these experiments was the AnaLight Bio 2000^{TM} attached to a Harvard 632695945 syringe injection system which are both connected to a PC and run via a software interface, AnaLight Daq. The instrument and software were developed by Farfield Sensors Ltd. and are situated at ISIS, Rutherford Appleton Labs. in Didcot, UK.

All samples were run on unmodified FB80 chips which have a hydrophilic silicon oxynitirde (SiO_xN_y) surface. They were supplied by the manufacturer, Farfield Sensors Ltd., and used without further modification. The running buffer was phosphate buffered saline which was degassed before use. A photo of the instrument and the chip mounting can be seen below in figure (2.8).

Before any measurements of phase changes are made it is necessary to manually choose the sharpest fringe image. Once an experiment has been started the run the calibration procedures and ensure that the surface is free of any contaminants. The surface of the chip was cleaned by flowing an 80 % ethanol solution over the surface for 10 minutes. This is repeated until the TM and TE signals for both channels return to the same level as before the injection and the chip is now considered clean. The chip thickness and bulk refractive index are calculated by references against known standards; a solution of 80:20 ethanol:H_2O and unbuffered H_2O respectively. The run off period of the 80 % ethanol solution can also be used for linearisation; an advanced calibration of the detector response. The accuracy of the phase position measurement is dependent of the quality of the fringes [26]. Defects in the image will result in small innacuracies in the phase response which will have a periodicity of 2π radians. The phase error is typically of the order of ± 50 milliradians and will have the greatest impact on thin or diffuse adsorbed layers [27]. A screenshot of

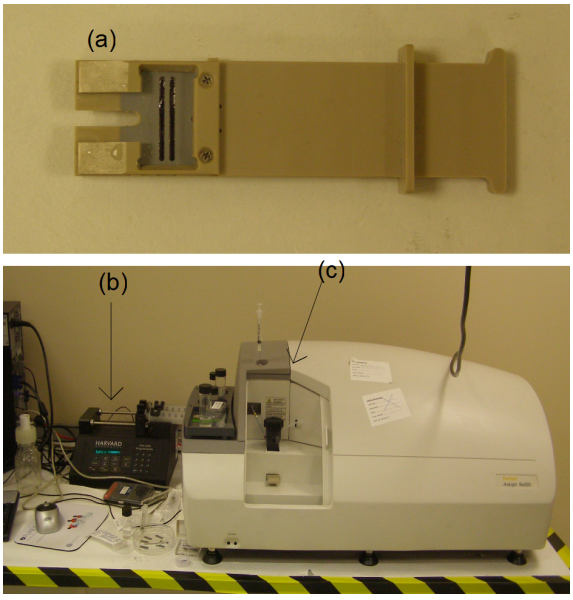


Figure 2.8: A photo of (a) the chip mounting, (b) the Harvard injection system and (c) the AnaLight Biosensor 2000.

the user interface software is shown in figure (2.9) with the cleaning and calibration procedure highlighted.

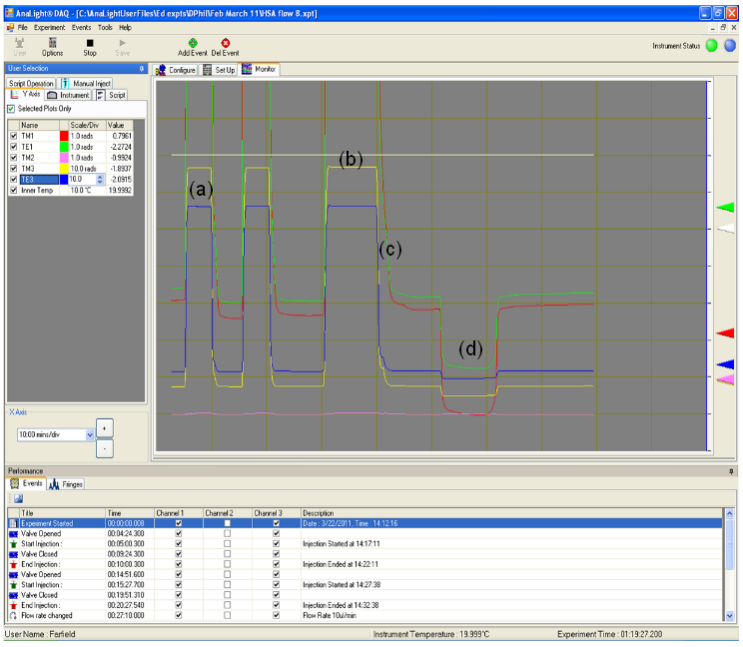


Figure 2.9: A screenshot of the AnaLight Daq software showing (a) Cleaning, (b) Chip calibration, (c) Linearisation region & (d) Bulk calibration

2.2.3 Data analysis

The analysis of the raw data is done using the software, AnaLight Explorer, and follows the method as described in section (2.2.1). The user is asked to manually choose the time points for the chip and bulk calibrations and linearisation. The refractive index increment of the adsorbent is taken to be 0.182 ml g^{-1}. It is possible to calculate the refractive index and layer thickness for all time points of the experiment but, given the long timescale of experiments of interest here and the slow changes observed it was found to be more convenient and less likely to induce an error in the software to select certain discrete data points. During periods of relatively fast changes e.g during the initial adsorption phase, these data points were chosen to be close together whereas during periods of slow changes one data point every hour was all that was deemed necessary. This process greatly reduced the time required to process the data when exported into a spreadsheet without any loss of information. The final output of an experiment and a screen shot of AnaLight Explorer is shown below in Figure (2.10)

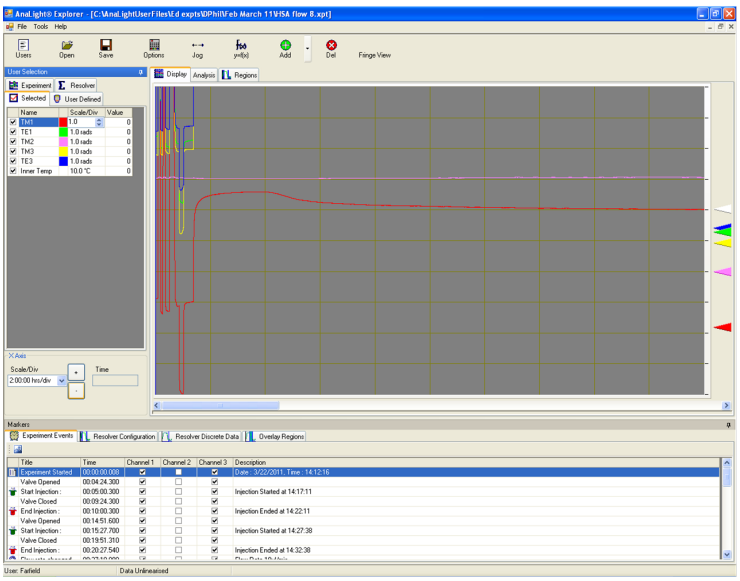


Figure 2.10: A screen shot of the AnaLight Explorer software used for data analysis.

2.3 Materials

HSA, LYS and PBS tablets were bought from Sigma and used without any further purification or modification with the exception of one batch of HSA which was then

purified by the research group of Sara Linse to remove any HSA dimers in the same manner as described in the supporting material of [28]. This did not have any measurable impact on the adsorption. Protonated Maltose binding protein (h-MBP) was bought from Rockland Immunochemicals Inc. and was supplied as a 5 mg ml^{-1} solution in PBS buffer. This was diluted as required.

Perdeuterated proteins are obtained by growing simple organisms, such as bacteria or yeasts, in fully deuterated media. Both the d-HSA and d-MBP were expressed and purified by the team in the deuteration lab at the Institut Laue-Langevin (Grenoble, France). d-HSA was expressed in the yeast strain *Pichia pastoris* using d_8-glycerol and d_4-methanol as the deuterated carbon source. d-MBP was expressed in *Escherichia coli* BL21(DE3) using d_8-glycerol. They were supplied in PBS buffer solution at a variety of concentrations and solvent (H_2O and D_2O) ratios depending on the batch. These were decided upon with the final desired solvent contrast in mind and varied depending on the experimental design for each batch. This imposed the limitation of a lack of control when wanting to make changes to the solvent contrast during the experiments to respond to the data as it was being recorded.

References

[1] H. L. Anderson, E. Fermi, A. Wattenberg, G. L. Weil, and W. H. Zinn, "Method for measuring neutron-absorption cross sections by the effect on the reactivity of a chain-reacting pile," *Phys. Rev.*, vol. 72, pp. 16–23, Jul 1947.

[2] R. R. Highfield, R. P. Humes, R. K. Thomas, P. G. Cummins, D. P. Gregory, J. Mingins, J. B. Hayter, and O. Schaerpf, "Critical reflection of neutrons from a soap film," *Journal of Colloid and Interface Science*, vol. 97, no. 2, pp. 367 – 373, 1984.

[3] C. S. Lee and G. Belfort, "Changing activity of ribonuclease A during adsorption: A molecular explanation," *Proceedings of the National Academy of Sciences*, vol. 86, no. 21, pp. 8392–8396, 1989.

[4] A. R. Rennie, R. J. Crawford, E. M. Lee, R. K. Thomas, T. L. Crowley, S. Roberts, M. S. Qureshi, and R. W. Richards, "Adsorption of poly(ethylene oxide) at the air-solution interface studied by neutron reflection," *Macromolecules*, vol. 22, no. 8, pp. 3466–3475, 1989.

[5] T. Cosgrove, T. G. Heath, J. S. Phipps, and R. M. Richardson, "Neutron reflectivity studies of polymers adsorbed on mica from solution," *Macromolecules*, vol. 24, no. 1, pp. 94–98, 1991.

[6] E. Dickinson, D. S. Horne, and R. M. Richardson, "Neutron reflectivity study of the competitive adsorption of ?-casein and watersoluble surfactant at the planar air-water interface," *Food Hydrocolloids*, vol. 7, no. 6, pp. 497 – 505, 1993.

[7] T. J. Su, J. R. Lu, R. K. Thomas, Z. F. Cui, and J. Penfold, "The effect of solution pH on the structure of lysozyme layers adsorbed at the silica-water interface studied by neutron reflection," *Langmuir*, vol. 14, pp. 438–445, 1998.

[8] G. Fragneto, R. K. Thomas, A. R. Rennie, and J. Penfold, "Neutron reflection study of bovine beta-casein adsorbed on OTS self-assembled monolayers.," *Science*, vol. 267(5198), pp. 657–60., 1995.

[9] G. Fragneto, F. Graner, T. Charitat, P. Dubos, and E. Bellet-Amalric, "Interaction of the third helix of antennapedia homeodomain with a deposited phospholipid bilayer: A neutron reflectivity structural study," *Langmuir*, vol. 16, no. 10, pp. 4581–4588, 2000.

[10] J. R. Lu, E. Lee, and R. Thomas, "The analysis and interpretation of neutron and X-ray specular reflection.," *Acta Crystallographica, Section A: Foundations of Crystallography*, vol. A52(1), pp. 11–41, 1996.

[11] T. Crowley, E. Lee, E. Simister, and R. Thomas, "The use of contrast variation in the specular reflection of neutrons from interfaces," *Physica B: Condensed Matter*, vol. 173, no. 1-2, pp. 143 – 156, 1991.

[12] M. Born and E. Wolf, *Principles of Optics*. Pergammon: Oxford, 1970.

[13] H. Kiessig, "Interferenz von rantgenstrahlen an dannen schichten," *Annalen der Physik*, vol. 402, no. 7, pp. 769–788, 1931.

[14] O. Heavens, *Optical Properties of Thin Films*. Butterworth, London, 1955.

[15] S. J. Perkins, "Chapter 6 X-ray and neutron solution scattering," in *Modern Physical Methods in Biochemistry* (A. Neuberger and L. van Deenen, eds.), vol. 11, Part 2 of *New Comprehensive Biochemistry*, pp. 143 – 265, Elsevier, 1985.

[16] A. Hvidt and S. O. Nielsen, "Hydrogen exchange in proteins," vol. 21 of *Advances in Protein Chemistry*, pp. 287 – 386, Academic Press, 1966.

[17] S. E. Radford, M. Buck, K. D. Topping, C. M. Dobson, and P. A. Evans, "Hydrogen exchange in native and denatured states of hen egg-white lysozyme," *Proteins: Structure, Function, and Bioinformatics*, vol. 14, no. 2, pp. 237–248, 1992.

[18] Y. M. Efimova, A. A. van Well, U. Hanefeld, B. Wierczinski, and W. Bouwman, "On the neutron scattering length density of proteins in H_2O/D_2O," *Physica B*, vol. 350, pp. e877–e880, 2004.

[19] Y. M. Efimova, A. A. van Well, U. Hanefeld, B. Wierczinski, and W. G. Bouwman, "On the scattering length density of proteins in H_2O/D_2O: Determination of H-D exchange using ES+I-MS," *Journal of Radioanalytical and Nuclear Chemistry*, vol. 264, pp. 271–275, 2005.

[20] A. Nelson, "Co-refinement of multiple-contrast neutron/X-ray reflectivity data using *motofit*," *Journal of Applied Crystallography*, vol. 39, pp. 273–276, Apr 2006.

[21] motofit.sourceforge.net/wiki/index.php/Benchmarking_fitting_programs.

[22] T. Young, "The bakerian lecture: Experiments and calculations relative to physical optics," *Philosophical Transactions of the Royal Society of London*, vol. 94, pp. pp. 1–16, 1804.

[23] G. H. Cross, A. Reeves, S. Brand, M. J. Swann, L. L. Peel, N. J. Freeman, and J. R. Lu, "The metrics of surface adsorbed small molecules on the Young's fringe dual-slab wave guide interferometer," *Journal of Physics D: Applied Physics*, vol. 37, pp. 74–80, 2004.

[24] J. A. de Feijter, J. Benjamins, and F. A. Veer, "Ellipsometry as a tool to study the adsorption of synthetic and biopolymers at the air-water interface.," *Biopolymers*, vol. 17, pp. 1759–1772, 1978.

[25] A. W. Sonesson, T. H. Callisen, H. Brismar, and U. M. Elofsson, "A comparison between dual polarisation interferometry (DPI) and surface plasmon resonance (SPR) for adsorption studies," *Colloids and Surface B: Biointerfaces*, vol. 54, pp. 236–240, 2007.

[26] Farfield Group Ltd., *Farfield Technical Notes 21v2- Short Description of Linearisation of AnaLight Detector Response.*

[27] Farfield Group Ltd., *Farfield Technical Notes 10v2- Linearisation of Detector Response on AnaLight Instruments.*

[28] S. Lindman, I. Lynch, E. Thulin, H. Nilsson, K. A. Dawson, and S. Linse, "Systematic investigation of the thermodynamics of HSA adsorption to N-iso-Propylacrylamide/ N-tert-Butylacrylamide compolymer nanoparticles. Effects of particle size and hydrophobicity," *Nano Letters*, vol. 7 (4), pp. 914–920, 2007.

Chapter 3

Results: Adsorption of single protein solutions

As discussed in chapter 1, before commencing an investigation into the sequential and competitive adsorption of proteins and the effect that the incubation time imparts it is necessary to have a detailed picture of the adsorption of single proteins both in terms of the layer structure and any changes to the gross morphology that occur over time. The subsequent focus in later chapters on sequential adsorption has been advantageous with respect to studying the single protein cases as it has allowed for the adsorption of the proteins under ostensibly the same experimental conditions to be characterised on numerous occasions; somewhat of a luxury where neutron reflectivity is the primary experimental technique. It will be shown that not all the data in each set agree as closely as might be expected. It will be argued that this is perhaps not overly surprising given the complex nature of protein adsorption and small changes may infer larger than expected impacts on the adsorption. However, general trends are observed which provide insights into the details of the adsorption process and post-adsorption changes that occur.

This chapter will outline the adsorption of four proteins, CA II, HSA, LYS and MBP. By comparing the adsorption of these proteins, some details of the adsorption process and relative importance of particular driving forces for adsorption will be discussed. The sections concerning CA II and LYS deal solely with adsorption of the protonated form studied using neutron reflectivity. In the sections following, a comparison is made between the protonated and deuterated forms of HSA and MBP. The ability of neutron reflectivity to distinguish between these two forms has

allowed for a detailed study of the adsorption dynamics of MBP by following the self exchange at the interface as a function of the incubation time. This is compared to the desorption process following the same incubation times.

During the fitting process, it was first attempted to fit the reflectivity profiles with the simplest model, a single uniform layer. In part, this was done for simplicity but it was also done to allow comparisons with later DPI results, where only a 1-layer model can be used. In the cases where this did not give a satisfactory fit to the data or did not allow for a consistent model of the adsorbed layer, a 2-layer model was used. The χ^2 values calculated by the fitting program offer a good indication of the improvement to the fit either for 1-layer vs 2-layer fits or comparing different sets of layer parameters for the same number of layers. When comparing the χ^2 values, it is necessary to take other factors into consideration such as the comparison to other similar data sets e.g. in a time sequence, whether the layer parameters describe a physically possible layer and also the weighting of the χ^2. For example, χ^2 values are normally lower (indicating a better fit) for D_2O runs compared to H_2O due to the high weighting and good fits achieved in the region below the critical Q value which is not present in H_2O runs. It is thus not possible to set absolute values which must be met to constitute an acceptable fit. It is also necessary to use some judgement concerning the look of the fit when compared to the data points. A combination of these factors has been used to achieve a consistent overall picture and the χ^2 values will be referred to in the text to illustrate some of the improvements made when comparing 1-layer and 2-layer models.

The thicknesses in the final layer parameters can then be compared to the dimensions of the proteins when in solution to provide some insight into the preferred orientation of the adsorbed protein.

3.1 Carbonic Anhydrase II

The adsorption of a 1 mg ml^{-1} solution of CA II was carried out in D_2O with PBS buffer at pH 7.4. The adsorbed layer was characterised immediately after injection of the solution and also after an incubation time, t_{inc}, of 6.5 and 11 hours. At t_{inc}=12.5 hours the bulk solution was exchanged for the buffer and another measurement was taken to ascertain the extent of readily desorbed protein molecules.

Initially the reflectivity profiles were fitted to a model consisting of one layer. The data, fits and scattering length profiles are shown in figure (3.1) with the layer

parameters given in table (3.1).

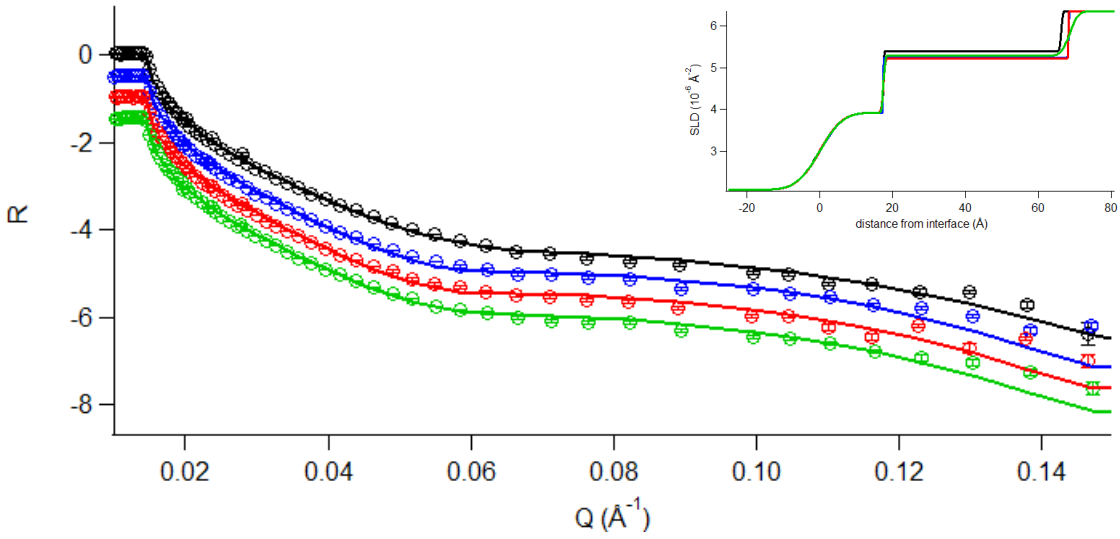


Figure 3.1: Reflectivity profiles and fits showing the changes over time for the adsorption of CA II in D_2O using a 1-layer model. The runs shown are $t_{inc} = 0$ (black), $t_{inc} = 6.5$ hours (blue), $t_{inc} = 11$ hours (red), $t_{inc} = 12.5$ hours and after exposure to protein-free buffer (green) with data being offset for clarity. The inset shows the scattering length density profiles and the layer parameters are in table (3.1).

t_{inc} \hrs	Thickness \±2 Å	% Solvent ±4	Roughness		Γ \±0.2 mg m^{-2}
			ox-1	1-s	
0	49	70	0	0	1.9
6.5	51	65	0	0	2.3
11	51	64	0	0	2.4
12.5	51	66	0	2	2.3

Table 3.1: Layer parameters for the 1-layer model of CA II adsorption. Data is shown in figure (3.1).

When in solution CA II is almost spherical with dimensions of 50 × 40 × 40 Å and the thickness of the 1-layer model is in good agreement with this suggesting that the protein is adsorbing in a single layer with no deformation. This model fits the observed reflectivity profiles well, however, all the fits do show a discrepancy from the data in the region between $Q = 0.05 - 0.1$ Å^{-1} which is reflected in the χ^2 range of 12-22. When the data is fitted using a 2-layer model, the χ^2 values for all the fits are reduced to a range of 6-16. These fits and the model layer parameters are shown in figure (3.2) and table (3.2).

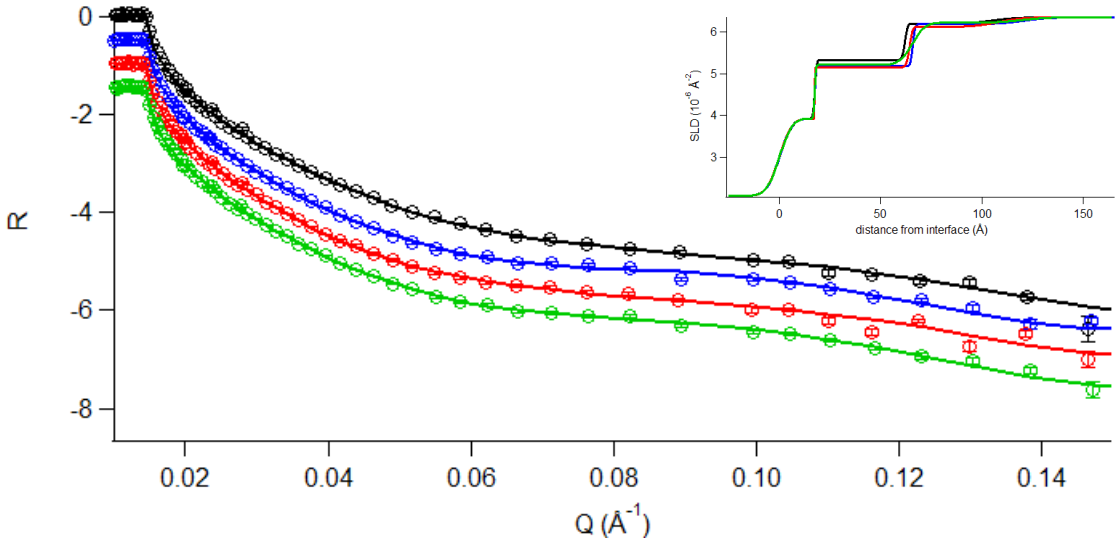


Figure 3.2: Reflectivity profiles and fits showing the changes over time for the adsorption of CA II in D_2O using a 2-layer model. The runs shown are $t_{inc} = 0$ (black), $t_{inc} = 6.5$ hours (blue), $t_{inc} = 11$ hours (red), $t_{inc} = 12.5$ hours and after exposure to protein-free buffer (green) with data being offset for clarity. The inset shows the scattering length density profiles and the layer parameters are in table (3.2).

t_{inc} \hrs	Layer number	Thickness \±2 Å	% Solvent ±4	Roughness			Γ \±0.2 mg m^{-2}
				ox-1	1-2	2-s	
0	1	44	68	1	1	10	1.8
	2	43	95				0.3
6.5	1	48	63	0	1	10	2.3
	2	55	95				0.4
11	1	47	62	0	0	10	2.3
	2	45	93				0.4
12.5	1	48	64	0	5	10	2.3
	2	55	95				0.4

Table 3.2: Layer parameters for the 2-layer model of CA II adsorption. Data is shown in figure (3.2).

A comparison of the 1-layer and 2-layer models reveals that they both show that the adsorption has neared completion by the end of the first measurement but with a small increase in the adsorbed amount up to a maximum after 6.5 hours. A combination of non-uniform charge distribution on the protein's surface, the protein being close to its IEP at this pH and the concentration of counter ions available means that there is no electrostatic attraction between the surface and the protein

to drive the adsorption but also there is no barrier due to repulsion between proteins. Under very similar physiochemical conditions Lindman et al.[1] have reported that the adsorption of CA II to copolymer nanoparticles involves no enthalpy change and thus the major driving force for adsorption is entropic in nature. CA II is a robust protein with respect to its structural stability and would not be expected to denature markedly on a hydrophilic surface. The favourable entropy change is due the dehydration of the binding surfaces of the substrate and the protein.

The two-layer model has an overall thickness of 87 Å initially and approximately 103 Å after a few hours. Both layers are approximately the same as the dimensions of the CA II molecule when in solution. This is consistent with a second layer adsorbing onto the first layer. This arrangement would maximise the protein-protein contact area resulting in a decrease in free energy due to release of solvent water molecules, van der Waals interactions and an increased possibility of specific interactions e.g. H-bonds between the proteins.

Another interesting feature of the 2-layer model is that the increase in adsorbed amount between the first two measurments occurs in both the layers. This is significant because it indicates that the formation of a second layer is occurring before the first layer has reached its jamming limit. It is most often assumed when deriving theoretical models or hypothesis regarding protein adsorption that a second layer is formed after the completion of the monolayer. It is also indicative of some degree of surface inhomogeneity whereby adsorption takes place more readily in some localised areas than others. This could be a result of the adsorption of surface impurities of variations in the local topography of the surface. Cuppett et al. have shown that polishing marks on silica promote the adsorption of LYS[2]. Specular neutron reflectivity only gives information about the structure normal to the surface and so it is assumed that the layers are homogeneous in the xy-plane and free from impurities. The exact nature of the adsorption process can not be deduced from this set of measurements but it is of note that some degree of lateral inhomogeneity can be hypothesised based on the model of adsorption for this protein. It is also possible that surface diffusion of the protein is occurring and exposing more binding sites on the surface[3].

The adsorbed protein layer, including the diffuse outer layer, is also resistant to desorption into protein free buffer as shown by the unchnaged adsorbed amounts between $t_{inc} = 11$ and 12.5 hours. A schematic of this model of CA II is shown below in figure (3.3).

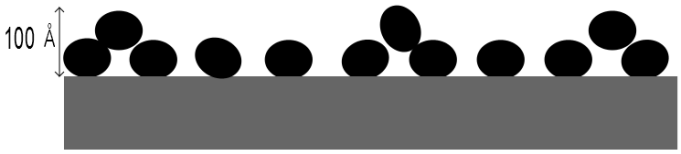


Figure 3.3: A schematic of the adsorption of CA II.

3.2 Lysozyme

The adsorption of 1 mg ml^{-1} LYS solutions onto hydrophilic silica surfaces was carried out in D_2O with PBS buffer at pH 7.4. Although there is only one water contrast, which could lead to the problem of distinguishing between the plausibility of the different proposed models, the adsorbed layer was characterised on numerous occasions with oxide layers that vary in thickness from 7.5 to 17 ÅLYS has been used as a model protein system in various studies so there is a wealth of data in the literature to compare these results to. Chapter 4 in this thesis will also re-examine the validity of the proposed models with respect to the new information of the addition of a second protein to the layer.

As stated previously, the reflectivity profiles were first fitted to a 1-layer adsorption model. A typical example of the reflectivity profiles, fits and scattering length density profiles is shown in figure (3.4) with the layer parameters in table (3.3). The other profiles, fits and layer parameters are shown in Appendix A at the end of this thesis.

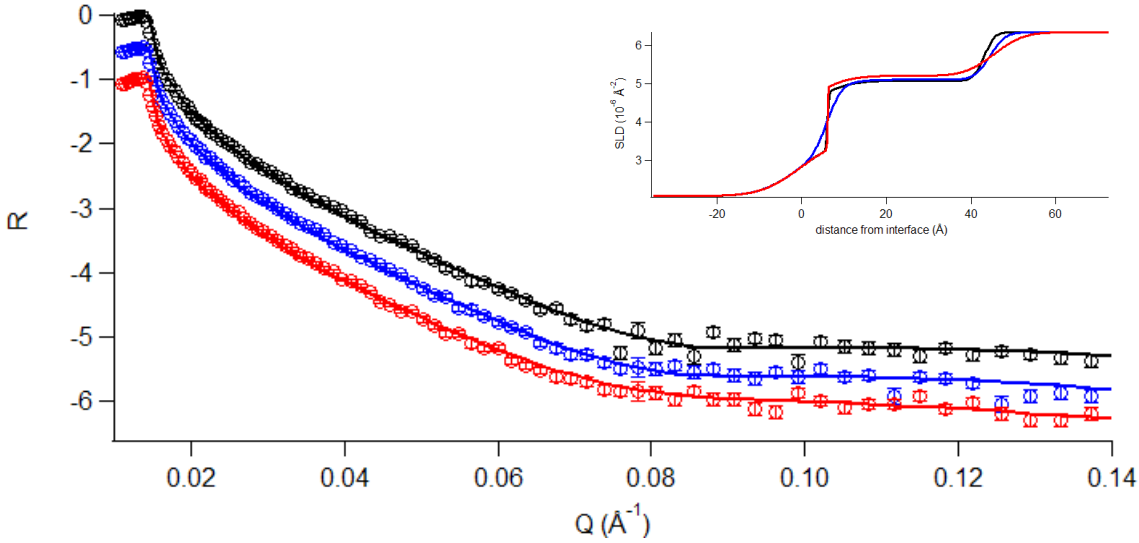


Figure 3.4: Reflectivity profiles and fits showing the changes over time for the adsorption of LYS in D_2O using a 1-layer model. The runs shown are $t_{inc} = 0$ (black), $t_{inc} = 5.5$ hours (blue) and $t_{inc} = 10$ hours (red) with data being offset for clarity. The inset shows the scattering length density profiles and the layer parameters are in table (3.3).

t_{inc} \hrs	Thickness \±2 Å	% Solvent ±3	Roughness		Γ \±0.2 mg m^{-2}
			ox-1	1-s	
0	37	54	0	2	2.3
5.5	38	55	3	3	2.3
10	39	59	0	6	2.1

Table 3.3: Layer parameters for the 1-layer model of LYS adsorption. Data is shown in figure (3.4).

The final thickness of the layer varies from 34 to 42 Å and the percentage of the solvent incorporated in the layer varies from 61 to 50. Given that the solution dimensions of LYS are 30 × 30 × 45 Å, this suggests that the LYS is adsorbed in a tilted orientation between side-on and end-on with the extent of the tilting varying.

A plot of the surface excess over time for the one layer model is shown in figure (3.5). This shows that the adsorption is fast with respect to the timescale of the experiment and that the adsorbed amount is comparable to that observed for CA II.

There are three anomalous data points on this graph. The blue data point refers to the fit for the $t_{inc} = 0$ profile in figure (A.3) and as can be seen from

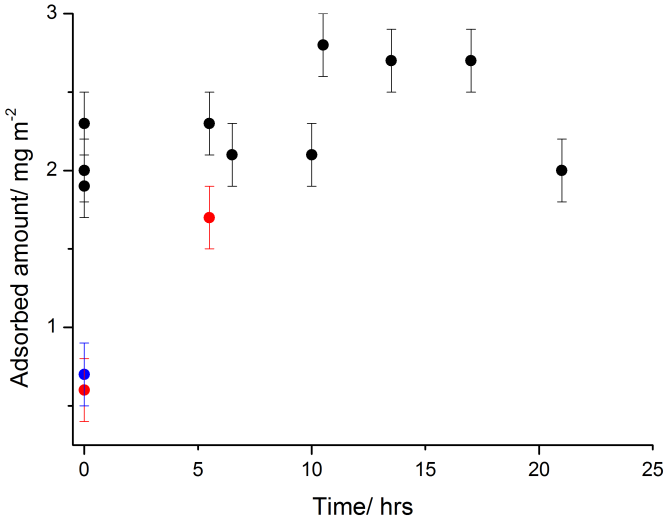


Figure 3.5: Adsorbed amount of LYS over time after injection of a 1 mg ml^{-1} LYS solution into the sample cell.

this figure, the lower than expected adsorbed amount can be attributed to the poor fit of the model to the experimental data (χ^2 = 36 compared to less than 10 for the other fits). The red data points at Γ =0.6 mg m^{-2} and Γ = 1.7 mg m^{-2} are from an anomalous data set and not included in the above discussion. This adsorbed layer was not used in any subsequent sequential adsorption models but it has been included as it highlights a salient point of this chapter. The experimental procedure outlined in chapter 2 describes the Piranha method for cleaning the silicon surface and producing an oxide layer. In the case of this particular silicon block, a slightly different procedure was used. The silicon surface was first treated using a Piranha solution at a temperature of $70 - 80\,^{\circ}$C before being illuminated by a UV light under flowing oxygen. Although the oxide layer is similar with respect to its thickness and roughness, the difference in surface preparation could subtly alter the oxide layer and in this case it has the impact of reducing the initial adsorption. Using ellipsometry Svesnsson and Arnebrant[4] have reported a marked difference in the adsorption of bovine serum albumin onto silica as a result of different surface cleaning regimes. Likewise, using neutron reflectivity to study the adsorption of non-ionic surfactants, Penfold et al.[5] found that the details of the surface treatment and its history critically affect its adsorption properties. It is important to take such factors into account when comparing data from different studies and the potential

for variability of the surface within the same study should not be overlooked as a source of error. The reflectivity profiles and fits are shown below in figure (3.6) and the layer parameters in table (3.4)

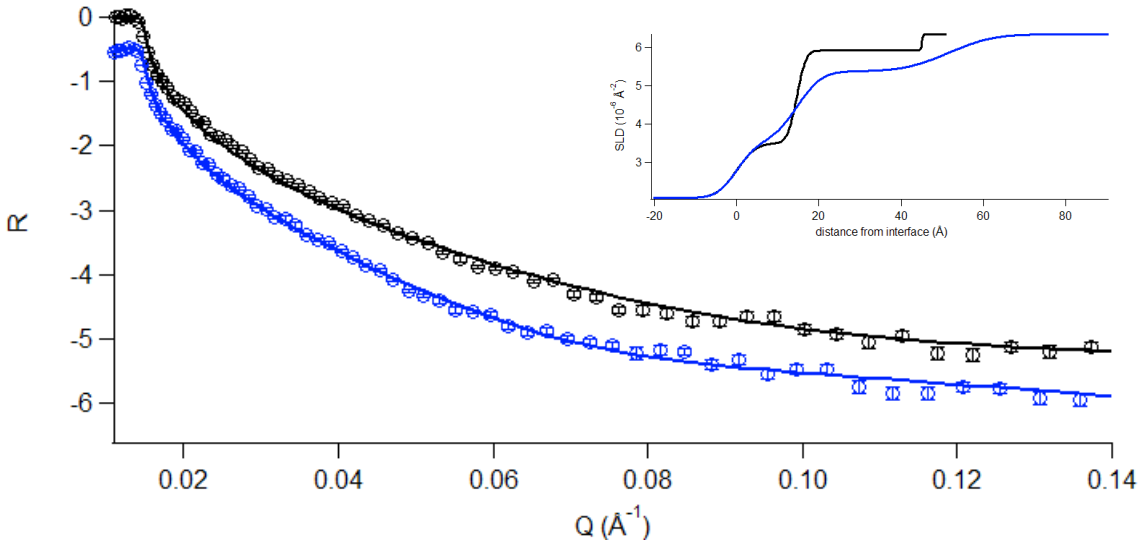


Figure 3.6: Reflectivity profiles and fits showing the changes over time for the adsorption of LYS in D_2O using a 1-layer model. The runs shown are $t_{inc} = 0$ (black) and $t_{inc} = 5.5$ hours (blue) with data being offset for clarity. The inset shows the scattering length density profiles and the layer parameters are in table (3.4).

t_{inc} \hrs	Thickness \±2 Å	% Solvent ±4	Roughness		Γ \±0.2 mg m^{-2}
			ox-1	1-s	
0	30	85	2	0	0.6
5.5	37	65	5	9	1.7

Table 3.4: Layer parameters for the 1-layer model of LYS adsorption in D_2O. Data is shown in figure (3.6).

In one set of reflectivity profiles (figure A.1), the 1-layer model does not give a satisfactory fit, particularly in the $Q >$ 0.07 Å^{-1} region, and the data was fitted using a 2-layer model. The χ^2 values are reduced by approximately 10 % in each case and the fits are visibliy improved. The reflectivity profiles and fits are shown below in figure (3.7) with the layer parameters in table (3.5). The total thickness of the adsorbed layer in this model is approximately 85 Å with the layer nearer the surface being thicker (35 Å) and denser (up to 58 % protein) than the outer layer (50 Å and 9% protein). This is consistent with the adsorption of two or more LYS

molecules adsorbed with the bottom one in a side-on orientation and the second loosely bound on top of the first layer; in a similar manner to the adsorption of CA II described previously.

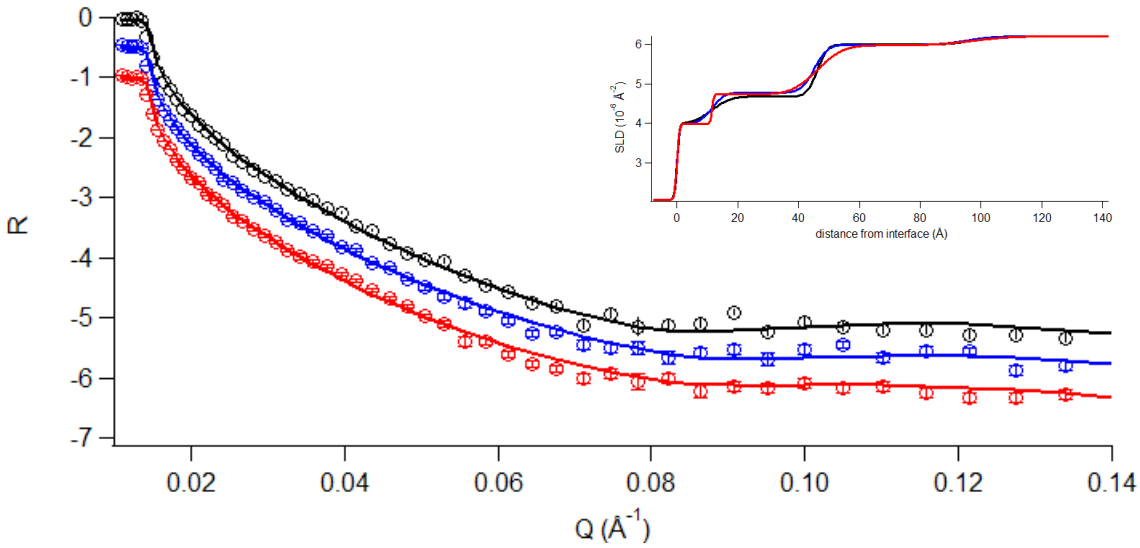


Figure 3.7: Reflectivity profiles and fits showing the changes over time for the adsorption of LYS in D_2O using a 2-layer model. The runs shown are t_{inc} = 10.5 hours (black), t_{inc} = 13.5 hours (blue) and t_{inc} = 17 hours (red) with data being offset for clarity. The inset shows the scattering length density profiles and the layer parameters are in table (3.5).

t_{inc} \hrs	Layer number	Thickness \±2 Å	% Solvent ±4	Roughness ox-1	Roughness 1-2	Roughness 2-s	Γ \±0.2 mg m^{-2}
10.5	1	35	42	5	3	6	2.7
	2	51	92				0.5
13.5	1	34	45	3	4	7	2.2
	2	50	92				0.5
17	1	35	44	1	7	10	2.6
	2	51	91				0.6

Table 3.5: Layer parameters for the 2-layer model of LYS adsorption in D_2O. Data is shown in figure (3.7).

3.2.1 Desorption of LYS

As well as monitoring the time evolution of the LYS layer, the extent to which the proteins were adsorbed irreversibly was studied by replacing the bulk solution with

protein free buffer after an incubation time of 1.5 hrs and following the changes to the layer for almost 30 hrs. The reflectivity profiles, fits and scattering length density profiles for a 1-layer model are shown in figure (3.8) with the layer parameters in table (3.6) . The initial adsorbed amount, 2.0 mg m^{-2}, is in good agreement with other data sets and it can be seen that most of the LYS remains on the surface. Even after 30 hours of being exposed to a protein-free bulk solution the adsorbed amount is still 1.4 mg m^{-2}. The remaining 70-90 % (depending on the time) of LYS can be thought of as irreversibly bound which is in excellent agreement with the findings of van der Veen et al.[6].

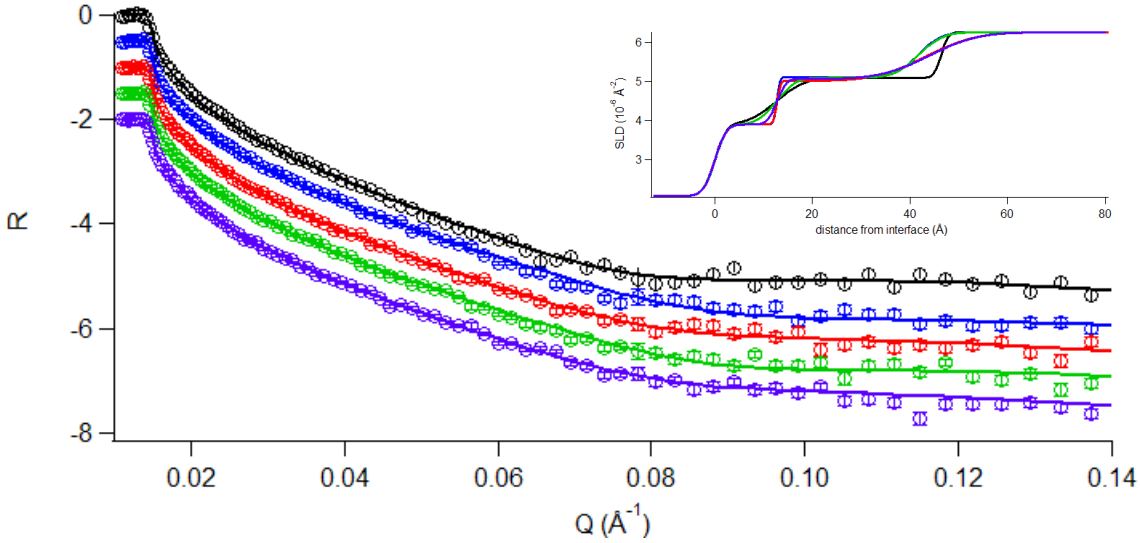


Figure 3.8: Reflectivity profiles and fits showing the adsorption of LYS in D_2O and changes after exposure to protein-free buffer using a 1-layer model. The runs shown are $t_{inc} = 0$ (black), $t = 1.75$ hours (blue), $t = 5$ hours (red), $t = 9.75$ hours (green) and $t = 30.5$ hours (purple) with data being offset for clarity. The inset shows the scattering length density profiles and the layer parameters are in table (3.6).

t_{inc} \hrs	Thickness \±2 Å	% Solvent ±4	Roughness		Γ \±0.2 mg m^{-2}
			ox-1	1-s	
0	34	56	5	2	2.0
1.75 (buffer only)	29	57	1	4	1.6
5	30	53	1	8	1.8
9.75	29	56	3	4	1.7
30.5	31	65	2	8	1.4

Table 3.6: Layer parameters for the 1-layer model of LYS desorption after an incubation period of 1.75 hours in D_2O. Data is shown in figure (3.8).

The adsorption of LYS onto silica using neutron reflectivity has been studied previously by Su et al. [7, 8] and Jackler et al. [9] under a range of solution conditions. Our results agree with the adsorption models proposed in these works although it is not possible to make a direct comparison due to the different solution conditions used. For the same concentration, the adsorbed amounts reported here are lower than those by Su et al.[7] which is to be expected given that the higher ionic strength of the solution used in this work reduces the strength of attraction between the surface and the protein. With regards to the structure of the layer and orientation of the protein, Su et al. propose a variety of models which are dependent on the solution conditions (from one layer side-on adsorption to a multilayer with the bottom layer being almost end-on orientated). The electrostatic interactions, both protein-surface and protein-protein, are considered to be an important factor as well as the protein concentration. The driving forces for adsorption are the favourable surface-protein electrostatic interactions and the entropically favourable dehydration of the protein and substrate surfaces upon adsorption. The effect of temperature change on LYS adsorption investigated by Jackler et al.[9] suggest that overall the process is endothermic and thus the entropy change associated with dehydration and structural modifications is the main driving force. The results here, taken under high salt conditions which mask the electrostatic attraction but also reduce the lateral repulsion, agree with these findings. A schematic of the proposed adsorption model is shown below in figure (3.9)

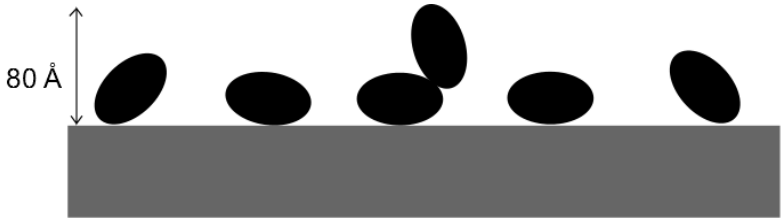


Figure 3.9: A schematic of the adsorption of LYS.

3.3 Human Serum Albumin

HSA is the most abundant protein in human serum and is thus of great importance when considering adsorption and has been extensively studied. Its bovine analogue, BSA, has also been widely studied and despite being 80 % homologous with respect to their primary amino acid sequences, having molecular weights differing by less than 1% and identical isoelectric points a direct comparison by Kurrat et al.[10] shows marked differences in their adsorption kinetics at silica-titania surfaces. Some differences in the layer thickness and adsorbed amount at the air/water interface have also been observed by Lu et al.[11] using neutron reflectivity. This highlights the sensitivity of the serum albumin system and also a feature of adsorption of proteins in general that, as with other protein functions, it is determined by small and specific changes in the amino acid composition or physicochemical conditions.

This section will discuss the adsorption of a 1 mg ml^{-1} solution of HSA in PBS buffer at pH 7.4 onto a hydrophilic silica surface. Initially the protonated form has been investigated in three different water contrasts- D_2O, H_2O and a mixture with a scattering length density of 5, referred to as CM5 from now on. The use of multiple solvent compositions in neutron reflectivity, known as contrast variation, reduces the possibility of the model being non-unique. CM5 was chosen as it lies between the scattering length densities of the protonated and perdeuterated forms of the protein. The adsorption of the perdeuterated form of the protein (d-HSA) has also been investigated and this will be discussed in comparison with the protonated form. To aid this discussion adsorption of a 50:50 mixture of the h and d forms has been investigated in both D_2O and H_2O.

When using the 1 and 2-layer models to infer preferred orientations of the adsorbed molecule, as has been done for CA II and LYS, it should be noted that this is done with less certainty due to the higher degree of structural flexibility shown by HSA. There is also some debate as to the dimensions of the protein when in solution

under certain conditions. It has been shown that a change in pH will induce conformational changes[12, 13]. Upon adsorption at an interface even if there is not enough evidence to suggest that denaturation (unfolding of the secondary structures) has occurred it is a reasonable assumption that the tertiary structure will not remain totally intact and the same as the crystal structure. Some authors, such as Forciniti and Hamilton[14] use an equilateral triangle/heart shape as a model, which is based on the crystal structure first determined by He and Carter[15]. Others, for example in work by Lu et al.[16], use a cigar shape with a length of 140 Å and diameter of 40 Å. The volume of the cigar shape model is approximately 117 kÅ^3 whereas the equilateral triangle has a volume of 83 kÅ^3. Calculating the volume using the individual amino acid volumes from Perkins[17] and the amino acid sequence gives a value of 85 kÅ^3 i.e. much closer to the equilateral triangle/ heart shaped model. This is not to say that this is necessarily the correct model to use when adsorption at an interface is concerned but if the cigar model is used this will include some solvent molecules as well as the protein and should be regarded as an excluded volume of the protein. It has been estimated from measurements of the electrophoretic mobility and using dynamic light scattering that the excluded radius caused by the hydration shell is 1.3 times larger than the packed radius (assuming the protein to be roughly spherical)[18, 19] which is close to the ratio of 1.38 for the cigar:amino acid volumes above.

3.3.1 h-HSA in D_2O, CM5 and H_2O

The adsorption of h-HSA has been investigated using three water contrasts- D_2O, CM5 and H_2O. A typical set of reflectivity profiles in D_2O is shown below with fits for a 1-layer model figure (3.10) and the layer parameters in table (3.7). The corresponding 2-layer model fits and layer parameters and given in figure (3.11) and table (3.8). The full set of reflectivity profiles, fits and layer parameters can be seen in Appendix B[1].

[1]Other D_2O data in figures B.1 to B.8 and with corresponding layer parameters in tables B.1 to B.8. CM5 in figure B.9 and table B.9. H_2O in figure B.10 and table B.10

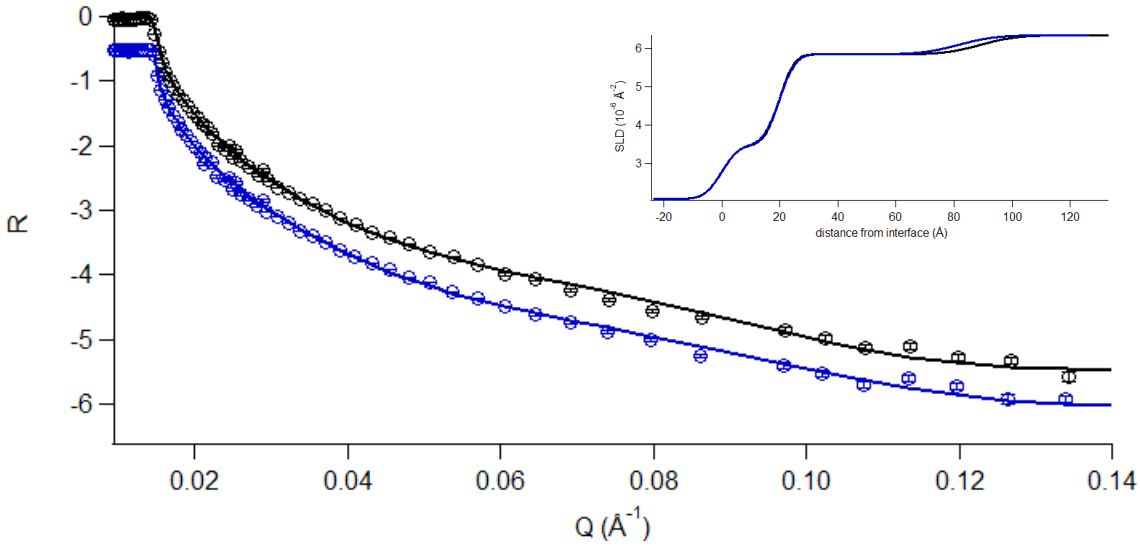


Figure 3.10: Reflectivity profiles and fits showing the changes over time for the adsorption of HSA in D_2O using a 1-layer model. The runs shown are t_{inc} = 4 hours (black) and t_{inc} = 13 hours (blue) with data being offset for clarity. The inset shows the scattering length density profiles and the layer parameters are in table (3.7).

t_{inc} \hrs	Thickness \±3 Å	% Solvent ±5	Roughness		Γ \±0.2 mg m^{-2}
			ox-1	1-s	
4	69	85	4	10	1.4
13	65	86	5	10	1.2

Table 3.7: Layer parameters for the 1-layer model of HSA adsorption in D_2O. Data is shown in figure (3.10).

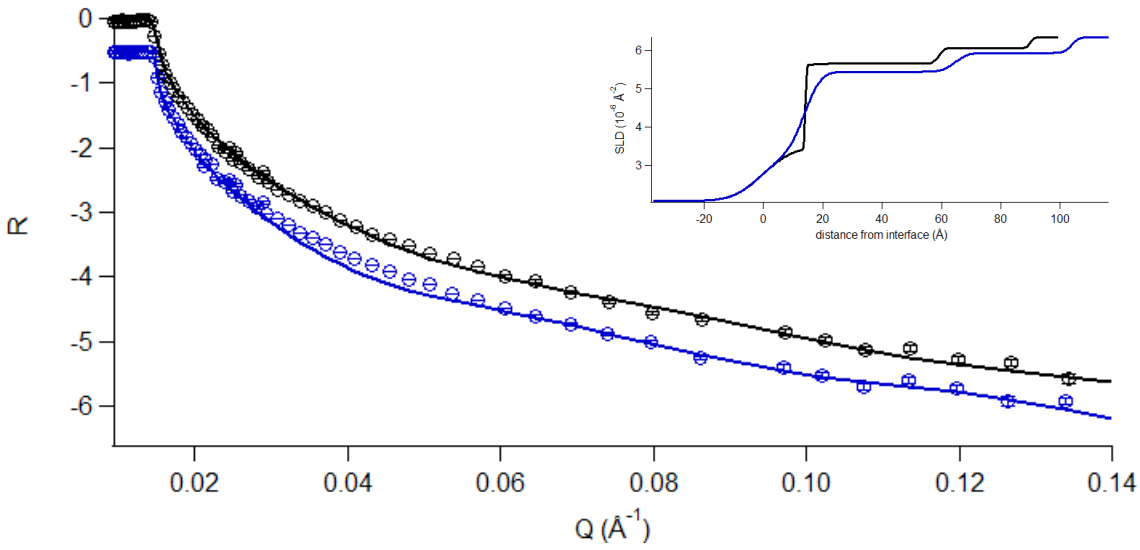


Figure 3.11: Reflectivity profiles and fits showing the changes over time for the adsorption of HSA in D_2O using a 2-layer model. The runs shown are t_{inc} = 4 hours (black) and t_{inc} = 13 hours (blue) with data being offset for clarity. The inset shows the scattering length density profiles and the layer parameters are in table (3.8).

t_{inc} \hrs	Layer #	Thickness \±3 Å	% Solvent ±5	Roughness			Γ \±0.2 mg m^{-2}
				ox-1	1-2	2-s	
4	1	57	83	2	2	6	1.3
	2	53	94				0.4
13	1	50	83	1	5	6	1.1
	2	49	95				0.3

Table 3.8: Layer parameters for the 2-layer model of HSA adsorption in D_2O. Data is shown in figure (3.11).

The adsorption of h-HSA in D_2O, CM5 and H_2O gives a variety of possible models. Generally, two things can be noted that are common to all; the adsorption is less than for CA II and LYS in terms of the proportion of protein in the layer. The thicknesses of the 1-layer model lie mostly in the range 30-73 Å although the thinner layers are only observed for initial adsorption. This is in good agreement with Forciniti and Hamilton [14] who observed a ∼ 65 Å thickness of HSA onto quartz at pH 7 and proposed this being due to the adsorption of the HSA molecules via their positively charged tip. In the cases where 2-layer models were required for a better fit, particularly in the low Q region, and all have qualitatively the same characteristics i.e. the outer layer is more diffuse. The thicknesses of the inner

layers vary between 41 and 71 Å suggesting that a variety of conformations exist but these can largely be thought of as in a slanted orientation given that the long axis of the HSA molecule is 80 Å (for the heart shaped model) or 140 Å (for the cigar shaped model). This is in good agreement with Monte Carlo simulations run by Hsu et al.[20]. They showed that when adsorbing onto a neutral, hydrophilic surface there are up to eight possible orientations that the HSA molecule adopts upon adsorption. HSA is also known to be a flexible protein and thus could undergo unfolding after attachment to the surface. The extent of unfolding would have an impact on the thickness of the adsorbed layer and also make comparisons with the solution dimensions of the molecule less important when considering the orientation of the molecule on the surface.

Another source of error that could account for the variability in the adsorbed amount, which varies from 0.2 to 1.6 mg m^{-2} for the 1-layer models, is the possible presence of impurities (both on the surface or in the bulk solution). This is likely to vary between different experiments given that they were taken on three different reflectometers (D17, INTER and SURF) on different occasions but no trend is apparent. Given that the biological function of HSA is as a carrier protein and has a number of binding sites[21], it is possible that even a small level of impurity will efficiently bind to HSA in solution and alter its adsorption characteristics. The effect of fatty acid binding is explored in more detail in chapter 6 of this thesis and our results indicate that fatty acid binding hinders HSA adsorption which is in good agreement with the findings of Lindman et al[1] and McClellan and Franses[22]. This suggests that variability could occur between different batches of the same protein. All of the h-HSA batches used in this study were purchased from Sigma who specify that it contains $\leq 0.02\%$ fatty acids but the presence of fatty acids or other substances was not directly accounted for thus there is also likely to be a variability in the purity of the protein between different batches. One of the experiments (results shown in figures (B.2) and (B.3) with layer parameters in tables (B.2) and (B.3)) used HSA purchased from Sigma and then purified by the research group of Sara Linse to remove any HSA dimers in the same manner as described in the supporting material of [1]. This extra purification step does not appear to make any difference to the adsorption of the protein.

When modelling multiple solvent contrasts in neutron reflectivity techniques, it is most usually assumed that the adsorbed layer is very similar when under different solvent compositions but this is not necessarily the case for the adsorption

of proteins. Cioni and Strambini[23] have shown that when in D_2O the rigidity of the native structure is significantly increased. When considering the importance of solvent isotope effects on the adsorption of surfactants to hydrophilic interfaces, Thomas[24] suggests that, aside from inducing phase changes which are not of importance here, the largest effects are seen in the adsorbed amount.

When fitting using the optical matrix method it is assumed that the oxide layer and surface topography is homogeneous but in reality this is unlikely to be the case. There are likely to be regions of higher and lower roughness and also other small variations, such as patches of a more hydrophobic nature or the presence of impurities on the surface, which can not be accounted for in this analysis. Using fluorescence and AFM techniques, Cuppett et al. have shown that the existence of polishing marks on silica have an impact on the adsorption of LYS [2] with localised changes to the surface topography on a nanometre scale being responsible for altering the degree of irreversibly adsorbed LYS. These changes are also likely to impact on the adsorbed state of the protein and would result in some degree of inhomogeneity in the adsorbed orientation of the HSA molecules. Similarly, Wehmeyer et al. [25] attribute the higher than predicted surface excess of BSA onto TiO_2 surfaces being due to the nanoscale topography in their experiments. Unfortunately in this study, due to the relatively small sample size, a comparison of the HSA adsorption with the characteristics of the oxide layer (thickness and roughness) did not reveal any trends although the underlying oxide layer parameters varied between 7-20 Å in thickness and 2-5Å roughness so this will be likely have induced some variability between the repeat measurements of adsorption. Overall, the range of thicknesses and adsorbed amounts is indicitative of the sensitivity of this system to a variety of factors.

The general trend observed is that adsorbed amounts are lower than for the other proteins in this study. This is a result of the overall net repulsion between the like-charged surface and HSA molecule at pH 7.4 as both carry a negative charge. Adsorption of HSA still occurs however due to the entropic driving force of the dehydration of the protein and surface, protein unfolding and the electrostatic attraction between the negatively charged surface and the positively charged region on HSA[14].

3.3.2 d-HSA in D_2O, CM5 and H_2O

The adsorption of d-HSA was investigated in three water contrasts, D_2O, CM5 and H_2O. The reflectivity when in D_2O was insensitive to adsorption i.e. the reflectivity profiles were too similar to the bare oxide layer before exposure to the protein solution. This is due to the small difference in the scattering length density of the solvent (6.35×10^{-6}Å^{-2}) and the protein (7.38×10^{-6}Å^{-2}) and also the small amount of adsorbed protein. These are shown in Appendix A (figures B.11 and B.12) and will be discussed further in chapter 4 with reference to the sequential adsorption but are not included in this section.

The reflectivity profiles where first analysed using a 1-layer model, shown below in figures (3.12), (3.13) and (3.14) with the layer parameters in tables (3.9), (3.10) and (3.11). The thickness of the 1-layer models varies from 34-60 Å with adsorbed amounts from 0.6-1.0 mg m^{-2} (Γ = 2.5mg m^{-2} in table (3.11) can be disregarded due to the poor fit of the 1-layer model in this case, $\chi^2 = 3.2$ compared to 1.1 for the 2-layer model). The thicknesses are generally lower than for h-HSA indicating the d-HSA is adsorbing with a higher degree of spreading or unfolding on the surface.

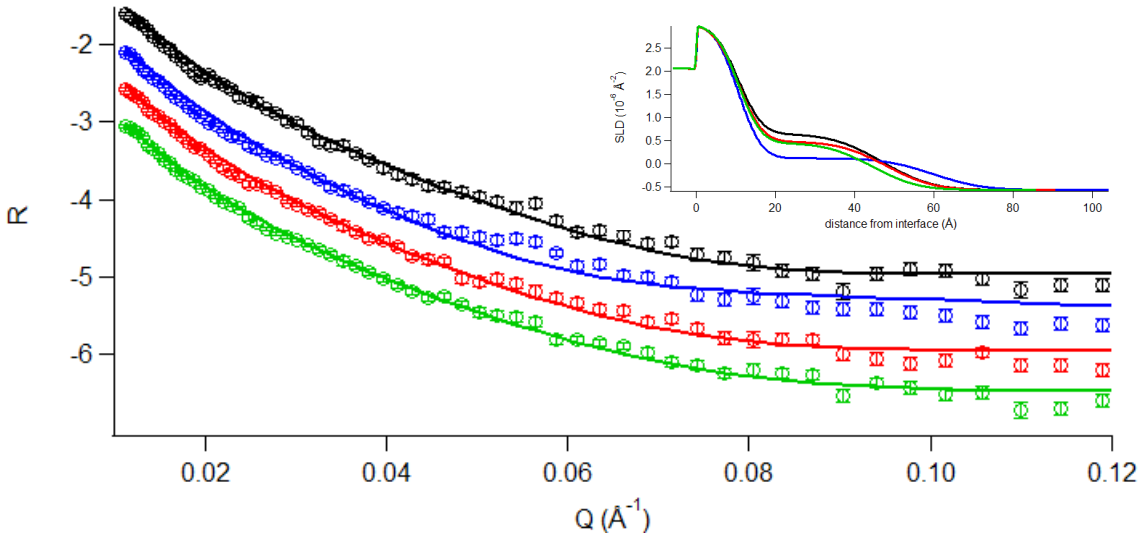


Figure 3.12: Reflectivity profiles and fits showing the adsorption of d-HSA in H_2O using a 1-layer model. The runs shown are t_{inc} = 0 (black solid= thin layer; black dashed= thick layer), t = 5 hours (blue), t_{inc} = 11 hours (red) and t_{inc} = 19 hours (green) with data being offset for clarity. The inset shows the scattering length density profiles and the layer parameters are in table (3.9).

t_{inc} \hrs	Thickness \±4 Å	% Solvent ±5	Roughness		Γ \±0.2 mg m^{-2}
			ox-1	1-s	
0	37	82	5	9	0.9
5	49	90	5	10	0.7
11	38	84	2	10	0.8
19	34	85	4	8	0.7

Table 3.9: Layer parameters for the 1-layer model of d-HSA adsorption in H_2O. Data is shown in figure (3.12).

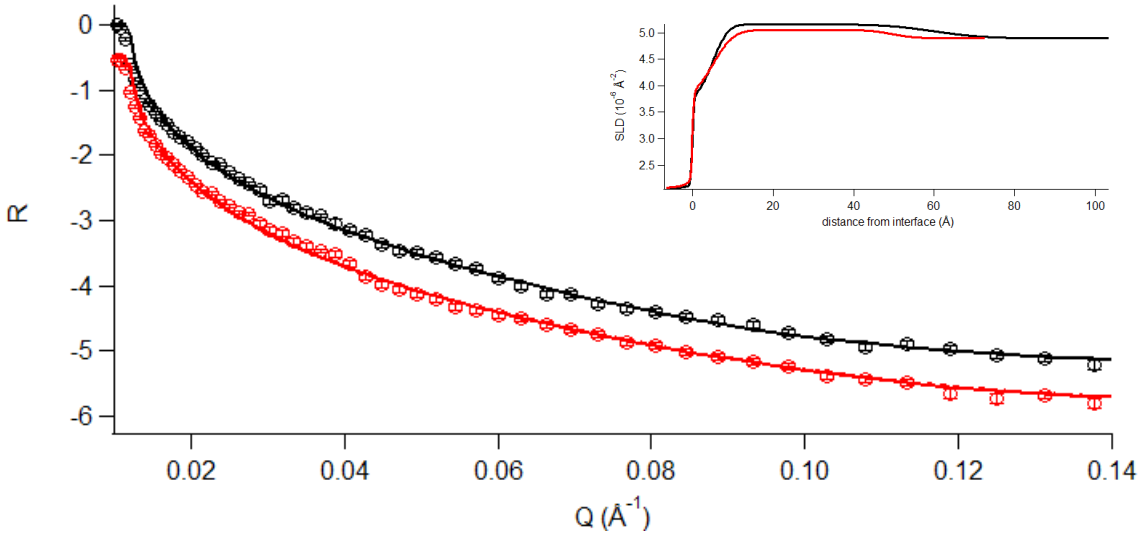


Figure 3.13: Reflectivity profiles and fits showing the adsorption of d-HSA in CM5 using a 1-layer model. The runs shown are $t_{inc} = 0$ (black), a thin layer for $t_{inc} = 0.75$ hours (red solid line) and a thick layer for $t_{inc} = 0.75$ hours (red dashed line) with data being offset for clarity. The inset shows the scattering length density profiles and the layer parameters are in table (3.10).

t_{inc} \hrs	Thickness \±3 Å	% Solvent ±5	Roughness		Γ \±0.2 mg m^{-2}
			ox-1	1-s	
0	55	87	5	9	1.0
0.75	45	90	5	1	0.6

Table 3.10: Layer parameters for the 1-layer model of d-HSA adsorption in CM5 with two possible fits for the $t_{inc} = 0.75$ hrs profile. Data is shown in figure (3.13).

In order to improve the fits in some cases a 2-layer model was used. The difference is best illustrated in figure (3.14) where the 1- and 2-layer fits are compared for the

same data set. The χ^2 value decreased from 3.2 to 1.1 for the 1-layer and 2-layer models respectively. The layer parameters are shown in table (3.11). The other 2-layer model fits are shown in figure (3.15) with the layer parameters in table (**??**). The 2-layer models show there to be 2 distinctive layers; a thinner, denser inner layer and a more diffuse but thicker outer layer. The inner layer thickness varies from 31 to 36 Å but the overall thickness is as high as 130 Å. This is in close agreement to the 2-layer models described previously for h-HSA and similarly, the formation of a thick, diffuse outer layer is in agreement with the 2-layer models for CA II and LYS.

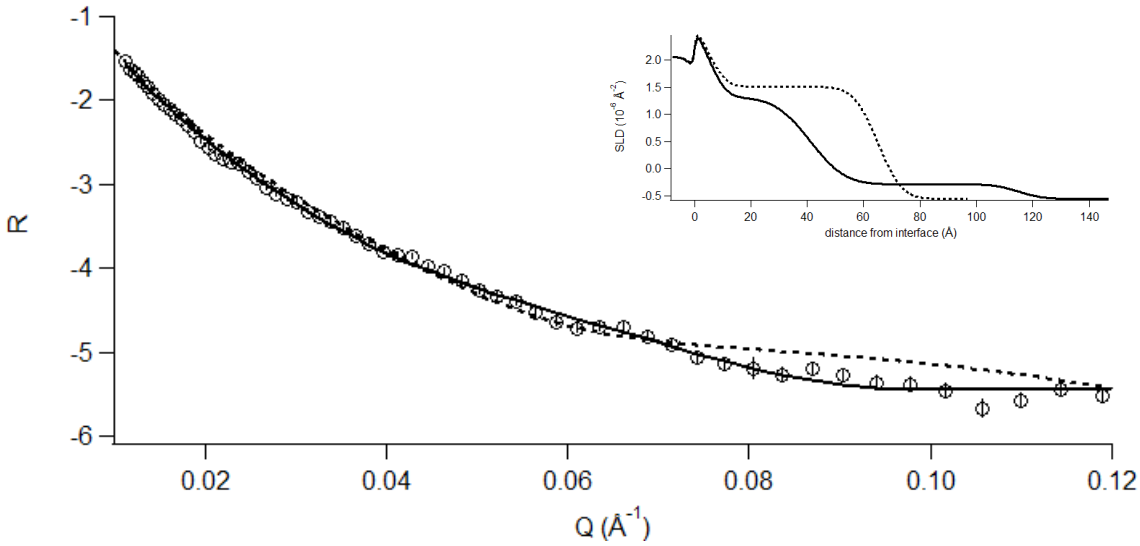


Figure 3.14: Reflectivity profiles and fits showing the adsorption of d-HSA in H_2O using a 1-layer and 2-layer model. The runs shown are 1-layer model for $t_{inc} = 0$ (black dashed line) and 2-layer model for $t_{inc} = 0$ (black solid line). The inset shows the scattering length density profiles and the layer parameters are in table (3.11).

t_{inc} \hrs	Layer number	Thickness \±2 Å	% Solvent ±3	Roughness			Γ \±0.2 mg m^{-2}
				ox-1	1-2	2-s	
0	1	60	69	5	10		2.5
0	1	36	72	5	10	10	1.4
	2	74	96				0.4

Table 3.11: Layer parameters for a 1-layer and 2-layer model of d-HSA in H_2O. Data is shown in figure (3.14).

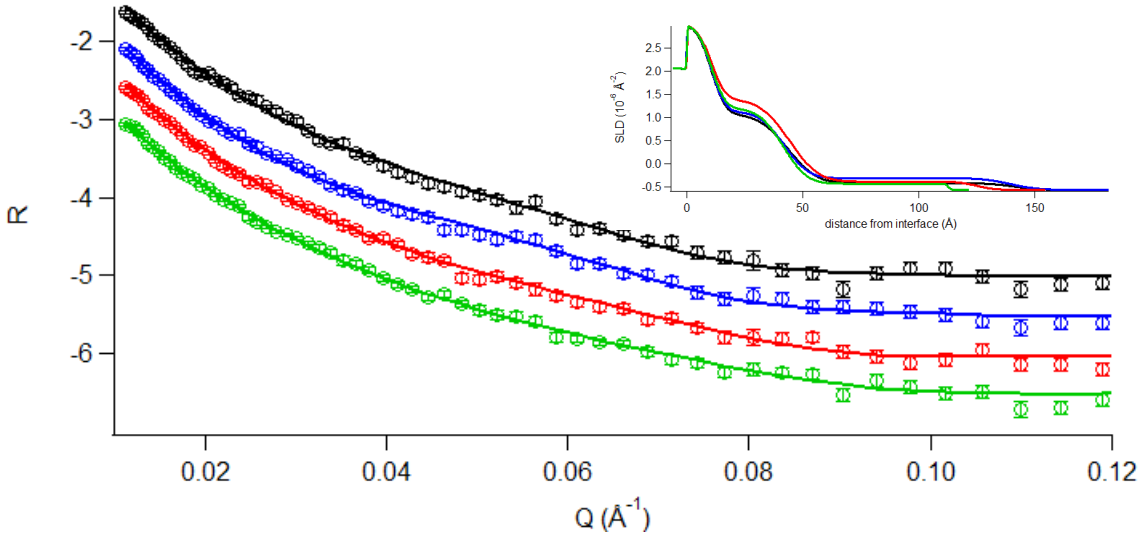


Figure 3.15: Reflectivity profiles and fits showing the adsorption of d-HSA in H_2O using a 2-layer model. The runs shown are $t_{inc} = 0$ (black), $t_{inc} = 5$ hours (blue), $t_{inc} = 11$ hours (red) and $t_{inc} = 19.5$ hours (green). The inset shows the scattering length density profiles and the layer parameters are in table (3.12).

t_{inc} \hrs	Layer #	Thickness \±3 Å	% Solvent ±5	Roughness			Γ \±0.2 mg m^{-2}
				ox-1	1-2	2-s	
0	1	33	76	3	8	2	1.1
	2	97	98				0.3
5	1	31	75	3	6	7	1.1
	2	98	96				0.5
11	1	34	71	4	5	4	1.3
	2	81	97				0.3
19.5	1	31	74	4	10	8	1.1
	2	71	98				0.2

Table 3.12: Layer parameters for the 2-layer model of d-HSA adsorption in H_2O. Data is shown in figure (3.15).

3.3.3 Mixture of d- and h-HSA in D_2O and H_2O

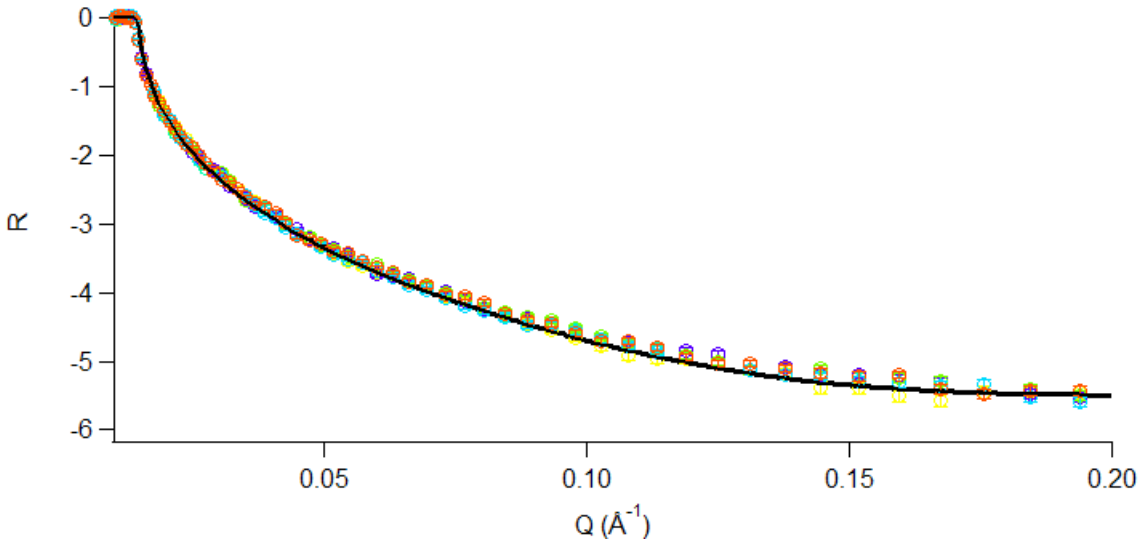


Figure 3.16: Reflectivity profiles for the adsorption of a 50:50 mix of h- and d-HSA in D_2O compared with the bare oxide layer (black line).

As can be seen from figure (3.16) the reflectivity profiles for the adsorption of a 50:50 mixture of d- and h-HSA in D_2O are indistinguishable from the buffer with no protein present. There are two scenarios that could account for this. Firstly this would arise if there is no adsorption of the protein. This can be disregarded given that it has been shown previously in this chapter that h-HSA and d-HSA adsorb onto silica in all the other water contrasts and that the adsorption of the mixture in H_2O does show a difference from the blank run. The alternative scenario that would give this result is that the scattering length density of the adsorbed layer is equal to the solvent, which in this case is D_2O ($\rho_{solvent} = 6.35 \times 10^{-6}$Å^{-2}). Given that the scattering length densities of the two protein variants (h- and d-HSA) are 7.38 and 3.02×10^{-6}Å^{-2} respectively then an adsorption ratio of approximately 3:1 for d:h would result in the neutrons not being able to distinguish between the protein layer and the solvent.

When in H_2O, the reflectivity profiles are distinguishable from the bare oxide layer and the overall scattering length density of the adsorbed layer is made up of contributions from the solvent, h-HSA and d-HSA. Even though the reflectivity profiles in D_2O are the same as in the absence of protein they still provide some information regarding the nature of the protein layer once it is assumed that adsorp-

tion is occurring and this can be used to more accurately determine the adsorbed layer characteristics for the H_2O data. The scattering length densities of the h- and d-HSA when in H_2O are 1.76 and 6.11×10^{-6}Å^{-2} respectively and if it is assumed that the 3:1 ratio is valid in H_2O as well as D_2O a 3:1 ratio of d:h variants gives the protein scattering length density as 5.02×10^{-6}Å^{-2}. Using this the reflectivity profiles were fit using 1-layer and 2-layer models. These can be seen below in figures (3.17) and (3.18) with the layer parameters in table (3.13). The thicknesses and adsorbed amount are in good agreement with the single protein cases.

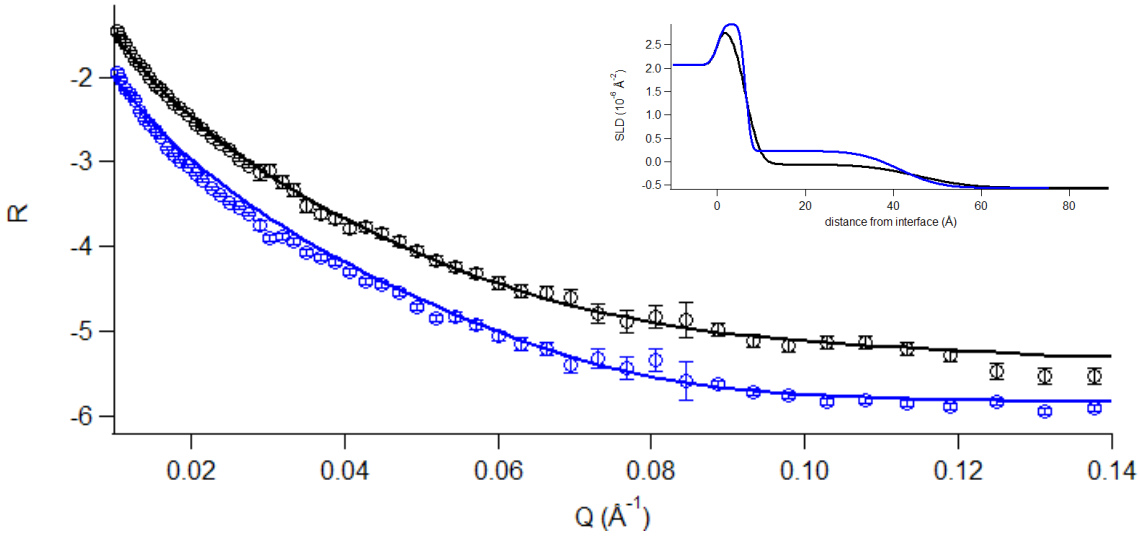


Figure 3.17: Reflectivity profiles and fits for the adsorption of a 50:50 mix of h- and d-HSA in H_2O assuming a 3:1 adsorption ratio (d:h) and fitted using a 1-layer model. The runs shown are $t_{inc} = 0$ and $t_{inc} = 6$ hours (blue). The inset shows the scattering length density profiles and the layer parameters are in table (3.13).

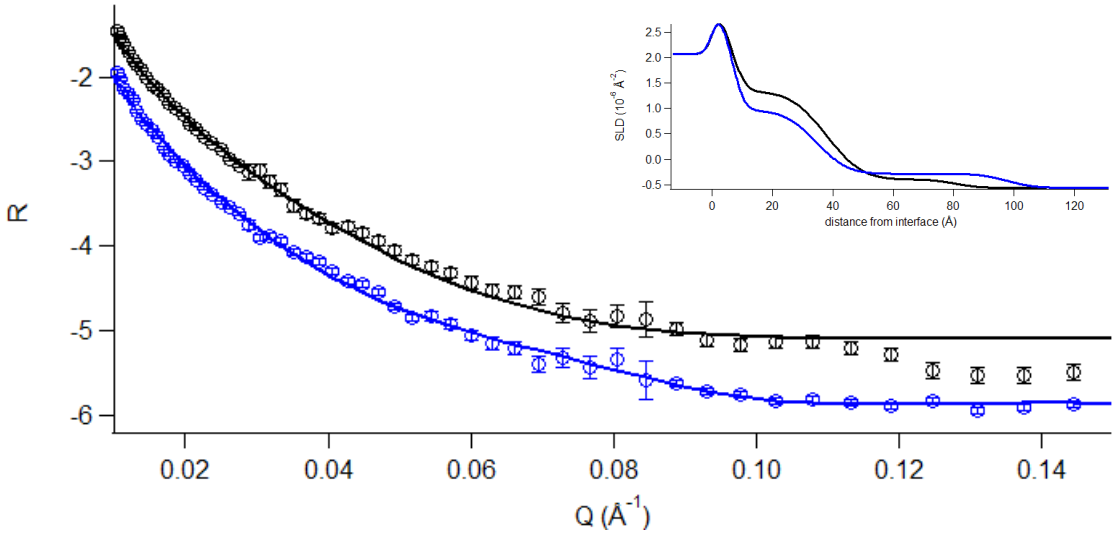


Figure 3.18: Reflectivity profiles and fits for the adsorption of a 50:50 mix of h- and d-HSA in H_2O assuming a 3:1 adsorption ratio (d:h) and fitted using a 2-layer model. The runs shown are $t_{inc} = 0$ (black) and $t_{inc} = 6$ hours (blue). The inset shows the scattering length density profiles and the layer parameters are in table (3.13).

t_{inc} \hrs	Layer number	Thickness \±2 Å	% Solvent ±4	Roughness			Γ \±0.2 mg m^{-2}
				ox-1	1-2	2-s	
0		42	90	5	9		0.6
6		45	88	5	9		0.7
0	1	32	66	1	2	6	1.5
	2	43	97				0.2
6	1	28	73	3	6	3	1.4
	2	63	95				0.4

Table 3.13: Layer parameters for the adsorption of a 50:50 mix of h- and d-HSA assuming a 3:1 adsorption ratio (d:h) for 1-layer and 2-layer models. The data is shown in figures (3.17) and (3.18).

3.4 Maltose Binding Protein

This section will discuss the adsorption of MBP and, in particular, the effect that incubation time has on the subsequent propensity for exchange and desorption. However, before undertaking an investigation into the exchange of the protonated and deuterated forms it is necessary to compare their individual adsorption characteristics. This has been achieved by monitoring the adsorption in different water

contrasts and also by adsorption of an equal mixture of the two forms.

3.4.1 h-MBP in H_2O, CM3.6 and CMSi

The adsorption of h-MBP was studied under 3 different water contrasts- H_2O, CM 3.6 and CMSi ($\rho_{solvent} = 2.07 \times 10^{-6}$Å^{-2}). The data from the CMSi contrast (not shown) provides very little information with respect to the adsorption of h-MBP due to the similarity of the scattering length densities of the solvent and the protein ($\rho_{h-MBP} = 2.2 \times 10^{-6}$Å^{-2}) but it does provide information in the subsequent exchange phase of the investigation and thus will be mentioned further in section (3.4.5).

In keeping with the aforementioned procedure, it was first attempted to fit the data using a 1-layer model. The reflectivity profiles and theoretical fits for a 1-layer model for the H_2O runs are shown in figure (3.19) with the layer parameters given in table (3.14).

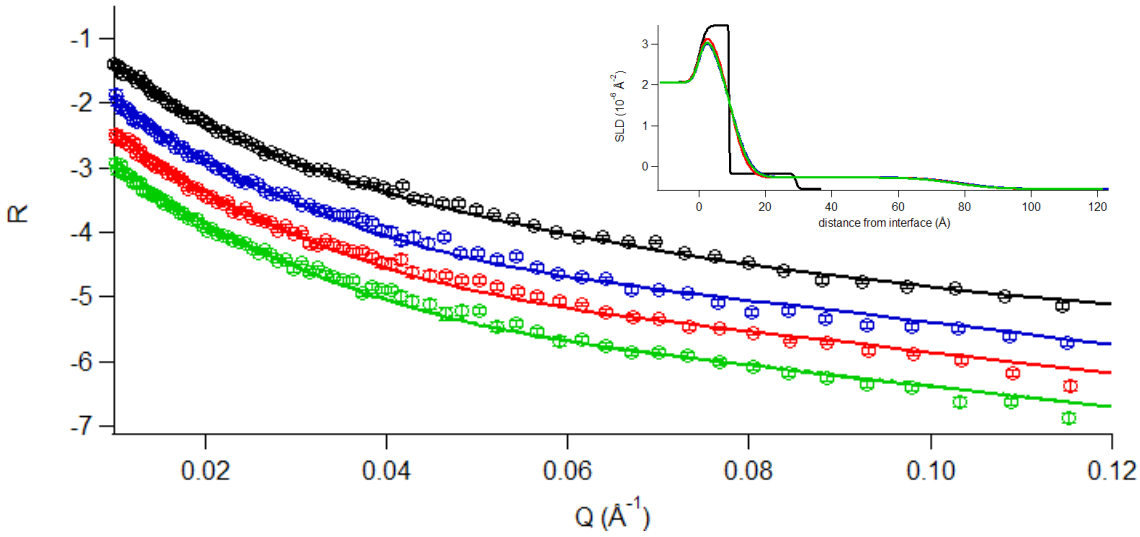


Figure 3.19: Reflectivity profiles and fits showing the changes over time for adsorption of h-MBP in H_2O using a 1-layer model. The runs shown are $t_{inc} = 0$ (black), $t_{inc} = 4$ hours (blue), $t_{inc} = 19.5$ hours (red) and $t_{inc} = 21.5$ hours (green dashed line is for a thick layer, green solid line is for a thin layer). The inset shows the scattering length density profiles and the layer parameters are in table (3.14).

t_{inc} \hrs	Thickness \±4 Å	% Solvent ±4	Roughness		Γ \±0.2 mg m^{-2}
			ox-1	1-s	
0	20	84	0	0	0.4
4	70	88	5	9	1.1
19.5	69	88	5	10	1.1
21.5 (wash)	68	89	5	10	1.0

Table 3.14: Layer parameters for the 1-layer model of h-MBP adsorption in H_2O. The data is shown in figure (3.19).

The fits for a 1-layer model and layer parameters for the CM 3.6 solvent contrast are shown below in figure (3.20) and table (3.15). These show that the 1-layer model does not adequately describe the adsorbed layer, except in the case of the initial adsorption with the fits being particularly poor fits in the Q¡0.05 Å^{-1} regions.

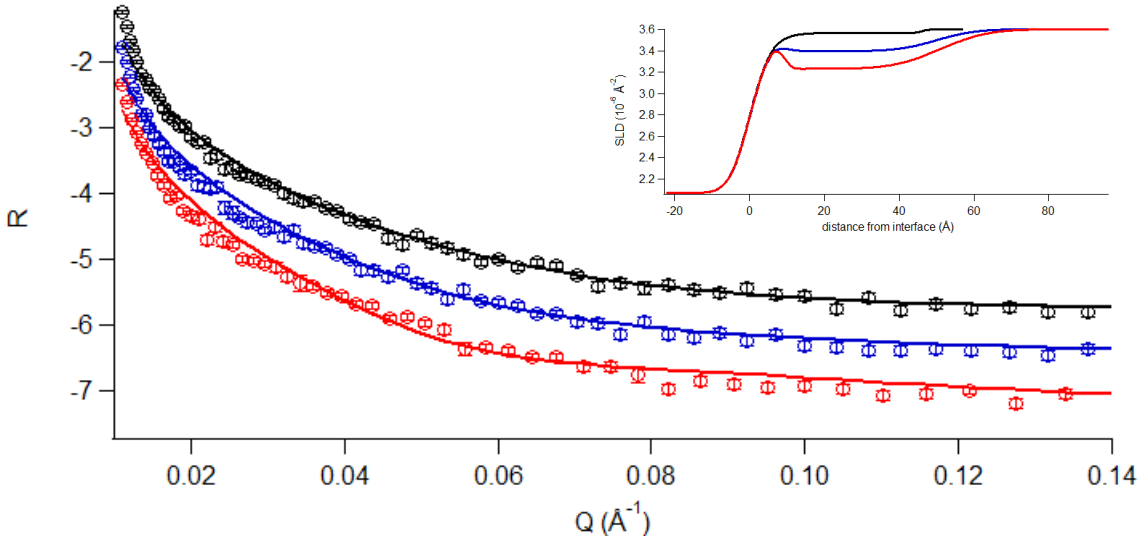


Figure 3.20: Reflectivity profiles and fits showing the changes over time for adsorption of h-MBP in CM3.6 using a 1-layer model. The runs shown are $t_{inc} = 0$ (black), $t_{inc} = 17$ hours (blue) and $t_{inc} = 23.5$ hours. The inset shows the scattering length density profiles and the layer parameters are in table (3.15).

t_{inc} \hrs	Thickness \±2 Å	% Solvent ±4	Roughness		Γ \±0.2 mg m^{-2}
			ox-1	1-s	
0	37	98	4	2	0.1
17	41	85	3	8	0.8
23.5	42	74	2	10	1.4

Table 3.15: Layer parameters for the 1-layer model of h-MBP adsorption in CM3.6. Data is shown in figure (3.20).

Given that the 1-layer model does not adequately fit the experimental data for either solvent contrast and the agreement between them in terms of layer thickness is not good it is now attempted to fit using a 2-layer model. The fits for the 2-layer models are shown in figures (3.21) and (3.22) with corresponding layer parameters in tables (3.16) and (3.17). The overall thickness is comparable with the model for the H_2O contrast but provides more information regarding the nature of the adsorbed protein. It can be seen that the bottom layer of the model (adjacent to the silica surface) is thinner and denser than the outer layer. Also, as time progresses, the layer becomes thinner and denser still. The thickness, 15 Å, is approximately 1/2 that of the shortest axis of the molecule when in solution and the solvent percentage is 50 %.

A high protein volume fraction in an adsorbed layer can be as a result of two processes; adsorption of more protein molecules or spreading of the protein that is attached to the surface. In this case, the discrepancy between the first and second layers in terms of solvent percentage suggests that the protein closest to the surface has unfolded and spread over the surface.

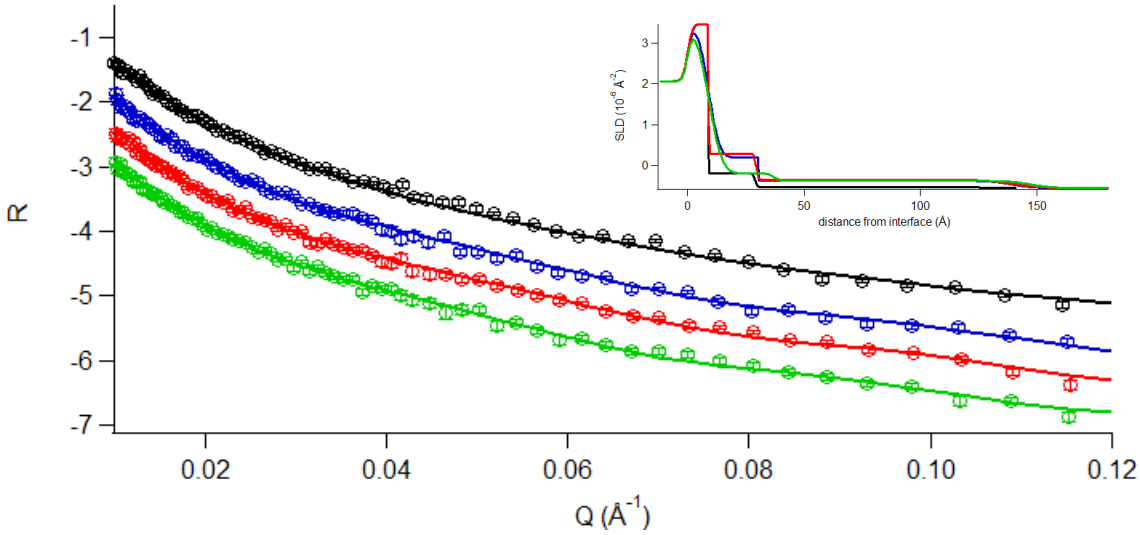


Figure 3.21: Reflectivity profiles and fits showing the changes over time for adsorption of h-MBP in H_2O using a 2-layer model. The runs shown are $t_{inc} = 0$ (black), $t_{inc} = 4$ hours (red), $t_{inc} = 19.5$ hours (blue) and $t_{inc} = 21.5$ hours (green). The inset shows the scattering length density profiles and the layer parameters are in table (3.16).

t_{inc} \hrs	Layer number	Thickness \±2 Å	% Solvent ±4	Roughness			Γ \±0.2 mg m^{-2}
				ox-1	1-2	2-s	
0	1	20	85	0	1	3	0.4
	2	96	99				0.1
4	1	22	68	3	0	7	0.9
	2	109	92				1.1
19.5	1	21	64	0	1	9	1.0
	2	109	91				1.2
21.5	1	26	81	4	0	9	0.6
	2	80	93				0.7

Table 3.16: Layer parameters for the 2-layer model of h-MBP adsorption in H_2O. Data is shown in figure (3.21).

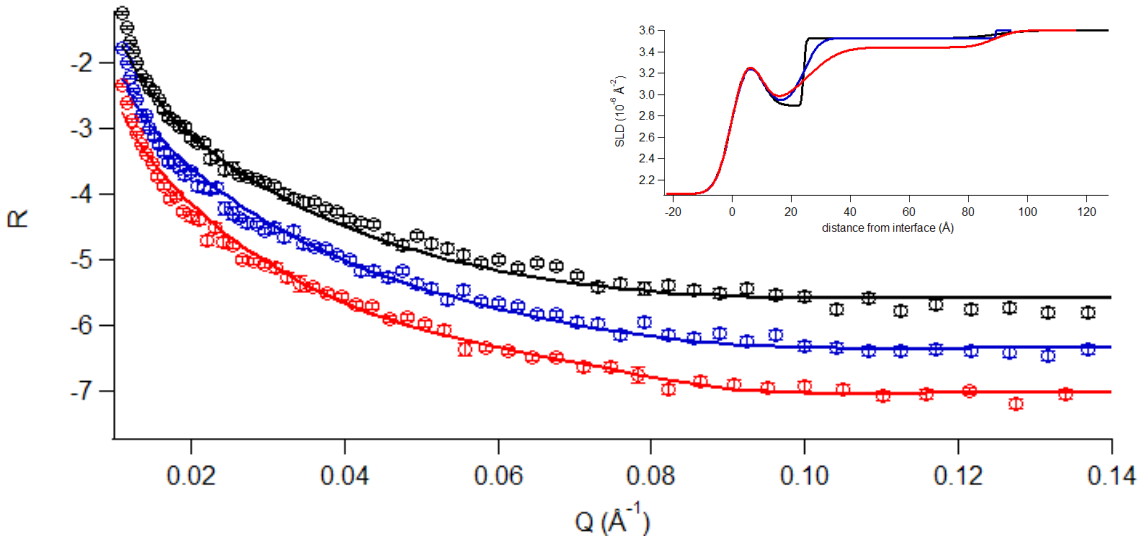


Figure 3.22: Reflectivity profiles and fits showing the changes over time for adsorption of h-MBP in CM3.6 using a 2-layer model. The runs shown are $t_{inc} = 0$ (black), $t_{inc} = 17$ hours (red) and $t_{inc} = 23.5$ hours (blue). The inset shows the scattering length density profiles and the layer parameters are in table (3.17).

t_{inc} \hrs	Layer number	Thickness \±2 Å	% Solvent ±4	Roughness			Γ \±0.2 mg m^{-2}
				ox-1	1-2	2-s	
0	1	15	50	3	4	0	1.0
	2	65	95				0.4
17	1	16	48	3	8	6	1.1
	2	64	89				0.9
23.5	1	15	50	4	1	5	1.0
	2	64	95				0.4

Table 3.17: Layer parameters for the 2-layer model of h-MBP adsorption in CM3.6 showing two possible fits for the t=23.5 hrs data. Data is shown in figure (3.22).

If the models from the two water contrasts are compared, it can be seen that the overall adsorbed amounts are comparable but the H_2O contrast does not show any evidence of the unfolding process suggested by the high protein content and thin inner layer observed in CM 3.6 data. The two 2-layer models show that they are also in good agreement with respect to the adsorbed layer characteristics; a thin, dense inner layer and a diffuse, thick outer layer. The differences could be attributed to the effect of the solvent on the protein properties or it could also reflect the differences in the sensitivity of the technique under the different solvent contrasts.

There is a greater difference in the scattering length densities between the solvent and the protein when in H_2O which increases the sensitivity but there is also a higher amount of non-coherent scattering which would limit the Q-range and increase the background signal. Given the diffuse nature of the outer layer and the differences in the solvent a fully quantative agreement should not be expected but the two solvent contrasts can be said to be in good agreement from a semi-quantative view point.

3.4.2 d-MBP in H_2O and CMSi

The adsorption of d-MBP was investigated in two water contrasts, H_2O and CMSi. D_2O was not used as a solvent contrast in this case due to the similarity of scattering length densities of the solvent and the protein which would reduce the sensitivity of the experiment as was observed for the d-HSA in D_2O in section 3.3.2. The reflectivity profiles and theoretical fits for a 1-layer model are shown below in figures (3.23), (3.24) and (3.25) with the corresponding layer parameters shown in tables (3.18), (3.19) and (3.20).

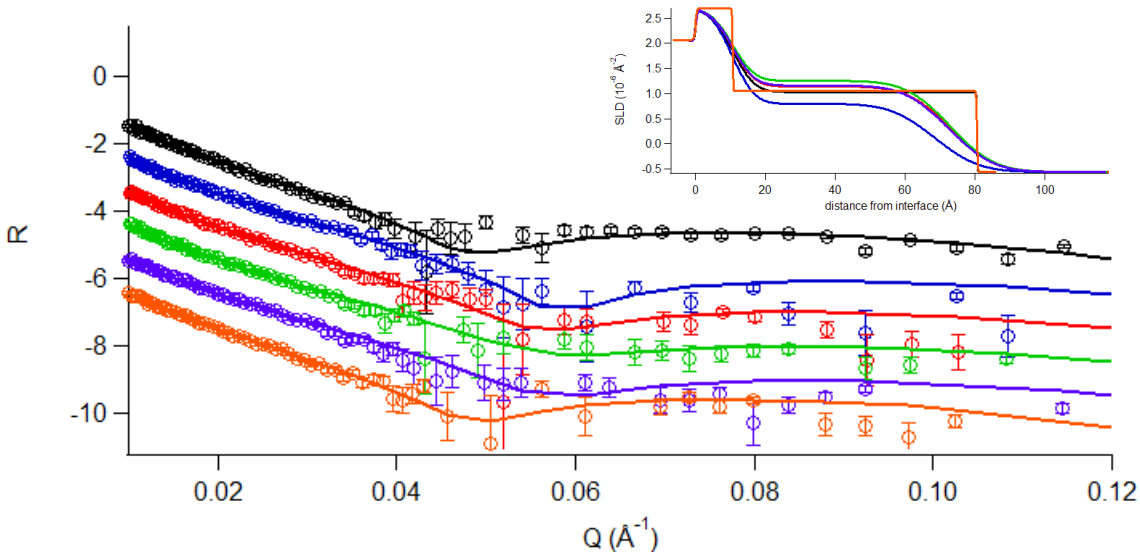


Figure 3.23: Reflectivity profiles and fits showing the changes over time for adsorption of d-MBP in H_2O using a 1-layer model. The runs shown are $t_{inc} = 0$ (black), $t_{inc} = 4.25$ hours (red), $t_{inc} = 11.75$ hours (blue), $t_{inc} = 17$ hours (green), $t_{inc} = 20$ hours (purple) and $t_{inc} = 20$ hours (yellow). The inset shows the scattering length density profiles and the layer parameters are in table (3.18).

t_{inc} \hrs	Thickness \±2 Å	% Solvent ±4	Roughness		Γ \±0.2 mg m^{-2}
			ox-1	1-s	
0	70	76	0	0	2.3
4.25	58	80	5	10	1.6
11.75	63	75	5	10	2.1
17	62	73	5	10	2.3
20	62	75	5	10	2.1
21 (wash)	70	76	0	0	2.3

Table 3.18: Layer parameters for the 1-layer model of d-MBP adsorption in H_2O. Data is shown in figure (3.23).

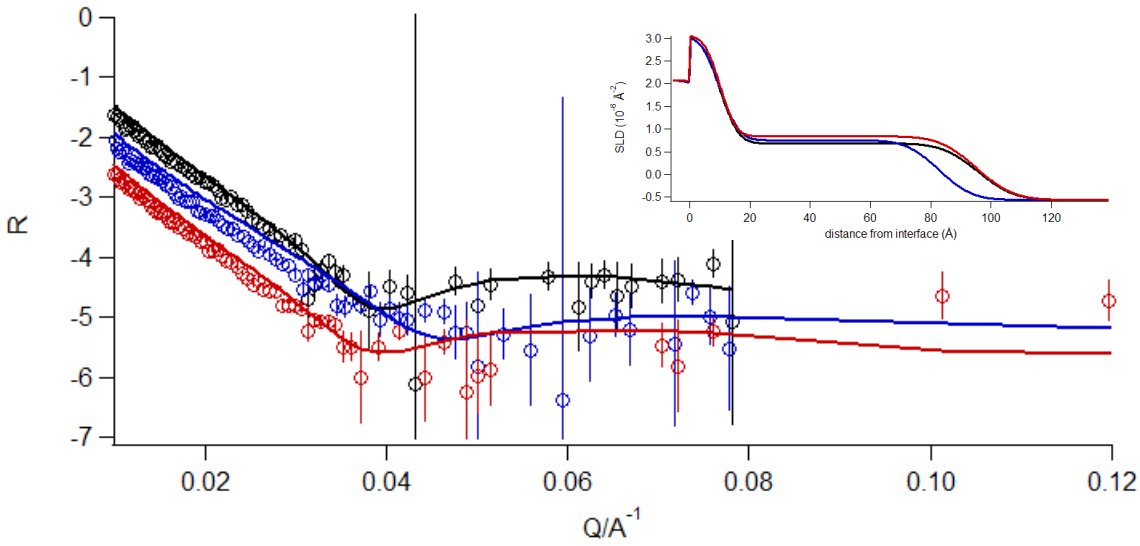


Figure 3.24: Reflectivity profiles and fits showing the changes over time for adsorption of d-MBP in H_2O using a 1-layer model. The runs shown are $t_{inc} = 0$ (black), $t_{inc} = 1.5$ hours (red) and $t_{inc} = 2.75$ hours (blue). The inset shows the scattering length density profiles and the layer parameters are in table (3.19).

t_{inc} \hrs	Thickness \±2 Å	% Solvent ±4	Roughness		Γ \±0.2 mg m^{-2}
			ox-1	1-s	
0	86	82	5	9	2.1
1.5	73	81	5	9	1.9
2.75	85	80	4	10	2.3

Table 3.19: Layer parameters for the 1-layer model of d-MBP adsorption in H_2O. Data is shown in figure (3.24).

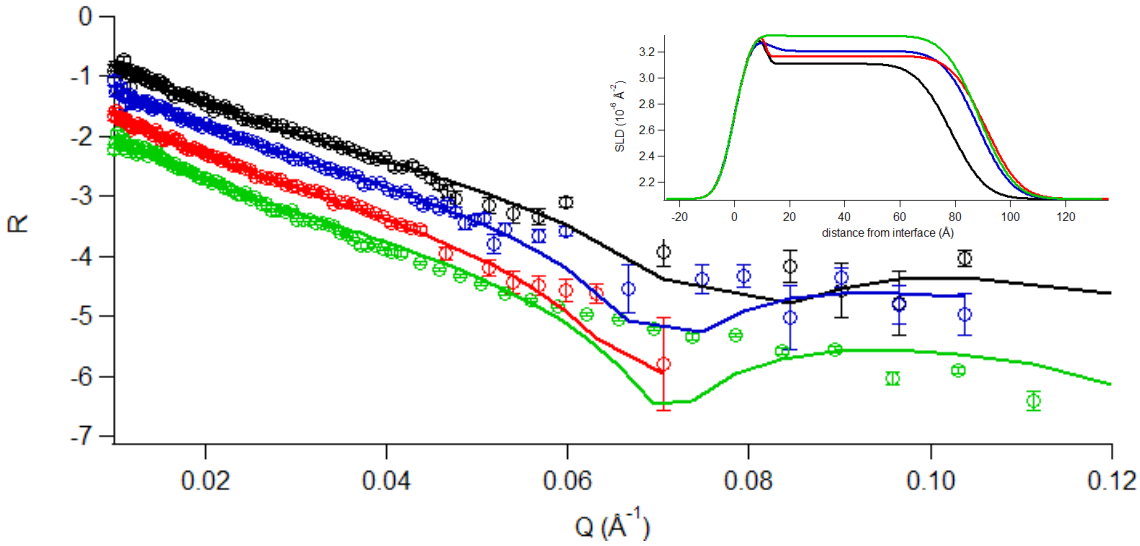


Figure 3.25: Reflectivity profiles and fits showing the changes over time for adsorption of d-MBP in CMSi using a 1-layer model. The runs shown are $t_{inc} = 0$ (black), $t_{inc} = 2$ hours (red), $t_{inc} = 4$ hours (blue) and $t_{inc} = 13$ hours (green). The inset shows the scattering length density profiles and the layer parameters are in table (3.20).

t_{inc} \hrs	Thickness \±2 Å	% Solvent ±4	Roughness		Γ \±0.2 mg m^{-2}
			ox-1	1-s	
0	67	76	2	10	2.2
2	77	74	4	10	2.7
4	80	75	1	10	2.7
13	77	71	4	10	3.0

Table 3.20: Layer parameters for the 1-layer model of d-MBP adsorption in CMSi. Data is shown in figure (3.25).

Although, a 1-layer model gives good agreement between the theoretically calculated reflectivity and the experimentally determined profiles in most cases the thicknesses of the adsorbed layers in this model are consistently greater than the longest axial dimension of the MBP molecule when in solution. This could occur if the molecule has unfolded to a different conformation and then adsorbs end-on. This is an unlikely scenario as it would involve a transition to a less favoured conformation of the protein and the exposure of hydrophobic side chains, previously hidden in the core, to the solvent. As the adsorption is end-on there would be no free energy gain from increased attachment to the surface and no driving force for this conformational change is apparent. The more likely scenario is that the adsorbed

layer is two proteins thick and either they are present with equal adsorption in both layers or the neutron reflectivity technique under these conditions is not sensitive enough to elucidate the finer details of the non-uniform density profile normal to the surface. To distinguish between these possibilities the data is re-examined and fit to a 2-layer model. The reflectivity profiles and fits are shown below in figures (3.26), (3.27) and (3.28) with the corresponding layer parameters shown in tables (3.21), (3.22) and (3.23).

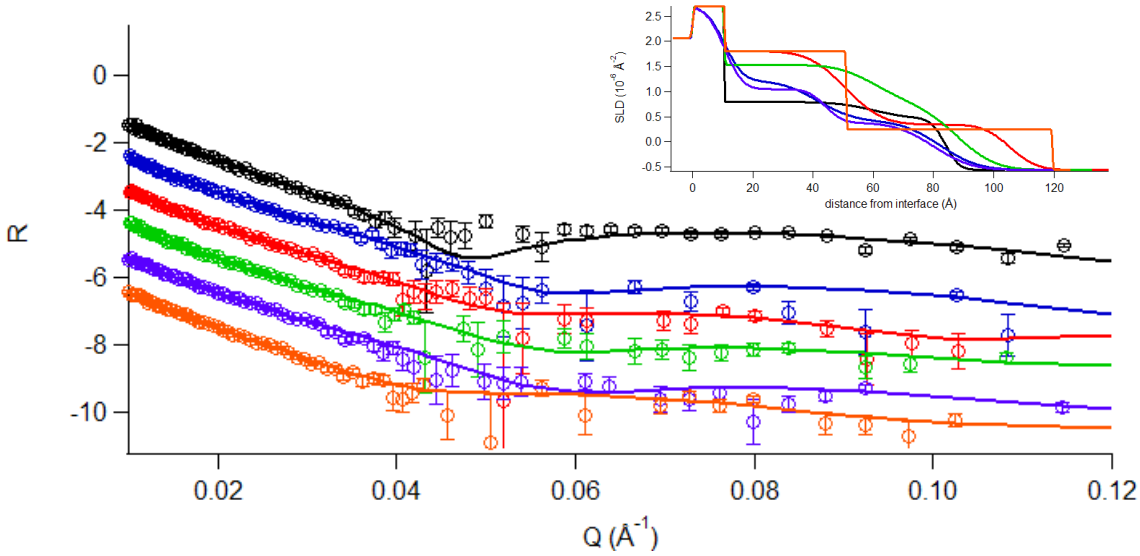


Figure 3.26: Reflectivity profiles and fits showing the changes over time for adsorption of d-MBP in H_2O using a 2-layer model. The runs shown are $t_{inc} = 0$ (black), $t_{inc} = 4.25$ hours (red), $t_{inc} = 11.75$ hours (blue), $t_{inc} = 17$ hours (green), $t_{inc} = 20$ hours (purple) and $t_{inc} = 20$ hours (yellow). The inset shows the scattering length density profiles and the layer parameters are in table (3.21).

t_{inc} \hrs	Layer number	Thickness \±2 Å	% Solvent ±4	Roughness			Γ \±0.2 mg m^{-2}
				ox-1	1-2	2-s	
0	1	50	80	0	10	4	1.4
	2	24	85				0.5
4.25	1	32	74	5	10	10	1.1
	2	41	86				0.8
11.75	1	40	65	0	10	7	1.9
	2	55	87				1.0
17	1	50	69	0	10	10	2.1
	2	28	80				0.8
20	1	34	76	4	4	0	1.1
	2	36	86				0.7
21 (wash)	1	40	65	0	0	0	1.9
	2	69	88				1.1

Table 3.21: Layer parameters for the 2-layer model of d-MBP adsorption in CMSi. Data is shown in figure (3.26).

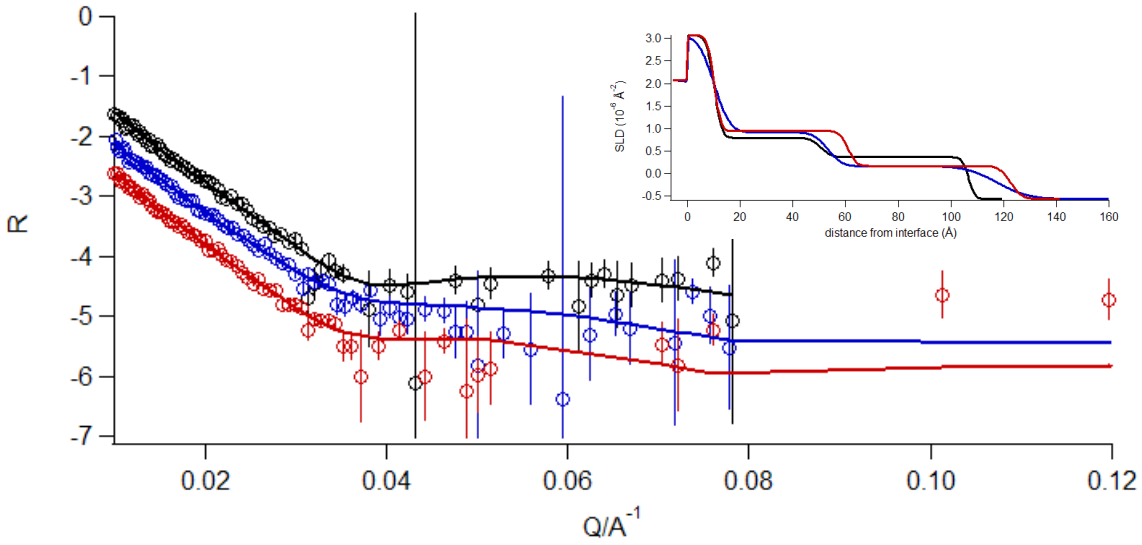


Figure 3.27: Reflectivity profiles and fits showing the changes over time for adsorption of d-MBP in H_2O using a 2-layer model. The runs shown are $t_{inc} = 0$ (black), $t_{inc} = 1.5$ hours (red) and $t_{inc} = 2.75$ hours (blue). The inset shows the scattering length density profiles and the layer parameters are in table (3.22).

t_{inc} \hrs	Layer number	Thickness \±2 Å	% Solvent ±4	Roughness			Γ \±0.2 mg m^{-2}
				ox-1	1-2	2-s	
0	1	41	80	2	3	2	1.1
	2	56	86				1.1
1.25	1	43	78	5	4	9	1.3
	2	64	89				1.0
2.5	1	51	78	2	3	3	1.5
	2	62	89				0.9

Table 3.22: Layer parameters for the 2-layer model of d-MBP adsorption in H_2O. Data is shown in figure (3.27).

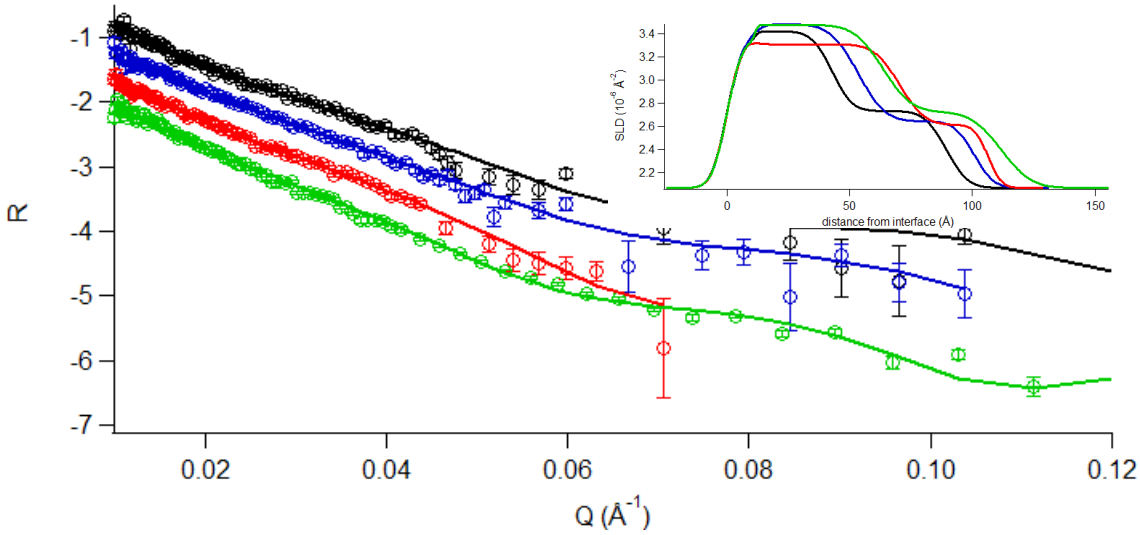


Figure 3.28: Reflectivity profiles and fits showing the changes over time for adsorption of d-MBP in CMSi using a 2-layer model. The runs shown are $t_{inc} = 0$ (black), $t_{inc} = 2$ hours (red), $t_{inc} = 4$ hours (blue) and $t_{inc} = 13$ hours (green). The inset shows the scattering length density profiles and the layer parameters are in table (3.23).

t_{inc} \hrs	Layer number	Thickness \±2 Å	% Solvent ±4	Roughness			Γ \±0.2 mg m^{-2}
				ox-1	1-2	2-s	
0	1	32	71	1	7	7	1.3
	2	47	86				0.9
2	1	42	69	4	9	6	1.8
	2	47	88				0.8
4	1	59	73	3	8	4	2.2
	2	36	88				0.6
13	1	52	69	1	9	10	2.2
	2	48	86				0.9

Table 3.23: Layer parameters for the 2-layer model of d-MBP adsorption in CMSi. Data is shown in figure (3.28).

The 2-layer model is an improved fit for this system with χ^2 values decreasing in all but two of the runs shown and in some cases the improvement is up to 50%. To an extent this is to be expected given that the fitting program can vary more parameters and should find an improved fit on an individual basis. In order to asses whether the 2-layer model provides any further insight the collective set of data must be looked at. There are numerous reflectivity profiles taken after different incubation times and under two different water contrasts and in every case the 2-layer model is consistent; the inner layer (adjacent to the surface) has a higher volume fraction of protein than the outer layer and the individual layers all have thicknesses comparable to the solution dimensions of the protein. This agreement over all the measured reflectivity profiles suggests that the 2-layer model is an accurate interpretation of the adsorbed protein layer. This is also in good agreement with the models proposed for CA II and LYS in previous sections. The thickness of the inner layer varies from 32 to 50 Å and the overall thickness from 85 to 113 Å. The wider range in the total thickness is a consequence of the more diffuse nature of the outer layer which results in a less accurate determination of the thickness of the layer. The inner layer proteins are adsorbed in a variety of orientations with most being in a tilted orientation between side-on and end-on. It is difficult to draw any firm conclusions about the orientation of the proteins in the outer layer given the wide range of values for the thickness as well as the diffuse nature of the adsorbed layer. It should also be noted that although this is a 2-layer model, it is not necessarily the case that the individual layers represent a "one protein layer" i.e. some proteins may span both layers as a result of having a different adsorption orientation of neighbouring

proteins or due to varying degrees of penetration into the inner layer by an adsorbed protein in the outer layer.

3.4.3 Mixture of h- and d-MBP in CMSi

The adsorption of a 50:50 w/v mixture of the perdeuterated and protonated forms of MBP in CMSi was investigated. The determination of the layer thickness and solvent percentage is complicated by the factor that the SLD of the protein is unknown due to it being a mixture of the h- and d-MBP forms. The overall SLD of the adsorbed layer is given by the equation

$$\rho_{layer} = \phi_p \rho_p + (1 - \phi_p)\rho_w \tag{3.1}$$

which for CMSi as the solvent can be rearranged to give

$$\rho_{layer} = \phi_p(\rho_p - 2.07) + 2.07 \tag{3.2}$$

Thus, for a given value of ρ_{layer} there can be a variety of possible combinations of ϕ_p and ρ_p that will satisfy equation (3.2). However, by comparison with the results for h-MBP and d-MBP adsorption described above it may be possible to discount some of these mathematically satisfactory solutions in preference of one that is most physically realistic.

An alternative approach is to fix the value (or, at least restrict the range of the parameter during the fitting process) of ρ_p based on some assumptions about the ratio of h:d in the layer. Three scenarios were investigated: equal adsorption (ρ_p=4.33), h-MBP dominant ($2.2 \leq \rho_p \leq 4.3$) and d-MBP dominant ($4.4 \leq \rho_p \leq 6.47$). The resultant layer parameters are shown in table (3.24) below.

t_{inc} \hrs	SLD of layer \x$10^{-6}$ Å^{-2}	Thickness \±2 Å	% Solvent ±4	Roughness		Γ \±0.2 mg m^{-2}
				ox-1	1-s	
0	4.33	71	64	1	10	3.4
3.5	4.33	62	55	2	10	3.7
13.5	4.33	63	53	3	10	3.9
0	3.1	73	19	4	9	7.7
3.5	3.1	63	2	2	10	8.0
13.5	3.5	63	25	5	10	6.1
0	5.2	64	73	4	8	2.3
3.5	5.7	67	73	2	6	2.4
13.5	5.5	64	69	5	8	2.7

Table 3.24: Layer parameters for the adsorption of a 50:50 mixture of d-MBP and h-MBP using a 1-layer model with 3 adsorption scenarios (see text for detail).

In order to decide which of these models is accurate the most useful information is the adsorbed amount. When h- and d-MBP are considered in isolation the average adsorbed amounts observed for the 1-layer models are 1.1 mg m^{-2} for h-MBP and 2.3 mg m^{-2} for d-MBP. The first two adsorption scenarios (equal and h-dominant) both give higher adsorbed amounts than these averages which are in much better agreement with the third scenario (d-dominant). The variation of adsorbed amount when changing the proportion of d-MBP in the adsorbed layer is shown below in figure (3.29).

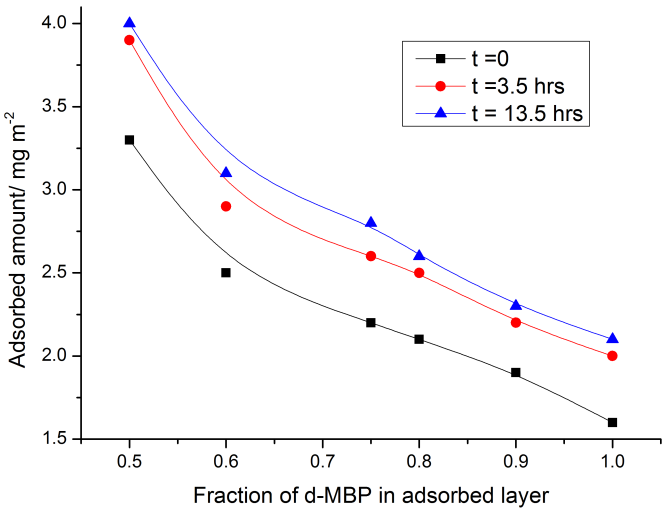


Figure 3.29: Effect on adsorbed amount with varying the proportion of d-MBP in the model. (Lines have been drawn to guide the eye.)

By comparison of these adsorbed amounts and those of the h- and d-MBP variant data sets, the most likely scenario is that d-MBP is dominant in the adsorbed layer but that accurate determination of the ratio is not possible given the uncertainty in the value of the adsorbed amounts. There are also two other sources of error which compound the problem; the possibility that the adsorbed amount and/or ratio is changing over time and the possibility that the h- and d-forms are not uniformly distributed throughout the layer. Further investigation including more data sets at different times and under different water contrasts would be required to more accurately determine the h:d ratio.

It has already been shown in section (3.3.3) that a mixture of d- and h-HSA adsorb in an approximate ratio of 3:1 and if this same ratio is applied to the MBP mixture, $\rho_p = 5.4$. The reflectivity profiles were fitted assuming this adsorption ratio and are shown in figure (3.30) with the layer parameters given in (3.25).

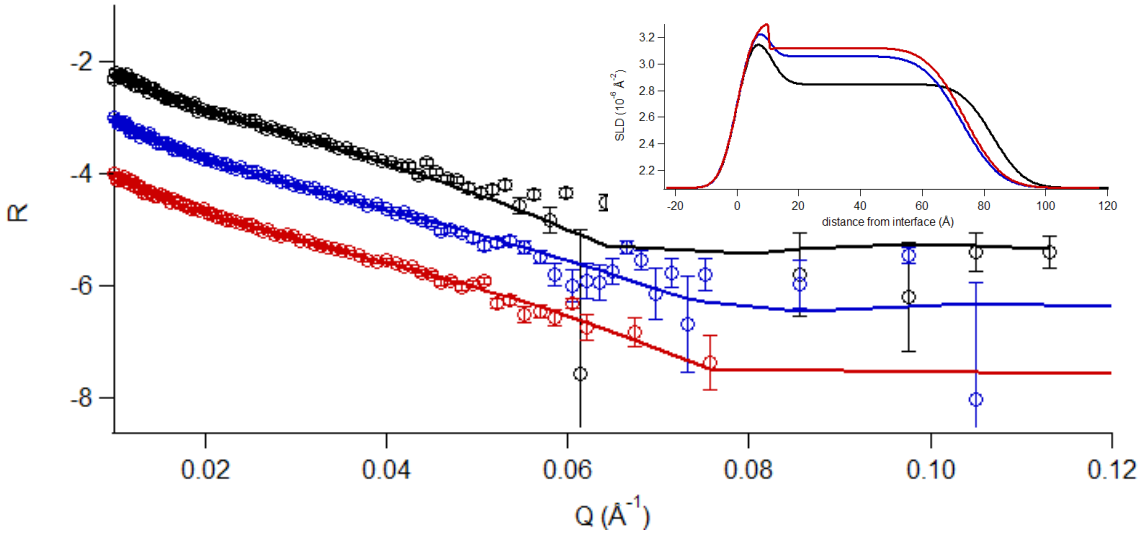


Figure 3.30: Reflectivity profiles and fits showing the changes over time for adsorption of d-MBP/h-MBP mixture in CMSi using a 1-layer model and assuming an adsorption ratio of 3:1. The runs shown are $t_{inc} = 0$ (black), $t_{inc} = 2$ hours (red) and $t_{inc} = 4$ hours (blue). The inset shows the scattering length density profiles and the layer parameters are in table (3.25).

The thicknesses and adsorbed amount are in agreement with the 1-layer models describing d-MBP in H_2O. As with the d-MBP and h-MBP 1-layer models the layer thickness is greater than the long axis of the MBP molecule and, if the same methodology were to be followed, the data would be subjected to analysis using a 2-layer model. In this case, however, given the uncertainties that have been outlined above for a 1-layer model, any conclusions drawn from fits to a 2-layer model would be speculative and would not add to the overall discussion.

t_{inc} \hrs	Thickness \±2 Å	% Solvent ±4	Roughness		Γ \±0.2 mg m^{-2}
			ox-1	1-s	
0	61	74	2	9	2.1
2	67	71	3	1	2.5
4	65	69	2	4	2.7

Table 3.25: Layer parameters for the adsorption a d-MBP/h-MBP mixture in CMSi assuming 3:1 (d:h) adsorption ratio. Data is shown in figure (3.30).

3.4.4 Effect of incubation time on the desorption of d-MBP

The effect of the incubation time on the desorption of d-MBP was investigated by replacing the bulk solution with protein-free buffer after elapsed times of 2 min, 30 min, 1.5 hrs and 4 hrs. The adsorbed layers were characterised for up to 22 hours after the removal of the protein from the bulk solution. The reflectivity profiles, fits and layer parameters can be seen in Appendix B. They are not included here as there are no features of particular interest that have not been discussed elsewhere. The main interest in studying the desorption of d-MBP lies in ascertaining the rate of desorption and the amount of protein that is irreversibly adsorbed. Figures (3.31) and (3.32) below shows the change in adsorbed amount after replacement of the bulk solution (taken as t=0) for the 1-layer and 2-layer models respectively.

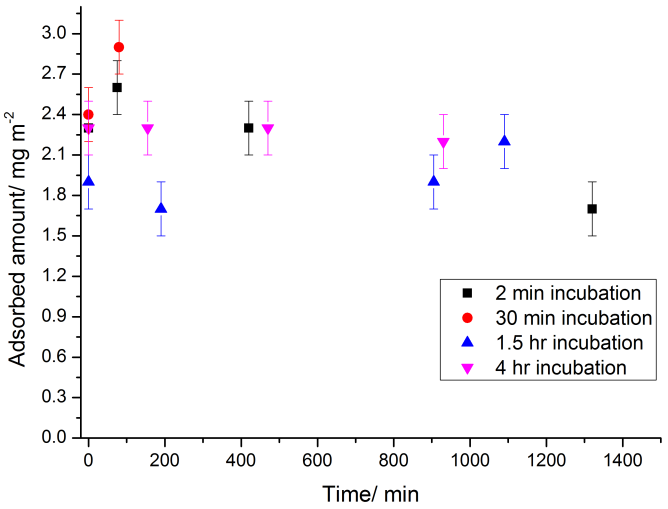


Figure 3.31: The desorption of d-MBP with time. t=0 on the x-axis is defined as the time of bulk solution replacement. Analysed using a 1-layer model.

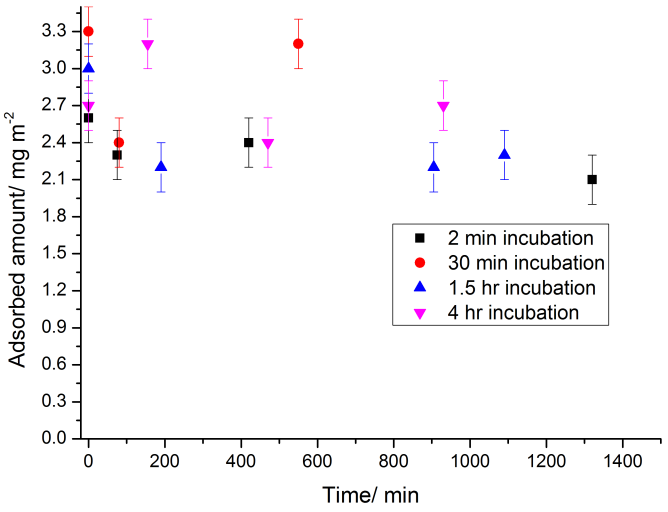


Figure 3.32: The desorption of d-MBP with time. t=0 on the x-axis is defined as the time of bulk solution replacement. Analysed using a 2-layer model.

For both the 1- and 2-layer models it can be seen that, even for the shortest incubation time of 2 minutes, almost all of the protein remains attached to the surface even after more than 20 hours have elapsed since the exchange of the protein solution for protein free buffer. There also appears to be no apparent trend in the effect of incubation time. A similar result has been reported by van der Veen et al.[6] who showed that after an incubation time of 20 minutes, any increase in incubation time had no appreciable effect on the proportion of desorbed protein. It is likely that the same effect is occurring for d-MBP in these experiments but the incubation time at which this transition occurs is much less than 20 minutes. In order for the desorption of proteins to occur all the attachments to the surface must be broken at the same time. Even if each link is of the order of kT the overall interaction energy of multiple attachments to the surface results in a very high activation energy for the desorption of a protein molecule [26].

3.4.5 Self exchange

Even though the proteins do not desorp to any great extent when exposed to protein free buffer, it is known from studies of protein mixtures that exchange of the incumbent proteins does occur [27]. To compare the exchange with the pure desorption process discussed in the previous section the rate of exchange for the protonated

form of the protein was investigated. The important feature of this is the changing ratio of h:d variants of the protein. As the d-MBP is replaced by the h-MBP the scattering length density of the adsorbed layer will decrease, as is the case with desorption of the protein i.e. it is not possible to distinguish between exchange of the proteins from an increase in the solvent percentage. If both the solvent percentage and protein scattering length density parameters were allowed to vary during the fitting process the resultant layer parameters would not be of much use. Instead, the exchange process is monitored by using fixed models where the only variable parameters are the scattering length density and the layer roughness.

The simplest case is using a 1-layer model with fixed values for the solvent percentage and thickness. For the 1-layer model, a thickness of 75 Å with 75 % solvent was used as it showed the most consistently acceptable fis when applied to all the single protein reflectivity profiles for both h- and d-MBP and the 50:50 mixture. The change in scattering length density over time for the various incubation times is shown below in figure (3.33).

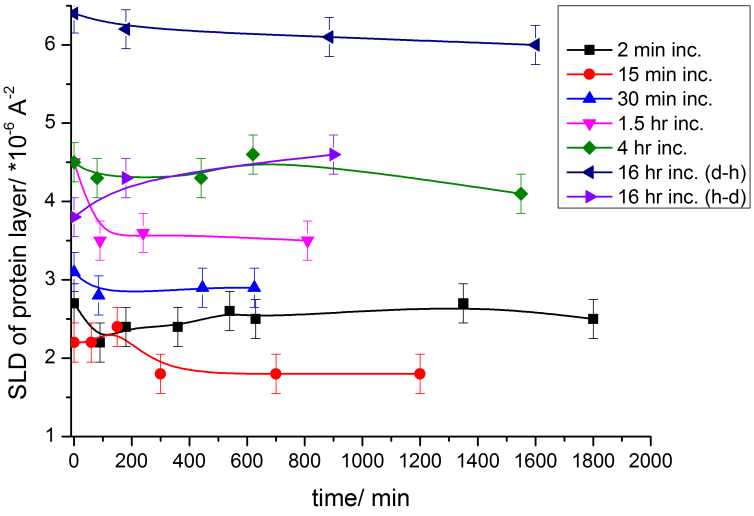


Figure 3.33: Variation of protein scattering length density over time ($t = 0$ refers to the time of exchanging the bulk solutions) with a fixed 1-layer model of $\tau = 75$ Å and solvent % = 75 %. (Lines have been drawn to guide the eye.)

The overall trend is that the extent of exchange increases with decreasing incubation times. This indicates that as time is progressing the number of MBP molecules that are irreversibly bound with respect to exchange is increasing. It can also be

seen that the majority of exchange occurs within the time it takes to record one reflectivity profile i.e. within the first few minutes after the exchange of the bulk solutions. After this initial period, exchange still occurs but at a much slower rate. Thus, the proteins on the surface could be classified into three different types based on their propensity for exchange; readily exchanged, exchangeable on intermediate timescales and irreversibly bound. In the case of the shortest incubation times (30 minutes and less), eventually up to 90 % of the perdeuterated form of the protein is exchanged for the protonated form.

This is in marked contrast to the results for desorption of the d-MBP discussed in section 3.4.4 whereby the d-MBP is almost all irreversibly bound to the silica surface. It is thus plausible to conclude that the protein molecule approaching the surface in some way actively displaces the resident protein molecule and that the rate of this exchange depends on the residence time of the incumbent protein on the surface. This is in contrast to an exchange mechanism consisting of a stepwise process consisting of desorption followed by re-adsorption in the vacant site. A theoretical model of multiple states developed by Szollosi et al.[28] proposes a mechanism whereby the adsorbed protein spreads out over time to increase its number of attachments to the surface. Exchange occurs by the adsorption of an incoming protein inducing the pre-adsorbed protein to be "ratcheted" up to smaller footprints before being expelled. This results in a higher rate of removal of the pre-adsorbed protein when compared to the scenario of desorption into protein-free buffer and also provides a mechanism whereby the rate of exchange is decreased due to longer incubation times. The longer the incubation time the more spreading that has occurred and thus the greater the activation energy required to remove the incumbent protein. This is in good agreement with our experimental findings; as time progresses the number of proteins that are readily exchangeable is decreasing whilst the proportion of irreversibly bound and exchangeable on intermediate timescales is increasing.

For the longest incubation time, 16 hours, the "d-then-h" and "h-then-d" exchanges were compared. When the perdeuterated form was initially adsorbed onto the surface, the "d-h" scenario, the scattering length density of the protein layer after nearly 27 hours is 5.9×10^{-6}Å^{-2} which corresponds to a d:h ratio of approximately 5:1. However, in the "h-d" case, the final $\rho_{protein} = 4.6 \times 10^{-6}$Å^{-2}; a d:h ratio of 3:2. This demonstrates that d-MBP more easily displaces h-MBP than *vice versa*.

As with the adsorption of only h- or d-MBP, a layer thickness of 75 Å is greater than the long axis of the molecule and so a 2-layer model is used. In some cases, there were measurements made of the protein layer before the replacement of the bulk solution and in these data sets, the thicknesses and solvent percentages were fixed at the same values as for the last run before the exchange occurred. For the shorter incubation times, however, it was not possible to characterise the adsorbed layer before the exchange occurred. In these cases (incubation times of 2 and 15 minutes) a 2-layer model was fitted to the data for the first reflectivity profile taken after the exchange of the bulk solutions. The layer parameters used are shown below in table (3.26).

t_{inc}	**Layer number**	**Thickness** \±4 **Å**	**% Solvent** ±4	**Γ** \±0.2 **mg m^{-2}**
2 min	1	41	75	1.4
	2	50	85	1.0
15 min	1	40	77	1.2
	2	37	83	0.8
30 min	1	41	80	1.1
	2	46	87	0.8
1.5 hrs	1	51	73	1.9
	2	57	90	0.8
4 hrs	1	51	78	1.5
	2	62	89	0.9
16 hrs (d-h)	1	52	69	2.2
	2	48	86	0.9
16 hrs (h-d)	1	48	75	1.6
	2	46	90	0.6

Table 3.26: Layer parameters for the 2-layer models of MBP used to monitor the self exchange of the deuterated and protonated protein. (Note: the roughnesses are not shown as these parameters were allowed to vary during the analysis of the exchange.)

When using a 2-layer model to study the exchange process it is necessary to consider the possible exchange scenarios. It has been shown that the outer layer is much more diffuse and likely to be less tightly bound thus, it is plausible that exchange occurs more in this layer than the inner layer. This may also be considered to be increasingly true with longer incubation times of the d-MBP as it will have had the possibility to increase its strength of attachment to the surface. In order to investigate this, two possible exchange mechanisms were modeled; exchange only

occurring in the outer layer and exchange occurring in both layers. The change in the scattering length density of the outer layer over time is shown below in figure (3.34).

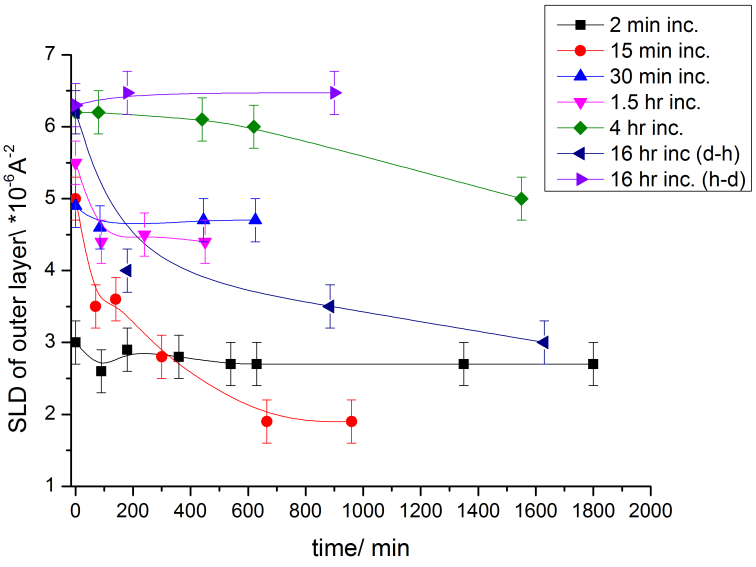


Figure 3.34: Variation of protein scattering length density over time for the outer layer when using a 2-layer model and assuming that exchange is only occurring in the outer layer ($t = 0$ refers to the time of exchanging the bulk solutions; Lines have been drawn to guide the eye.).

This model shows that there is no apparent trend between incubation time and the extent of exchange if it is assumed that this is occurring solely in the outer layer. Although the longest incubation time shows the least extent of exchange the assumption of exchange only occurring in the outer layer is probably also most realistic for this time as the proteins on the surface will have had a great time in which to unfold and create a stronger attachment to the surface. For the shorter times, however, the changes in scattering length density over time follow no trend and in one case, $t_{inc} = 2$ min, this mechanism of exchange would suggest that the proportion of d-MBP in the outer layer is increasing between t_{ex} =180 and 1800 minutes which cannot be the case as d-MBP is no longer present in the bulk solution. However, this scenario only reflects the best possible fits under a quite restrictive range of parameters which can be relaxed to gain a more accurate appraisal of the exchange process.

When the experiments were run in H_2O, as for the short incubation times (up to 4 hours), the theoretical fits when assuming all exchange is occurring in the outer

layer are generally a good fit to the experimental data with χ^2 values of less than 5 for almost all fits. This is not the case for the $t_{inc} = 16$ hrs runs (in CMSi) where the theoretical fits do not match the experimental data unless exchange is assumed to take place in both layers. The fits are compared for the two scenarios in figure (3.35) for both $t_{inc} = 16$ hrs (d-h and h-d) sets and for $t_{inc} = 30$ min, which is a typical example of the data sets taken in H_2O. This shows that the assumption of all exchange occurring in the outer layer is not valid and both layers need to be considered.

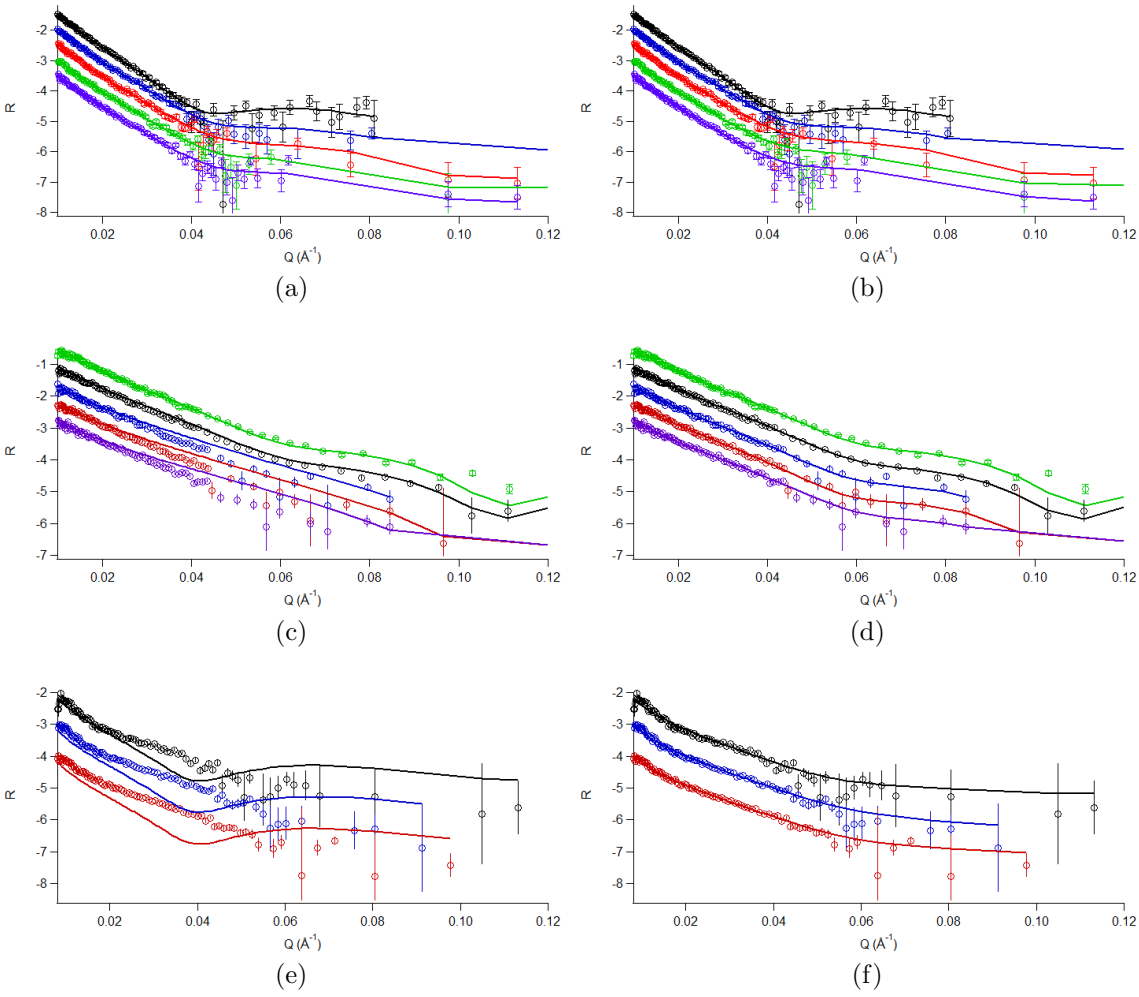


Figure 3.35: Reflectivity profiles and fits comparing the different exchange scenarios for the 2-layer model. (a) $t_{inc} = 30$ min in H_2O with only outer layer exchange. (b) $t_{inc} = 30$ min in H_2O with exchange occurring from both layers. (c) $t_{inc} = 16$ hrs "d-then-h" in CMSi with only outer layer exchange. (d) $t_{inc} = 16$ hrs "d-then-h" in CMSi with exchange occurring from both layers. (e) $t_{inc} = 16$ hrs "h-then-d" in CMSi with only outer layer exchange. (f)$t_{inc} = 16$ hrs "h-then-d" with exchange occurring from both layers. The reflectivity profiles for the other incubation times are shown in Appendix C (figures C.6 and C.7).

The change in scattering length densities for both layers with time is shown below in figure (3.36). The general trend of increasing exchange with incubation time observed above for the 1-layer model is apparent again under this exchange scenario. It can also be seen that there is more exchange from the outer layer than the inner layer for all incubation times with the exception of $t_{inc} = 16$ hrs (d-h). In this case, exchange appears to occur more extensively in the inner layer which is in

contradiction to other conclusions in this chapter. This is most likely caused by the fixed solvent percentage used in the 2-layer model. If during the fitting process the solvent percentage is allowed to vary to be within 5% of the initial model for both layers it is seen that the solvent percentage of the inner layer increases from 69 to 74% and the outer layer reduces from 86 to 84 %. The trend in the scattering length densities is then in good agreement with the other incubation times studies. The final scattering length densities are 5.8 and 5.6×10^{-6}Å^{-2} for the inner and outer layers i.e. the same extent of exchange occurs, within error, for both layers. The other slight anomaly is that there is more extensive exchange for the outer layer for $t_{inc} = 1.5$ hrs than $t_{inc} = 15$ and 30 mins. This is also likely to be due to a greater change in the solvent percentage of the outer layer in 2-layer model used. If the proportion of the solvent in the layer is increasing then this will result in an overall decrease in the scattering length density of the layer. It is assumed in the analysis here that the solvent percentage is constant and that the only change in scattering length density is due to exchange of the d-MBP for h-MBP.

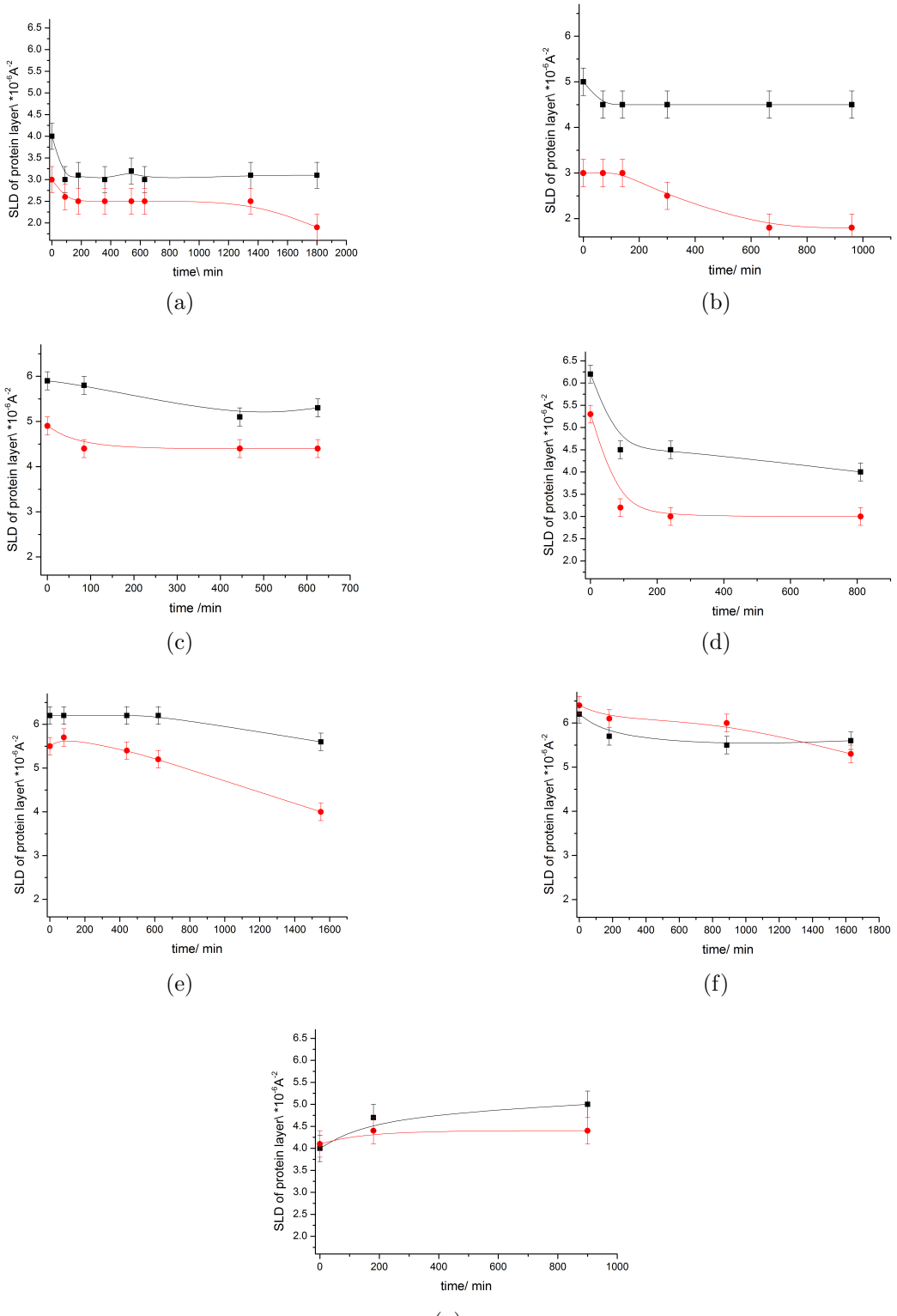


Figure 3.36: Change in scattering length density over time with t=0 on the x-axis defined as when the exchange of bulk solutions occurred. Red = top layer and black = bottom layer. (a) t_{inc} = 2 min, (b) t_{inc} = 15 min, (c) t_{inc} = 30 min, (d) t_{inc} = 1.5 hrs, (e) t_{inc} = 4 hrs, (f) t_{inc} = 16 hrs (d-h) and (g) t_{inc} = 16 hrs (h-d). (Lines have been drawn to guide the eye.)

3.5 Discussion

3.5.1 Comparison of different protonated proteins

A good basis for comparing the adsorption of different proteins and the governing driving forces is the adsorbed amount. For the protonated proteins (deuterated will be considered later in the discussion) the general trend is that the order of the adsorbed amount is CA II, LYS >MBP, HSA. As has been mentioned previously, there is a wider range of observed amounts for HSA and also some differences occur due in different solvents but the underlying trend follows that from what would be expected from an electrostatic description. Under the experimental condition used MBP and HSA both have IEP<pH and thus carry a net negative charge which will cause the proteins to be repelled away from the negatively charged surface and require an excess of counterions to be adsorbed to neutralise the negative charge. LYS is positively charged and will be attracted to the surface but the possibility of lateral repulsion will reduce the overall adsorbed amount predicted from protein-surface interactions alone[8]. Similarly, for CA II the net neutral charge reduces the lateral repulsion and it is a commonly observed feature of protein adsorption that adsorption is greatest when the pH is equal to the IEP of the protein[29, 30, 31, 32, 33]. The main driving force for the adsorption of CA II is entropic in nature and likely to be mostly due to the dehydration of the interface as it is considered to be a rigid protein and does not undergo any significant structural unfolding. The adsorption of HSA to silica has been shown to be endothermic[34] but is less rigid than CA II and will have the added entropic contribution of increased rotational freedom of the polypeptide backbone when unfolding upon adsorption.

Most of the adsorbed layers have qualitatively the same characteristics when comparing the 2-layer models; a denser inner layer and a thicker, more diffuse outer layer which is representative of a loosely bound second protein. The exception is LYS which does not so readily form a second layer due to the repulsion of the positively charged adsorbed first layer repelling any incoming protein. The 2-layers do not commonly fit to the dimensions of the proteins when in solution which suggests that both layers are comprised of a variety of differently orientated proteins and also likely is some degree of inhomogeneity in different areas of the surface which would show this.

3.5.2 Comparison of protonated and deuterated proteins

When comparing the adsorption of the perdeuterated and protonated forms of HSA, it can be seen that when using a 1-layer model the thickness is generally less for d-HSA. This is also true when comparing the inner layers of the 2-layer models. As stated previously, HSA is a flexible protein and undergoes some degree of unfolding or spreading after adsorption onto a surface. Various studies have shown that perdeuteration of proteins results in a decrease in their thermal stability [35, 36, 37, 38] but do not change their tertiary structure or enzymatic ability. The reduced stability suggests that the perdeuterated forms of proteins will be more likely to unfold or spread upon adsorption at an interface which is in agreement with our observations and with Brockwell et al. who state that even if a protein is not markedly different from its protonated counterpart both the global unfolding equilibrium and the activation barriers for transient local unfolding fluctuations are reduced on perdeuteration[36]. It is also possible that the perdeuterated proteins will not fold correctly when being expressed. This would result in a more hydrophobic exterior and a resultant increase in the driving force for adsorption of dehydration of the protein surface. The mis-folded proteins could also be less stable and prone to conformational changes after adsorption to further increase their attachment to the surface. The isotope effect on the stability is likely to be the more important of these factors as anecdotal evidence suggests that mis-folding is not a commonly observed phenomena as the deuterated forms crystallise under similar conditions to protonated proteins[39].

When comparing the two forms of MBP, the overall thickness are similar but h-MBP has a thinner bottom layer and a more diffuse, thicker outer layer. This results in a higher adsorbed amount for d-MBP ($\Gamma_{average}$ = 2.3 mg m^{-}2 compared to 1.1 mg m^{-}2 for h-MBP) suggesting the deuteration provides an additional driving force for the adsorption particularly in the formation of a second layer. The increase in molecular weight due to the isotopic substitution is only 5% and so can not account for the magnitude of the increase that is observed. It has been shown that deuteration of proteins often leads to the promotion of dimer association[36] or the formation of a collection of oligiomers not seen for the protonated proteins[35]. The adsorption of insulin onto hydrophilic silica only occurs at a high enough concentration and when oligomers are present[40]. Both the formation of a denser outer layer upon adsorption and association in the bulk solution would involve the

same protein-protein interactions. It has been shown for some proteins, insulin and β-lactoglobulin, that dimerisation occurs via shared β-sheets where H-bonding is important[41] and given that HSA contains no β-sheets whereas MBP's secondary structure has approximately 20% β-sheets[42] this could also explain why the effect is more noticeable for MBP than HSA.

When considering the mixture both the isotope effects for individual proteins and the possibility that more dimers or trimers are formed could impact on the adsorption. The rate of arrival to the surface will not necessarily be the same for both but even assuming they have reached the surface in an equal ratio the deuterated form will bind more strongly and be more resistant to subsequent exchange processes. The approximate 3:1 ratio of d-HSA:h-HSA and d-MBP:h-MBP thus reflects both the difference in stability of the two forms and the increased likelihood of association of protein monomers. The reduced stability is perhaps of more importance when in the mixture as the formations of mixed (h + d) oligomers could also be enhanced. This is in good agreement with the work of Lee et al.[43] that, in otherwise very similar LYS mutant variants, the less stable variants exhibited an advantage in competitive adsorption.

References

[1] S. Lindman, I. Lynch, E. Thulin, H. Nilsson, K. A. Dawson, and S. Linse, "Systematic investigation of the thermodynamics of HSA adsorption to N-iso-Propylacrylamide/ N-tert-Butylacrylamide compolymer nanoparticles. Effects of particle size and hydrophobicity," *Nano Letters*, vol. 7 (4), pp. 914–920, 2007.

[2] C. M. Cuppett, L. J. Doneski, and M. J. Wirth, "Irreversible adsorption of lysozyme to polishing marks on silica," *Langmuir*, vol. 16, no. 18, pp. 7279–7284, 2000.

[3] R. D. Tilton, *Surfactant Science Series Volume 110: Biopolymers at Interfaces (2nd ed.)*, ch. 9. Mobility of Biomolecules at Interfaces, pp. 221–257. Marcel Dekker, Inc., 2003.

[4] O. Svensson and T. Arnebrant, "Adsorption of serum albumin on silica - the influence of surface cleaning procedures," *Journal of Colloid and Interface Science*, vol. 344, no. 1, pp. 44 – 47, 2010.

[5] J. Penfold, E. Staples, and I. Tucker, "On the consequences of surface treatment on the adsorption of nonionic surfactants at the hydrophilic silica-solution interface," *Langmuir*, vol. 18, no. 8, pp. 2967–2970, 2002.

[6] M. van der Veen, M. C. Stuart, and W. Norde, "Spreading of proteins and its effect on adsorption and desorption kinetics," *Colloids and Surface B: Biointerfaces*, vol. 54, pp. 136–142, 2007.

[7] T. J. Su, J. R. Lu, R. K. Thomas, Z. F. Cui, and J. Penfold, "The effect of solution pH on the structure of lysozyme layers adsorbed at the silica-water interface studied by neutron reflection," *Langmuir*, vol. 14, pp. 438–445, 1998.

[8] T. J. Su, J. R. Lu, R. K. Thomas, Z. F. Cui, and J. Penfold, "The adsorption of lysozyme at the silica-water interface: A neutron reflection study," *Journal of Colloid and Interface Science*, vol. 203, pp. 419–429, 1998.

[9] G. Jackler, R. Steitz, and C. Czeslik, "Effect of temperature on the adsorption of lysozyme at the silica/water interface studied by optical and neutron reflectometry," *Langmuir*, vol. 18, no. 17, pp. 6565–6570, 2002.

[10] R. Kurrat, J. E. Prensoil, and J. J. Ramsden, "Kinetics of human and bovine serum albumin adsorption at silicatitania surfaces," *Journal of Colloid and Interface Science*, vol. 185, pp. 1–8, 1997.

[11] J. R. Lu, T. J. Su, and J. Penfold, "Adsorption of serum albumins at the air/water interface," *Langmuir*, vol. 15, no. 20, pp. 6975–6983, 1999.

[12] J. R. Olivieiri and A. F. Craievich, "The subdomain structure of human serum albumin in solution under different pH conditions studied by small angle X-ray scattering," *European Biophysics Journal*, vol. 24, pp. 77–84, 1995.

[13] O. J. Bos, J. F. Labro, M. J. Fischer, J. Wilting, and L. H. Janssen, "The molecular mechanism of the neutral-to-base transition of human serum albumin. Acid/base titration and proton nuclear magnetic resonance studies on a large peptic and a large tryptic fragment of albumin.," *Journal of Biological Chemistry*, vol. 264, no. 2, pp. 953–959, 1989.

[14] D. Forciniti and W. A. Hamilton, "Surface enrichment of proteins at quartz/water interfaces: A neutron reflectivity study," *Journal of Colloid and Interface Science*, vol. 285, pp. 458–468, 2005.

[15] X. M. He and D. C. Carter, "Atomic structure and chemistry of human serum albumin," *Nature*, vol. 358, pp. 209–215, 1992.

[16] J. R. Lu, X. Zhao, and M. Yaseen, "Protein adsorption studied by neutron reflection," *Current Opinion in Colloid & Interface Science*, vol. 12, pp. 9–16, 2007.

[17] S. J. Perkins, "Chapter 6 X-ray and neutron solution scattering," in *Modern Physical Methods in Biochemistry* (A. Neuberger and L. van Deenen, eds.), vol. 11, Part 2 of *New Comprehensive Biochemistry*, pp. 143 – 265, Elsevier, 1985.

[18] E. A. Vogler, "Protein adsorption in three dimensions," *Biomaterials*, vol. 33, pp. 1201–1237, 2012.

[19] A. Krishnan, C. A. Siedlecki, and E. A. Vogler, "Traube-rule interpretation of protein adsorption at the liquid-vapor interface," *Langmuir*, vol. 19, no. 24, pp. 10342–10352, 2003.

[20] H.-J. Hsu, S.-Y. Sheu, and R.-Y. Tsay, "Preferred orientation of albumin adsorption on a hydrophilic surface from molecular simulation," *Colloids and Surfaces B: Biointerfaces*, vol. 67, no. 2, pp. 183 – 191, 2008.

[21] S. Curry, P. Brick, and N. P. Franks, "Fatty acid binding to human serum albumin: new insights from crystallographic studies," *Biochimica et Biophysica Acta*, vol. 1441, pp. 131–140, 1999.

[22] S. J. McClellan and E. I. Franses, "Mechanisms of competitive adsorption of albumin and sodium myristate at the silicon oxide/aqueous interface," *Langmuir*, vol. 21, pp. 10148–10153, 2005.

[23] P. Cioni and G. B. Strambini, "Effect of heavy water on protein flexibility," *Biophysical Journal*, vol. 82, pp. 3246–3253, 2002.

[24] R. K. Thomas, "Neutron reflection from liquid interfaces," *Annual Review of Physical Chemistry*, vol. 55, pp. 391–426, 2004.

[25] J. L. Wehmeyer, R. Synowicki, R. Bizios, and C. D. Garcia, "Dynamic adsorption of albumin on nanostructured TiO_2 thin films," *Materials Science and Engineering C*, vol. 30, pp. 277–282, 2010.

[26] D. Sarkar and D. Chattoraj, "Activation parameters for kinetics of protein adsorption at silica-water interface," *Journal of Colloid and Interface Science*, vol. 157, no. 1, pp. 219 – 226, 1993.

[27] V. Ball, P. Schaaf, and J.-C. Voegel, *Surfactant Science Series Volume 110: Biopolymers at Interfaces (2nd ed.)*, ch. 11. Mechanisms of Interfacial Excahnge Phenomena for Proteins Adsorbed at Solid-Liquid Interfaces, pp. 295–320. Marcel Dekker, Inc., 2003.

[28] G. Szollosi, I. Derenyi, and J. Voros, "Reversible mesoscopic model of protein adsorption: From equilibrium to dynamics," *Physica A*, vol. 343, pp. 359–375, 2004.

[29] T. J. Su, J. R. Lu, R. K. Thomas, and Z. F. Cui, "Effect of pH on the adsorption of bovine serum albumin at the silica/water interface studied by neutron reflection," *The Journal of Physical Chemistry B*, vol. 103 (18), pp. 3727–3736, 1999.

[30] M. G. Bremer, J. Duval, W. Norde, and J. Lyklema, "Electrostatic interactions between immunoglobulin (IgG) molecules and a charged sorbent," *Colloids and Surfaces A: Physicochemical and Engineering Aspects*, vol. 250, no. 1-3, pp. 29 – 42, 2004. In honour of the 250th volume of Colloid and Surfaces A and the 25th Anniversary of the International Association of Colloid and Interface Scientists (IACIS).

[31] S. Demanche, J.-P. Chapel, L. J. Monrozier, and H. Quiquampoix, "Dissimilar pH-dependent adsorption features of bovine serum albumin and α-chymotrypsin on mica probed by AFM," *Colloids and Surfaces B: Biointerfaces*, vol. 70, no. 2, pp. 226 – 231, 2009.

[32] F. Hook, M. Rodahl, B. Kasemo, and P. Brzezinski, "Structural changes in haemoglobin during adsorption to solid surfaces: Effects of pH, ionic strength, and ligand binding," *PNAS*, vol. 95, pp. 12271–12276, 1998.

[33] R. Maheshwari and A. Dhathathreyan, "Mucin at solution/air and solid/solution interfaces," *Journal of Colloid and Interface Science*, vol. 293, no. 2, pp. 263 – 269, 2006.

[34] G. A. Kulikova, I. V. Ryabinina, S. S. Guseynov, and E. V. Parfenyuk, "Calometric study of adsorption of human serum albumin onto silica particles," *Thermochemica Acta*, vol. 503-504, pp. 65–69, 2010.

[35] G. Piszczek, J. C. Lee, N. Tjandra, C.-R. Lee, Y.-J. Seok, R. L. Levine, and A. Peterkofsky, "Deuteration of Escherichia coli enzyme INtr alters its stability," *Archives of Biochemistry and Biophysics*, vol. 507, pp. 332–342, 2011.

[36] D. Brockwell, L. Yu, S. Cooper, S. Mccleland, A. Cooper, D. Attwood, S. J. Gaskell, and J. Barber, "Physicochemical consequences of the perdeuteriation of glutathione S-transferase from S. japonicum," *Protein Science*, vol. 10(3), pp. 572–580, 2001.

[37] F. Meilleur, J. Contzen, D. Myles, and C. Jung, "Structural stability and dynamics of hydrogenated and perdeuterated cytochrome P450cam (CYP101)," *Biochemistry*, vol. 43, pp. 8744–8753, 2004.

[38] A. Hattori, H. L. Crespi, and J. J. Katz, "Effect of side-chain deuteration on protein stability," *Biochemistry*, vol. 4, no. 7, pp. 1213–1225, 1965.

[39] T. Forsyth (private communication).

[40] P. Nilsson, T. Nylander, and S. Havelund, "Adsorption of insulin on solid surfaces in relation to the surface properties of the monomeric and oligomeric forms.," *Journal of Colloid and Interface Science*, vol. 144, pp. 145–152, 1991.

[41] T. Nylander, *Surfactant Science Series Volume 110: Biopolymers at Interfaces (2nd ed.)*, ch. 10. Protein Adsorption in Relation to Solution Association and Aggregation, pp. 259–294. Marcel Dekker, Inc., 2003.

[42] J. C. Spurlino, *The three-dimensional structure of the D-maltose-binding protein from Escherichia coli*. PhD thesis, Rice University, 1988.

[43] W.-K. Lee, J. McGuire, and M. K. Bothwell, "Competitive adsorption of bacteriophage T4 lysozyme stability variants at hydrophilic glass surfaces," *Journal of Colloid and Interface Science*, vol. 269, no. 1, pp. 251 – 254, 2004.

Chapter 4

Results: Sequential adsorption of proteins

In the previous chapter it has been demonstrated that although the proteins are stable with respect to desorption into pure buffer, homogeneous exchange is occurring and that the extent of this exchange is dependent on the incubation time of the protein. The aim of this chapter is to elucidate similar features of this exchange process but with heterogeneous systems whereby the incoming protein is of a different type to the pre-adsorbed layer. It is also necessary to distinguish between the process of exchange, whereby the incumbent protein is displaced by the incoming one, and the formation of a multilayer of different proteins. Ultimately, the biological response of any surface covered in a protein corona is governed by the "seen" surface [1] and the extent of exchange vs multilayer formation to present a mixed layer will be paramount in this regard. Neutron reflectivity has been used by Forciniti and Hamilton to investigate the sequential adsorption of HSA and Fibrinogen and marked differences in the reflectivity profiles were observed[2]. However, this study only used protonated proteins and the effects of varying the incubation time were not investigated.

When analysing sequential adsorption experiments there are two time frames of interest; the incubation time of the first protein (referred to as t_{inc}) and the time after the exposure to the second protein occurred (t_{ex}). In the cases of LYS and MBP interacting with HSA the effect of incubation time has been investigated. In all cases where time allowed reflectivity profiles were recorded for as long as possible after the exposure occurred to investigate the influence of t_{ex} on the subsequent

exchange and/or additional adsorption.

Initially, the interaction of three different proteins (CA II, LYS and MBP) with a pre-adsorbed HSA layer is discussed. The later sections will discuss details of the interaction of HSA with the pre-adsorbed layers of the same three proteins.The stability with respect to homogeneous exchange of h-MBP adsorbed onto an h-HSA layer has also been investigated by a second change in the bulk solution; h-MBP being replaced by d-MBP. This replicates the self-exchange methodology used in Chapter 3 but in the case presented in this chapter the adsorption and exchange is occurring on a pre-adsorbed h-HSA layer rather than a clean and relatively smooth silica surface.

When fitting the reflectivity profiles, the starting point was always the final fit of the pre-adsorbed layer. When this was adequately described using a 1-layer model then a 1-layer model was initially tried for the sequential adsorption profiles also. If the pre-adsorbed layer required a 2-layer model to describe it then a fit was still attempted using a 1-layer model but in all cases these were deemed to be poor fits of the data either in terms of a high χ^2 value or an observed discrepancy between the fit and the data points in a region where the weighting of χ^2 value is low. The 1-layer models are not shown. In all cases a 2-layer model gave good fits to the data.

4.1 Adsorption onto a pre-adsorbed HSA layer

The coating of biomaterials with serum albumin has often been used to reduce unspecific protein adsorption and subsequent platelet adhesion[3]. Although this does have an empirically observed beneficial effect in many cases of reducing the subsequent biological impacts [4, 5, 6], a detailed understanding of the underlying reasons is not apparent and some recent results suggest that the blocking effect of HSA is not universal[7].

4.1.1 CA II

The adsorption of a 1 mg ml^{-1} CA II solution onto a pre-adsorbed h-HSA layer, t_{inc} = 27.5 hours, was investigated. The reflectivity profiles and fits are shown in figure (4.1) with layer parameters in table (4.1). The overall thickness is reduced from 115 ± 4 Å for the final HSA layer up to 112 ± 4 ÅṪhere is also an increase in the adsorbed amount from 1.7 up to 2.7 mg m^{-2}. The additional material is divided

equally between the two layers indicating that the incoming CA II is adsorbing both directly onto the surface and also on top of the pre-adsorbed protein. Given that CA II and HSA both have the same scattering length densities it is not possible to determine whether the additional protein is simply an addition to the HSA or whether any of the HSA is being exchanged. The changes that occur show no long term time dependence i.e. all the changes occur within the timescale of the first measurement.

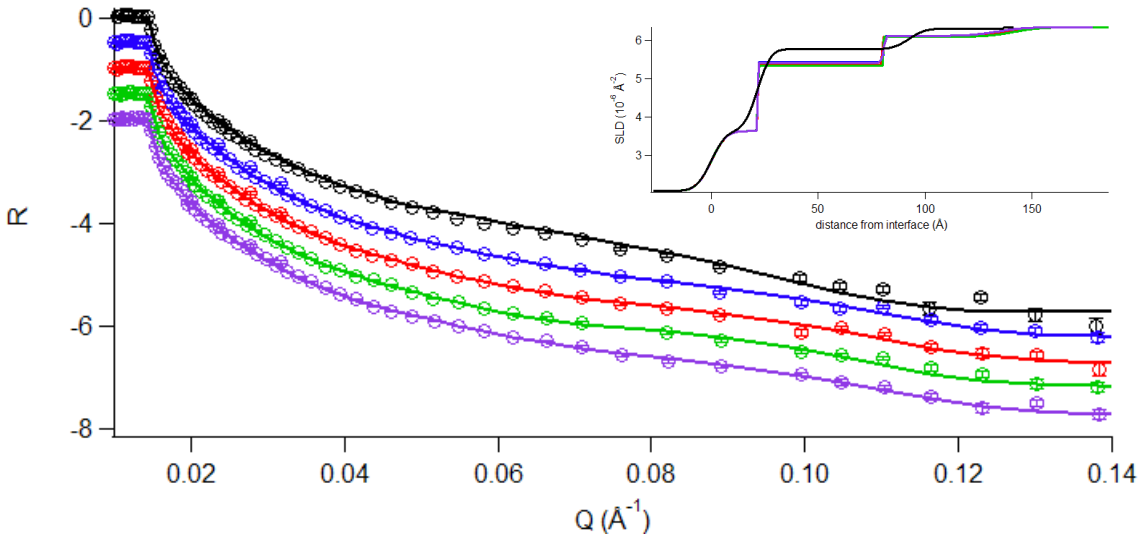


Figure 4.1: Reflectivity profiles and fits showing the changes over time for adsorption of CA II onto a pre-adsorbed HSA layer in D_2O. A 2-layer model was used and the runs are the final HSA, $t_{inc} = 27.5$ hrs (black), $t_{ex} = 0$ (blue), $t_{ex} = 6.5$ hours (red), $t_{ex} = 13$ hours (green) and $t_{ex} = 17$ hours (purple) with data being offset for clarity. The inset shows the scattering length density profiles and the layer parameters are in table (4.1).

t_{ex} \hrs	Layer number	Thickness \±2 Å	% Solvent ±4	Roughness			Γ \±0.2 mg m^{-2}
				ox-1	1-2	2-s	
final HSA	1	71	83	5	9	8	1.6
	2	44	99				0.1
0	1	59	73	0	0	10	2.1
	2	53	93				0.5
6.5	1	58	71	0	0	10	2.2
	2	57	93				0.5
13	1	59	70	0	0	10	2.3
	2	61	93				0.6
17	1	59	72	0	1	10	2.2
	2	53	93				0.5

Table 4.1: Layer parameters for the 2-layer model for the adsorption of CA II onto a pre-adsorbed HSA layer in D_2O. The data is shown in figure (4.1).

4.1.2 LYS

The adsorption of a 1 mg ml^{-1} LYS solution onto a pre-adsorbed HSA layer was investigated with variations in the incubation time (t_{inc}) of the HSA before the exchange of the bulk solution was carried out. The use of h- and d-HSA allows for a more accurate determination of the proportions of each protein in the adsorbed layer and thus the dynamic nature of the exchange/adsorption process can be followed.

In order to investigate the effect of incubation time of h-HSA on exposure to a bulk solution of LYS three different incubation times were studied. The reflectivity profiles for the shortest time (t_{inc} = 1.5 hrs) are shown in figure (4.2) with the layer parameters in table (4.2). The pre-adsorbed HSA layer in the experiment was very diffuse with only 5 % protein in the layer. This is likely to be a result of the short incubation time resulting in weak attachment to the surface or the presence of impurities that hinder the adsorption of HSA. Given the low proportion of HSA the scattering length density during the fitting process was assumed to be equal to that of pure LYS (3.6×10^{-6} Å $^{-2}$). On exposure to the LYS, the resultant layer had a thickness of 43 ±2 Å and a solvent percentage of 52 ±2 %. This is in good agreement with the single protein adsorption scenario discussed in section 3.2 which suggests that with only a short incubation time of HSA this has no impact on the adsorption of LYS.

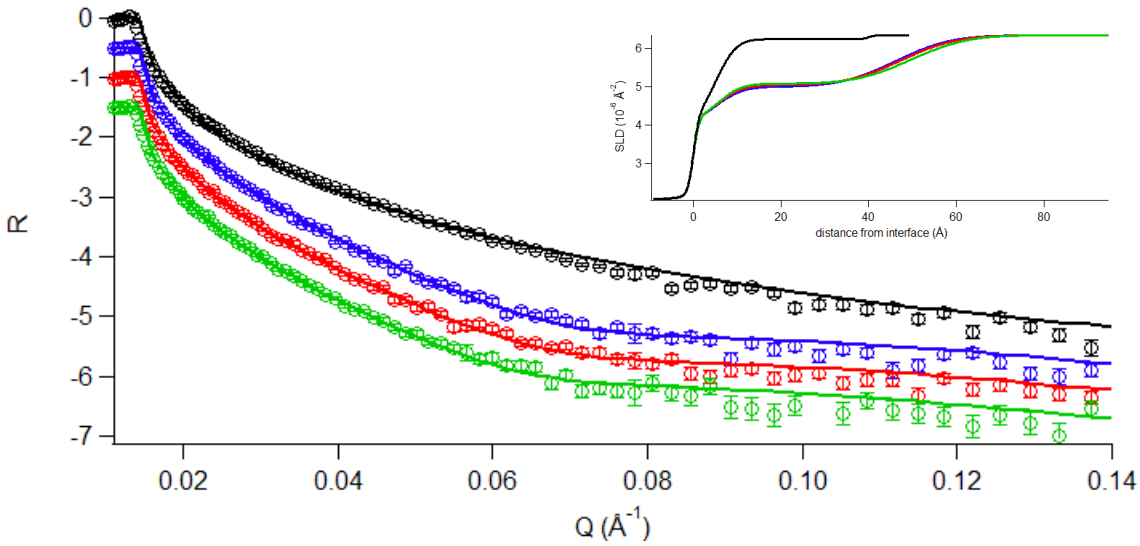


Figure 4.2: Reflectivity profiles and fits showing the changes over time for adsorption of LYS onto a pre-adsorbed HSA layer in D_2O. A 1-layer model was used and the runs are the final HSA, $t_{inc} = 1.5$ hrs (black), $t_{ex} = 0$ (blue), $t_{ex} = 9.5$ hours (red)and $t_{ex} = 15.5$ hours (green) with data being offset for clarity. The inset shows the scattering length density profiles and the layer parameters are in table (4.2).

t_{ex} \hrs	Thickness \±2 Å	% Solvent ±4	Roughness		Γ \±0.2 mg m^{-2}
			ox-1	1-s	
final HSA	35	97	2	1	0.2
0	41	51	5	10	2.6
9.5	43	53	5	10	2.7
15.5	45	54	5	10	2.7

Table 4.2: Layer parameters for the 1-layer model of adsorption of LYS onto a pre-adsorbed h-HSA layer in D_2O ($t_{inc} = 1.5$ hours). The data is shown in figure (4.2)

The reflectivity profiles for the adsorption of LYS onto a pre-adsorbed HSA with $t_{inc} = 3$ hours are shown in figure (4.3) with the layer parameters in table (4.3). The scattering length density of the protein layer was taken as 3.3×10^{-6} Å $^{-2}$ which corresponds approximately to a 50:50 ratio of HSA:LYS. The choice of scattering length density does not have an effect on the thickness of the layer in the model but does alter the solvent percentage and consequently the adsorbed amount. For example, for the final reflectivity profile ($t_{ex} = 9.5$ hours) if it is assumed that all the HSA has been exchanged by this time, the solvent percentages for the 1st and 2nd layers would be 47 % and 85 % respectively (with adsorbed amounts of 3.6

and 0.9 mg m^{-2}). Even when taking into account the error in the scattering length density there is an increase in the adsorbed amount of protein on the surface and this predominantly occurs in the first layer (if $\rho_{protein} = 3 \times 10^{-6}$ Å $^{-2}$ i.e. equal to HSA, $\Gamma = 2.8$ and 0.8 mg m^{-2}).

Attachment of LYS directly onto the surface could occur via exchange of the pre-adsorbed HSA or it is possible that the HSA is preferentially adsorbed in patches and the LYS is filling in the spaces between the HSA. This would act to reduce some of the lateral electrostatic repulsion between the LYS molecules and as a result the adsorbed amount is greater than that observed for the adsorption of LYS onto a clean silica surface. It is not possible to distinguish between these two adsorption regimes with this set of measurements but it is likely that both processes are occurring. Both would show the observed changes; an increased adsorbed amount which is predominantly in the bottom layer. The thicknesses of both layers are comparable with that of the pre-existing HSA layer. This suggests that its presence induces the LYS to form a thick dense inner layer with LYS in an end-on orientation. The final adsorbed amount, 3.9 mg m^{-2}, is greater than any observed in the case of LYS adsorbing onto a clean surface as shown in section 3.2.

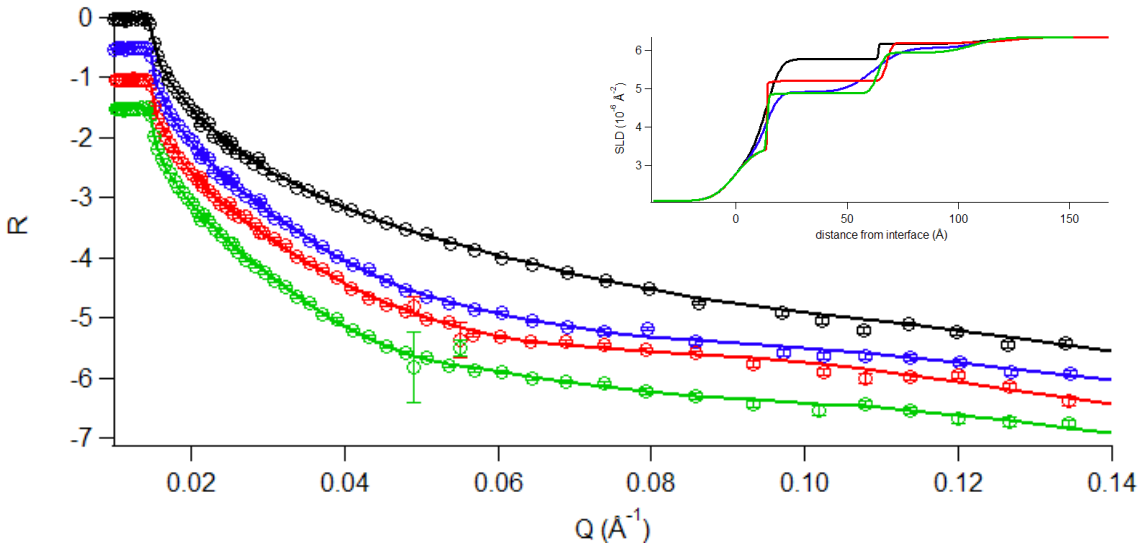


Figure 4.3: Reflectivity profiles and fits showing the changes over time for adsorption of LYS onto a pre-adsorbed HSA layer in D_2O. A 2-layer model was used and the runs are the final HSA, $t_{inc} = 13$ hrs (black), $t_{ex} = 0$ (blue), $t_{ex} = 5.5$ hours (red) and $t_{ex} = 9.5$ hours (green) with data being offset for clarity. The inset shows the scattering length density profiles and the layer parameters are in table (4.3).

t_{ex} \hrs	Layer number	Thickness \±2 Å	% Solvent ±5	Roughness			Γ \±0.4 mg m^{-2}
				ox-1	1-2	2-s	
final HSA	1	50	83	1	5	6	1.1
	2	49	95				0.3
0	1	48	53	5	10	10	3.0
	2	49	91				0.6
5.5	1	54	62	0	8	10	2.7
	2	55	95				0.4
9.5	1	50	52	1	3	10	3.2
	2	43	87				0.7

Table 4.3: Layer parameters for the 2-layer model of adsorption of LYS onto a pre-adsorbed h-HSA layer in D_2O (t_{inc} = 13 hours). The data is shown in figure (4.3)

The reflectivity profiles for the adsorption of LYS onto a pre-adsorbed HSA with an incubation time of 23 hours are shown in figures (4.4) and (4.5) with the corresponding layer parameters in tables (4.4) and (4.5). The scattering length density of the protein layer was taken as 3.3×10^{-6} Å $^{-2}$ which corresponds approximately to a 50:50 ratio of HSA:LYS.

Initially a 1-layer model was used to fit the data and this shows similar results to that of LYS adsorbing onto a clean silica surface or onto a pre-adsorbed HSA layer after t_{inc} = 1.5 hrs. The only difference being that the thickness is slightly greater and more closely resembles that of LYS in an end-on orientation. It can also be seen in figure (4.4) that the fit is not optimal at low Q values. For this reason a 2-layer model was used which decreased the χ^2 values by 10% for all the fits. The 2-layer model is in good agreement with that of the intermediate t_{inc}; an increase in adsorbed amount, mostly in the bottom layer. The overall thickness of ∼130 Å is equal to three LYS molecules in an end-on orientation and it is very diffuse, similar to the pre-existing HSA layer, suggesting that even the loosely bound HSA in this layer is not displaced by the incoming LYS. In this case, the effect of HSA after t_{inc} = 23 hours appears to be inducing LYS to adsorb in a different orientation than when adsorbing onto a clean surface and that the HSA is not significantly displaced. This is similar to the observations made for t_{inc} = 13 hours.

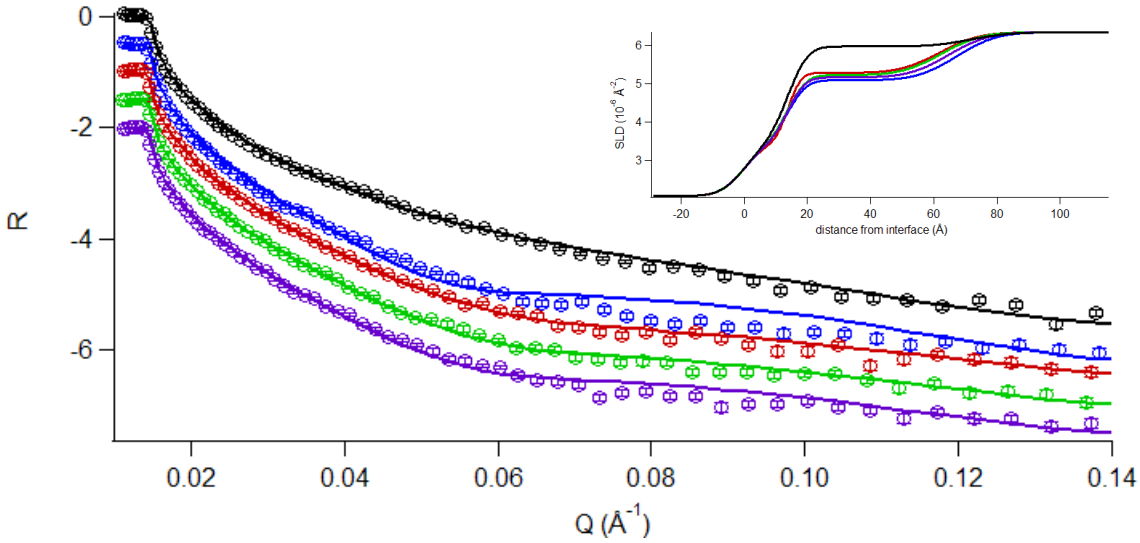


Figure 4.4: Reflectivity profiles and fits showing the changes over time for adsorption of LYS onto a pre-adsorbed HSA layer in D_2O. A 1-layer model was used and the runs are the final HSA, $t_{inc} = 23$ hrs (black), $t_{ex} = 0$ (blue), $t_{ex} = 6$ hours (red), $t_{ex} = 14.5$ hours (green) and $t_{ex} = 21.5$ hours (purple) with data being offset for clarity. The inset shows the scattering length density profiles and the layer parameters are in table (4.4).

t_{ex} \hrs	**Thickness** \±2 **Å**	**% Solvent** ±4	**Roughness**		Γ \±0.3 **mg m^{-2}**
			ox-1	1-s	
final HSA	58	89	5	8	0.8
0	53	59	5	10	2.7
6	48	65	3	9	2.2
14.5	49	63	5	10	2.4
21.5	51	61	4	9	2.6

Table 4.4: Layer parameters for the 1-layer model of adsorption of LYS onto a pre-adsorbed h-HSA layer in D_2O ($t_{inc} = 23$ hours). The data is shown in figure (4.4)

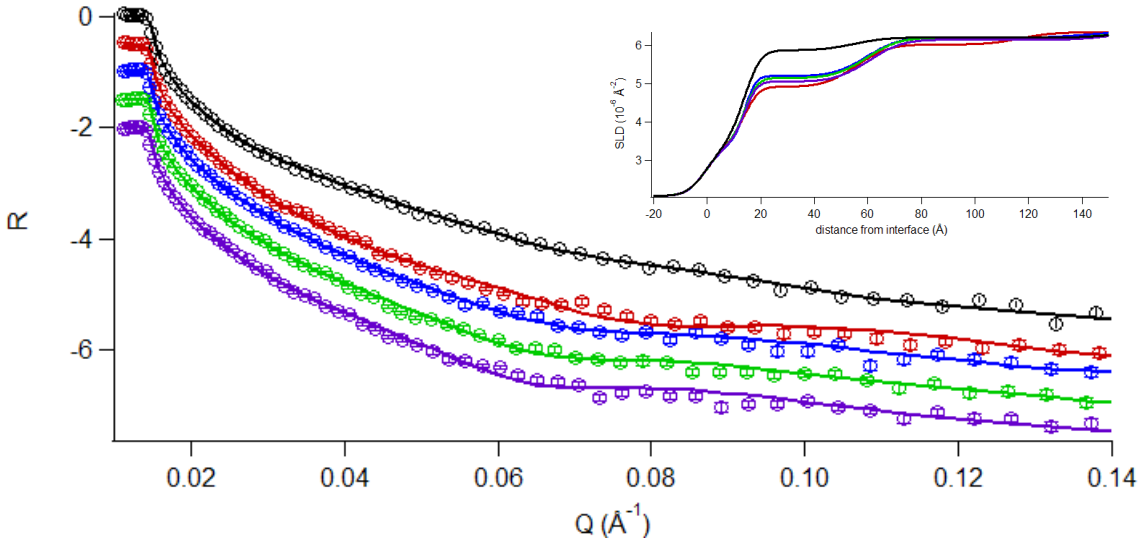


Figure 4.5: Reflectivity profiles and fits showing the changes over time for adsorption of LYS onto a pre-adsorbed HSA layer in D_2O. A 2-layer model was used and the runs are the final HSA, $t_{inc} = 23$ hrs (black), $t_{ex} = 0$ (blue), $t_{ex} = 6$ hours (red), $t_{ex} = 14.5$ hours (green) and $t_{ex} = 21.5$ hours (purple) with data being offset for clarity. The inset shows the scattering length density profiles and the layer parameters are in table (4.5).

t_{ex} \hrs	Layer number	Thickness \±2 Å	% Solvent ±4	Roughness			Γ \±0.3 mg m^{-2}
				ox-1	1-2	2-s	
final HSA	1	41	86	2	5	9	0.8
	2	96	96				0.5
0	1	42	53	5	9	10	2.6
	2	61	90				0.8
6	1	46	63	3	10	10	2.3
	2	81	96				0.4
14.5	1	45	61	4	10	9	2.3
	2	89	95				0.6
21.5	1	46	58	4	9	10	2.6
	2	90	94				0.7

Table 4.5: Layer parameters for the 2-layer model of adsorption of LYS onto a pre-adsorbed h-HSA layer in D_2O ($t_{inc} = 23$ hours). The data is shown in figure (4.5)

Now the effect of incubation time when considering the exchange of protonated proteins has been established it is possible to use this information to determine more accurately the proportions of the individual proteins within the adsorbed layer by using d-HSA instead of h-HSA. Following the same experimental protocol as for protonated case, t_{inc} values of 1 and 24 hours were chosen for the d-HSA before

exposure to the LYS. Two different solvent contrasts were used for each t_{inc} so as to reduce the possibility of non-unique solutions.

For the t_{inc} =1 hour sets, the solvents used were CM5 and H_2O. CM5 was chosen as it is an intermediate value between the two proteins of interest, d-HSA and LYS. The reflectivity profiles for the 1-layer model are shown in figure (4.6) with the layer parameters in table (4.6). In order to determine the scattering length density of the adsorbed protein, and hence the proportions of each protein in the layer, it is initially assumed that the d-HSA/LYS system behaves in the same manner as the h-HSA/LYS system with respect to the adsorbed amount. For the same number of proteins d-HSA will have a greater mass so values for the thickness and solvent percentage were found which correspond to and adsorbed amount of 2.7 $\pm$ 0.3 mg m^{-2} . The scattering length densities for the individual proteins in CM5 water are 3.3 $\times 10^{-6}$ Å $^{-2}$ for LYS and 6.9 $\times 10^{-6}$ Å $^{-2}$ for d-HSA. The best fit for the $t_{ex} = 0$ uses a scattering length density of 5.5 $\times$ 10^{-6} Å $^{-2}$ which corresponds to 60% of the adsorbed protein being d-HSA which, given the adsorbed amount has increased from 0.5 to 2.9 mg m^{-2} cannot be the case. It is likely that the actual scattering length density is closer to 5 but around this value it is contrast matched to the solvent and sensitivity to the adsorbed amount is greatly reduced.

The ratio of d-HSA:LYS for the t_{ex} = 1 hour is 1:1 and for t_{ex} = 2 hours it is 1:2. These values are again not possible due to the small amount of d-HSA that was present initially and shows that d-HSA and h-HSA respond differently to the exposure of LYS. However, if at t_{ex} = 2 hours it is assumed that all d-HSA has been removed from the surface i.e $\rho_{protein} = 3.3 \times 10^{-6}$ Å $^{-2}$ the layer parameters are τ = 31 Å and solvent %= 79 % which corresponds to an adsorbed amount of 0.9 mg m^{-2}. This is less than half that of the values for h-HSA/LYS system despite a similar starting amount of HSA and also less than LYS adsorbing onto a clean silica surface. The conclusion drawn from this is that most of the d-HSA adsorbed on the surface is irreversibly bound with respect to exchange by LYS even after an incubation time of just 1 hour but it should be noted that there is some uncertainty arising from the lack of sensitivity in this solvent contrast. This is in contrast to the h-HSA case which concluded that the presence of HSA had little to no impact on the adsorption of LYS.

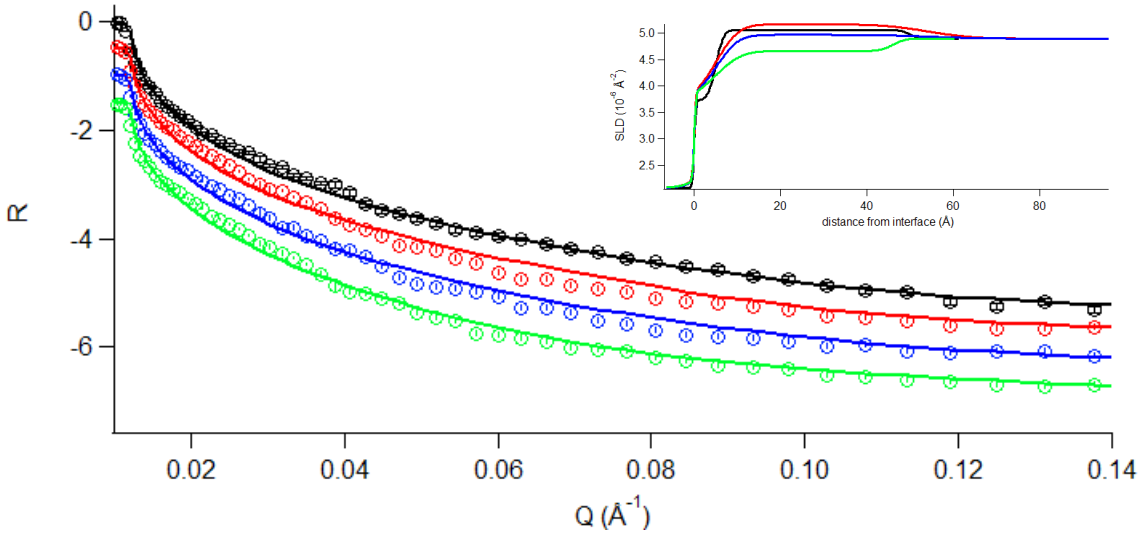


Figure 4.6: Reflectivity profiles and fits showing the changes over time for adsorption of LYS onto a pre-adsorbed d-HSA layer in CM5. A 1-layer model was used and the runs are the final HSA, $t_{inc} = 1$ hour (black), $t_{ex} = 0$ (blue), $t_{ex} = 1$ hour (red) and $t_{ex} = 2$ hours (green) with data being offset for clarity. The inset shows the scattering length density profiles and the layer parameters are in table (4.6).

t_{ex} \hrs	**Thickness** \±2 **Å**	**% Solvent** ±4	$\rho_{protein}$ \$\times 10^{-6}$ Å $^{-2}$	**Roughness**		Γ \±0.2 **mg m**$^{-2}$
				ox-1	1-s	
final HSA	45	92	6.9	5	5	0.5
0	49	56	5.5	5	7	2.9
1	50	52	5.0	5	0	3.0
2	41	56	4.4	9	2	2.5

Table 4.6: Layer parameters for the 1-layer model of adsorption of LYS onto a pre-adsorbed d-HSA layer in CM5 ($t_{inc} = 1$ hour). The data is shown in figure (4.6)

To provide more information on the d-HSA/LYS system the experiment was repeated with H_2O as the solvent. Although the background will be higher in H_2O, it was chosen in order to avoid the possibility of contrast matching the adsorbed protein layer with the solvent and to increase the sensitivity of the measurements. The scattering length densities of the proteins in this solvent are 1.9 and 6.1 $\times 10^{-6}$ Å^{-2} for LYS and d-HSA respectively. The other noticeable difference is the d-HSA layer that is pre-adsorbed onto the silica. Although the overall thicknesses are comparable, the adsorbed amount in the H_2O runs is greater (1.7 compared to 0.5 mg m^{-2}). Subsequently when the d-HSA is exposed to a LYS solution the adsorbed

amount is greater than previously seen, up to 4.4 mg m^{-2}, with an overall thickness of up to 145 Å. The increase in adsorbed amounts, however, is consistent with the h-HSA/LYS system given that in the d-HSA/LYS system there is a greater error resulting from a greater uncertainty in the scattering length density of the protein layer.

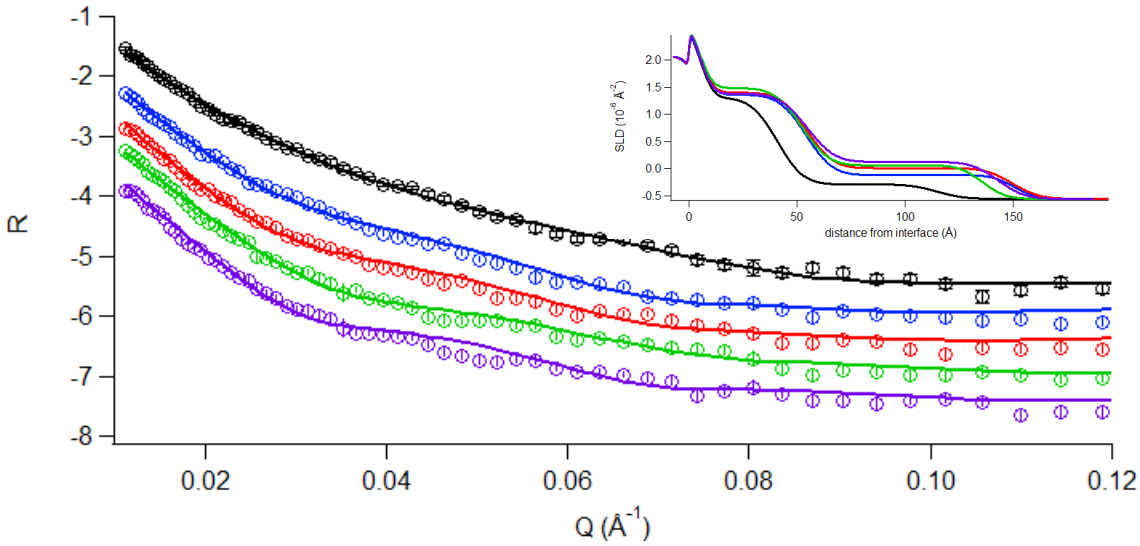


Figure 4.7: Reflectivity profiles and fits showing the changes over time for adsorption of LYS onto a pre-adsorbed d-HSA layer in H_2O. A 2-layer model was used and the runs are the final d-HSA, $t_{inc} = 1$ hour (black), $t_{ex} = 0$ (blue), $t_{ex} = 6$ hours (red), $t_{ex} = 16$ hours (green) and $t_{ex} = 22$ hours (purple) with data being offset for clarity. The inset shows the scattering length density profiles and the layer parameters are in table (4.7).

To compare with the short t_{inc} data above, d-HSA with $t_{inc} = 24$ hours was investigated in both D_2O and H_2O. The reflectivity profiles are shown in figures (4.8) and (4.9) with the layer parameters in tables (4.8) and (4.9). CM5 was not used so as to avoid the possibility of the protein layer and solvent having the same scattering length density as discussed above for the shorter incubation time.

The final d-HSA layer in the D_2O runs represents the best fit based on the χ^2 values but, as discussed in section 3.3.2, the small difference in scattering length densities between the protein and solvent mean it is not very sensitive to the adsorption and thus there is not much confidence in the adsorbed amount. To demonstrate this, the dashed and solid black lines represents fits of the same thickness but 80 % solvent ($\Gamma = 1.1$ mg m^{-2}) and 52 % solvent ($\Gamma = 2.5$ mg m^{-2}) respectively. For the d-HSA/LYS reflectivity profile, the same methodology as above is used to determine the scattering length density of the protein layer i.e. it is assumed that the adsorbed

t_{ex} \hrs	Layer number	Thickness \±3 Å	% Solvent ±4	$\rho_{protein}$ \$\times 10^{-6}$ Å $^{-2}$	Roughness			Γ \±0.4 mg m^{-2}
					ox-1	1-2	2-s	
final HSA	1	36	72	6.1	5	9	9	1.3
	2	74	96	6.1				0.4
0	1	50	67	5.2	5	9	9	2.2
	2	96	86	2.5				1.8
6	1	50	60	4.4	5	10	9	2.7
	2	95	86	3.6				1.7
16	1	47	60	4.6	5	8	9	2.5
	2	83	82	2.9				1.8
22	1	50	58	4.1	5	10	10	2.7
	2	88	85	3.1				1.7

Table 4.7: Layer parameters for the 2-layer model of adsorption of LYS onto a pre-adsorbed d-HSA layer in H_2O (t_{inc} = 1 hour). The data is shown in figure (4.7)

amount is the same (after taking into account the increase due to deuteration of the HSA) as for the h-HSA/LYS system in table (4.4). Based on this assumption the ratio of d-HSA:LYS in the protein layer is approximately 1:1 and the LYS is adsorbed in a nearly end-on orientation.

A comparison of the D_2O and H_2O data shows the same trend as for the $t_{inc} = 1$ hour data. When adsorption occurs in H_2O the adsorbed layer is thicker and denser, in particular with respect to the outer layers, and this results in a higher adsorbed amount. There is more uncertainty regarding the scattering length density of the bottom layer as it can not be determined how much of the d-HSA is displaced in each individual case. A scattering length density of 4.2 $\times 10^{-6}$ Å $^{-2}$ corresponds to a d-HSA:LYS ratio of about 1:1. It can also be seen that the outer layer is up to 85 ± 2 Å thick and the amount of protein in this layer increases over time from 0.2 mg m^{-2} initially up to 1.5 mg m^{-2}. Overall, it can be concluded that most of the d-HSA is irreversibly bound and that the presence of this pre-adsorbed layer acts to promote the adsorption of LYS both directly onto the silica surface and on top of the pre-existing protein layer.

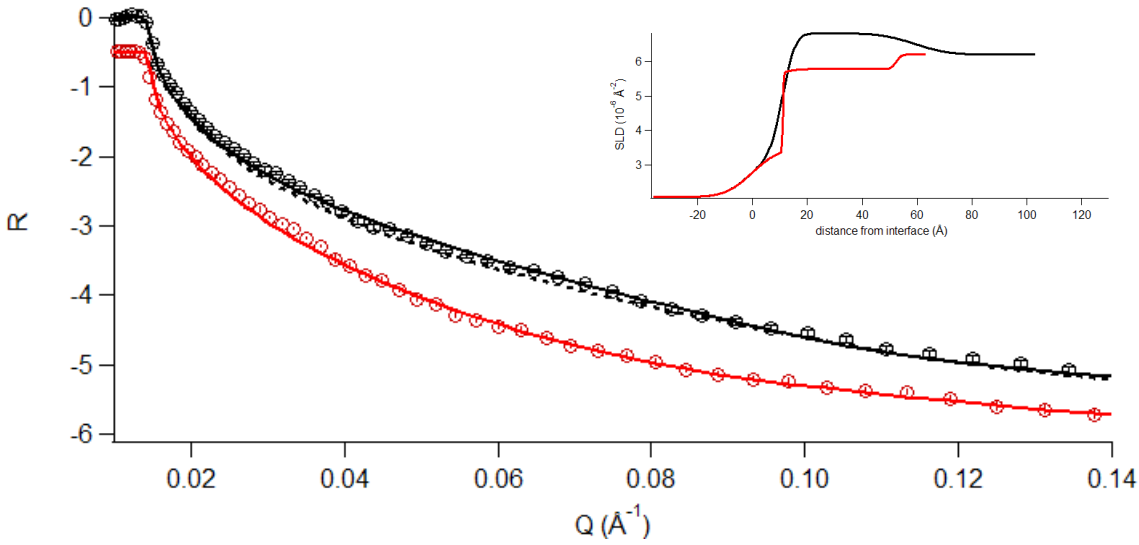


Figure 4.8: Reflectivity profiles and fits showing the changes over time for adsorption of LYS onto a pre-adsorbed d-HSA layer in D_2O. A 1-layer model was used and the runs are the final HSA, $t_{inc} = 24$ hrs (black) and $t_{ex} = 0$ (blue) with data being offset for clarity. The inset shows the scattering length density profiles and the layer parameters are in table (4.8).

t_{ex} \hrs	Thickness \±2 Å	% Solvent ±4	$\rho_{protein}$ \$\times 10^{-6}$ Å $^{-2}$	Roughness		Γ \±0.2 mg m^{-2}
				ox-1	1-s	
final HSA	41	52	7.4	4	9	2.7
final HSA	41	80	7.4	4	8	1.1
0	41	46	5.4	0	3	2.9

Table 4.8: Layer parameters for the 1-layer model of adsorption of LYS onto a pre-adsorbed d-HSA layer in D_2O (t_{inc} = 24 hours). The data is shown in figure (4.8)

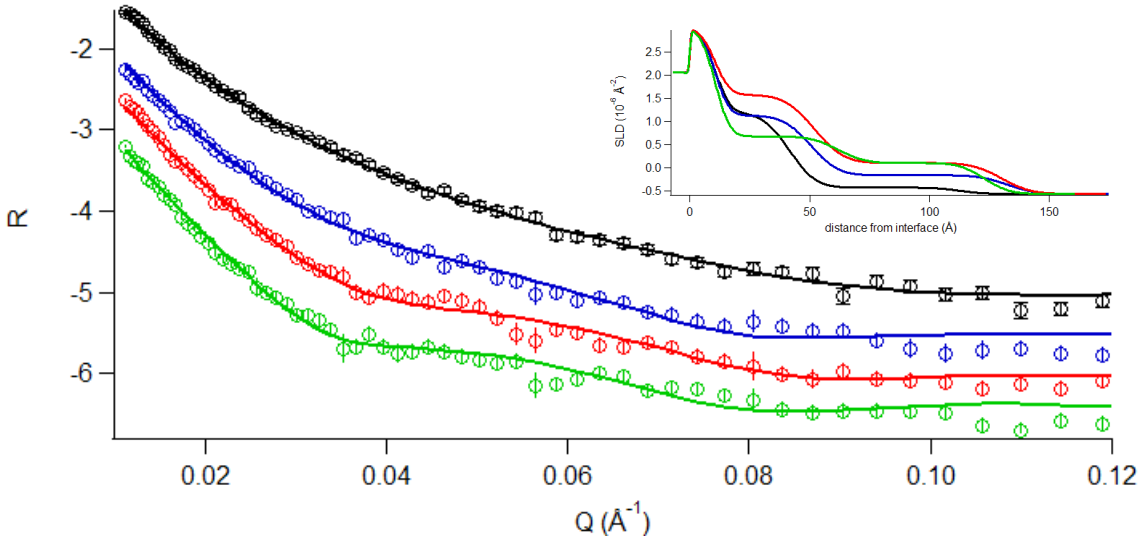


Figure 4.9: Reflectivity profiles and fits showing the changes over time for adsorption of LYS onto a pre-adsorbed d-HSA layer in H_2O. A 2-layer model was used and the runs are the final HSA, t_{inc} = 24 hrs (black), t_{ex} = 0 (blue), t_{ex} = 5.5 hours (red) and t_{ex} = 11 hours (green) with data being offset for clarity. The inset shows the scattering length density profiles and the layer parameters are in table (4.9).

4.1.3 MBP

In chapter 3 the exchange of d-MBP and h-MBP was discussed. In this section, a pre-adsorbed HSA layer (t_{inc} = 21 hours) is exposed to 1 mg ml^{-1} solutions of the two forms of MBP. In the case of the h-HSA/h-MBP system, after t_{ex} = 25 hours the bulk solution was again replaced by a solution of d-MBP to investigate the stability of the protein layer with respect to exchange.

Initially the data was analysed using a 1-layer model but this did not provide satisfactory fits and so a 2-layer model was used. h-MBP and h-HSA have the same

t_{ex} \hrs	Layer number	Thickness \±2 Å	% Solvent ±4	$\rho_{protein}$ \$\times 10^{-6}$ Å $^{-2}$	Roughness			Γ \±0.3 mg m^{-2}
					ox-1	1-2	2-s	
final HSA	1	31	74	6.1	4	10	5	1.1
	2	71	98	6.1				0.2
0	1	40	64	4.2	5	8	10	1.9
	2	85	89	3.1				1.2
5.5	1	41	64	4.6	4	10	8	2.0
	2	78	85	4.4				1.6
11	1	51	75	4.4	5	0	10	1.7
	2	61	81	2.9				1.5

Table 4.9: Layer parameters for the 2-layer model of adsorption of LYS onto a pre-adsorbed d-HSA layer in H_2O ($t_{inc} = 24$ hours). The data is shown in figure (4.9)

scattering length density so although the proportions of each in the adsorbed layer can not be determined, the thickness and percentage of solvent are unambiguous. The reflectivity profiles, fits and scattering length density profiles for the 1-layer model are shown in figure (4.10) and the corresponding layer parameters in table (4.10).

The best fits to a 1-layer model for the exposure of h-MBP to a pre-adsorbed HSA layer in H_2O show that initially the thickness is reduced to 40 Å but after $t_{ex} = 6$ hours it increases to 75 Å which is in good agreement with the h-MBP layers adsorbing onto a clean silica surface in section 3.4.1. This could occur due to HSA being partially or totally displaced by h-MBP. When the h-MBP solution is removed and replaced by a solution of d-MBP at $t_{ex} = 25$ hours a change in the reflectivity profiles is observed suggesting that slow exchange of the pre-adsorbed layer is occurring. During the fitting it was assumed that the layer structure in terms of thickness and solvent percentage was the same and that the only difference occurring was in the scattering length density due to exchange of d-MBP for either h-HSA or h-MBP. These reflectivity profiles could not be adequately fitted using a 1-layer model and so a 2-layer model was used to fit the final h-MBP reflectivity profile and the exchange for d-MBP was then followed.

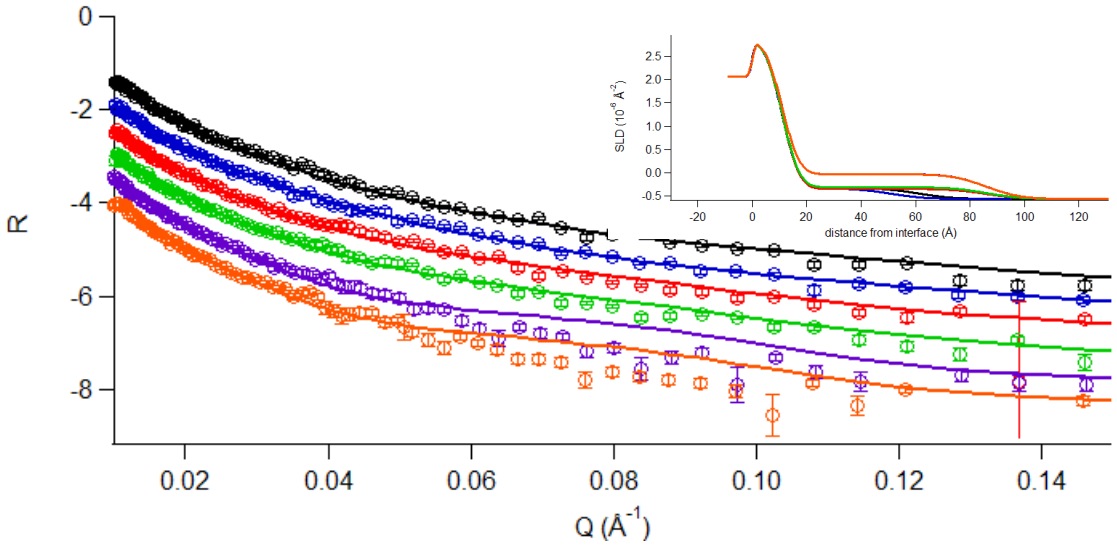


Figure 4.10: Reflectivity profiles and fits showing the changes over time for adsorption of h-MBP and then d-MBP onto a pre-adsorbed HSA layer in H_2O. A 1-layer model was used and the runs are the final HSA, t_{inc} = 21 hrs (black), t_{ex} = 0 (blue), t_{ex} = 6 hours (red), t_{ex} = 11 hours (green), $t_{ex,d-MBP}$ = 25 hours (purple) and $t_{ex,d-MBP}$ = 30 hours (orange) with data being offset for clarity. The inset shows the scattering length density profiles and the layer parameters are in table (4.10).

t_{ex} \hrs	**Thickness** \±2 **Å**	**% Solvent** ±4	$\rho_{protein}$ \$\times 10^{-6}$ Å $^{-2}$	**Roughness**		Γ \±0.2 **mg m**$^{-2}$
				ox-1	1-s	
final HSA	50	90	1.75	5	10	0.7
0	40	90	1.75	5	10	0.5
6	75	91	1.75	5	10	0.9
11	75	89	1.75	5	10	1.1
25	75	89	4.40	5	10	1.1
30	75	89	4.36	5	10	1.1

Table 4.10: Layer parameters for the 1-layer model of adsorption of h-MBP (d-MBP replaces h-MBP for t_{ex} = 25 and 30 hours) onto a pre-adsorbed HSA layer in H_2O (t_{inc} = 21 hours). The data is shown in figure (4.10)

The reflectivity profiles, fits and scattering length density profiles for the 2-layer model are shown in figure (4.11) and the corresponding layer parameters in table (4.11). It was again assumed that during the exposure to the d-MBP solution the protein layer thickness and percentage of solvent was unchanged and the only variable parameter is the scattering length density. The results show that exchange is continuing to occur after the h-MBP/d-MBP solution exchange. By this time,

the h-HSA has been in contact with the surface for 46 hours. This exchange also occurs immediately after exposure to the d-MBP with the ratio of h:d proteins (h being a mixture of h-HSA and h-MBP) at t_{ex} = 25 hours (1st run after d-MBP exposure) is approximately 1:1 in both layers. In light of other conclusions regarding the difference between h-MBP and d-MBP it is likely that the rate and extent of exchange is increased when h-MBP is replaced by d-MBP in the bulk phase. Also, the apparent greater extent of exchange in the bottom layer is likely to be a result of the assumption that the protein layer is not changing with respect to thickness and solvent percentage.

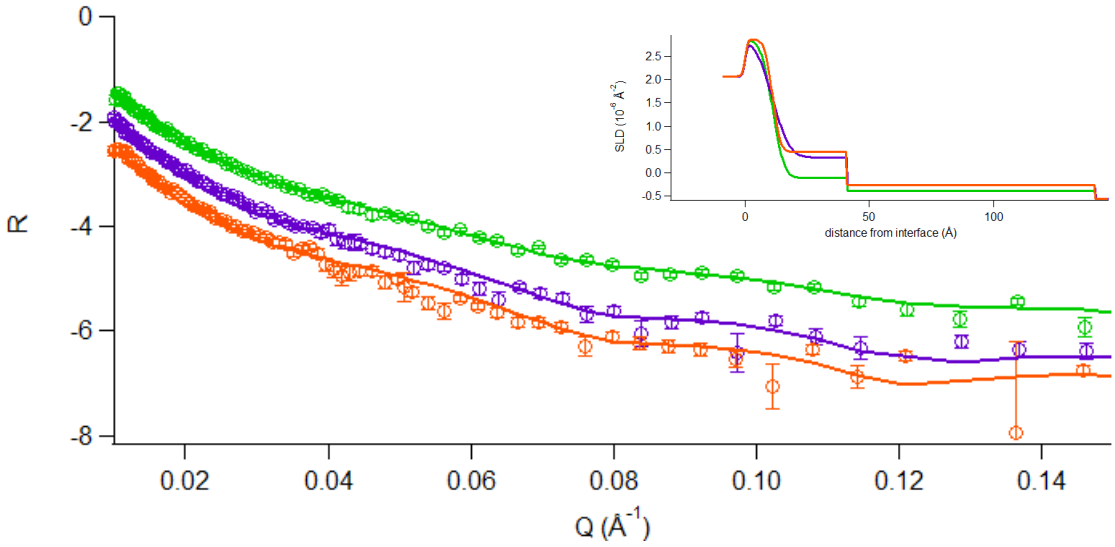


Figure 4.11: Reflectivity profiles and fits showing the changes over time for adsorption of h-MBP and then d-MBP onto a pre-adsorbed HSA layer in H_2O. A 2-layer model was used and the runs are the final HSA, t_{inc} = 21 hrs (black), t_{ex} = 0 (blue), t_{ex} = 6 hours (red), t_{ex} = 11 hours (green), $t_{ex,d-MBP}$ = 25 hours (purple) and $t_{ex,d-MBP}$ = 30 hours (orange) with data being offset for clarity. The inset shows the scattering length density profiles and the layer parameters are in table (4.11).

To provide more information on the layer structure, the experiment was repeated with the same incubation time of h-HSA and the pre-adsorbed protein layer was exposed to a 1 mg ml^{-1} solution of d-MBP. This was carried out in CM5 water contrast. The reflectivity profiles, fits and scattering length density profiles for the 1-layer model are shown in figure (4.12)and the corresponding layer parameters in table (4.12). It was first attempted to find values for the thickness and solvent percentage that corresponded to the same adsorbed amount as for the h-HSA/h-MBP system (1.1 ± 0.3 mg m^{-2}). This was only possible for t_{ex} = 0 and the layer

t_{ex} \hrs	Layer number	Thickness \±2 Å	% Solvent ±4	$\rho_{protein}$ $\times 10^{-6}$ Å $^{-2}$	Roughness			Γ \±0.2 mg m^{-2}
					ox-1	1-2	2-s	
11	1	30	81	1.75	4	0	0	0.7
	2	100	93	1.75				0.9
25	1	30	81	4.0	5	0	10	0.7
	2	100	93	3.45				0.9
30	1	30	81	4.0	5	8	10	0.7
	2	100	93	4.0				0.9

Table 4.11: Layer parameters for the 2-layer model of adsorption of h-MBP and then d-MBP onto a pre-adsorbed HSA layer in H_2O (t_{inc} = 21 hours). The data is shown in figure (4.11)

is almost entirely composed of d-MBP. For the other times the lowest adsorbed amount was found with a scattering length density equal to that of just d-MBP being present. The layer parameters and adsorbed amounts are comparable with those shown in section 3.4.2 for the adsorption of d-MBP onto a clean silica surface. It can be concluded from this that the presence of h-HSA does not significantly effect the adsorption of d-MBP. This is not a surprising result given the diffuse nature of the pre-adsorbed HSA layer in this case. It is also in agreement with that observed for the $t_{inc} = 1.5$ hours followed by LYS adsorption in section 4.1.2.

With reference to the h-HSA/h-MBP system discussed previously, it was stated that it was not possible to determine the extent of exchange in the protein layer due to the proteins having the same scattering length density. With the additional information the h-HSA/d-MBP system provides, it could be possible to draw further conclusions based on the a comparison between the propensity of h-HSA to exchange for h- vs d-MBP. However, the h-HSA layers in the two cases are different in both adsorbed amount and layer structure. This variability in the HSA adsorption is likely to be the main factor in the difference between the final layer structures although it should be noted that even if the HSA layers were the same, the differences in the ability to exchange pre-adsorbed proteins for h-MBP and d-MBP would still make this a very difficult parameter to determine with any certainty.

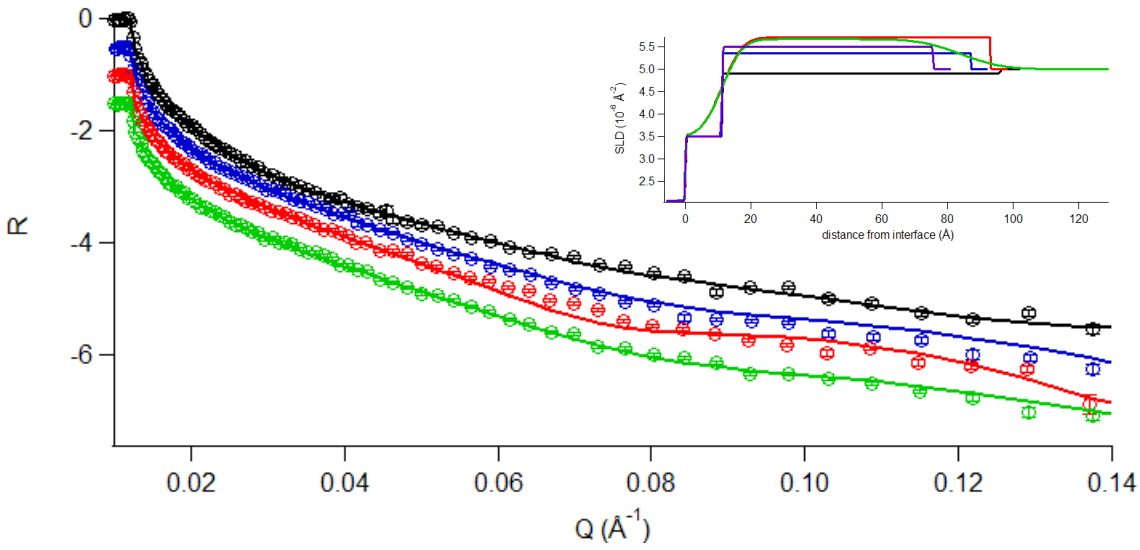


Figure 4.12: Reflectivity profiles and fits showing the changes over time for adsorption of d-MBP onto a pre-adsorbed HSA layer in CM5. A 1-layer model was used and the runs are the final HSA, t_{inc} = 21 hrs (black), t_{ex} = 0 (blue), t_{ex} = 5.5 hours (red) and t_{ex} = 17 hours (green) with data being offset for clarity. The inset shows the scattering length density profiles and the layer parameters are in table (4.12).

t_{ex} \hrs	**Thickness** \±3 **Å**	**% Solvent** ±4	$\rho_{protein}$ \$\times 10^{-6}$ Å $^{-2}$	**Roughness**		Γ \±0.2 **mg m**$^{-2}$
				ox-1	1-s	
final HSA	59	93	2.9	5	4	0.6
0	75	86	6.9	4	3	1.4
5.5	80	75	7.1	5	10	2.6
17	80	74	7.1	5	10	2.7

Table 4.12: Layer parameters for the 1-layer model of adsorption of d-MBP onto a pre-adsorbed HSA layer in CM5 (t_{inc} = 21 hours). The data is shown in figure (4.12)

4.2 Adsorption of HSA onto a pre-adsorbed protein layer

This chapter has so far been concerned with the exchange or addition to a pre-adsorbed HSA layer. The following section details the reverse situation; the exposure of pre-adsorbed CA II, LYS and MBP layers to a bulk solution of HSA.

4.2.1 CA II

The adsorption of a 1 mg ml^{-1} solution of HSA on to a pre-adsorbed CA II layer (t_{inc} = 12.5 hours) was investigated. The reflectivity profiles, fits and scattering length density profiles are shown in figure (4.13) with the corresponding layer parameters in table (4.13). The results show that there is no significant change in the structure of the adsorbed protein layer or the adsorbed amount. This could occur if exchange is occurring in a like-for-like manner or if the CA II is irreversibly bound with respect to exchange and also blocking the HSA from adsorbing further. Given that the CA II carries no net charge at this pH and both the HSA and silica surface are negatively charged the removal of CA II and replacement by HSA would be unfavourable. HSA is bigger than CA II (66 kDa compared to 29 kDa) and thus if exchange is occurring to maintain the same adsorbed amount, one HSA molecule would displace two CA II molecules which is entropically favourable. However, this is balanced by the increased number of solvent molecules required to solvate the desorbing protein molecules and the additional number of counter ions required for charge neutrality in the adsorbed layer. Even if the exchange were shown to be thermodynamically favourable, the lack of any strong driving force suggests that it would be very slow and the most likely conclusion is that CA II is irreversible with respect to exchange by HSA, although the possibility of a small amount of exchange can not be totally ruled out.

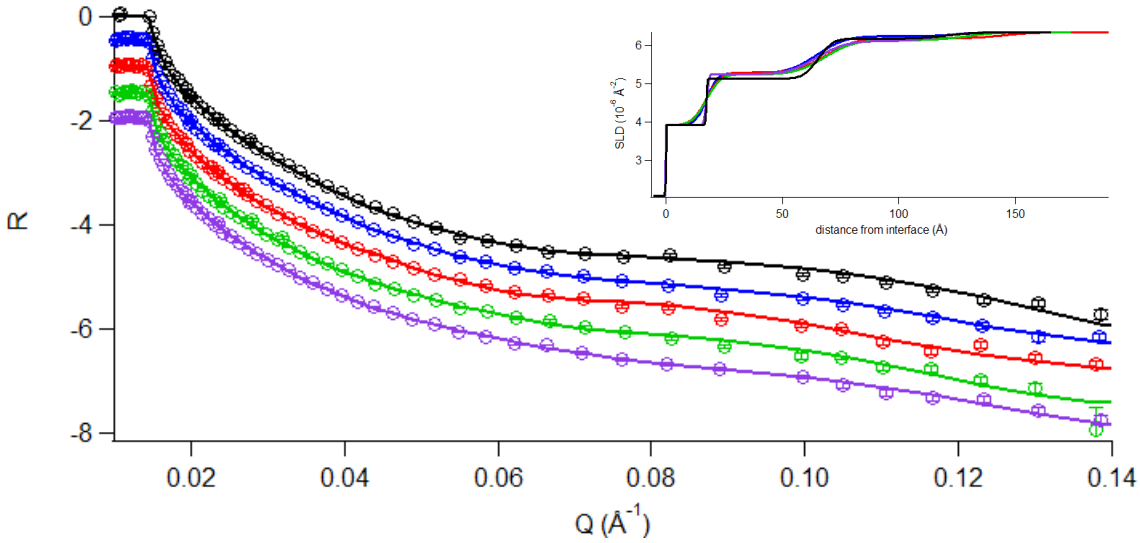


Figure 4.13: Reflectivity profiles and fits showing the changes over time for adsorption of HSA onto a pre-adsorbed CA II layer in D_2O. A 2-layer model was used and the runs are the final CA II, $t_{inc} = 22.5$ hrs (black), $t_{ex} = 0$ (blue), $t_{ex} = 8$ hours (red), $t_{ex} = 17$ hours (green) and $t_{ex} = 22$ hours (purple) with data being offset for clarity. The inset shows the scattering length density profiles and the layer parameters are in table (4.13).

t_{ex} \hrs	Layer number	Thickness \±2 Å	% Solvent ±4	Roughness			Γ \±0.2 mg m^{-2}
				ox-1	1-2	2-s	
final CA II	1	48	64	0	5	10	2.3
	2	55	95				0.4
0	1	48	68	4	10	9	2.0
	2	60	97				0.2
8	1	52	69	5	10	10	2.1
	2	76	95				0.5
17	1	51	67	5	10	10	2.2
	2	61	94				0.5
22	1	47	67	1	10	10	2.0
	2	52	93				0.5

Table 4.13: Layer parameters for the 2-layer model of adsorption of HSA onto a pre-adsorbed CA II layer in D_2O ($t_{inc} = 21$ hours). The data is shown in figure (4.13)

4.2.2 LYS

For all HSA/LYS fitting a scattering length density of 3.3×10^{-6} Å $^{-2}$ was used which is equal to a 1:1 mixture of LYS:HSA. This assumption is reflected in the greater stated errors in the tables for the adsorbed amount. All runs were done in

D_2O with four different incubation times for the LYS, 1.5, 10, 17 and 21 hours. The reflectivity profiles, fits and scattering length density profiles are shown in figures (4.14), (4.15),(4.16), (4.17) and (4.18) with the corresponding layer parameters in tables (4.14), (4.15), (4.16), (4.17) and (4.18).

The incubation time of the LYS has little effect on the final protein layer after exposure to HSA. In most cases analysed using a 1-layer model there is a small increase in adsorbed amount and layer thickness but there is no trend with respect to the incubation time of the pre-adsorbed LYS. In the data sets where a 1-layer model gave good fits the increase in adsorbed amount is not significant and the layer thickness only increases up to 50 Å suggesting that the final layer is still comprised predominantly of LYS.

The only set requiring a 2-layer model is for $t_{inc} = 17$ hours. The χ^2 values for the 2-layer model are in the range 2.8-5.0 compared with 6.9-15 for the 1-layer fits. The 2-layer analysis shows an increase in the adsorbed amount and the layer thickness but the solvent percentage in the bottom layer is only slightly increased. The increase in thickness could result from the HSA displacing some of the LYS attached to the surface or this could be undisturbed and the HSA adsorbs into the gaps left in the outer LYS layer. Van der Veen et al.[8] have shown that after $t_{inc} = 20$ min only 80 % of LYS is irreversibly bound with respect to desorption into protein-free buffer. These findings agreed with the 1-layer model of LYS when exposed to buffer discussed in section 3.2. Given that the addition of HSA provides another mechanism for actively removing the LYS the most likely scenario is that the changes seen are as a result of a small proportion of the adsorbed LYS being replaced by HSA. The positively charged LYS also provides an electrostatic driving force for the negatively charged HSA to adsorb in the gaps of the outer LYS layer which accounts for the observed increases in the outer layer.

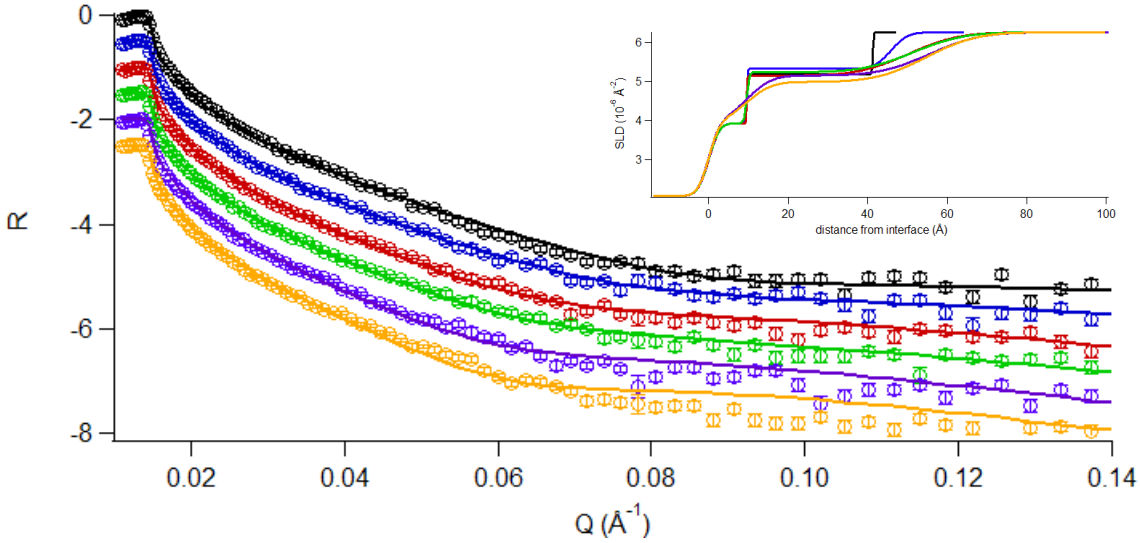


Figure 4.14: Reflectivity profiles and fits showing the changes over time for adsorption of HSA onto a pre-adsorbed LYS layer in D_2O. A 1-layer model was used and the runs are the final LYS, t_{inc} = 1.5 hrs (black), t_{ex} = 0 (blue), t_{ex} = 3 hours (red), t_{ex} = 12 hours (green), t_{ex} = 16 hours (purple) and t_{ex} = 34 hours (orange) with data being offset for clarity. The inset shows the scattering length density profiles and the layer parameters are in table (4.14).

t_{ex} \hrs	Thickness \±2 Å	% Solvent ±5	Roughness		Γ \±0.3 mg m^{-2}
			ox-1	1-s	
final LYS	34	58	2	0	1.9
0	36	65	0	3	1.7
3	41	63	0	10	2.0
12	42	66	1	10	1.9
16	46	63	5	10	2.3
34	45	57	5	10	2.6

Table 4.14: Layer parameters for the 2-layer model of adsorption of HSA onto a pre-adsorbed LYS layer in D_2O (t_{inc} = 1.5 hours). The data is shown in figure (4.14)

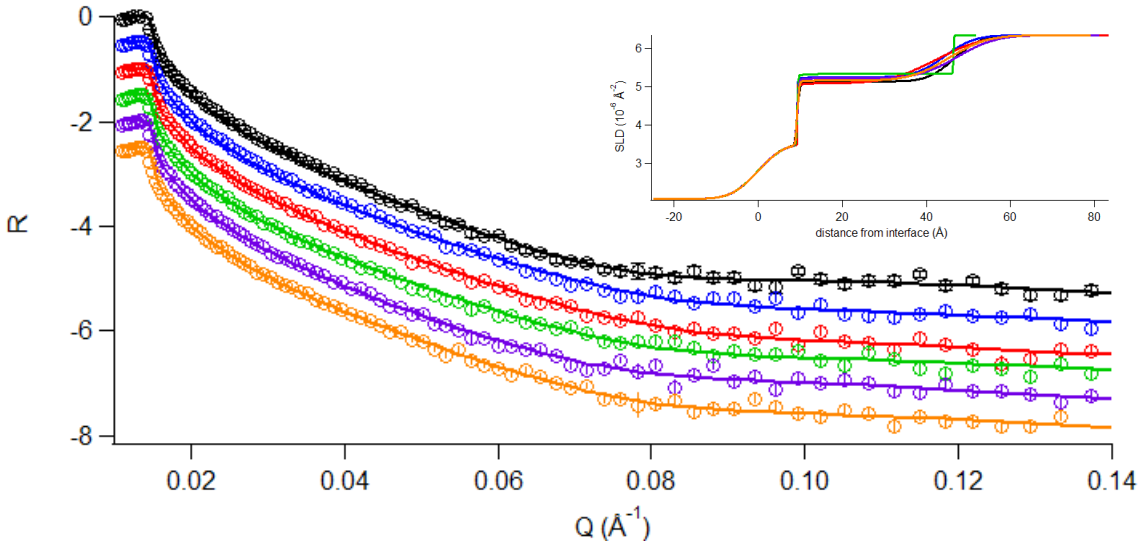


Figure 4.15: Reflectivity profiles and fits showing the changes over time for adsorption of HSA onto a pre-adsorbed LYS layer in D_2O. A 1-layer model was used and the runs are the final LYS, t_{inc} = 10 hrs (black), t_{ex} = 0 (blue), t_{ex} = 2 hours (red), t_{ex} = 14 hours (green), t_{ex} = 19 hours (purple) and t_{ex} = 24.5 hours (orange) with data being offset for clarity. The inset shows the scattering length density profiles and the layer parameters are in table (4.15).

t_{ex} \hrs	Thickness \±2 Å	% Solvent ±5	Roughness		Γ \±0.3 mg m^{-2}
			ox-1	1-s	
final LYS	34	56	0	5	2.0
0	35	64	2	6	1.7
2	33	59	0	9	1.8
14	37	67	0	1	1.6
19	38	63	0	7	1.9
24.5	36	61	0	7	1.9

Table 4.15: Layer parameters for the 1-layer model of adsorption of HSA onto a pre-adsorbed LYS layer in D_2O (t_{inc} = 10 hours). The data is shown in figure (4.15)

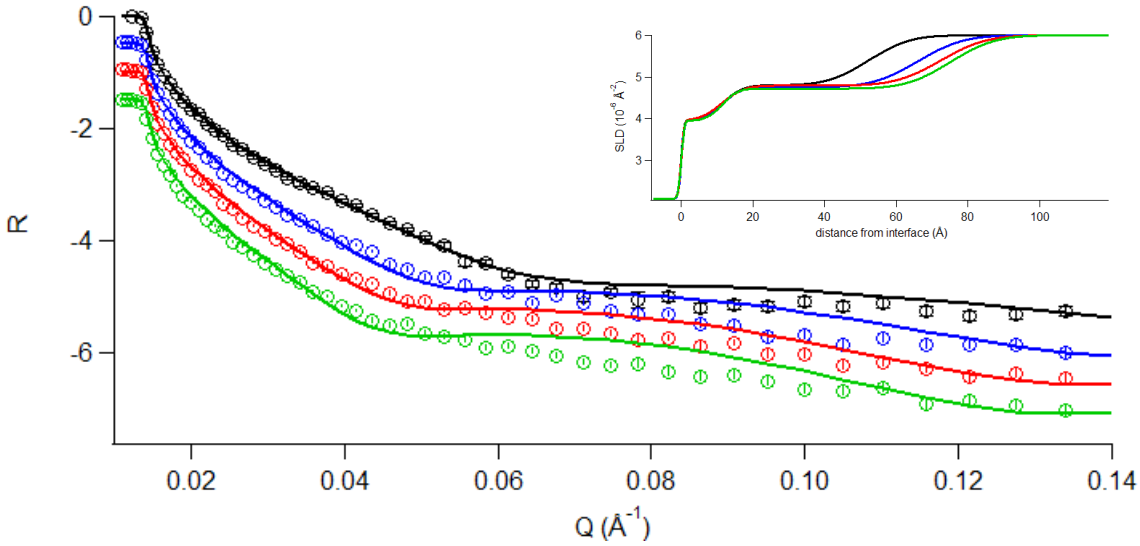


Figure 4.16: Reflectivity profiles and fits showing the changes over time for adsorption of HSA onto a pre-adsorbed LYS layer in D_2O. A 1-layer model was used and the runs are the final LYS, t_{inc} = 17 hrs (black), t_{ex} = 0 (blue), t_{ex} = 2 hours (red), t_{ex} = 14 hours (green), t_{ex} = 19 hours (purple) and t_{ex} = 24.5 hours (orange) with data being offset for clarity. The inset shows the scattering length density profiles and the layer parameters are in table (4.16).

t_{ex} \hrs	Thickness \±2 Å	% Solvent ±5	Roughness		Γ \±0.4 mg m^{-2}
			ox-1	1-s	
final LYS	41	50	5	7	2.7
0	60	56	4	10	3.5
3.5	61	54	5	10	3.6
5.5	64	55	3	10	3.7

Table 4.16: Layer parameters for the 1-layer model of adsorption of HSA onto a pre-adsorbed LYS layer in D_2O (t_{inc} = 10 hours). The data is shown in figure (4.15)

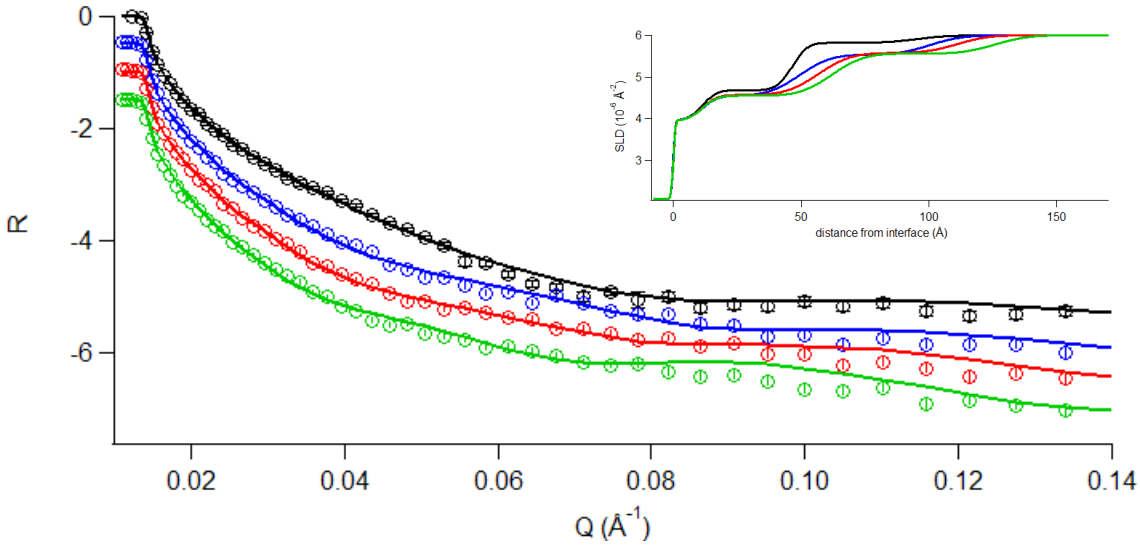


Figure 4.17: Reflectivity profiles and fits showing the changes over time for adsorption of HSA onto a pre-adsorbed LYS layer in D_2O. A 2-layer model was used and the runs are the final LYS, t_{inc} = 17 hrs (black), t_{ex} = 0 (blue), t_{ex} = 3.5 hours (red) and t_{ex} = 5.5 hours (green) with data being offset for clarity. The inset shows the scattering length density profiles and the layer parameters are in table (4.17).

t_{ex} \hrs	Layer number	Thickness \±2 Å	% Solvent ±5	Roughness			Γ \±0.3 mg m^{-2}
				ox-1	1-2	2-s	
final LYS	1	35	45	3	1	8	2.6
	2	49	93				0.5
0	1	38	46	2	10	9	2.7
	2	51	83				1.1
3.5	1	45	47	3	8	10	3.1
	2	54	84				1.1
5.5	1	51	46	5	10	10	3.6
	2	64	84				1.4

Table 4.17: Layer parameters for the 2-layer model of adsorption of HSA onto a pre-adsorbed LYS layer in D_2O (t_{inc} = 17 hours). The data is shown in figure (4.17)

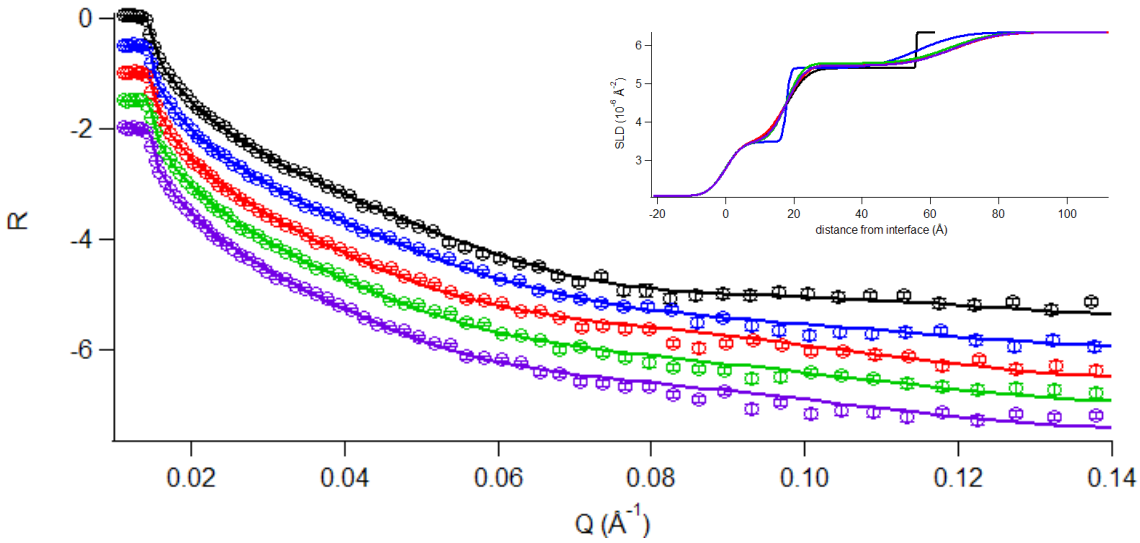


Figure 4.18: Reflectivity profiles and fits showing the changes over time for adsorption of HSA onto a pre-adsorbed LYS layer in D_2O. A 1-layer model was used and the runs are the final LYS, t_{inc} = 21 hrs (black), t_{ex} = 0 (blue), t_{ex} = 6 hours (red), t_{ex} = 13.5 hours (green) and t_{ex} = 21.5 hours (purple) with data being offset for clarity. The inset shows the scattering length density profiles and the layer parameters are in table (4.18).

t_{ex} \hrs	Thickness \±2 Å	% Solvent ±5	Roughness ox-1	Roughness 1-s	Γ \±0.3 mg m^{-2}
final LYS	38	66	5	0	1.7
0	39	70	5	10	1.7
6	50	73	5	10	1.8
13.5	48	73	4	10	1.7
21.5	49	72	4	10	1.8

Table 4.18: Layer parameters for the 1-layer model of adsorption of HSA onto a pre-adsorbed LYS layer in D_2O (t_{inc} = 21 hours). The data is shown in figure (4.18)

4.2.3 MBP

The adsorption of a 1 mg ml^{-1} solution of HSA on to a pre-adsorbed MBP layer (t_{inc} = 21 hours) was investigated using both d- and h-MBP. The h-MBP was recorded under two water contrasts, H_2O and CM3.6, whereas the d-MBP was only recorded in H_2O. The h-MBP case will be considered first with the reflectivity profiles, fits and scattering length density profiles for the 1-layer models shown in figures (4.19) and (4.20) for the H_2O and CM 3.6 solvent contrasts respectively. The corresponding layer parameters are shown in tables (4.19) and (4.20).

The results for both the H_2O and CM 3.6 solvent contrasts are in good agreement with respect to the adsorbed amount of 1.1 ± 0.3 mg m^{-2} which is unchanged from the final h-MBP layer but for the CM3.6 data the fits are poor with χ^2 values in excess of 20 so a 2-layer model was used to analyse this solvent contrast. A 2-layer model was also applied to the H_2O solvent contrats due to the thickness of the layer being longer than the longest axis of h-MBP.

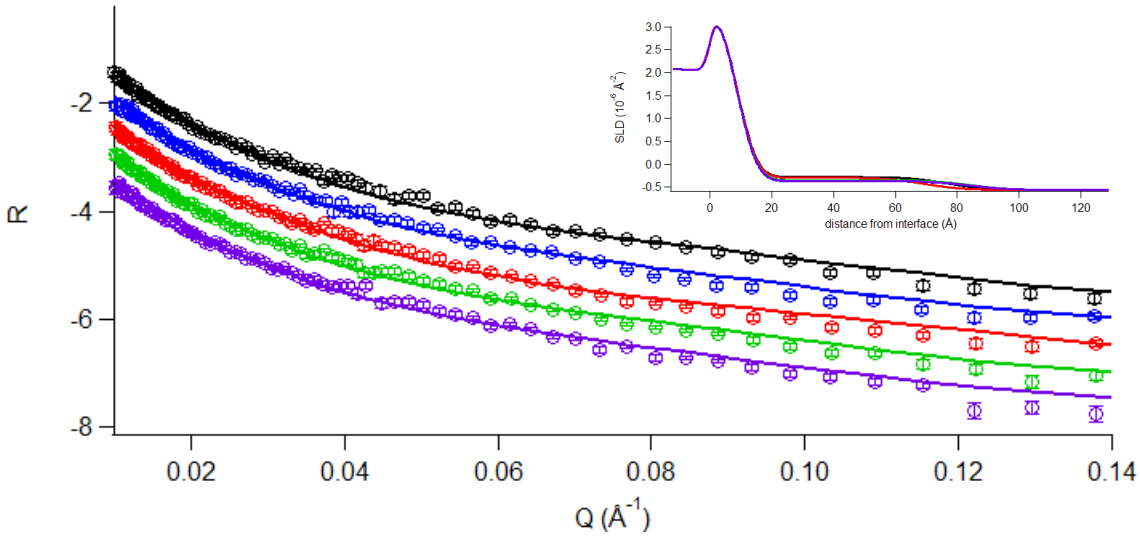


Figure 4.19: Reflectivity profiles and fits showing the changes over time for adsorption of HSA onto a pre-adsorbed h-MBP layer in H_2O. A 1-layer model was used and the runs are the final h-MBP, $t_{inc} = 21$ hrs (black), $t_{ex} = 0$ (blue), $t_{ex} = 4.5$ hours (red), $t_{ex} = 13.5$ hours (green) and $t_{ex} = 18.5$ hours (purple) with data being offset for clarity. The inset shows the scattering length density profiles and the layer parameters are in table (4.19).

t_{ex} \hrs	Thickness \±2 Å	% Solvent ±4	Roughness		Γ \±0.2 mg m^{-2}
			ox-1	1-s	
final h-MBP	68	88	5	10	1.1
0	75	92	5	10	0.9
4.5	60	88	5	9	0.9
13.5	75	91	5	10	0.9
18.5	75	92	5	9	0.8

Table 4.19: Layer parameters for the 1-layer model of adsorption of HSA onto a pre-adsorbed h-MBP layer in H_2O ($t_{inc} = 21$ hours). The data is shown in figure (4.19)

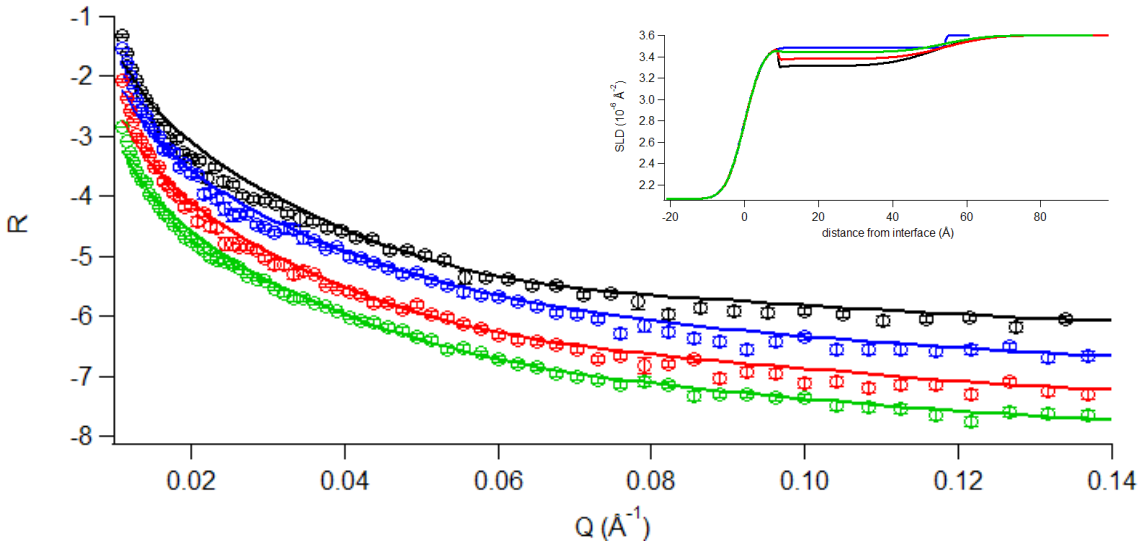


Figure 4.20: Reflectivity profiles and fits showing the changes over time for adsorption of HSA onto a pre-adsorbed h-MBP layer in CM3.6. A 1-layer model was used and the runs are the final h-MBP, t_{inc} = 21 hrs (black), t_{ex} = 0 (blue), t_{ex} = 9 hours (red) and t_{ex} = 23 hours (green) with data being offset for clarity. The inset shows the scattering length density profiles and the layer parameters are in table (4.20).

t_{ex} \hrs	Thickness \±2 Å	% Solvent ±4	Roughness		Γ \±0.2 mg m^{-2}
			ox-1	1-s	
final h-MBP	42	74	2	10	1.4
0	45	90	4	0	0.6
9	45	80	5	10	1.2
23	45	85	2	9	0.9

Table 4.20: Layer parameters for the 1-layer model of adsorption of HSA onto a pre-adsorbed h-MBP layer in CM3.6 (t_{inc} = 21 hours). The data is shown in figure (4.20)

The reflectivity profiles, fits and scattering length density profiles for the 2-layer model can be seen in figure (4.21) for the CM 3.6 solvent contrast. The corresponding layer parameters are shown in table (4.21). As discussed in section 3.4.1, the 2-layer model for the adsorption of h-MBP in CM 3.6 shows evidence for the denaturation and unfolding of the protein to form a thin but dense layer attached to the surface and a thick, diffuse outer layer. After exposure to the HSA, the inner layer thickness is unchanged but some there is a small reduction in the protein volume fraction. The outer layer shows a small increase in the adsorbed amount and also a large increase in thickness when in H_2O suggesting that the

HSA molecules are adsorbing onto the pre-adsorbed h-MBP and forming a thick but diffuse multilayer. Over time both are relatively stable and show no evidence that HSA is exchanging for or displacing the adsorbed MBP to any great extent. However, it should be noted that h-MBP and h-HSA have the same scattering length densities.

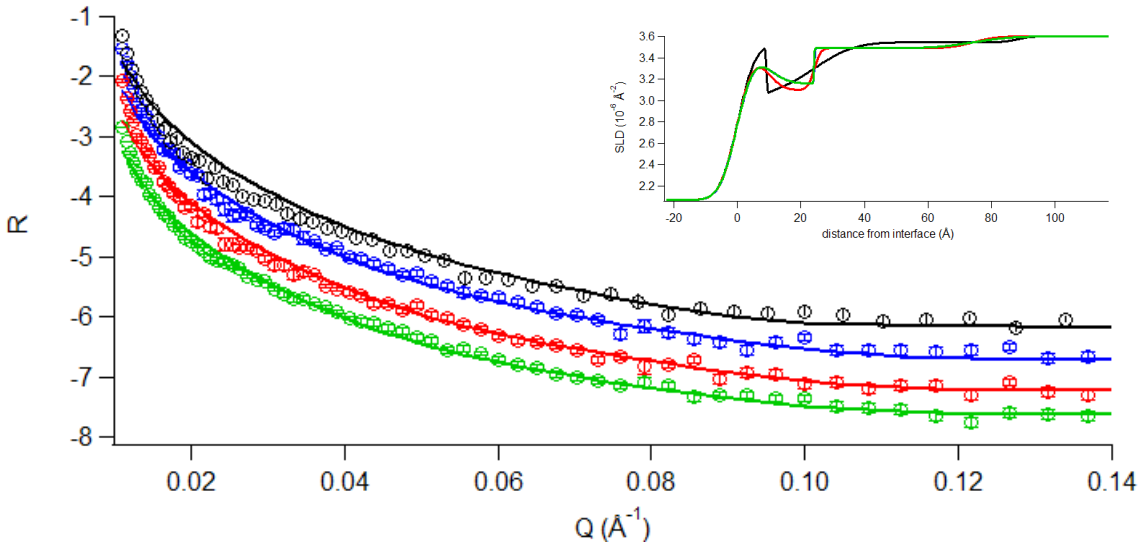


Figure 4.21: Reflectivity profiles and fits showing the changes over time for adsorption of HSA onto a pre-adsorbed h-MBP layer in CM3.6. A 1-layer model was used and the runs are the final h-MBP, t_{inc} = 21 hrs (black), t_{ex} = 0 (blue), t_{ex} = 9 hours (red) and t_{ex} = 23 hours (green) with data being offset for clarity. The inset shows the scattering length density profiles and the layer parameters are in table (4.21).

t_{ex} \hrs	Layer number	Thickness \±2 Å	% Solvent ±4	Roughness ox-1	Roughness 1-2	Roughness 2-s	Γ \±0.2 mg m^{-2}
final h-MBP	1	15	50	5	6	9	1.0
	2	64	95				0.4
0	1	15	60	5	0	2	0.8
	2	50	90				0.7
9	1	15	54	5	0	6	0.9
	2	50	90				0.7
23	1	15	60	5	0	10	0.9
	2	50	90				0.7

Table 4.21: Layer parameters for the 2-layer model of adsorption of HSA onto a pre-adsorbed h-MBP layer in CM3.6 (t_{inc} = 21 hours). The data is shown in figure (4.21)

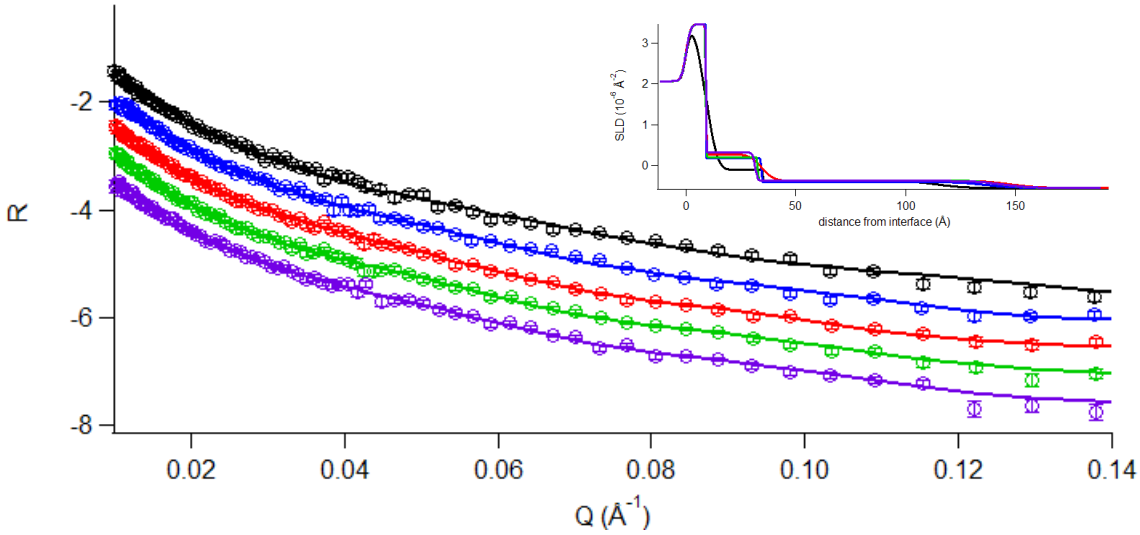


Figure 4.22: Reflectivity profiles and fits showing the changes over time for adsorption of HSA onto a pre-adsorbed h-MBP layer in H_2O. A 2-layer model was used and the runs are the final h-MBP, $t_{inc} = 21$ hrs (black), $t_{ex} = 0$ (blue), $t_{ex} = 4.5$ hours (red), $t_{ex} = 13.5$ hours (green) and $t_{ex} = 18.5$ hours (purple) with data being offset for clarity. The inset shows the scattering length density profiles and the layer parameters are in table (4.22).

t_{ex} \hrs	Layer number	Thickness \±2 Å	% Solvent ±4	Roughness			Γ \±0.2 mg m^{-2}
				ox-1	1-2	2-s	
final h-MBP	1	26	81	1	0	1	0.6
	2	80	93				0.7
0	1	25	69	5	0	10	1.0
	2	102	94				0.8
4.5	1	26	64	5	0	10	1.2
	2	113	92				1.2
13.5	1	24	67	4	0	10	1.0
	2	110	92				1.1
18.5	1	23	62	0	0	10	1.1
	2	113	93				1.0

Table 4.22: Layer parameters for the 2-layer model of adsorption of HSA onto a pre-adsorbed h-MBP layer in H_2O ($t_{inc} = 21$ hours). The data is shown in figure (4.22)

To provide more information regarding the possibility of HSA/MBP exchange, a pre-adsorbed d-MBP layer was exposed to a bulk solution of HSA after the same incubation time (21 hours) as for the h-MBP/HSA experiments. Given that during the h-MBP/HSA sequential adsorption experiments, there was no discernable change in the adsorbed amount, this was assumed to be true also for the d-MBP/HSA system.

This assumption makes it possible to get a more accurate result for the scattering length density of the protein layer and hence the ratio of d-MBP:HSA. When this was done using a 1-layer model it can be seen that some of the d-MBP is displaced by HSA resulting in afinal layer ratio of 3:1 d-MBP:HSA. However, the d-MBP thickness is greater than the long axis of the molecule so it was also attempted to fit to a 2-layer model.

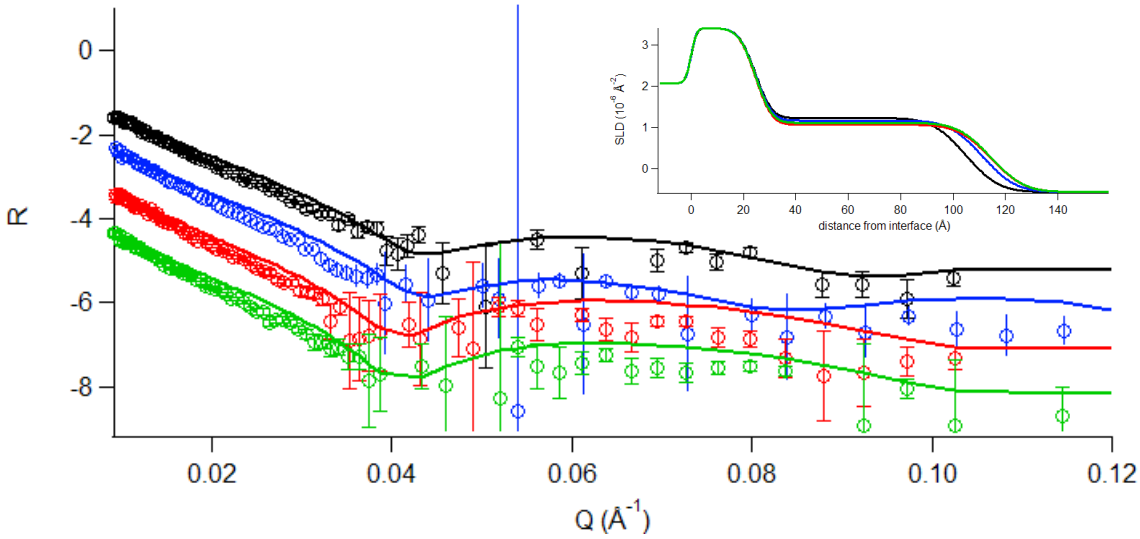


Figure 4.23: Reflectivity profiles and fits showing the changes over time for adsorption of HSA onto a pre-adsorbed d-MBP layer in H_2O. A 1-layer model was used and the runs are the final d-MBP, t_{inc} = 21 hrs (black), t_{ex} = 0 (blue), t_{ex} = 12.5 hours (red) and t_{ex} = 18.5 hours (green) with data being offset for clarity. The inset shows the scattering length density profiles and the layer parameters are in table (4.23).

t_{ex} \hrs	Thickness \±2 Å	% Solvent ±4	$\rho_{protein}$ \$\times 10^{-6}$ Å $^{-2}$	Roughness		Γ \±0.2 mg m^{-2}
				ox-1	1-s	
final d-MBP	70	76	6.2	5	10	2.4
0	78	80	5.1	5	10	2.1
12.5	80	79	5.1	5	10	2.2
18.5	80	79	5.0	5	10	2.2

Table 4.23: Layer parameters for the 1-layer model of adsorption of h-HSA onto a pre-adsorbed d-MBP layer in H_2O (t_{inc} = 21 hours). The data is shown in figure (4.23)

Following the same methodology as for the self-exchange experiments detailed in section 3.4.5, a 2-layer model was used starting with the assumption that the

only changes occurring did so in the outer layer. The parameters for the bottom layer were kept the same. When using the 2-layer model assuming exchange only occurred from the outer layer it was only possible to obtain satisfactory fits for the same adsorbed amount if the scattering length density was set at 6.2 $\times 10^{-6}$ Å $^{-2}$ i.e. 100% d-MBP. This is not in agreement with the 1-layer model thus some exchange must be occurring from the bottom layer also. The reflectivity profiles, fits and scattering length density profiles for the 2-layer model are shown in figure (4.24) with the corresponding layer parameters in table (4.24). These conclusions are supported by the analysis if the parameters for both layers are allowed to vary, as shown in figure (4.25) and table (4.25). The small changes in the scattering length density of the bottom layer show that not much, if any, exchange and/or adsorption of HSA is occurring. However, the reduced scattering length density and increased adsorbed amount in the outer layer suggest that HSA is adsorbing into the outer layer.

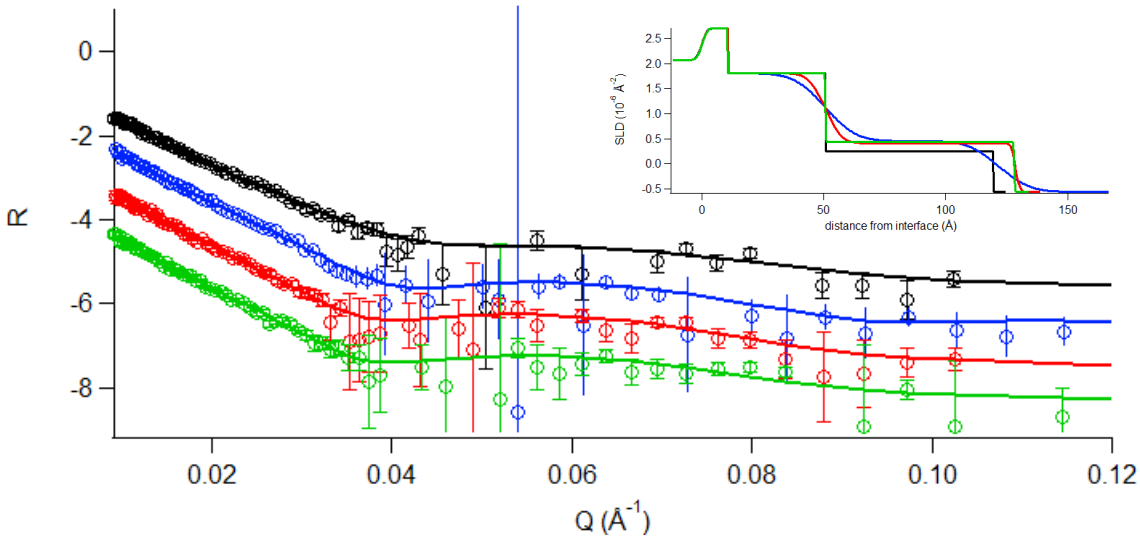


Figure 4.24: Reflectivity profiles and fits showing the changes over time for adsorption of HSA onto a pre-adsorbed d-MBP layer in H_2O. A 2-layer model assuming changes only occurred in the outer layer was used and the runs are the final d-MBP, t_{inc} = 21 hrs (black), t_{ex} = 0 (blue), t_{ex} = 12.5 hours (red) and t_{ex} = 18.5 hours (green) with data being offset for clarity. The inset shows the scattering length density profiles and the layer parameters are in table (4.24).

t_{ex} \hrs	Layer number	Thickness \±3 Å	% Solvent ±4	$\rho_{protein}$ \$\times 10^{-6}$ Å $^{-2}$	Roughness			Γ \±0.2 mg m^{-2}
					ox-1	1-2	2-s	
final d-MBP	1	40	65	6.2	5	10	10	1.9
	2	69	88	6.2				1.1
0	1	40	65	6.2	5	0	10	1.9
	2	71	85	6.2				1.3
12.5	1	40	65	6.2	5	10	10	1.9
	2	78	85	5.9				1.3
18.5	1	40	65	6.2	5	10	10	1.9
	2	78	85	6.2				1.3

Table 4.24: Layer parameters for the 2-layer model (assuming changes were only occurring in the outer layer) of adsorption of h-HSA onto a pre-adsorbed d-MBP layer in H_2O (t_{inc} = 21 hours). The data is shown in figure (4.24)

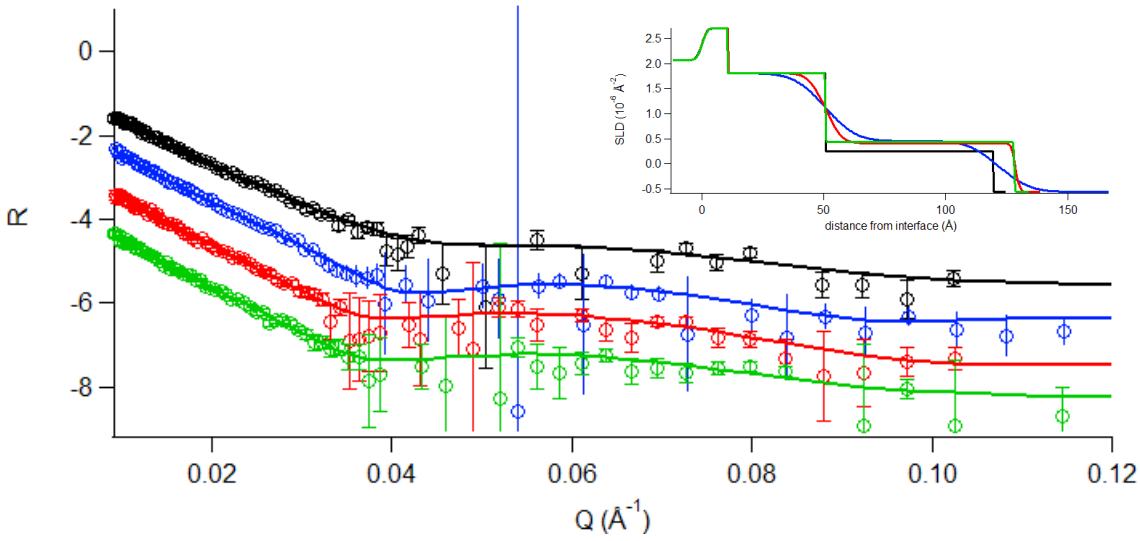


Figure 4.25: Reflectivity profiles and fits showing the changes over time for adsorption of HSA onto a pre-adsorbed d-MBP layer in H_2O. A 2-layer model assuming changes occurred in both layers was used and the runs are the final d-MBP, $t_{inc} = 21$ hrs (black), $t_{ex} = 0$ (blue), $t_{ex} = 12.5$ hours (red) and $t_{ex} = 18.5$ hours (green) with data being offset for clarity. The inset shows the scattering length density profiles and the layer parameters are in table (4.25).

4.3 Discussion

In the previous sections the three proteins, CA II, MBP and LYS and their interactions with HSA have been considered separately both with respect to adsorption onto a pre-adsorbed HSA layer and as an incumbent protein exposed to HSA in the bulk solution. The aims of this section are twofold; firstly a comparison is made between the proteins of interest and their interaction with HSA. Secondly, the underlying experimental methodology will be commented on with respect to the differences caused by using protonated and deuterated proteins.

As a basis of comparison, it is useful to consider the change in adsorbed amount when the pre-adsorbed protein layer is exposed to a different protein. These are shown below in figures (4.26) for the addition to an HSA layer and figure (4.27) for the addition of HSA to the other proteins.

For the addition of proteins onto a pre-adsorbed HSA layer, even when taking into account the variability of the HSA system commented on in section 3.3, there are two noteworthy comparisons; the difference between the three protonated proteins

t_{ex} \hrs	Layer number	Thickness \±3 Å	% Solvent ±4	$\rho_{protein}$ \$\times 10^{-6}$ Å $^{-2}$	Roughness ox-1	Roughness 1-2	Roughness 2-s	Γ \±0.2 mg m^{-2}
final d-MBP	1	40	65	6.2	5	10	10	1.9
	2	69	88	6.2				1.1
0	1	40	65	5.9	1	10	7	1.9
	2	68	84	5.5				1.4
12.5	1	41	60	5.9	5	5	8	2.2
	2	79	81	5.0				1.9
18.5	1	40	63	6.0	5	0	1	2.0
	2	79	82	5.0				1.9

Table 4.25: Layer parameters for the 2-layer model (with changes occurring in the both layers) of adsorption of h-HSA onto a pre-adsorbed d-MBP layer in H_2O (t_{inc} = 21 hours). The data is shown in figure (4.25)

and the difference between h-MBP and d-MBP. CA II and h-MBP show small increases in the adsorbed amount whereas LYS consistently shows an increase of between 1.8 and 2.7 mg m^{-2}. This is best illustrated by comparing the results in tables (4.1), (4.3) and (4.22) which show the adsorption of CA II, LYS and h-MBP respectively onto very similar HSA layers. All three of the proteins can be considered to be rigid with respect to their tertiary structure and all are smaller than HSA with the only major difference being that of their electrostatic properties. At pH 7.4, CA II carries no net charge, HSA and MBP are negatively charged (IEP=4.7 and 5.2[9] respectively) but LYS carries a large, net positive charge due to is IEP being 11.16[10]. An entropic contribution from dehydration of the interface can account for the small addition of CA II but the charge difference between HSA and LYS is providing the main driving force for the adsorption in this case. The apparent importance of charge is perhaps somewhat surprising, as has been noted also by Malmsten[11], given the Debye screening length under these conditions (PBS buffer, [NaCl]=0.137 M) is less than 1 nm but under these conditions the contribution of electrostatics to the overall free energy of adsorption, $\Delta_{ads}G_{el}$ typically varies from a few RT up to a few tens of RT per mol of protein[12]. Similarly, in an adsorption model derived from electrostatic arguments proposed by Hartvig et al.[13] it was assumed that the non-electrostatic contribution to the free energy, $\Delta_{ads}G_{chem}$, is approximately the same for proteins that are otherwise similar and differences in the adsorption of LYS and α-lactalbumin are due to the overall charge and charge distribution. An AFM study of interactions between BSA-BSA and apoferritin-apoferritin adsorbed onto silica showed an attractive force between the protein layers when the pH was below the IEP of the protein which was attributed to the van der Waals forces[14] and this is in the case when the proteins are of the same charge. The additional electrostatic attraction between HSA and LYS will add to this at short ranges.

The other difference of note is the increased adsorbed amount of d-MBP when compared to h-MBP. It can also be seen from table (4.12) that the final layer in this model has a scattering length density of 7.1 $\times 10^{-6}$ Å $^{-2}$ i.e. all d-MBP. This highlights the difference noted in chapter 3 that d-MBP much more readily displaces adsorbed protonated proteins than h-MBP due to the greater affinity for the surface.

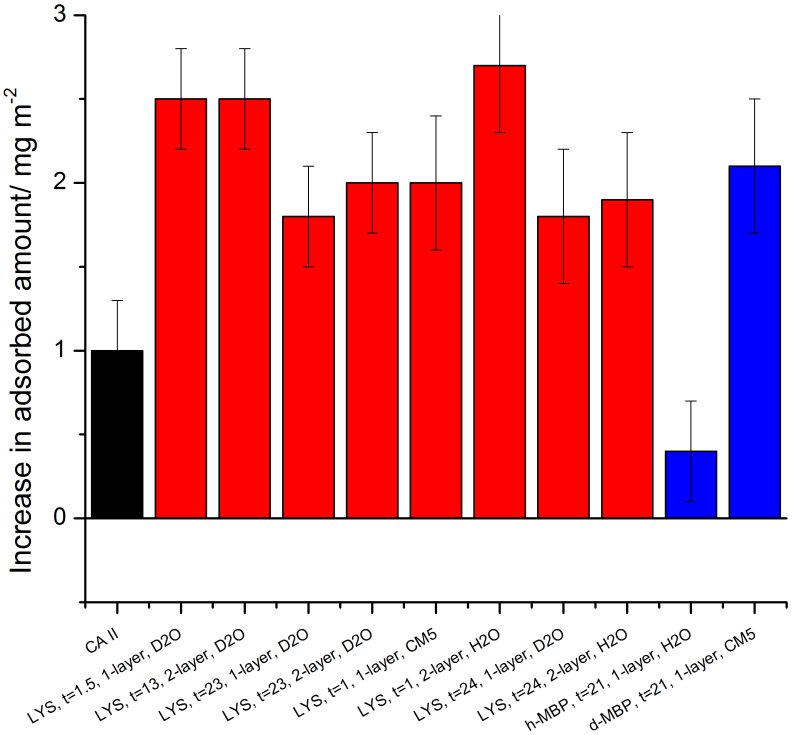


Figure 4.26: The changes in adsorbed amount for the longest t_{ex} timestamps when a pre-adsorbed HSA layer was exposed to other proteins (CA II, LYS and MBP).

When considering the adsorbed amount changes of the exposure of a pre-adsorbed protein layer to HSA, no clear trends emerge with the change in adsorbed amounts being variable. This lack of consistency was also observed in chapter 3 for HSA adsorbing onto a clean silica surface. There are some experiments that show no change or a reduction in the adsorbed amount which is not observed in the pre-adsorbed HSA experiments. For LYS, the t_{inc} =17 hours is anomalous. It is the only data set that required a 2-layer model and also the only one with an increase in the adsorbed amount of greater than 1 mg m^{-2}. The MBP experiments show no noticeable difference between h-MBP and d-MBP, although, taken as an average h-MBP showed less of an increase in the adsorbed amount. These results also show the importance of the order that the surface is exposed to the proteins in determining the final protein layer. With respect to LYS, Arai and Norde [15] have observed with myoglobin and ribonuclease on a negatively charged, hydrophobic PS surface that additional LYS adsorption occurs onto a pre-adsorbed ribonuclease or myoglobin surface but not vice-versa. They attributed this to the dehydration of the hydrophobic patch

on LYS being the driving force. The same phenomena is observed here with HSA on the silica surface even though HSA and RNase are different with respect to their size (66 vs 15 kDa) and charge (-ve vs +ve).

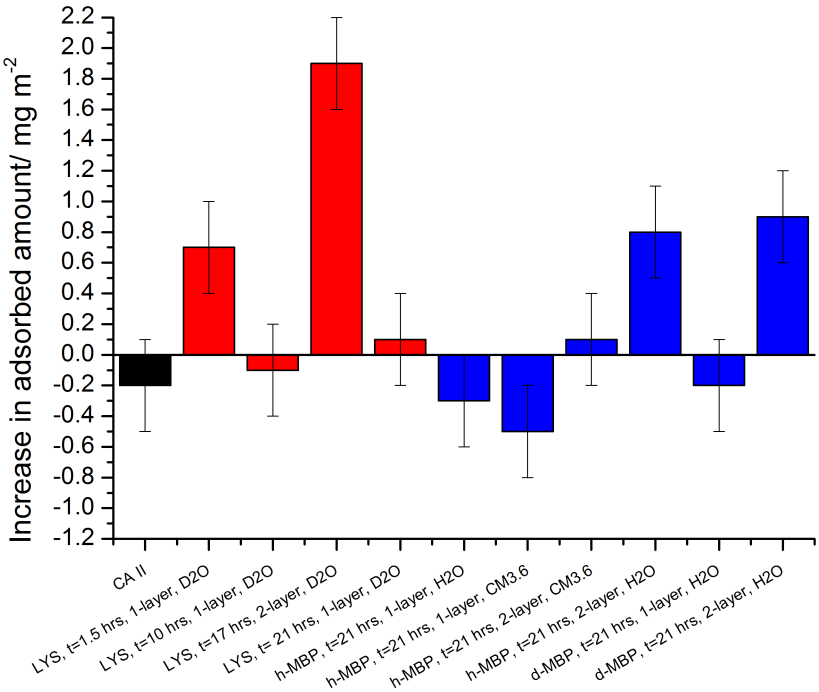


Figure 4.27: The changes in adsorbed amount for the longest t_{ex} timestamps when pre-adsorbed protein layers (CA II, LYS and MBP) were exposed to a solution of HSA.

When considering neutron reflectivity as a technique, it is often quoted that one of its main strengths lies in the ability to distinguish between hydrogen and deuterium containing species. This is certainly true and for many systems the use of contrast variation (altering the deuterium content of either the solvent or the components in a mixture) makes it possible to determine high resolution structural details of multi-component adsorbed layers[16]. This is done with the underlying assumption that the protonated and deuterated components show similar adsorption characteristics. When investigating proteinaceous systems that contain more than one protein species with neutron reflectivity, as is of interest in this work, the use of protonated and deuterated proteins is a very attractive one. This study provides a detailed examination of the limitations of such studies both with respect to the choice of experimental conditions, such as solvent contrast, and the difficulties encountered during the analysis of the data. Similarly, the isotope effects observed show the potential of using the perdeuterated proteins in a different way than previously

imagined. The details of the differences in adsorption and exchange properties provide information on the factors impacting on protein adsorption.

The scattering length density of almost all protonated proteins lies within a small range and thus changing the solvent does not provide sufficient information to determine the composition of the adsorbed layers with respect to the ratio of each protein. If one of the proteins is then substituted for a deuterated form and the experiment repeated, any differences in the scattering length density of the layers from the H/H adsorbed layer could then be attributable to either exchange or added adsorption if it is assumed that h-Protein and d-Protein are the same. However, it is equally possible to assume that the adsorption of the two forms is not the same and thus, the H/D exchange experiments can not be used as a quantitative guide to determine the ratio of h-A and h-B in a mixed A/B layer, which is the ultimate aim of these experiments given that deuterated proteins do not occur in any practical applications. Even if the adsorption of h-Protein and d-Protein from single protein solutions is used as a guide this still does not provide any information regarding the strength of interactions with other proteins which is of importance when considering exchange processes or the additional adsorption in sequential experiments. It has already been shown both in chapter 3 and in the literature [17, 18] that the process of exchange is an active one (rather than via a purely desorption/re-adsorption mechanism) and the nature of the incoming protein is of importance.

When attempting to accurately determine the ratio of h-A:d-B, it is necessary to use multiple solvent contrasts. It has been shown that the properties of proteins are effected by changing the solvent composition with varying ratio of H_2O:D_2O as the labile hydrogens on the protein will exchange for the solvent hydrogens and this exchange of ^1H for ^2H increases the rigidity of the native structure[19, 20, 21]. On a macroscopic level, D_2O is often considered to be a worse solvent than H_2O and attempts to reduce the surface area of contact with the protein molecules[19]. In order to solve the problems in analysis posed by isotope effects (both with respect to the protein itself and the solvent) it is necessary to consider what information is required and the different information provided from different solvent contrasts. For example, if the solvent is contrast matched to the substrate the reflectivity profile is highly sensitive to the adsorbed amount. This can then be used as a guide to determine the thickness and solvent percentage from other water contrasts, albeit allowing for some variability in the parameters to allow for changes in the adsorption under different solvent conditions. This is the commonly accepted procedure when

analysing surfactant adsorption data and has, to an extent, been applied here. However, in this investigation it has been shown that the isotope effects when concerning proteins are of greater importance than in surfactant systems and when considered from this view point the preferred experimental design would have been to investigate fewer systems with more solvent contrasts. It should also be considered though that this would not have revealed the inconsistency with regards to the adsorption of HSA (both onto a clean silica surface and onto pre-adsorbed layers of other proteins), which is possibly one cause of disagreement and lack of consensus within the literature where different techniques, experimental procedures etc. have been used. The greater likelihood of the formation of diffuse multilayers and the range of adsorbed thicknesses concerned also provide another layer of added complexity when compared to surfactant systems.

References

[1] I. Lynch, "Are there generic mechanisms governing interactions between nanoparticles and cells? Epitope mapping the outer layer of the protein-material interface," *Physica A: Statistical and Theoretical Physics*, vol. 373, pp. 511 – 520, 2007.

[2] D. Forciniti and W. A. Hamilton, "Surface enrichment of proteins at quartz/water interfaces: A neutron reflectivity study," *Journal of Colloid and Interface Science*, vol. 285, pp. 458–468, 2005.

[3] S. Guha Thakurta and A. Subramanian, "Evaluation of in situ albumin binding surfaces: a study of protein adsorption and platelet adhesion," *Journal of Materials Science: Materials in Medicine*, vol. 22, pp. 137–149, 2011. 10.1007/s10856-010-4169-3.

[4] T. J. Kinnari, E.-M. Salonen, and J. Jero, "New method for coating tympanostomy tubes to prevent tube occlusions," *International Journal of Pediatric Otorhinolaryngology*, vol. 58, no. 2, pp. 107 – 111, 2001.

[5] N. Maalej, R. Albrecht, J. Loscalzo, and J. D. Folts, "The potent platelet inhibitory effects of S-nitrosated albumin coating of artificial surfaces," *Journal of the American College of Cardiology*, vol. 33, no. 5, pp. 1408 – 1414, 1999.

[6] K. Ogawara, K. Furumoto, S. Nagayama, K. Minato, K. Higaki, T. Kai, and T. Kimura, "Pre-coating with serum albumin reduces receptor-mediated hepatic disposition of polystyrene nanosphere: implications for rational design of nanoparticles," *Journal of Controlled Release*, vol. 100, no. 3, pp. 451 – 455, 2004.

[7] M. Holmberg and X. Hou, "Fibrinogen adsorption on blocked surface of albumin," *Colloids and Surfaces B: Biointerfaces*, vol. 84, no. 1, pp. 71 – 75, 2011.

[8] M. van der Veen, M. C. Stuart, and W. Norde, "Spreading of proteins and its effect on adsorption and desorption kinetics," *Colloids and Surface B: Biointerfaces*, vol. 54, pp. 136–142, 2007.

[9] S. Raghava, S. Aquil, S. Bhattacharyya, R. Varadarajan, and M. N. Gupta, "Strategy for purifying maltose binding protein fusion proteins by affinity precipitation," *Journal of Chromatography A*, vol. 1194, no. 1, pp. 90 – 95, 2008. 27th International Symposium on the Separation of Proteins, Peptides & Polynucleotides.

[10] D. E. Kuehner, J. Engmann, F. Fergg, M. Wernick, H. W. Blanch, and J. M. Prausnitz, "Lysozyme net charge and ion binding in concentrated aqueous

electrolyte solutions," *The Journal of Physical Chemistry B*, vol. 103, no. 8, pp. 1368–1374, 1999.

[11] M. Malmsten, "Ellipsometry studies of the effects of surface hydrophobicity on protein adsorption," *Colloids and Surfaces B: Biointerfaces*, vol. 3, no. 5, pp. 297 – 308, 1995.

[12] W. Norde, *Surfactant Science Series Volume 110: Biopolymers at Interfaces (2nd ed.)*, ch. 2. Driving Forces for Protein Adsorption at Solid Surfaces, pp. 21–44. Marcel Dekker, Inc., 2003.

[13] R. A. Hartvig, M. van de Weert, J. stergaard, L. Jorgensen, and H. Jensen, "Protein adsorption at charged surfaces: The role of electrostatic interactions and interfacial charge regulation," *Langmuir*, vol. 27, no. 6, pp. 2634–2643, 2011.

[14] J. J. Valle-Delgado, J. A. Molina-Bolvar, F. Galisteo-Gonzlez, M. J. Glvez-Ruiz, A. Feiler, and M. W. Rutland, "Measurement of interactions between protein layers adsorbed on silica by atomic force microscopy," *Journal of Physics: Condensed Matter*, vol. 16(26), pp. S2383–22392, 2004.

[15] T. Arai and W. Norde, "The behavior of some model proteins at solid-liquid interfaces. 2. Sequential and competitive adsorption," *Colloids and Surfaces*, vol. 51, pp. 17–28, 1990.

[16] J. Penfold, R. M. Richardson, A. Zarbakhsh, J. R. P. Webster, D. G. Bucknall, A. R. Rennie, R. A. L. Jones, T. Cosgrove, R. K. Thomas, J. S. Higgins, P. D. I. Fletcher, E. Dickinson, S. J. Roser, I. A. McLure, A. R. Hillman, R. W. Richards, E. J. Staples, A. N. Burgess, E. A. Simister, and J. W. White, "Recent advances in the study of chemical surfaces and interfaces by specular neutron reflection," *J. Chem. Soc., Faraday Trans.*, vol. 93(22), pp. 3899–3917, 1997.

[17] V. Ball, P. Schaaf, and J.-C. Voegel, *Surfactant Science Series Volume 110: Biopolymers at Interfaces (2nd ed.)*, ch. 11. Mechanisms of Interfacial Excahnge Phenomena for Proteins Adsorbed at Solid-Liquid Interfaces, pp. 295–320. Marcel Dekker, Inc., 2003.

[18] G. Szollosi, I. Derenyi, and J. Voros, "Reversible mesoscopic model of protein adsorption: From equilibrium to dynamics," *Physica A*, vol. 343, pp. 359–375, 2004.

[19] P. Cioni and G. B. Strambini, "Effect of heavy water on protein flexibility," *Biophysical Journal*, vol. 82, pp. 3246–3253, 2002.

[20] A. Hattori, H. L. Crespi, and J. J. Katz, "Effect of side-chain deuteration on protein stability," *Biochemistry*, vol. 4, no. 7, pp. 1213–1225, 1965.

[21] L. Fu, S. Villette, S. Petoud, F. Fernandez-Alonso, and M.-L. Saboungi, "H/D isotope effects in protein thermal denaturation: The case of bovine serum albumin," *The Journal of Physical Chemistry B*, vol. 115, no. 8, pp. 1881–1888, 2011.

Chapter 5

Results: Adsorption of binary protein mixtures

In the previous two chapters the adsorption of single proteins and sequential adsorption scenarios have been investigated and discussed. However, in practically all applications adsorption to a solid surface occurs from a mixture of proteins and although it is necessary to understand the adsorption of single proteins and the impact of changing the protein environment in the bulk phase this should always be done with the aim of applying what has been learnt from these experiments to understand further what governs the competitive adsorption of proteins from a mixture. With this aim in mind this chapter is concerned with the adsorption of binary protein mixtures.

Often adsorption from a mixture is not directly compared to the sequential case as one may be favoured over the other depending on the researchers' aims. A study by Noh and Vogler[1] which did compare them showed no difference between competitive adsorption and sequential with an incubation time of 1 hour but this is an exception to the general findings that pre-adsorption of a protein will result in it being found in a higher proportion in the final layer compared to when adsorbed from a mixture. For example, when adsorbed onto polymer surfaces from a bulk mixture with HSA, Fibrinogen and IgG dominated the layer but in sequential studies they could not displace the pre-adsorbed HSA[2].

Another motivation for investigating the adsorption of mixtures is the possibility of observing cooperative effects such as those for protein/ surfactant[3] and polyectrolyte/ surfactant[4] systems. Cooperativity in protein systems is often observed

as faster kinetics or a S-shaped isotherm or an increased adsorbed amount[5]. The mechanism proposed by Rabe et al. [5, 6] is that when a protein from the bulk comes into contact with a pre-adsorbed protein it is not necessarily repelled from the surface but can diffuse laterally and be directed to a free binding site on the surface.

The total concentration is the same as for the single protein experiments, 1 mg ml^{-1}, to allow for a direct comparison of adsorbed amounts and layer structures and the only mixtures that were looked at were 50:50 by mass i.e. 0.5 mg ml^{-1} of each protein. This was chosen rather than an equimolar mixture as it has been shown that interfacial energetics of protein adsorption are very similar when scaled on a w/v basis[7, 8, 9].

5.1 HSA and CA II

As has been noted previously, the scattering length densities of CA II and HSA are the same so it is not possible to determine the composition in the final adsorbed layer with respect to protein ratios but there is less error in the determination of the layer parameters and total adsorbed amount. A 1-layer model was first used to fit the reflectivity profiles which can be seen in figure (5.1) and the corresponding layer parameters in table (5.1). The 1-layer model did not give satisfactory fits or consistent values for the thickness and adsorbed amounts. A 2-layer model was then used, which improved the χ^2 values by 10%. The fits and scattering length density profiles shown in figure (5.2) and the corresponding layer parameters in table (5.2).

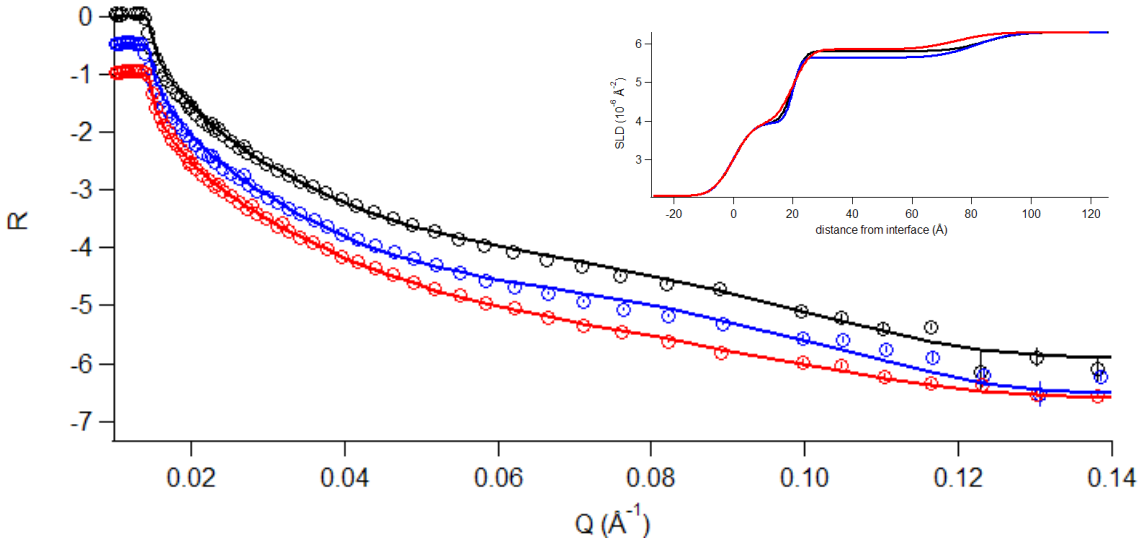


Figure 5.1: Reflectivity profiles and fits showing the changes over time for the adsorption of a 50:50 mixture of HSA and CA II in D_2O. A 1-layer model was used and the runs are t_{inc} = 0 hrs (black), t_{inc} = 8.5 (blue) and t_{inc} = 10.5 hours (red) with data being offset for clarity. The inset shows the scattering length density profiles and the layer parameters are in table (5.1).

t_{inc} \hrs	Thickness \±2 Å	% Solvent ±4	Roughness		Γ \±0.2 mg m^{-2}
			ox-1	1-s	
0	65	85	5	10	1.3
8.5	62	80	5	10	1.6
10.5 (wash)	55	87	0	2	0.9

Table 5.1: Layer parameters for the 1-layer model of adsorption of a 50:50 mixture of HSA and CA II in D_2O. The data is shown in figure (5.1)

The 2-layer model is similar to that of the single protein adsorption for both HSA and CA II, a denser inner layer and more diffuse outer layer and the thicknesses of the layers are comparable with the solution dimensions of the proteins. The layer formed from the mixture is more susceptible to desorption into the bulk than the single proteins and also desorption occurs from both layers. From these results it can be concluded that the interaction between HSA and CA II is weak and does not effect the adsorption in any dramatic fashion. This is to be expected given the net neutral charge on CA II and small negative charge on HSA. There are also no structural features on the exteriors of either protein that would allow for any specific interactions.

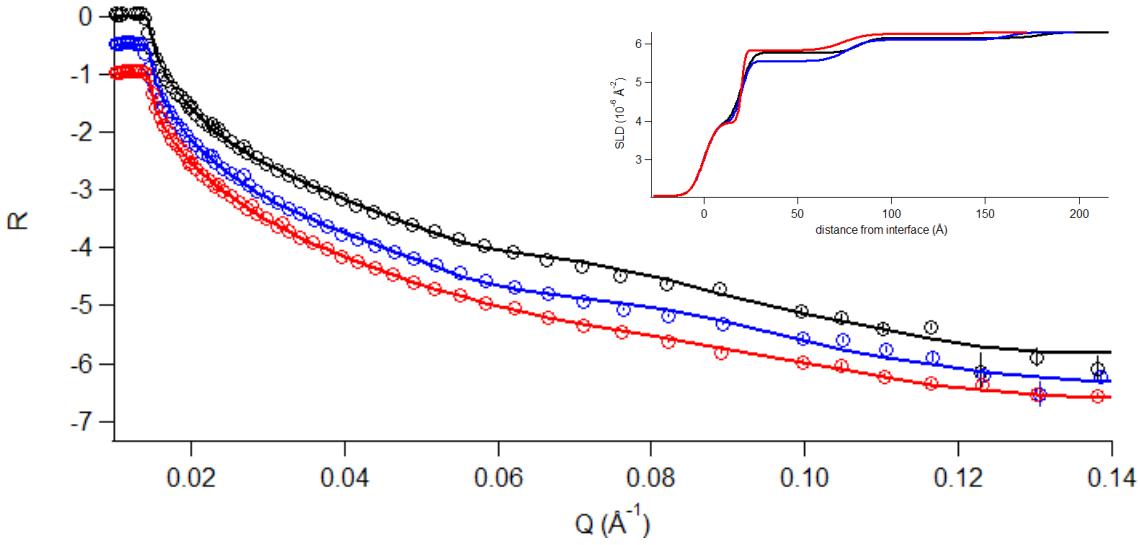


Figure 5.2: Reflectivity profiles and fits showing the changes over time for the adsorption of a 50:50 mixture of HSA and CA II in D_2O. A 2-layer model was used and the runs are t_{inc} = 0 hrs (black), t_{inc} = 8.5 (blue) and t_{inc} = 10.5 hours (red) with data being offset for clarity. The inset shows the scattering length density profiles and the layer parameters are in table (5.2).

t_{inc} \hrs	Layer number	Thickness \±3 Å	% Solvent ±4	Roughness			Γ \±0.2 mg m^{-2}
				ox-1	1-2	2-s	
0	1	63	84	4	7	8	1.3
	2	96	96				0.5
8.5	1	56	77	4	9	8	1.7
	2	86	94				0.7
10.5 (wash)	1	55	86	2	10	6	1.0
	2	70	98				0.2

Table 5.2: Layer parameters for the 2-layer model of adsorption of a 50:50 mixture of HSA and CA II in D_2O. The data is shown in figure (5.2)

5.2 HSA and LYS

The adsorption of a 50:50 mixture of h-HSA and LYS (total concentration = 1 mg ml^{-1}) onto a clean silica surface was investigated in D_2O. During the fitting, it was assumed that the scattering length density of the adsorbed layer was 3.3×10^{-6} Å $^{-2}$ which represents an equal amount of LYS and HSA being adsorbed. The reflectivity profiles, fits and scattering length densities for a 1-layer model can be seen in figure

(5.3) with the corresponding layer parameters in table (5.3). The layer thickness is in good agreement with the 1-layer models for LYS in section 3.2. The adsorbed amounts are slightly lower than the single LYS adsorption result. However, if it is assumed that all the adsorbed protein in this case is LYS and taking into account the reduced bulk concentration of LYS the adsorption from a mixture is consistent with the adsorbed layer being composed almost entirely of LYS. This is in good agreement with Palacio et al.[10] who showed that with a mixture of BSA and LYS, fouling during microfiltration is dominated by the LYS.

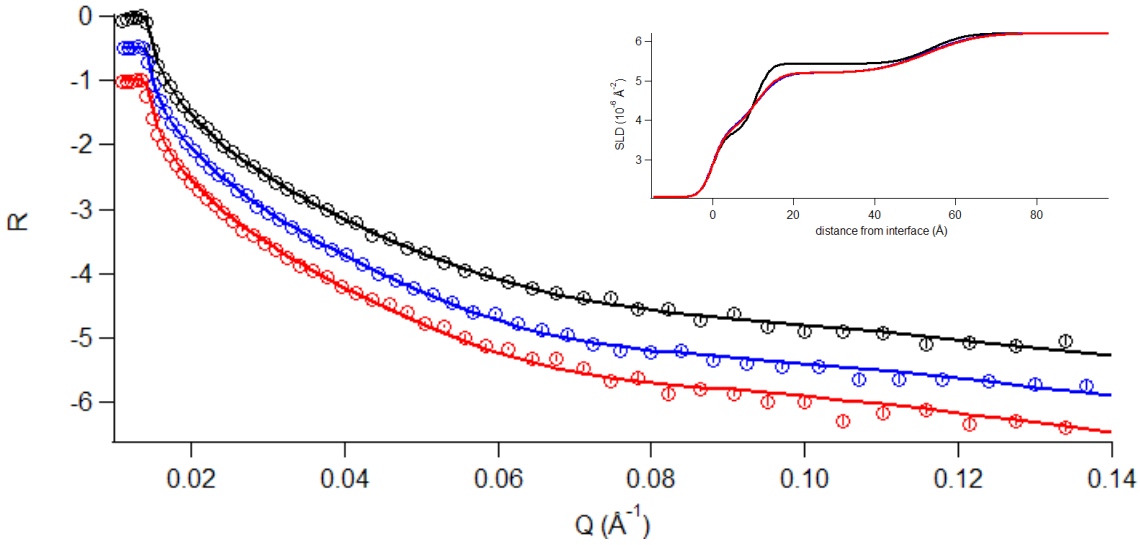


Figure 5.3: Reflectivity profiles and fits showing the changes over time for the adsorption of a 50:50 mixture of HSA and LYS in D_2O. A 2-layer model was used and the runs are $t_{inc} = 0$ hrs (black), $t_{inc} =$ (blue) and $t_{inc} =$ hours (red) with data being offset for clarity. The inset shows the scattering length density profiles and the layer parameters are in table (5.3).

t_{inc} \hrs	Thickness \±2 Å	% Solvent ±4	Roughness		Γ \±0.2 mg m^{-2}
			ox-1	1-s	
0	43	74	2	3	1.5
4	42	66	1	8	1.9
16.5	43	66	0	10	1.9

Table 5.3: Layer parameters for the 1-layer model of adsorption of a 50:50 mixture of HSA and LYS in D_2O. The data is shown in figure (5.3)

When fitting the d-HSA/LYS mixture it was first assumed that the layer structure would be approximately the same as for the h-HSA/LYS system and so the layer

parameters where restricted to the following ranges: $38 \leq \tau \leq 48$, $61 \leq$ solvent % ≤ 71. The reflectivity profiles and fits shown in figure (5.4) clearly show that this model does not fit the data. The constraints were then relaxed and the data was fitted to a 1-layer model. The reflectivity profiles, fits and scattering length density profiles for this 1-layer model are shown in figure (5.5) with the corresponding layer parameters in table (5.4). The best fits to the 1-layer model suggest that the layer is thicker than in the h-HSA/LYS system but the fits are poor, particularly in the region around Q= 0.06 $Å^{-1}$ so a 2-layer model was used.

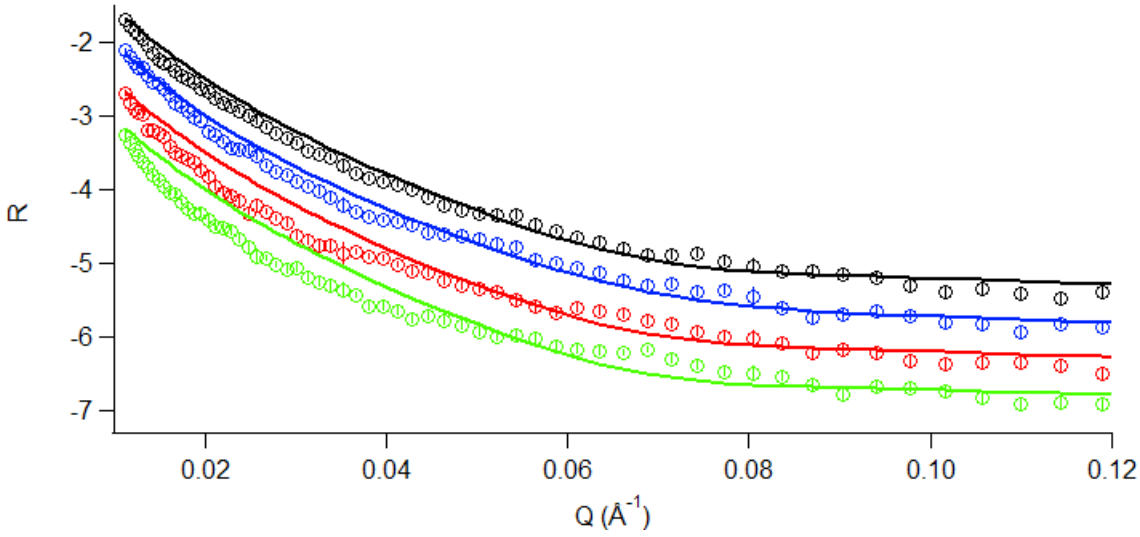


Figure 5.4: Reflectivity profiles and fits showing the changes over time for the adsorption of a 50:50 mixture of d-HSA and LYS in H_2O. A 1-layer model was used with similar layer parameters as the h-HSA/LYS mixture. The runs are $t_{inc} = 0$ hrs (black), $t_{inc} = 4$hrs (blue), $t_{inc} = 10$ hours (red) and $t_{inc} = 16$ hours (green) with data being offset for clarity. The inset shows the scattering length density profiles.

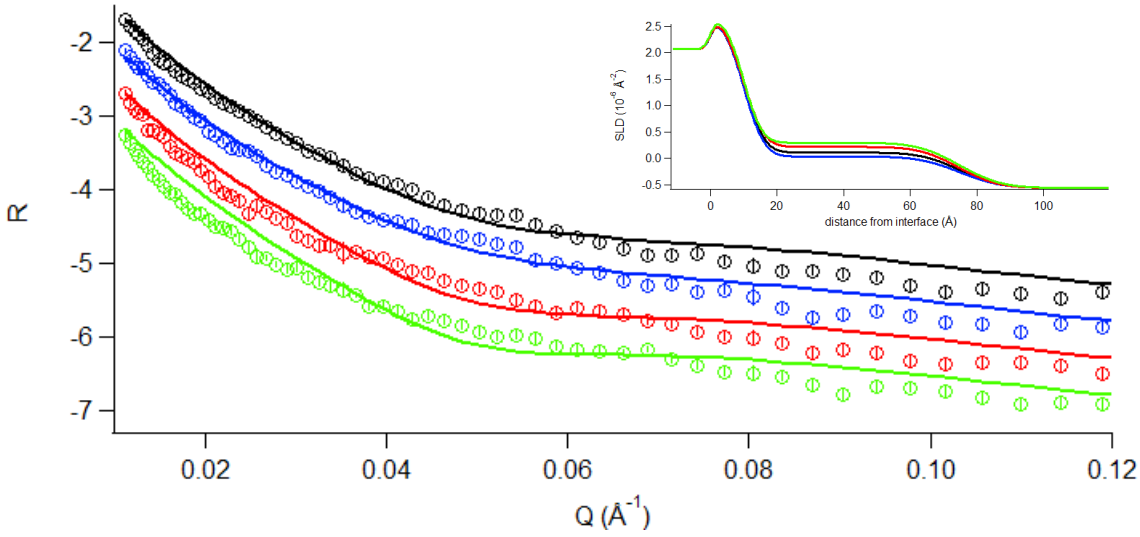


Figure 5.5: Reflectivity profiles and fits showing the changes over time for the adsorption of a 50:50 mixture of d-HSA and LYS in H_2O. A 1-layer model was used and the runs are $t_{inc} = 0$ hrs (black), $t_{inc} = 4$hrs (blue), $t_{inc} = 10$ hours (red) and $t_{inc} = 16$ hours (green) with data being offset for clarity. The inset shows the scattering length density profiles and the layer parameters are in table (5.4).

t_{inc} \hrs	Thickness \±2 Å	% Solvent ±4	$\rho_{protein}$ \$\times 10^{-6}$ Å $^{-2}$	Roughness		Γ \±0.2 mg m^{-2}
				ox-1	1-s	
0	65	82	3.2	5	10	1.6
4.5	65	85	3.4	5	10	1.4
10	65	80	3.1	5	9	1.7
16	65	83	4.3	4	10	1.5

Table 5.4: Layer parameters for the 1-layer model of adsorption of a 50:50 mixture of d-HSA and LYS in H_2O. The data is shown in figure (5.5)

The reflectivity profiles, fits and scattering length density profiles for the 2-layer model are shown in figure (5.6) with the corresponding layer parameters in table (5.5). The adsorbed amount is similar to that observed for adsorption from a solution of only LYS but the overall thickness is more comparable with that of a 2-layer model of d-HSA adsorption in section 3.3.2. However, the scattering length densities of the layers in this case suggest that most of the adsorbed protein is LYS in the bottom layer and that the outer layer is comprised more of d-HSA. The individual scattering length densities in H_2O are 1.9 and 6.1×10^{-6} Å $^{-2}$ for LYS and d-HSA respectively. Therefore a value of 4.0×10^{-6} Å $^{-2}$ represents a 1:1 ratio

of LYS:d-HSA.

Overall this result is in good agreement with the h-HSA/LYS conclusion. In a 50:50 w/v mixture of LYS and HSA adsorbing onto a clean silica surface the adsorbed layer formed is composed mostly of LYS. The higher adsorbed amount and higher proportion of HSA in the layer when considering the d-HSA/LYS system is a result of the higher affinity for the surface of the perdeuterated protein when compared to its protonated counterpart as has been discussed in the previous chapter.

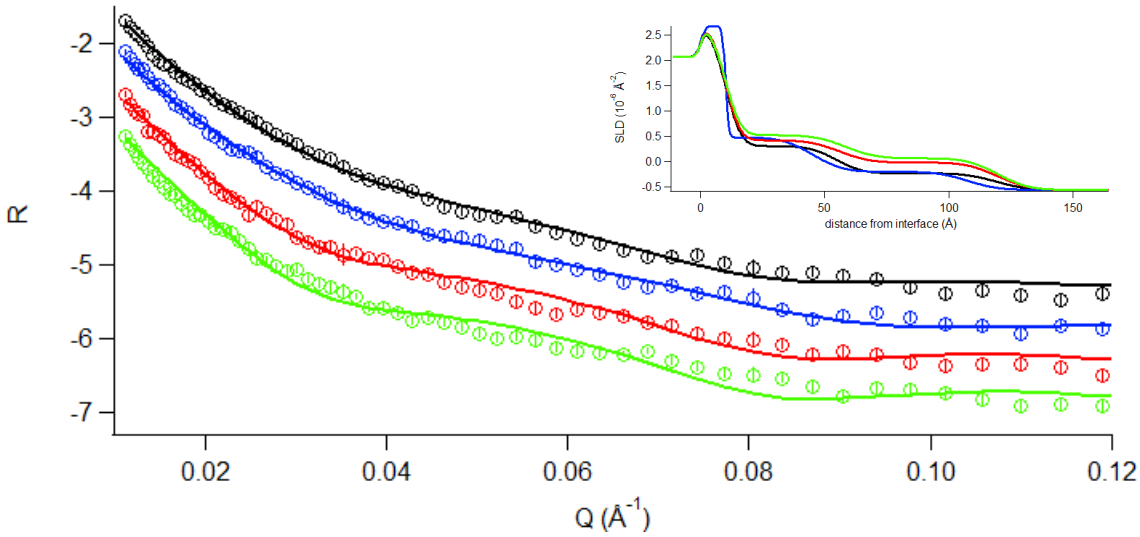


Figure 5.6: Reflectivity profiles and fits showing the changes over time for the adsorption of a 50:50 mixture of d-HSA and LYS in H_2O. A 2-layer model was used and the runs are t_{inc} = 0 hrs (black), t_{inc} = (blue) and t_{inc} = hours (red) with data being offset for clarity. The inset shows the scattering length density profiles and the layer parameters are in table (5.5).

t_{ex} \hrs	Layer number	Thickness \±2 Å	% Solvent ±5	$\rho_{protein}$ \$\times 10^{-6}$ Å $^{-2}$	Roughness			Γ \±0.4 mg m^{-2}
					ox-1	1-2	2-s	
0	1	45	70	2.3	5	8	10	1.8
	2	65	94	5.2				0.5
4.5	1	35	67	2.5	1	10	10	1.5
	2	63	90	3.2				0.9
10	1	46	71	2.8	5	4	10	1.8
	2	64	89	4.4				0.9
16	1	48	69	2.9	5	10	10	2.0
	2	62	86	4.0				1.2

Table 5.5: Layer parameters for the 2-layer model of adsorption of a 50:50 mixture of d-HSA and LYS in H_2O. The data is shown in figure (5.6)

5.3 HSA and MBP

The adsorption of a 50:50 mixture of h-HSA and h-MBP (total concentration = 1 mg ml^{-1}) onto a clean silica surface was investigated in CM5[1]. The reflectivity profiles, fits and scattering length density profile for a 1-layer model are shown in figure (5.7) with the corresponding layer parameters in table (5.6). This model shows that the adsorbed layer is quite diffuse with only 14 % protein and both the adsorbed amount and thickness are within the ranges of the single protein solution adsorption, especially when compared to the 2-layer models in these cases. For the mixture, however, a 2-layer model does not improve the 1-layer model fit.

[1]This solvent contrast was used because the supplied h-MBP was in H_2O buffer and this was the highest possible scattering length density achievable in order to maximise the difference between the scattering length densities of the protein and the solvent whilst keeping to a minimum the non-coherent scattering from H_2O.

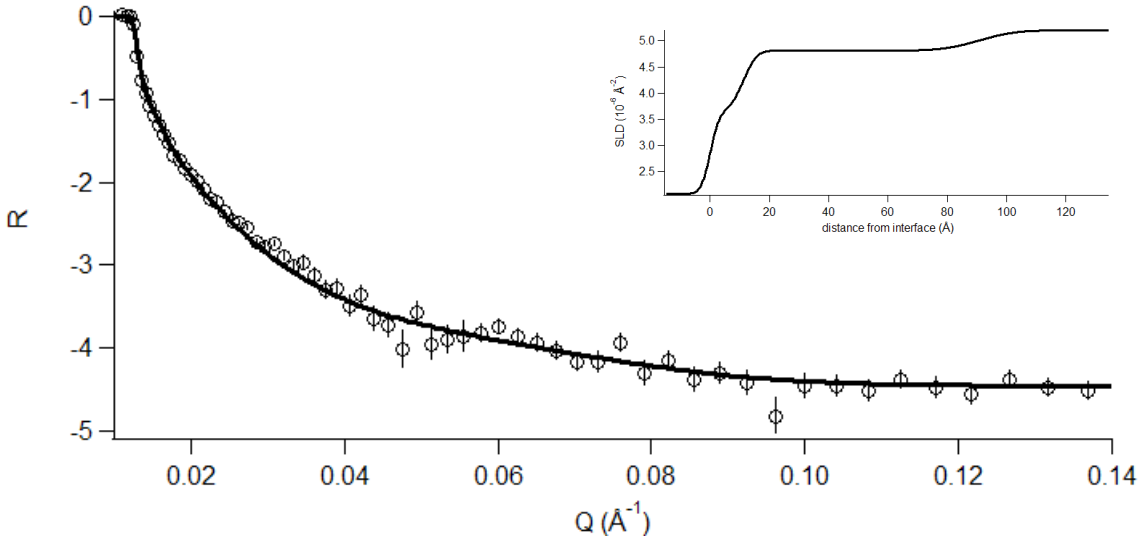


Figure 5.7: Reflectivity profiles and fits showing the changes over time for the adsorption of a 50:50 mixture of HSA and h-MBP in CM5. A 1-layer model was used and the runs are t_{inc} = 0 hrs (black). The inset shows the scattering length density profile and the layer parameters are in table (5.6).

t_{inc} \hrs	Thickness \±2 Å	% Solvent ±4	Roughness		Γ \±0.2 mg m^{-2}
			ox-1	1-s	
0	80	84	4	10	1.7

Table 5.6: Layer parameters for the 1-layer model of adsorption of a 50:50 mixture of HSA and h-MBP in CM5. The data is shown in figure (5.7)

With the aim of providing more information on the MBP/HSA mixture, the adsorption of a 50:50 mixture of d-MBP and HSA was investigated in CM5. Following the protocol outlined for the HSA/LYS system, it was attempted to fit the reflectivity profiles with a model that was similar to the h-MBP/HSA model. The layer parameters were constrained to the following ranges: $75 \leq \tau \leq 85$, $79 \leq$ solvent % ≤ 89 i.e. the h-MBP values ±5. The reflectivity profiles, fits and scattering length density profile for this 1-layer model are shown in figure (5.8) with the corresponding layer parameters in table (5.7). These show that the fits are good at low Q but are not at $0.03 \leq Q \leq 0.07$ Å^{-1} and the fits are progressively worse as time processes.

A 1-layer model was then used but with the constraints on the fitting parameters removed. The reflectivity profiles, fits and scattering length density profile for this model are shown in figure (5.9) with the corresponding layer parameters in table

(5.8). This model shows that the adsorbed amount is greater than the h-MBP/HSA system and the thickness is less. It can also be seen from the values for the scattering length densities that the adsorbed layer is composed almost entirely of d-MBP rather than HSA. Despite the lack of other solvent contrasts and the interdependency of the protein scattering length density and the solvent percentage this result is unambiguous. Due to the adsorption of the protein layer the reflectivity profile is shifted upwards compared with the oxide layer and this occurs because the scattering length density of the adsorbed layer is greater than that of the bulk solvent, which is 5×10^{-6} Å $^{-2}$. The scattering length densities of the individual proteins are 2.8 and 7.1×10^{-6} Å $^{-2}$ for h-HSA and d-MBP when in CM5 water. The thicknesses, solvent percentage and adsorbed amount are all in good agreement with the adsorption of d-MBP discussed in chapter 3. From this evidence it can be concluded that d-MBP dominates over HSA when adsorbed from an equal mixture. This is in good agreement with the sequential adsorption studies in section 4.1.3 where the d-MBP was shown to totally displce a pre-adsorbed HSA layer.

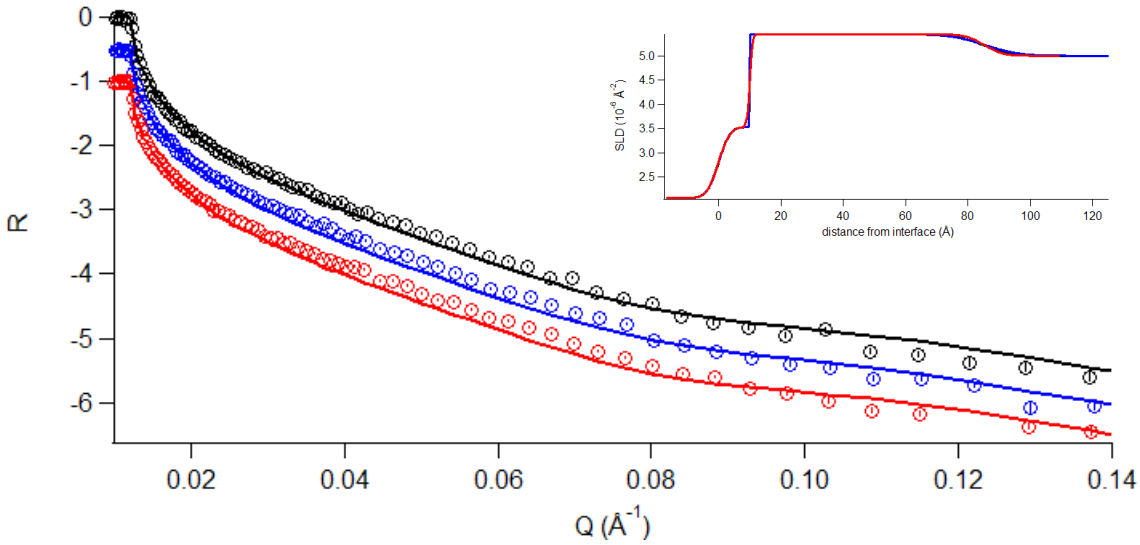


Figure 5.8: Reflectivity profiles and fits showing the changes over time for the adsorption of a 50:50 mixture of HSA and d-MBP in CM5. A 1-layer model was used with layer parameters restricted to ±5 the HSA/h-MBP mixture and the runs are t_{inc} = 0 hrs (black), t_{inc} = 10.5 hours (blue) and t_{inc} = 15.5 hours (red) with data being offset for clarity. The inset shows the scattering length density profiles and the layer parameters are in table (5.8).

t_{inc} \hrs	Thickness \±3 Å	% Solvent ±4	$\rho_{protein}$ \$\times 10^{-6}$ Å $^{-2}$	Roughness		Γ \±0.2 mg m^{-2}
				ox-1	1-s	
0	75	79	7.1	0	7	2.1
10.5	76	79	7.1	0	9	2.1
15.5	75	79	7.1	1	5	2.1

Table 5.7: Layer parameters for the 1-layer model of adsorption of a 50:50 mixture of HSA and d-MBP in CM5 with layer parameters restricted to ±5 the HSA/h-MBP mixture. The data is shown in figure (5.8)

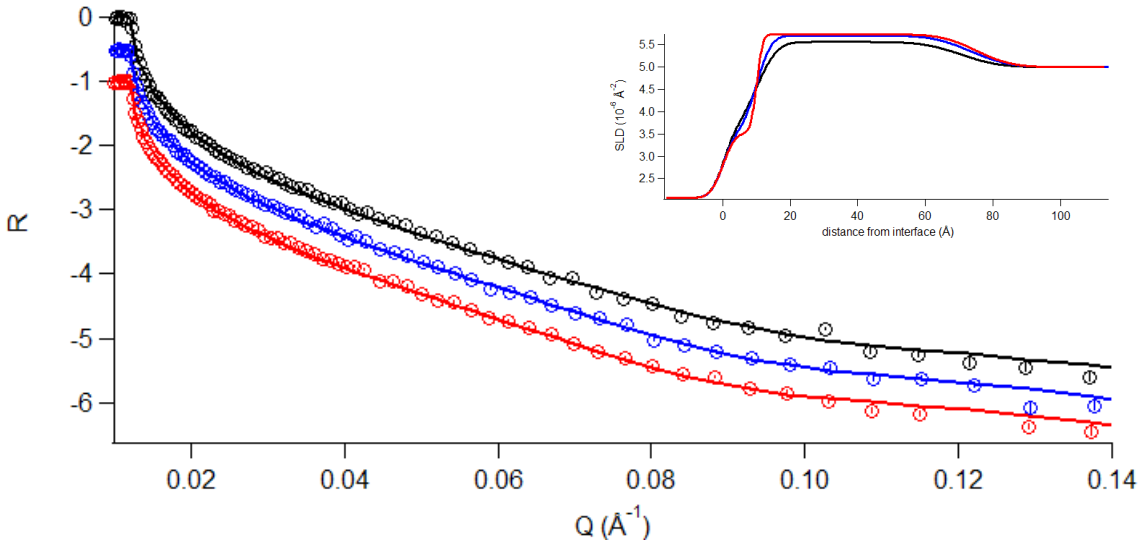


Figure 5.9: Reflectivity profiles and fits showing the changes over time for the adsorption of a 50:50 mixture of HSA and d-MBP in CM5. A 1-layer model was used and the runs are t_{inc} = 0 hrs (black), t_{inc} = 10.5 hours (blue) and t_{inc} = 15.5 hours (red) with data being offset for clarity. The inset shows the scattering length density profiles and the layer parameters are in table (5.8).

t_{inc} \hrs	Thickness \±3 Å	% Solvent ±4	$\rho_{protein}$ \$\times 10^{-6}$ Å $^{-2}$	Roughness		Γ \±0.2 mg m^{-2}
				ox-1	1-s	
0	61	73	7.1	5	9	2.2
10.5	64	66	7.1	3	9	2.9
15.5	65	65	7.1	1	8	3.0

Table 5.8: Layer parameters for the 1-layer model of adsorption of a 50:50 mixture of HSA and d-MBP in CM5 with no constraints on the layer parameters during fitting. The data is shown in figure (5.9)

5.4 Discussion

The adsorption of HSA and CA II are similar in terms of their layer thicknesses when from single protein solutions thus in this case it is not possible to determine the proportion of each protein in the layer when adsorbed from a mixture when using only protonated forms. The thickness of the 1-layer model more closely resembles that of HSA suggesting that the layer is not entirely CA II but beyond this conjecture no conclusions can be drawn.

For the other mixtures studied, HSA & LYS and HSA & MBP, the availability of deuterated proteins provides the possibility of being able to determine the ratios of each protein in the adsorbed layer using neutron reflectivity. The comparison of h + h and h + d mixtures to elucidate this information relies on the characteristics of the adsorbed layer in terms of thickness and solvent percentage to be similar for the two cases. This is commonly the case for surfactant and surfactant/polymer systems but the results presented above demonstrate that when protein mixtures are of interest the assumption no longer holds. This is shown most clearly by attempting to fit the d-HSA & LYS and d-MBP & h-HSA mixtures with similar layer characteristics to the h & h mixtures. The poor agreement between the reflectivity profiles and fits can be seen in figures (5.4) and (5.8). In both these cases the deuterated protein is presented in a greater proportion in the adsorbed layer than would be predicted from the h & h systems. This is in good agreement with the conclusions drawn in chapters 3 and 4 that the isotopic substitution of d for h in the polypeptide backbone has the effect of increasing the affinity of the protein for the silica surface.

As well as this isotope effect, the h-HSA & LYS layer characteristics being very similar to that of the adsorption of LYS alone (see section 3.2) suggest that in this case LYS is dominant in the layer. At the air/liquid interface it has been argued that the interfacial activities can be scaled on a molecular weight basis [7, 8, 11]. Similarly, at the solid/liquid interface the sequence of adsorption is often found to follow that of molecular weights[12, 13]. The evidence of LYS (14.3 kDa) and d-MBP (42.5 kDa) both out competing HSA (67 kDa) when adsorbed from an equal weight mixture as well as the differences between the deuterated and protonated forms shows that when adsorption to hydrophilic silica is of interest then molecular weight is not the most important factor. Other contributions come from electrostatic interactions and the proteins propensity to unfold at the interface to increase the rotational freedom of the polypeptide backbone.

If the competitive adsorption scenario is compared with that for sequential adsorption discussed in chapter 4 the effect of incubation time can be seen. When adsorbed from a mixture, LYS dominates the layer over HSA but in the case when LYS is added sequentially it can not displace the pre-adsorbed HSA to such a great extent. This is due to the HSA being attached more strongly to the surface after an incubation time as it has had time to unfold and form more links to the surface before LYS is present. This agrees with the trends observed in chapter 3 for the self exchange of MBP. However, in the case of d-MBP & HSA there is no discernable difference in the final adsorbed layer characteristics between the sequential and competitive adsorption scenarios. Noh et al.[1] have shown that there is no difference between the sequential and competitive adsorption, which concurs with the HSA\d-MBP system, whereas other authors, for example Nasir et al. and Wertz and Santore [14, 15] have demonstrated a clear effect of incubation time on the extent of exchange, as per the HSA\LYS system. The fact that in this study both agreement and disagreement between the adsorption protocols are observed shows that it should not be inferred that one school of thought is necessarily correct and the other wrong. The extent to which the adsorption scenarios differ can be seen as a complex interdependency of many factors. The degree of differences in terms of the final appearance of the protein layer can clearly vary from a dramatic change for some systems, for example the incubation time has more effect when adsorbing onto hydrophobic surfaces [2, 16], through a sliding scale of differences until systems that show no change are observed.

References

[1] H. Noh and E. A. Vogler, "Volumetric interpretation of protein adsorption: Competition from mixtures and the Vroman effect," *Biomaterials*, vol. 28, pp. 405–422, 2007.

[2] B. Lassen and M. Malmsten, "Competitive protein adsorption at plasma polymer surfaces," *Journal of Colloid and Interface Science*, vol. 186, no. 1, pp. 9 – 16, 1997.

[3] R. J. Green, T. J. Su, J. R. Lu, and J. Penfold, "The interaction between SDS and lysozyme at the hydrophilic solid-water interface," *Journal of Physical Chemistry B*, vol. 105, p. 1594, 2001.

[4] J. Penfold, I. Tucker, E. Staples, and R. K. Thomas, "Manipulation of the adsorption of ionic surfactants onto hydrophilic silica using polyelectrolytes," *Langmuir*, vol. 20, no. 17, pp. 7177–7182, 2004. PMID: 15301503.

[5] M. Rabe, D. Verdes, J. Zimmermann, and S. Seeger, "Surface organization and cooperativity during nonspecific protein adsorption events," *The Journal of Physical Chemistry B*, vol. 112, no. 44, pp. 13971–13980, 2008. PMID: 18842014.

[6] M. Rabe, D. Verdes, and S. Seeger, "Understanding protein adsorption phenomena at solid surfaces," *Advances in Colloid and Interface Science*, vol. 162, pp. 87–106, 2011.

[7] E. A. Vogler, "Protein adsorption in three dimensions," *Biomaterials*, vol. 33, pp. 1201–1237, 2012.

[8] A. Krishnan, C. A. Siedlecki, and E. A. Vogler, "Traube-rule interpretation of protein adsorption at the liquid-vapor interface," *Langmuir*, vol. 19, no. 24, pp. 10342–10352, 2003.

[9] A. Krishnan, C. A. Siedlecki, and E. A. Vogler, "Mixology of protein solutions and the Vroman effect," *Langmuir*, vol. 20, no. 12, pp. 5071–5078, 2004. PMID: 15984270.

[10] L. Palacio, C.-C. Ho, P. Prdanos, A. Hernndez, and A. Zydney, "Fouling with protein mixtures in microfiltration: BSA-lysozyme and BSA-pepsin," *Journal of Membrane Science*, vol. 222, no. 12, pp. 41 – 51, 2003.

[11] P. Cha, A. Krishnan, V. F. Fiore, and E. A. Vogler, "Interfacial energetics of protein adsorption from aqueous buffer to surfaces with varying hydrophilicity," *Langmuir*, vol. 24, no. 6, pp. 2553–2563, 2008. PMID: 18229964.

[12] W. Norde, *Physical Chemistry of Biological Interfaces*, ch. 4. Proteins at Solid Surfaces, pp. 115–135. Marcel Dekker, Inc., 2000.

[13] L. Vroman and A. L. Adams, "Adsorption of proteins out of plasma and solutions in narrow spaces," *Journal of Colloid and Interface Science*, vol. 111, no. 2, pp. 391 – 402, 1986.

[14] A. Nasir and J. McGuire, "Sequential and competitive adsorption of bovine serum albumin and β-lactoglobulin, and their resistance to exchange with α-lactalbumin and β-casein," *Food Hydrocolloids*, vol. 12, no. 1, pp. 95 – 103, 1998.

[15] C. F. Wertz and M. M. Santore, "Adsorption and relaxation kinetics of albumin and fibrinogen on hydrophobic surfaces: Single-species and competitive behavior," *Langmuir*, vol. 15, no. 26, pp. 8884–8894, 1999.

[16] N. Podhipleux, J. McGuire, M. Bothwell, and T. Horbett, "Sequential adsorption of bacteriophage T4 lysozyme stability variants at solidwater interfaces," *Colloids and Surfaces B: Biointerfaces*, vol. 27, no. 4, pp. 277 – 285, 2003.

Chapter 6

Results: Effect of fatty acids on the adsorption of HSA

6.1 Introduction

It is widely accepted that when a solid substrate is in contact with a biological mileu after a matter of seconds it will be covered with an adsorbed layer of proteins. The nature of this layer and its biological response is a complex one and an aim of this work is to ellucidate some of the factors involved in protein adsorption. Thus far this has been done by investigating protein only systems but it is also necessary to consider the effect of non-proteinaceous species present. They may or may not be adsorbed onto the solid substrate but by binding to proteins in the bulk, either through specific binding sites or non-specific physisorption, they will alter the physicochemical properties of the protein which could impact on the adsorption characteristics of that protein.

One of the main proteins of interest in this work is HSA which has a biological function of transporting fatty and amino acids. The fatty acid binding sites have been well characterised and are each slightly different but all comprise a hydrophobic pocket capped at one end with basic or polar side chains [1]. In the absence of fatty acids the binding sites will be solvated by water molecules and counterions, an unfavourable hydrophobic interaction. Upon binding of the fatty acid to a site, the solvent water will be replaced by more favourable interactions between the fatty acid hydrocarbon chain and the hydrophobic amino acid residues. This will act to reduce the overall hydrophobicity of the protein exterior. The crystal structure of the

HSA-myristate complex shows that the binding induces a significant conformational change in the protein[2]. It has also been shown that the presence of small molecular weight surfactants, such as SDS, will bind to the adsorbed protein layer[3, 4] and when present at high enough concentrations act to remove adsorbed protein layers from a solid surface via co-adsorption which alters their surface activity[4].

It is the aim of this chapter to investigate the effect of the binding of deuterated myristic acid (d-MA) to HSA on the adsorption. This is done first from a bulk mixture of the two species and second following the sequential adsorption methodology in chapter 4 i.e. after an incubation time of HSA the bulk solution was replaced by a protein-free solution of the fatty acid.

6.2 Sample preparation

The d-MA solutions were prepared by making up a stock solution of d-MA in chloroform at a concentration of 1 mg ml^{-1}. Small aliquots of this were added to the aqueous buffer and then sitrred vigorously with a magnetic stirring bar for enough time to allow chloroform to evaporate. It is assumed that the chloroform has evaporated to enough of an extent such that any residual chloroform in the aqueous phase has no impact on the properties of the protein or fatty acid. The solutions were filtered before use to remove any undissolved fatty acid. To make the mixture of HSA and d-MA the chloroform solution was spread on the surface and left to evaporate. The solutions were stirred for a short period of time before use as it is was found that if they were prepared in the same way as the solutions without protein a foam was created. This is likely to contain proteins and the stirring process could alter the structure of the proteins in the bulk solution after the foam has broken down.

6.3 Adsorption from a mixture

The adsorption of a 1 mg ml^{-1} solution of HSA and 1.5×10^{-4} mol dm^{-3} d-MA (a 1:10 molar ratio) in D_2O onto a clean silica surface was investigated. During the fitting process the scattering length density of the adsorbed layer was assumed to be 3×10^{-6} Å $^{-2}$ i.e no contribution from the fatty acid. The scattering length density of d-MA is 6.6×10^{-6} Å $^{-2}$ and even if it is assumed that all the d-MA is bound to the HSA and it remains bound during the adsorption process the scattering length density of the complex is 3.35×10^{-6} Å $^{-2}$. However, given that there are

only 6 well defined binding sites[2] and it is thought that the adsorption process occurs in a step-wise manner which starts with the unbinding of the fatty acid[5] the contribution of the d-MA to the overall scattering length density of the complex once adsorbed is likely to be negligible. The critical micelle concentration (CMC) of sodium myristate has been reported between 4.5 mmol[6] and 7 mmol[7] so it is safe to assume that the interaction of the fatty acid and protein in this study is not via encapsulation in micelles but via interactions of individual fatty acid molecues and the protein.

The reflectivity profiles, fits and scattering length density profiles are shown in figure (6.1) with the corresponding layer parameters in table (6.1). The results show that the presence of d-MA reduces the amount of HSA adsorbed to the surface to essentially nothing. This is in good agreement with McClellan et al. who showed the same was true for a mixture of sodium myristate and BSA[8]. Lindman et al.[5] have shown that the adsorption of HSA to copolymer nanoparticles is exothermic whereas in the presence of oleic acid the adsorption becomes endothermic. This was interpreted as due to a two stage adsorptiopn process where the fatty acid ligand unbinds from the protein before adsorption of the protein occurs. This suggests that the driving force for adsorption is entropic in nature and is most likely to be the dehydration of the interface. It also explains why the adsorbed amount would be reduced. The higher adsorbed amount in the Lindman study can be attributed to the increased hydrophobicity of the surface used.

These results also provide an explanation for the variability in the HSA system observed in section 3.3. It was proposed that the main reason for this was the presence of impurities either in the bulk solution or on the surface. The results presented here suggest that this is indeed a major contributing factor to the observed cases when HSA is present in a much lower amount than could otherwise be expected.

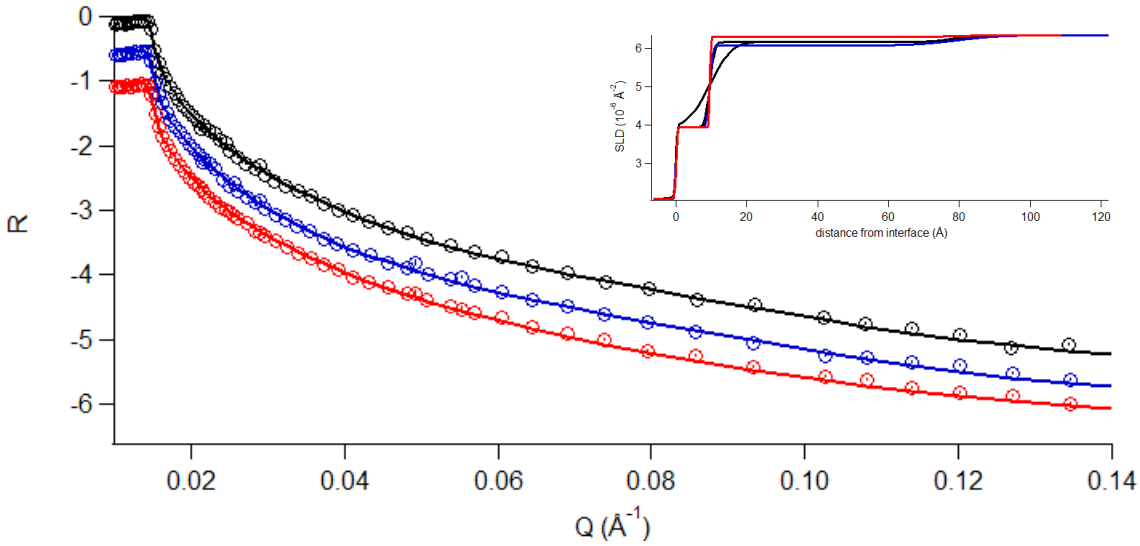


Figure 6.1: Reflectivity profiles and fits showing the changes over time for adsorption of HSA/d-MA mixture in D_2O. A 1-layer model was used and the runs $t_{inc} = 0$ hrs (black) and 0 (blue) with data being offset for clarity. The inset shows the scattering length density profiles and the layer parameters are in table (6.1).

t_{inc} \hrs	Thickness \±2 Å	% Solvent ±4	Roughness		Γ \±0.2 mg m^{-2}
			ox-1	1-s	
0	70	95	0	9	0.4
6	70	95	0	10	0.4
9.5	68	99	0	6	0.1

Table 6.1: Layer parameters for the 1-layer model of adsorption of HSA/d-MA mixture in D_2O. The data is shown in figure (6.1)

6.4 Sequential adsorption

The adsorption of a 1 mg ml^{-1} solution of HSA in PBS buffer at pH 7.4 was adsorbed onto a bare silica surface and left to incubate for 20 hours. After this time the bulk solution was replaced with a saturated solution of d-MA and the changes to reflectivity profile were recorded. After 4 hours there was no change due to the presence of d-MA but after 12 hours had elapsed the reflectivity profile was the same as the bare oxide layer before any adsorption of HSA. The reflectivity profiles, fits and scattering length density profiles are shown in figure (6.2) with the layer parameters in table (6.2). These results show that d-MA can displace pre-adsorbed

HSA even after it has been on the surface for more than 20 hours. This is in good agreement with McClellan et al.[8] who have shown that sodium myristate can remove some BSA from a silica surface by displacement. It is unclear whether the d-MA is itself adsorbed onto the silica surface. The lack of a difference between the bare oxide layer before the adsorption and after HSA displacement could be as a result of there being no adsorption of the fatty acid directly onto the solid surface which is the most likely scenario given that both surface and fatty acid carry a negative charge so there is no driving force for the adsorption to occur. However, the scattering length density of the d-MA is 6.6×10^{-6} Å $^{-2}$ which is close to that of the solvent (6.35×10^{-6} Å $^{-2}$) and so the experiment is not sensitive to the adsorption of d-MA.

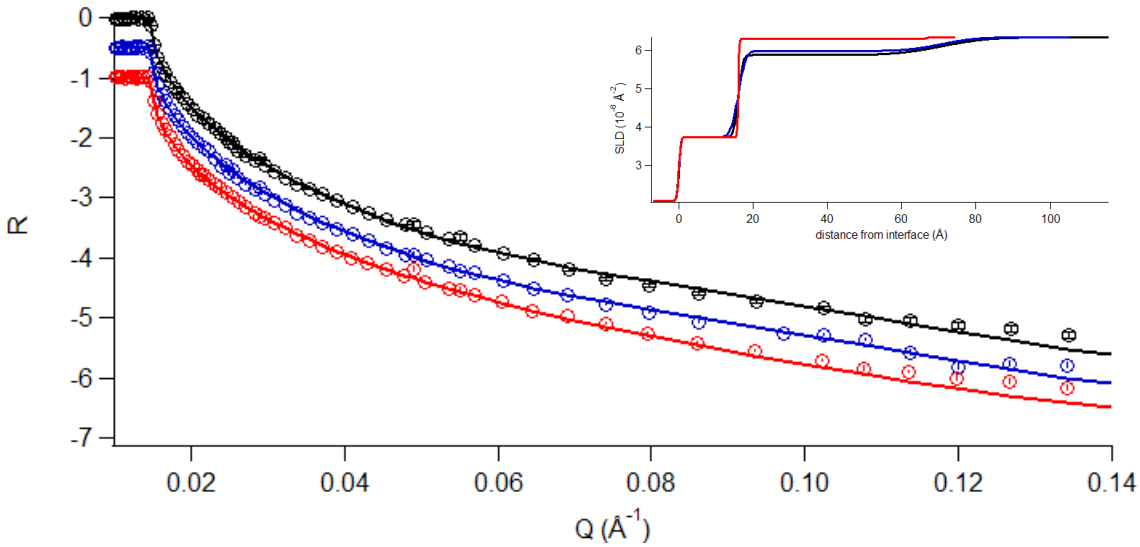


Figure 6.2: Reflectivity profiles and fits showing the adsorption of HSA and subsequent displacement by d-MA. A 1-layer model was used and the runs are the final HSA, $t_{inc} = 21$ hrs (black), $t_{ex} = 0$ (blue) and $t_{ex} = 6$ hours (red) with data being offset for clarity. The inset shows the scattering length density profiles and the layer parameters are in table (6.2).

t_{ex} \hrs	Thickness \±2 Å	% Solvent ±4	Roughness		Γ \±0.2 mg m^{-2}
			ox-1	1-s	
final HSA	55	86	1	10	1.0
4	55	89	2	7	0.8
12	51	99	0	0	0.1

Table 6.2: Layer parameters for the 1-layer model of adsorption of HSA and subsequent displacement by d-MA. The data is shown in figure (6.2).

References

[1] S. Curry, P. Brick, and N. P. Franks, "Fatty acid binding to human serum albumin: new insights from crystallographic studies," *Biochimica et Biophysica Acta*, vol. 1441, pp. 131–140, 1999.

[2] M. H. B. P. F. N. Curry, S., "Crystal structure of human serum albumin complexed with fatty acid reveals an asymmetric distribution of binding sites," *Nature Structural Biology*, vol. 5, no. 9, pp. 827–835, 1998. cited By (since 1996) 515.

[3] J. R. Lu, T. J. Su, R. K. Thomas, and J. Penfold, "Binding of sodium dodecyl sulfate to bovine serum albumin layers adsorbed at the silica-water interface," *Langmuir*, vol. 14, no. 21, pp. 6261–6268, 1998.

[4] R. J. Green, T. J. Su, J. R. Lu, and J. Penfold, "The interaction between SDS and lysozyme at the hydrophilic solid-water interface," *Journal of Physical Chemistry B*, vol. 105, p. 1594, 2001.

[5] S. Lindman, I. Lynch, E. Thulin, H. Nilsson, K. A. Dawson, and S. Linse, "Systematic investigation of the thermodynamics of HSA adsorption to N-iso-Propylacrylamide/ N-tert-Butylacrylamide compolymer nanoparticles. Effects of particle size and hydrophobicity," *Nano Letters*, vol. 7 (4), pp. 914–920, 2007.

[6] X. Wen and E. I. Franses, "Effect of protonation on the solution and phase behavior of aqueous sodium myristate," *Journal of Colloid and Interface Science*, vol. 231, no. 1, pp. 42 – 51, 2000.

[7] A. N. Campbell and D. G. R. Lakshminxrayan, "Conductances and surface tensions of aqueous solutions of sodium decanoate, sodium laurate, and sodium myristate, at 25° and 35°," *Canadian Journal of Chemistry*, vol. 43, pp. 1729–1737, 1965.

[8] S. J. McClellan and E. I. Franses, "Mechanisms of competitive adsorption of albumin and sodium myristate at the silicon oxide/aqueous interface," *Langmuir*, vol. 21, pp. 10148–10153, 2005.

Chapter 7

Dual Polarisation Interferometry results

7.1 Introduction

The previous chapters have considered solely the results obtained using the experimental technique of neutron reflectivity. Although this technique does have many advantages such as high structural resolution and the possibility of using isotopic labelling it does offer certain practical limitations given the necessity for a syncotron or nuclear reactor source, the high cost, the limited experimental time and some limitations on the time resolution of the data. In order to compliment the neutron reflectivity results it was decided to repeat some of the experiments carried out using the lab top apparatus of dual polarisation interferometry (DPI). DPI offers the advantages of being able to investigate the shorter timescales of the first few minutes of adosprtion, greater accessibility meaning more samples can be run and the potential to deconvolve the layer parameters of thickness and density which is not possible in some other evanescent wave techniques such as surface plasmon resonance. As a comparison to neutron reflectivity it is good because the substrates used, silicon and silicon oxynitride, are very similar in their chemistry and hydrophobicity. A similar comparison for the LYS system has previously been made by Lu et al.[1] which concluded that the results between the two techniques were in good agreement and the subtle differences could be attributed to the slightly altered surface chemistry.

In this study, two different proteins were investigated to compare with neutron reflectivity results; LYS and HSA adsorption. With respect to the sequential ad-

sorption and adsorption of a mixture of proteins some preliminary experiments were performed but it was decided not to investigate these systems further as it is not possible to make any conclusions about the structure with respect to the position of each protein within the adsorbed layer. Also, the differences noted between the two techniques for the single protein system meant that any results obtained from the binary protein systems would not aid the interpretation of the neutron reflectivity data.

7.2 Results

In the results presented below there are two values of uncertainty which are represented by the two error bars in the figures. The technique is precise with respect to the uncertainty in each individual measurement (as designated by the small error bars in the figures below) but due to differences between each run, such as varying degrees of surface roughness or differences in the protein solutions, the larger error bars represent the spread of results on repeated measurements. Lu et al.[1] report a variation of 15 % from measurement to measurement for a 1 mg ml^{-1} LYS solution at pH 7 which is commensurate with the error observed here for LYS whereas the spread is greater for the adsorption of HSA.

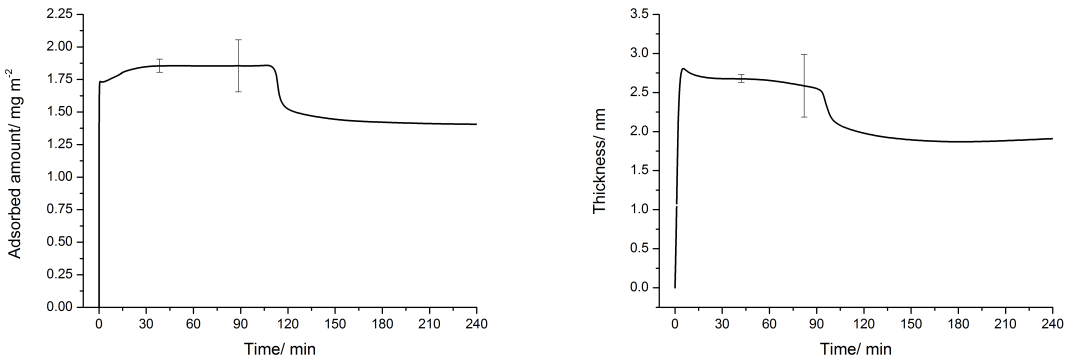
7.2.1 LYS adsorption

A 1 mg ml^{-1} solution of LYS in PBS buffer at pH 7.4 was flowed over a silicon oxynitride surface for 1.5 hours at a flow rate of 2 μl min^{-1} before being returned to running buffer for up to 20 hours to follow the desorption. A typical result for the adsorbed amount, in figure (7.1a) below, show that there is no lag time between the protein reaching the surface and the protein nearing the maximum adsorption. The slight initial curvature is due to the slow flow rate such that only partial coverage of the surface with the protein solution occurs for the first few minutes and there is often a small difference between the two channels due to the distance between the sample loop (where the protein solution is injected) and the start of the sensor surface. A slow flow rate was required due to the small volume of the injection port and the need for $t_{inc} = 1.5$ hours to compare with the neutron reflectivity data.

The maximum adsorbed amounts lie in the range 1.7-2.1 mg m^{-2} and the thickness of the adsorbed layer, figure (7.1b), range from 22-33 Å. The shortest axial

dimension of LYS when in solution is 30 Å so the results here are consistent with LYS molecules spreading over the surface which is a driving force for adsorption at this temperature due to the associated entropy gain[2].

With respect to the desorption phase of the experiment, when the protein solution is displaced by running buffer, the adsorbed amount and thickness both show a decrease to final values ranging from 0.9-1.6 mg m^{-2} and 10-22 Å respectively. The desorption is characterised by an initial period of fast desorption followed by a slow, asymptotic decay to the final value. The simultaneous reduction in adsorbed amount and thickness is consistent with a model whereby the spreading of the proteins on the surface increases their attachment and are irreversibly bound. The protein molecules that do not spread are those that are most likely to be desorbed. The proportion of protein that remains on the surface, on average 60%, is lower than that of the neutron reflectivity results and also the findings of van der Veen et al.[3].



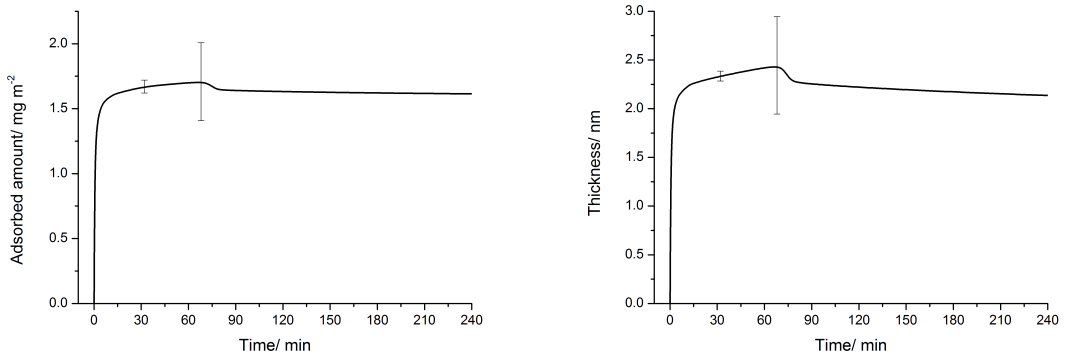
(a) (b)

Figure 7.1: Typical measurements showing changes over time in (a) adsorbed amount and (b) the layer thickness for the adsorption of a 1 mg/ml solution of LYS.

7.2.2 HSA adsorption

A 1 mg ml^{-1} solution of HSA in PBS buffer at pH 7.4 was flowed over a silicon oxynitride surface for 1 hour using a range of flow rates from 1-4 μl min^{-1}. The different flow rates had no noticeable impact on the adsorption parameters observed. The maximum adsorbed amounts lie in the range 1.2-2.0 mg m^{-2} and the thickness of the adsorbed layer, figure (7.2b), range from 15-34 Å. The thicknesses are mostly

less than that of the shortest axial dimension of the protein when in solution, 30 Å, which is consistent with the HSA spreading over the surface. This is in good agreement with the investigation of BSA by Freeman et al.[4] who reported a 39 Å layer at pH 5 with an adsorbed amount of 2.11 mg m^{-2}. The electrostatic conditions in the two solutions are similar given the high ionic strength in this study and the net neutral charge on the protein in Freeman's work. The extent of spreading also results in a high degree of irreversibly bound protein as noted by the small change after 60 min when the protein solution was replaced with running buffer.



(a) (b)

Figure 7.2: Typical measurements showing changes over time in (a) adsorbed amount and (b) the layer thickness for the adsorption of a 1 mg ml^{-1} solution of HSA.

7.3 Discussion

The adsorbed amounts for the two proteins studied is similar which suggests that the charge on the protein is of little consequence which is in contrast to the findings of the neutron reflectivity results in previous chapters. For the DPI studies, the lack of electrostatic importance and the greater extent of spreading suggests that the main driving factor for adsorption is entropic in nature and most likely due to the extra freedom of the polypeptide chains upon unfolding as well as a contribution from the dehydration of the interface as the number of solvent molecules liberated per protein molecule will increase with increasing surface area occupied by the protein.

7.3.1 Comparison of DPI with other techniques

To aid the discussion of the comparison, the main results of the two techniques are shown in table (7.1) below.[1]

For the adsorption of LYS, the two techniques are in good agreement with respect to the adsorbed amounts but the thickness is 11 Å less for the DPI. However, the DPI does show a higher degree of desorption from the silicon oxynitride surface than from the silica used for the neutron reflectivity experiments and in the study be van der Veen et al.[3]. Given the reduced thickness the mostly plausible scenario is that in the competition for the available surface the increased degree of spreading of some of the molecules reduces the available area for others to form strong enough bonds with the surface to remain attached after the replacement of the bulk solution with protein free buffer.

For the adsorption of HSA there is less agreement but the DPI results do replicate the variety observed with the neutron reflectivity experiments with a wider range of adsorbed amounts and thicknesses observed. The range is less in the DPI case as the technique allows for a higher number of repeat experiments and it should be noted that due to the higher number of runs it was possible to remove some anomalous results with low adsorbed amounts. The observation that the anomalous points observed agree with some of the neutron reflectivity results supports the conclusions made in chapters 3 and 6 that the reduction in HSA adsorption is very sensitive to levels of surface active impurities.

The thickness of the adsorbed layer is less using the DPI which is in good agreement with the LYS study here and also a similar comparison made by Freeman et al.[4] with BSA.

The differences between the two techniques can be attributed to the differences in the surface chemistry. Although both use a predominantly silicon dioxide surface, the surface of the chip used for DPI has been manufactured using chemical vapour deposition and been doped with silicon nitride. Thus, the two surfaces are likely to vary in their degrees of roughness as well as composition. The modeling of neutron reflectivity data allows for the inclusion of a roughness term whereas in DPI it is assumed that the surface is smooth. Similarly, neutron reflectivity analysis can model multiple, homogeneous layers but DPI is limited to a 1-layer model. As has

[1]For a more comprehensive view of the neutron reflectivity results of interest, LYS adsorption study is in section 3.2 with specific focus on the desorption shown in figure (3.8) and table (3.6). The neutron reflectivity results for HSA are in section 3.3 and Appendix B.

been shown in previous chapters a 1-layer model is often unsuitable for accurately describing the adsorbed protein layer and this constraint in the DPI analysis is a contributing factor to the error in the measurements as the presence of a diffuse second layer will not be appropriately accounted for. However, it should also be noted than the evanescent wave decays exponentially from the sensor surface and the effect of a thick diffuse multilayer, as observed in the neutron reflectivity data, is likely to be small.

Protein	**DPI**		**Neutron Reflectivity**	
	Γ **\mg m^{-2}**	**Average thickness \Å**	Γ **\mg m^{-2}**	**Average† thickness \Å**
LYS	1.9 ±0.2	28	2.2±0.2	39
HSA	1.6 ±0.4	25	1.1 ±0.5	53

Table 7.1: Comparison of adsorbed amounts and thicknesses from DPI and neutron reflectivity techniques.(†The thicknesses for neutron reflectivity data are for the 1-layer models in order to make a better comparison with DPI where only 1-layer models are possible.)

As well as the variation in surface chemistry and analysis the two techniques do have some practical differences. The neutron reflectivity experiments are done under static conditions whilst DPI is performed under flowing buffer. The flow rates were kept to a minimum (up to 5μl min^{-1}) to reduce this difference and it has also been shown in other studies that the flow rate is not important in the adsorption of single proteins to silicon surfaces[5]. Similarly, with respect to the time resolution, to gain the full Q range in neutron reflectivity experiments it is necessary to measure at two or three angles with a measurement time between 15 and 90 minutes (depending on the neutron flux, angle and solvent contrast) whereas DPI takes multiple data points per second. The neutron reflectivity profiles are thus a time averaged measurement for each angle. In both cases presented above when using DPI there is no discernable time lag between the protein coming into contact with the surface and adsorption reaching a maximum value which provides a strong indication that the potential problem due to time averaging in neutron reflectivity is negated.

Overall, the results presented here show the two techniques agree well. The slight discrepancies are most likely to be caused by the different surface chemistry and in a comparison of the same two techniques by Lu et al.[1], the DPI results also showed a reduced adsorbed amount and a reduced thickness. Other contributing factors are possibly the different temperatures of the experiments (20°C for DPI and

25°C for neutron reflectivity) and the different solvents used (DPI in H_2O, neutron reflectivity predominantly in D_2O). The effect of the temperature difference is likely to be small given that it is only 5°C and in a region where the protein is stable with respect to denaturation. For the solvent effect, D_2O increases the rigidity of the protein compared to H_2O[6, 7, 8] and thus the propensity to unfold will be expected to be greater in the DPI experiments, which is in good agreement with the results presented here.

Another technique that is often used to investigate the adsorption of proteins on a silica surface is ellipsometry[9, 10, 11, 12]. It (and other optical techniques) are very sensitive to the adsorbed amount but the degree of certainty in structural information is low due to the necessary assumptions that are required in order to derive such parameters[13]. It is difficult to make direct comparisons due to the different experimental methods used with regards to the concentration of protein, pH and ionic strength. Generally, the adsorbed amounts are lower when recorded using ellipsometry on a silica surface and the thicknesses are comparable or greater. Both of these differences can be attributable to the higher degree of surface unfolding on the silicon oxynitride surface when compared to silica. Both surfaces and HSA at the pH values of interest (i.e. approx. 7) have a net negative charge and thus the Coulombic forces between protein and solvent will be repulsive and the adsorption of HSA onto silica has been shown to be endothermic[14] thus the driving force is entropic but with only a small degree of unfolding the entropy increase will be a result of surface dehydration. In the case of the silicon oxynitride there is an additional entropic contribution from the protein unfolding and therefore the adsorbed amount is greater and the thicknesses reduced. In the work by Silva-Bermudez et al.[12] a variety of metal oxide surfaces with varying degrees of hydrophobicity were used to measure the adsorption of BSA and the lowest value for the thickness for a 1 mg ml^{-1} solution was 56 ± 3Å but the highest adsorbed amount recorded was just 1.0 mg m^{-2}.

References

[1] J. R. Lu, M. J. Swann, L. L. Peel, and N. J. Freeman, "Lysozyme adsorption studies at the silica/water interface using dual polarisation interferometry," *Langmuir*, vol. 20, pp. 1827–1832, 2004.

[2] C. Czeslik, G. Jackler, and C. Royer, "Driving forces for the adsorption of enzymes at the water/silica interface studied by total internal reflection fluorescence spectroscopy and optical reflectometry," *Spectroscopy*, vol. 16, p. 139145, 2002.

[3] M. van der Veen, M. C. Stuart, and W. Norde, "Spreading of proteins and its effect on adsorption and desorption kinetics," *Colloids and Surface B: Biointerfaces*, vol. 54, pp. 136–142, 2007.

[4] N. J. Freeman, L. L. Peel, M. J. Swann, G. H. Cross, A. Reeves, S. Brand, and J. R. Lu, "Real time, high resolution studies of protein adsorption and structure at the solidliquid interface using dual polarization interferometry," *Journal of Physics: Condensed Matter*, vol. 16, p. S2493S2496, 2004.

[5] J. Ortega-Vinuesa, P. Tengvall, B. Wlivaara, and I. Lundstrm, "Stagnant versus dynamic conditions: A comparative adsorption study of blood proteins," *Biomaterials*, vol. 19, no. 1-3, pp. 251 – 262, 1998.

[6] P. Cioni and G. B. Strambini, "Effect of heavy water on protein flexibility," *Biophysical Journal*, vol. 82, pp. 3246–3253, 2002.

[7] A. Hattori, H. L. Crespi, and J. J. Katz, "Effect of side-chain deuteration on protein stability," *Biochemistry*, vol. 4, no. 7, pp. 1213–1225, 1965.

[8] L. Fu, S. Villette, S. Petoud, F. Fernandez-Alonso, and M.-L. Saboungi, "H/D isotope effects in protein thermal denaturation: The case of bovine serum albumin," *The Journal of Physical Chemistry B*, vol. 115, no. 8, pp. 1881–1888, 2011.

[9] M. Malmsten, "Ellipsometry studies of the effects of surface hydrophobicity on protein adsorption," *Colloids and Surfaces B: Biointerfaces*, vol. 3, no. 5, pp. 297 – 308, 1995.

[10] R. Seitz, R. Brings, and R. Geiger, "Protein adsorption on solid-liquid interfaces monitored by laser-ellipsometry," *Applied Surface Science*, vol. 252, no. 1, pp. 154 – 157, 2005. 13th Applied Surface Analysis Workshop.

[11] J. Benesch, A. Askendal, and P. Tengvall, "Quantification of adsorbed human serum albumin at solid interfaces: a comparison between radioimmunoassay (ria) and simple null ellipsometry," *Colloids and Surfaces B: Biointerfaces*, vol. 18, no. 2, pp. 71 – 81, 2000.

[12] P. Silva-Bermudez, S. Rodil, and S. Muhl, "Albumin adsorption on oxide thin films studied by spectroscopic ellipsometry," *Applied Surface Science*, vol. 258, no. 5, pp. 1711 – 1718, 2011.

[13] M. Malmsten, "Ellipsometry studies of protein layers adsorbed at hydrophobic surfaces," *Journal of Colloid and Interface Science*, vol. 166, no. 2, pp. 333 – 342, 1994.

[14] G. A. Kulikova, I. V. Ryabinina, S. S. Guseynov, and E. V. Parfenyuk, "Calometric study of adsorption of human serum albumin onto silica particles," *Thermochemica Acta*, vol. 503-504, pp. 65–69, 2010.

Chapter 8

Conclusions

There are two main themes of interest running through this thesis; the various adsorption scenarios of proteins, and the importance of isotope effects with reference to both the impact on protein adsorption and as an analysis of the experimental technique and methodology. The organisiation of the results chapters in this thesis largely reflects the first of these, the experimental narrative, with discussions on the second theme interspersed as appropriate. The aim of this concluding chapter is to summarise the main findings of this work and in so doing provide a clearer link between the points of thematic interest in each chapter.

In chapter 3 a comparison was made between the adsorption of four protonated proteins, HSA, CA II, LYS and MBP, onto a clean silica surface which revealed that the general trend for adsorbed amounts followed the order CA II, LYS >MBP, HSA which could largely be explained by considering the electrostatic driving forces for adsorption; both protein-protein and protein-surface. The apparent importance of favourable electrostatic interactions being the driving force for adsorption was also observed when a pre-adsorbed HSA layer was exposed to CA II, LYS and MBP in chapter 4. LYS (positively charged) consistently showed an increase in adsorbed amount which was independent of both the initial adsorbed amount and the incubation time of the HSA whereas CA II (neutral) and h-MBP (negatively charged) did not significantly change the amount of protein adsorbed.

In the single protein adsorption, sequential adsorption and adsorption from a mixture it was often found that a 2-layer model was needed to accurately fit the experimental data to the theoretically calculated reflectivity profile using the optical matrix method and that the characteristics of the 2-layer model were common to all the protein systems studied. The inner layer bound to the surface is more dense and

generally thinner. The thicker, diffuse outer layer is characteristic of a loosely bound and patchy second protein layer adsorbing on top of the surface bound molecules. This highlights an advantage of neutron reflectivity over other techniques as analysis using the optical matrix method allows for the adsorbed protein layer to be broken down into multiple homogeneous layers. A comparison between neutron reflectivity and dual polarisation interferometry (DPI) in chapter 7 showed that the adsorption of LYS and HSA is similar. The greater extent of LYS desorption and smaller layer thicknesses for both proteins when using DPI can mostly be attributed to the difference in surface chemistry but other factors such as limitations in the DPI analysis and solvent used could also contribute. DPI is restricted to the assumption of a 1-layer model which limits its usefulness when compared to neutron reflectivity.

Of the proteins studied, HSA had the highest degree of variability between samples in terms of the adsorbed amounts both when adsorbing onto a clean silica surface (chapter 3) and onto a pre-adsorbed protein layer (chapter 4). It was postulated that the extent of the variability was due to the presence of impurities (in the bulk solution and on the surface) which efficiently bind to the hydrophobic pockets on the exterior of HSA which are used to perform its main biological function as a carrier protein. This argument is supported by the results presented in chapters 6 and 7. Chapter 6 showed that the presence of a low concentration deuterated myristic acid prohibits the adsorption of HSA and when added sequentially acts to remove the pre-adsorbed HSA. In chapter 7, DPI was the experimental technique used and due to the increased accessibility of the bench top instrument compared to neutron reflectometers, it was possible to run more samples. There was less variability and some anomalous results which did occur could be discounted with more confidence than those from neutron reflectivity. These anomalous samples were those with lower adsorbed amounts than the consensus values.

As well as measuring the adsorbed amount and layer structure it was hoped to determine the importance of the incubation time on the adsorption of the proteins. There was no evidence to suggest that gross morphological changes were occurring over time and this was reflected in the extent of desorption of d-MBP showing no difference with varying incubation times from 2 min up to 4 hours. Rather than looking for changes to the morphology of the adsorbed layer, another route to monitoring the changes occurring over time is by using a less direct measurement- the extent of exchange in sequential adsorption using either different proteins (as in chapter 4) or the deuterated and protonated forms of the same protein (as for

the self exchange of MBP in chapter 3). When considering sequential adsorption of the proteins some effect of incubation time is apparent but no definitive results emerged due to the variability of the HSA adsorption. The exchange of h-MBP for pre-adsorbed d-MBP showed a clear trend that with increasing incubation time, the strength of attachment to the surface is increased and the extent of exchange is decreased. It is also apparent that the exchange process is an active one because the passive process (desorption into protein-free buffer and re-adsorption into the vacant binding sites) did not occur to any appreciable extent. Thus the nature of the incoming protein should be considered to be of as much importance as that of the incumbent protein. Using a 2-layer model showed that exchange is occurring from both layers because modeling the exchange with the assumption that it is occurring from just the outer layer did not reveal a sensible physical description or any trend with respect to the incubation time. This was in contrast to the findings of the 1-layer model (using fixed layer parameters of $\tau = 75$Å and solvent percentage= 75 %) and following the exchange from both layers in the 2-layer model. This difference was only apparent from the acceptability of the theoretical fits to the experimental data when in the CMSi solvent contrast.

Another interesting feature of the self exchange investigation is the finding that d-MBP more readily displaces h-MBP than *vice versa*. This influence of isotopic substitution was also observed when investigating the adsorption of 50:50 h+d mixtures (HSA and MBP) in chapter 3 where a 3:1 d:h ratio was observed and the mixtures of HSA and LYS. In this case, the LYS was thought to dominate the adsorbed layer when mixed with h-HSA but when adsorption occurred from an equal mixture of d-HSA and LYS, a mixed layer was observed. These differences provide an interesting and unexpected route to providing more information on the driving forces for protein adsorption. It is known that perdeuteration influences the stability of the protein and this is suggested as the main reason for the observed adsorption affinities. Other factors such as the importance of H-bonding and the hydrophobic effect could also be of importance as perdeuterated proteins have been shown in some studies to more readily form aggregates due to these processes. More information on the physicochemical properties of perdeuterated proteins is required for future studies to fully exploit this difference in determining important details regarding the relative importance of different driving forces for adsorption.

From a technical perspective the isotope effects observed have proved to be a good test of the assumptions used in neutron reflectivity. When investigating adsorp-

tion from a mixture and the sequential adsorption scenarios the aim is to determine the proportion of each protein in the adsorbed layer. Initially it was assumed that the protonated and perdeuterated proteins would behave similarly or, at worst, introduce a small error in the final determination of the protein ratio in the layer. Thus by comparing the h-h systems with h-d and keeping the adsorbed amount, thickness and solvent percentage parameters within a small range the variation in scattering length density of the protein layer would provide an accurate description of the adsorbed protein layer with respect to the position and relative proportions of the proteins in the layer. The observed differences in the two forms of the proteins have revealed the limitations in this methodology when applied to protein mixtures. A more in depth investigation using more solvent contrasts of the d-h system would still not provide more information on the h-h system. In the h-h system, the extent of the conclusions drawn with respect to protein proportions within the adsorbed layer is limited by the similarities in the scattering length densities of most protonated proteins. Similarly it is also assumed that the adsorption behaviour of proteins is the same under different solvent contrasts as these are required to reduce the possibility of finding non-unique solutions. Changing the D_2O:H_2O ratio in the solvent has been shown to have some effect with more extensive adsorption sometimes observed in H_2O compared to other contrasts.

Overall this work has confirmed the advantages of using neutron reflectivity for studying protein adsorption to gain high structural resolution of the adsorbed layers. However, it has also uncovered some difficulties with respect to studying binary systems using perdeuterated proteins. For future studies to continue to be successful a more detailed examination of the differences and similarities between perdeuterated and protonated proteins is required. A wide range of solvent contrasts would give the best possible route to uncovering the effect of both polypeptide backbone deuteration and solvent effects. As deuteration methods and techniques advance it is hoped that a wider range of proteins can be studied as well as more extensive studies on existing proteins such as HSA and MBP. Likewise, the increased flux of neutron reflectometers will provide greater opportunities to focus attention on the time dependence of the exchange process which has been shown in this work.

Appendix A

LYS neutron reflectivity data

The reflectivity profiles, fits and layer parameters are referred to in section 3.2 where a typical example is also shown.

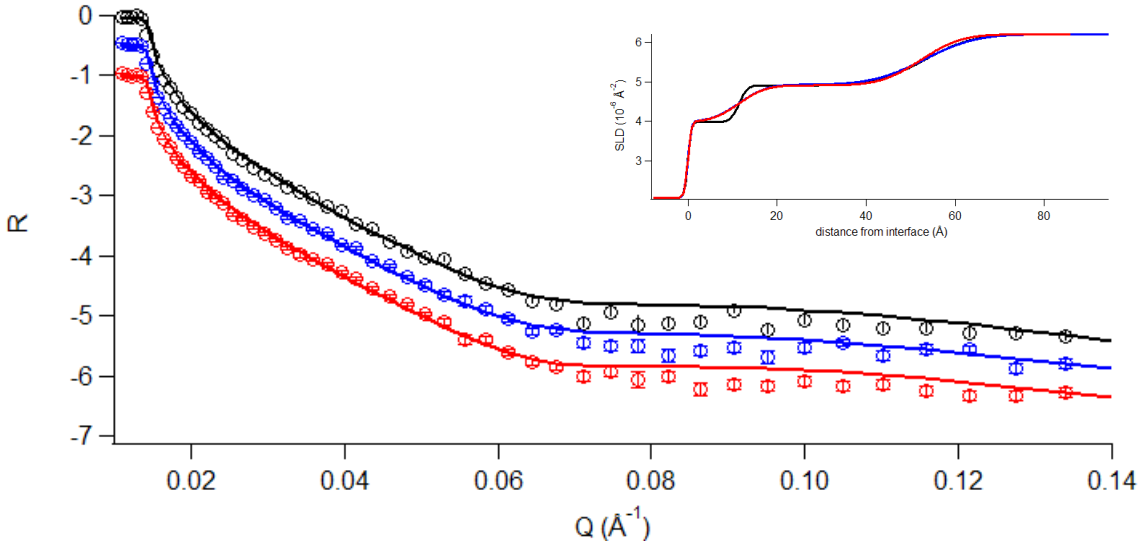


Figure A.1: Reflectivity profiles and fits showing the changes over time for the adsorption of LYS in D_2O using a 1-layer model. The runs shown are t_{inc} = 10.5 hours (black), t_{inc} = 13.5 hours (blue) and t_{inc} = 17 hours (red) with data being offset for clarity. The inset shows the scattering length density profiles and the layer parameters are in table (A.1).

t_{inc} \hrs	Thickness \±2 Å	% Solvent ±4	Roughness		Γ \±0.2 mg m^{-2}
			ox-1	1-s	
10.5	42	50	2	9	2.8
13.5	42	51	5		2.7
17	41	50	5	7	2.7

Table A.1: Layer parameters for the 1-layer model of LYS adsorption in D_2O. Data is shown in figure (A.1).

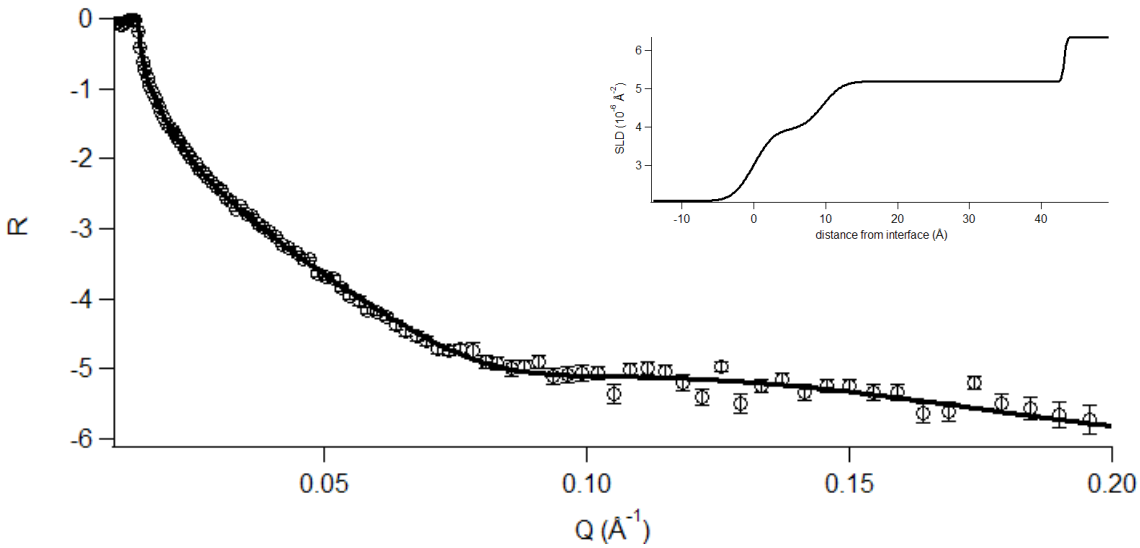


Figure A.2: Reflectivity profiles and fits showing the changes over time for the adsorption of LYS in D_2O using a 1-layer model. The run shown is $t_{inc} = 0$ hours (black). The inset shows the scattering length density profiles and the layer parameters are in table (A.2).

t_{inc} \hrs	Thickness \±2 Å	% Solvent ±4	Roughness		Γ \±0.2 mg m^{-2}
			ox-1	1-s	
0	34	58	2	0	1.9

Table A.2: Layer parameters for the 1-layer model of LYS adsorption in D_2O. Data is shown in figure (A.2).

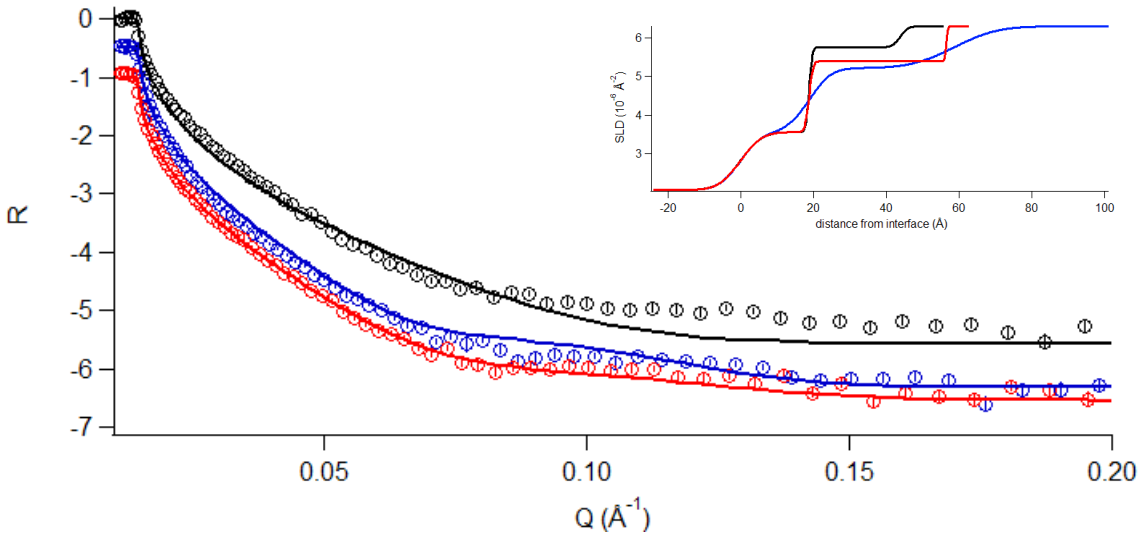


Figure A.3: Reflectivity profiles and fits showing the changes over time for the adsorption of LYS in D_2O using a 1-layer model. The runs shown are $t_{inc} = 0$ hours (black), $t_{inc} = 6.5$ hours (blue) and $t_{inc} = 21$ hours (red) with data being offset for clarity. The inset shows the scattering length density profiles and the layer parameters are in table (A.3).

t_{inc} \hrs	Thickness \±2 Å	% Solvent ±4	Roughness		Γ \±0.2 mg m^{-2}
			ox-1	1-s	
0	25	80	0	2	0.7
6.5	40	60	2	4	2.1
21	38	61	1	0	2.0

Table A.3: Layer parameters for the 1-layer model of LYS adsorption in D_2O. Data is shown in figure (A.3).

Appendix B

HSA neutron reflectivity data

The reflectivity profiles, fits and layer parameters are referred to in section (3.3) where a typical example is also shown.

B.1 h-HSA

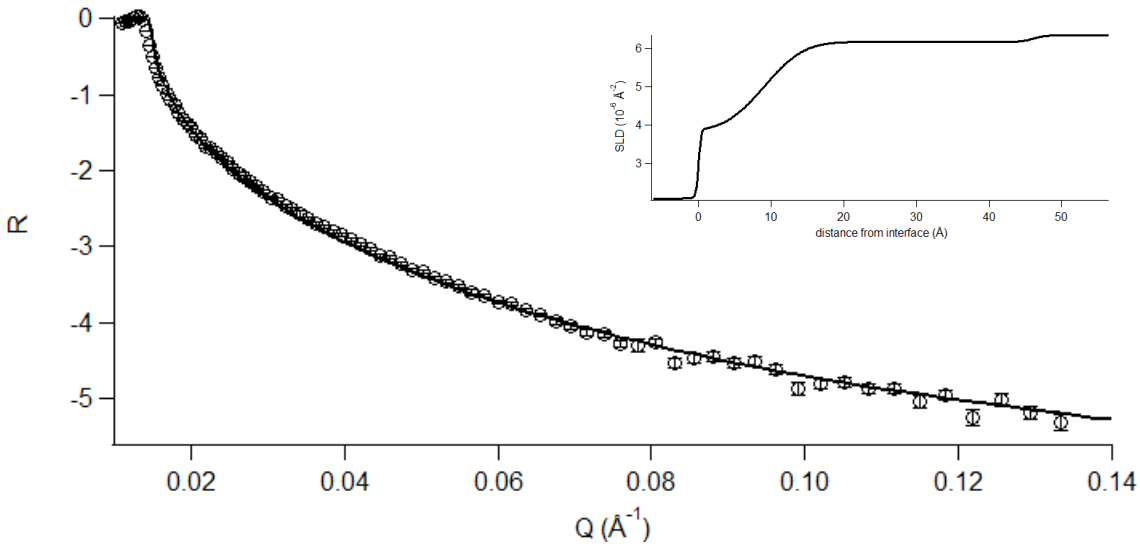


Figure B.1: Reflectivity profiles and fits showing the adsorption of HSA in D_2O using a 1-layer model. The run shown is $t_{inc} = 0$ (black). The inset shows the scattering length density profile and the layer parameters are in table (B.1).

t_{inc} \hrs	Thickness \±3 Å	% Solvent ±5	Roughness		Γ \±0.2 mg m^{-2}
			ox-1	1-s	
0	37	95	4	1	0.2

Table B.1: Layer parameters for the 1-layer model of HSA adsorption in D_2O. Data is shown in figure (B.1).

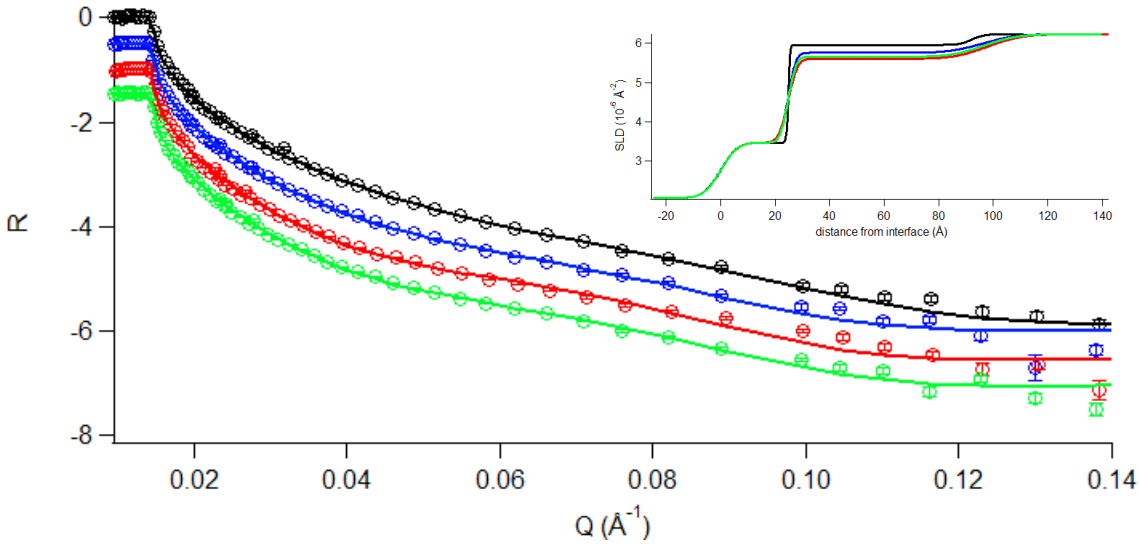


Figure B.2: Reflectivity profiles and fits showing the changes over time for the adsorption of HSA in D_2O using a 1-layer model. The runs shown are $t_{inc} = 0$ hours (black), $t_{inc} = 4.5$ hours (blue), $t_{inc} = 23$ hours (red) and $t_{inc} = 27.5$ hours (green) with data being offset for clarity. The inset shows the scattering length density profiles and the layer parameters are in table (B.2).

t_{inc} \hrs	Thickness \±3 Å	% Solvent ±5	Roughness		Γ \±0.2 mg m^{-2}
			ox-1	1-s	
0	68	92	1	4	0.7
4.5	71	85	2	10	1.4
23	73	81	3	10	1.8
27.5	73	83	4	10	1.6

Table B.2: Layer parameters for the 1-layer model of HSA adsorption in D_2O. Data is shown in figure (B.2).

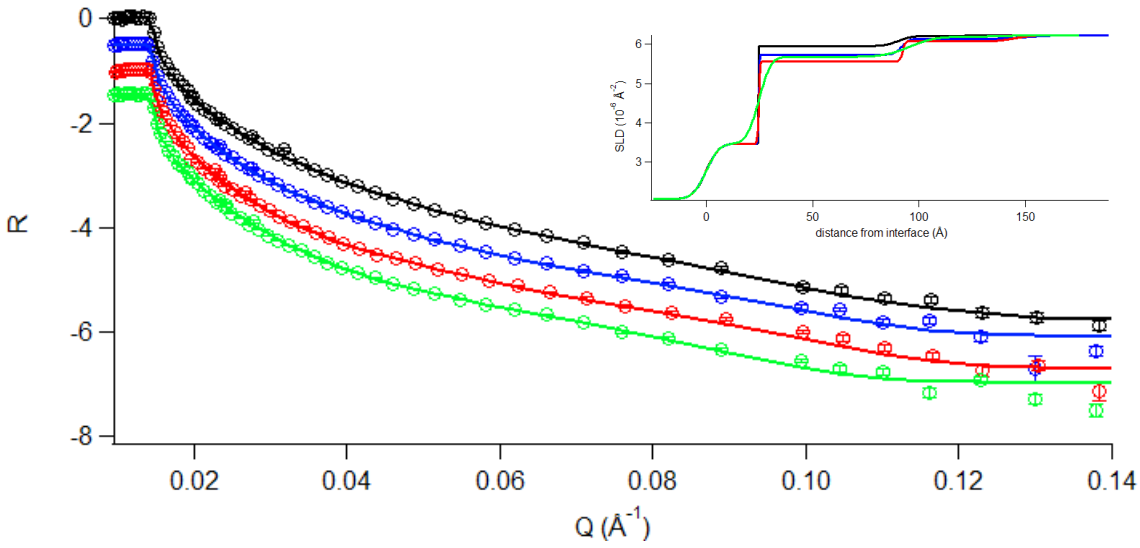


Figure B.3: Reflectivity profiles and fits showing the changes over time for the adsorption of HSA in D_2O using a 2-layer model. The runs shown are $t_{inc} = 0$ hours (black), $t_{inc} = 4.5$ hours (blue), $t_{inc} = 23$ hours (red) and $t_{inc} = 27.5$ hours (green) with data being offset for clarity. The inset shows the scattering length density profiles and the layer parameters are in table (B.3).

t_{inc} \hrs	Layer number	Thickness \±3 Å	% Solvent ±5	Roughness			Γ \±0.2 mg m^{-2}
				ox-1	1-2	2-s	
0	1	67	92	0	5	7	0.7
	2	32	99				0.0
4.5	1	67	85	0	3	8	1.3
	2	59	97				0.2
23	1	68	80	1	1	6	1.8
	2	53	95				0.3
27.5(wash)	1	71	83	5	9	8	1.6
	2	44	99				0.1

Table B.3: Layer parameters for the 2-layer model of HSA adsorption in D_2O. Data is shown in figure (B.3).

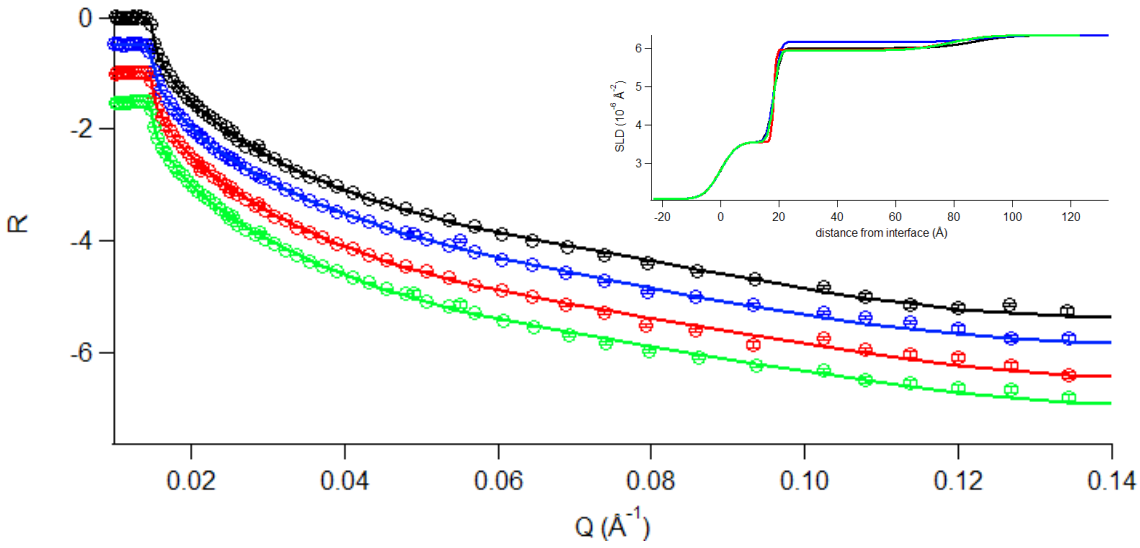


Figure B.4: Reflectivity profiles and fits showing the changes over time for the adsorption of HSA in D_2O using a 1-layer model. The runs shown are $t_{inc} = 0$ hours (black), $t_{inc} = 4$ hours (blue), $t_{inc} = 12$ hours (red) and $t_{inc} = 17$ hours (green) with data being offset for clarity. The inset shows the scattering length density profiles and the layer parameters are in table (B.4).

t_{inc} \hrs	Thickness \±3 Å	% Solvent ±5	Roughness		Γ \±0.2 mg m^{-2}
			ox-1	1-s	
0	69	90	2	10	0.9
4	70	95	2	10	0.5
12	61	89	1	10	0.9
17	60	88	2	10	0.9

Table B.4: Layer parameters for the 1-layer model of HSA adsorption in D_2O. Data is shown in figure (B.4).

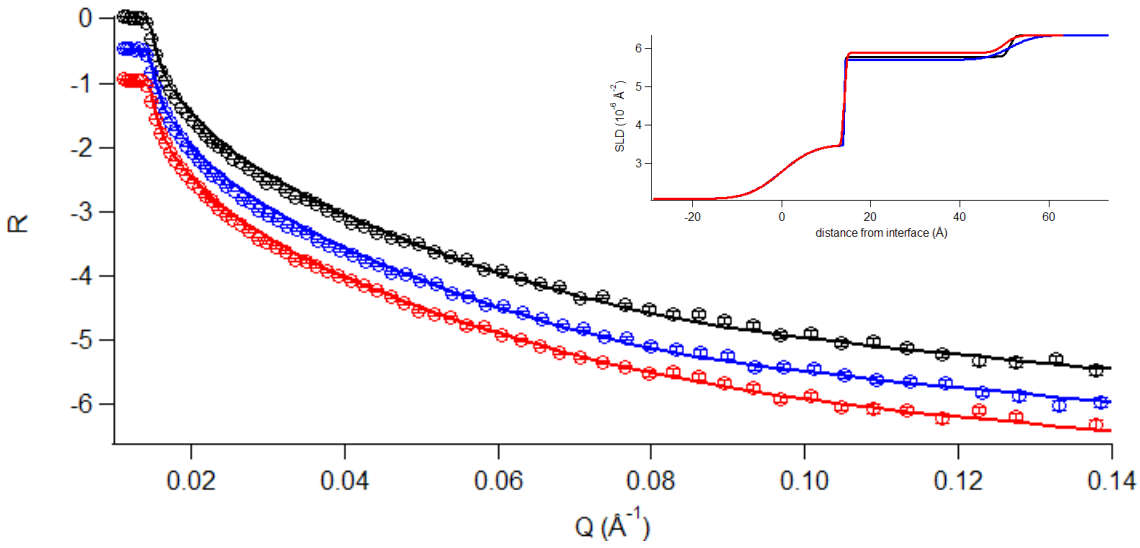


Figure B.5: Reflectivity profiles and fits showing the changes over time for the adsorption of HSA in D_2O using a 1-layer model. The runs shown are $t_{inc} = 0$ hours (black), $t_{inc} = 6.5$ hours (blue) and $t_{inc} = 21$ hours (red) with data being offset for clarity. The inset shows the scattering length density profiles and the layer parameters are in table (B.5).

t_{inc} \hrs	Thickness \±3 Å	% Solvent ±5	Roughness		Γ \±0.2 mg m^{-2}
			ox-1	1-s	
0	56	84	4	9	1.2
6.5	54	83	4	10	1.2
21	58	89	5	8	0.8

Table B.5: Layer parameters for the 1-layer model of HSA adsorption in D_2O. Data is shown in figure (B.5).

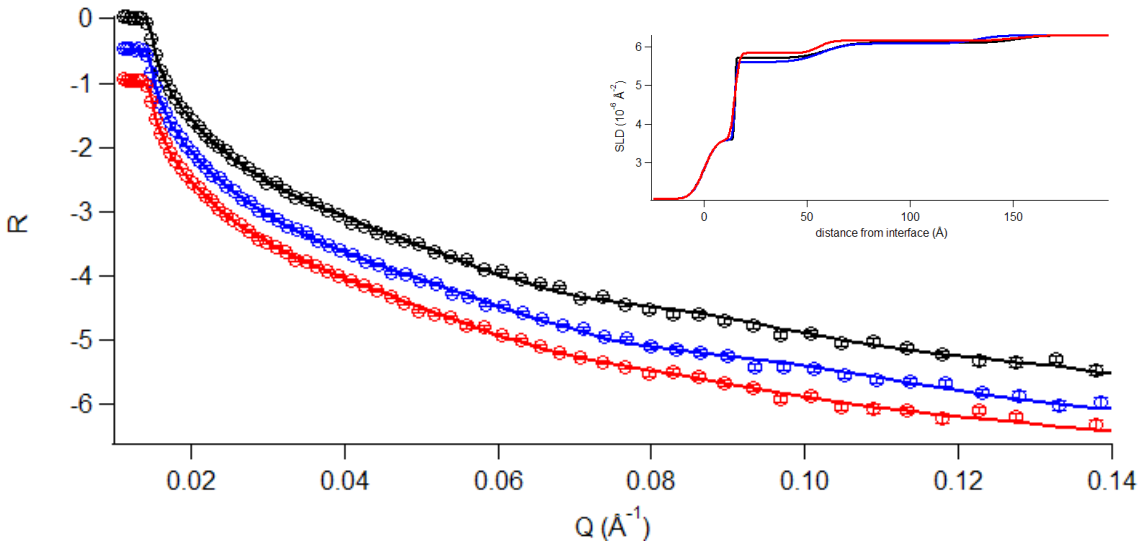


Figure B.6: Reflectivity profiles and fits showing the changes over time for the adsorption of HSA in D_2O using a 2-layer model. The runs shown are $t_{inc} = 0$ hours (black), $t_{inc} = 6.5$ hours (blue) and $t_{inc} = 21$ hours (red) with data being offset for clarity. The inset shows the scattering length density profiles and the layer parameters are in table (**??**).

t_{inc} \hrs	Layer number	Thickness \±3 Å	% Solvent ±5	Roughness			Γ \±0.2 mg m^{-2}
				ox-1	1-2	2-s	
0	1	45	82	0	10	9	1.1
	2	92	94				0.7
6.5	1	42	79	1	10	9	1.2
	2	75	94				0.6
20	1	41	86	2	5	9	0.8
	2	96	96				0.5

Table B.6: Layer parameters for the 2-layer model of HSA adsorption in D_2O. Data is shown in figure (B.6).

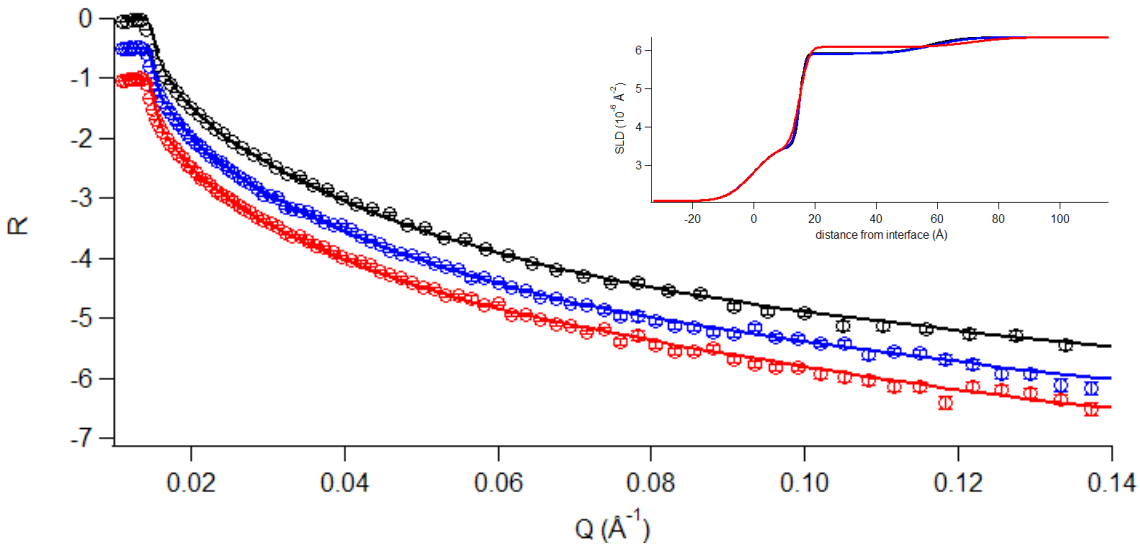


Figure B.7: Reflectivity profiles and fits showing the changes over time for the adsorption of HSA in D_2O using a 1-layer model. The runs shown are $t_{inc} = 0$ hours (black), $t_{inc} = 1.5$ hours (blue) and $t_{inc} = 8$ hours (red) with data being offset for clarity. The inset shows the scattering length density profiles and the layer parameters are in table (B.7).

t_{inc} \hrs	Thickness \±3 Å	% Solvent ±5	Roughness		Γ \±0.2 mg m^{-2}
			ox-1	1-s	
0	42	87	1	1	0.7
1.5	43	87	3	6	0.7
8	56	92	1	6	0.6

Table B.7: Layer parameters for the 1-layer model of HSA adsorption in D_2O. Data is shown in figure (B.7).

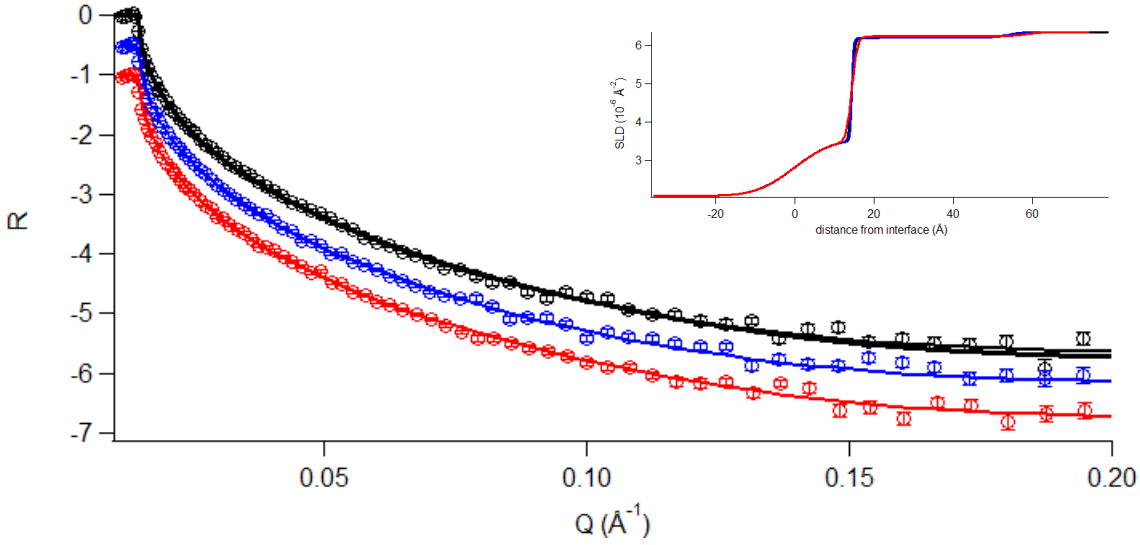


Figure B.8: Reflectivity profiles and fits showing the changes over time for the adsorption of HSA in D_2O using a 1-layer model. The runs shown are $t_{inc} = 0$ hours (black), $t_{inc} = 5$ hours (blue) and $t_{inc} = 19$ hours (red) with data being offset for clarity. The inset shows the scattering length density profiles and the layer parameters are in table (B.8).

t_{inc} \hrs	Thickness \±3 Å	% Solvent ±5	Roughness		Γ \±0.2 mg m^{-2}
			ox-1	1-s	
0	40	96	1	5	0.2
5	40	96	0	2	0.2
19	44	97	1	3	0.2

Table B.8: Layer parameters for the 1-layer model of HSA adsorption in D_2O. Data is shown in figure (B.8).

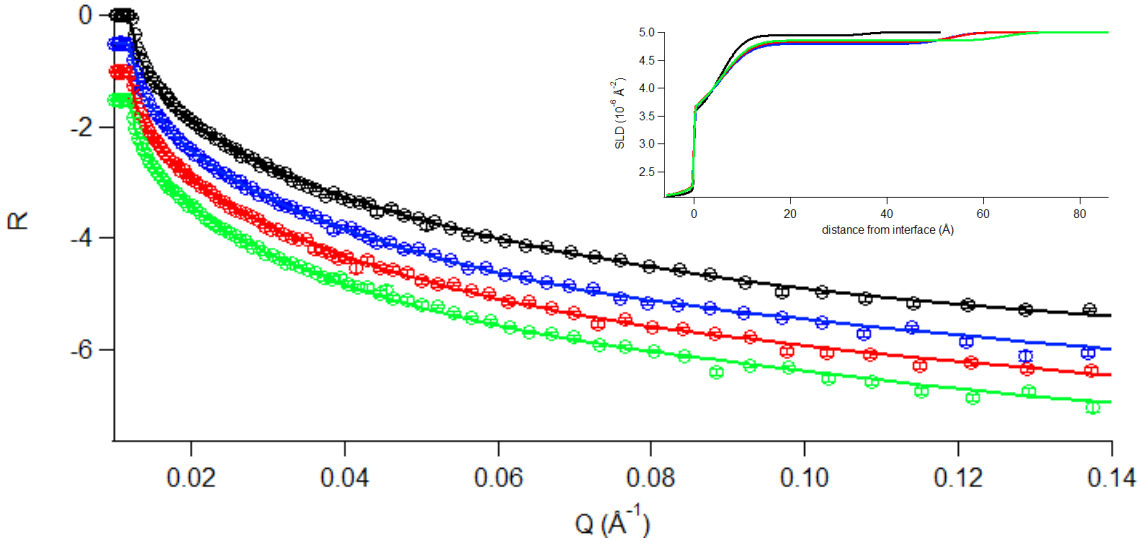


Figure B.9: Reflectivity profiles and fits showing the changes over time for the adsorption of HSA in CM5 using a 1-layer model. The runs shown are $t_{inc} = 0$ hours (black), $t_{inc} = 6$ hours (blue), $t_{inc} = 20$ hours (red) and $t_{inc} = 21$ hours (green) with data being offset for clarity. The inset shows the scattering length density profiles and the layer parameters are in table (B.9).

t_{inc} \hrs	Thickness \±3 Å	% Solvent ±5	Roughness ox-1	Roughness 1-s	Γ \±0.2 mg m^{-2}
0	30	98	4	3	0.1
6	47	91	5	4	0.6
20	49	92	5	4	0.5
21	59	93	5	4	0.5

Table B.9: Layer parameters for the 1-layer model of HSA adsorption in CM5. Data is shown in figure (B.9).

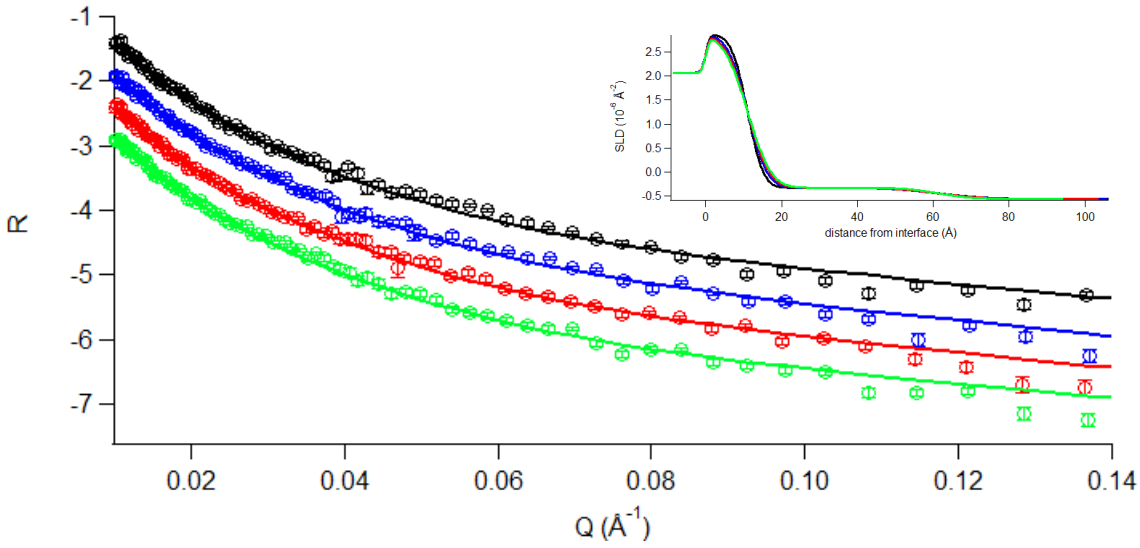


Figure B.10: Reflectivity profiles and fits showing the changes over time for the adsorption of HSA in H_2O using a 1-layer model. The runs shown are $t_{inc} = 1.5$ hours (black), $t_{inc} = 7$ hours (blue), $t_{inc} = 18.5$ hours (red) and $t_{inc} = 20$ hours (green) with data being offset for clarity. The inset shows the scattering length density profiles and the layer parameters are in table (B.10).

t_{inc} \hrs	Thickness \±3 Å	% Solvent ±5	Roughness		Γ \±0.2 mg m^{-2}
			ox-1	1-s	
1.5	50	90	5	6	0.7
7	50	89	5	10	0.7
18.5	51	89	5	10	0.7
20	50	90	5	3	0.7

Table B.10: Layer parameters for the 1-layer model of HSA adsorption in H_2O. Data is shown in figure (B.10).

B.2 d-HSA

Due to the similarities of the scattering length densities between the protein and the solvent, neutron reflectivity is insensiitve to the adsorption of d-HSA in D_2O and so the layer parameters are not given. The reflectivity profiles, fits and scattering length density profiles are included for the sake of completeness and the other solvent contrasts are discussed in section 3.3.2.

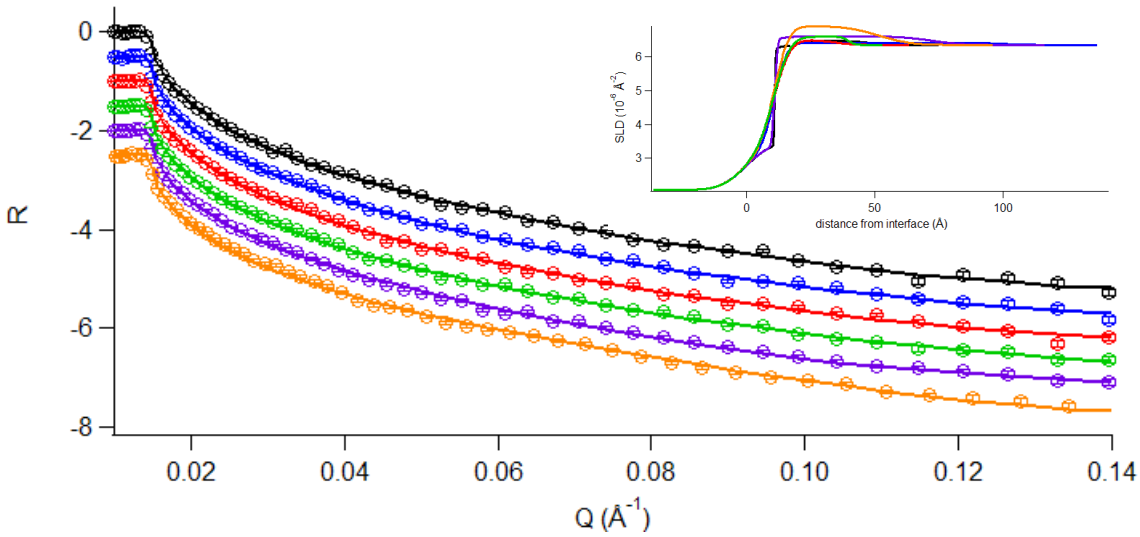


Figure B.11: Reflectivity profiles and fits showing the changes over time for adsorption of d-HSA in D_2O using a 1-layer model. The runs shown are $t_{inc} = 0$ (black), $t_{inc} = 0.75$ hrs (blue), $t_{inc} = 1.5$ hrs (red), $t_{inc} = 2.25$ hrs (green), $t_{inc} = 6$ hrs (purple) and $t_{inc} = 23$ hrs (orange) with data being offset for clarity. The inset shows the scattering length density profiles.

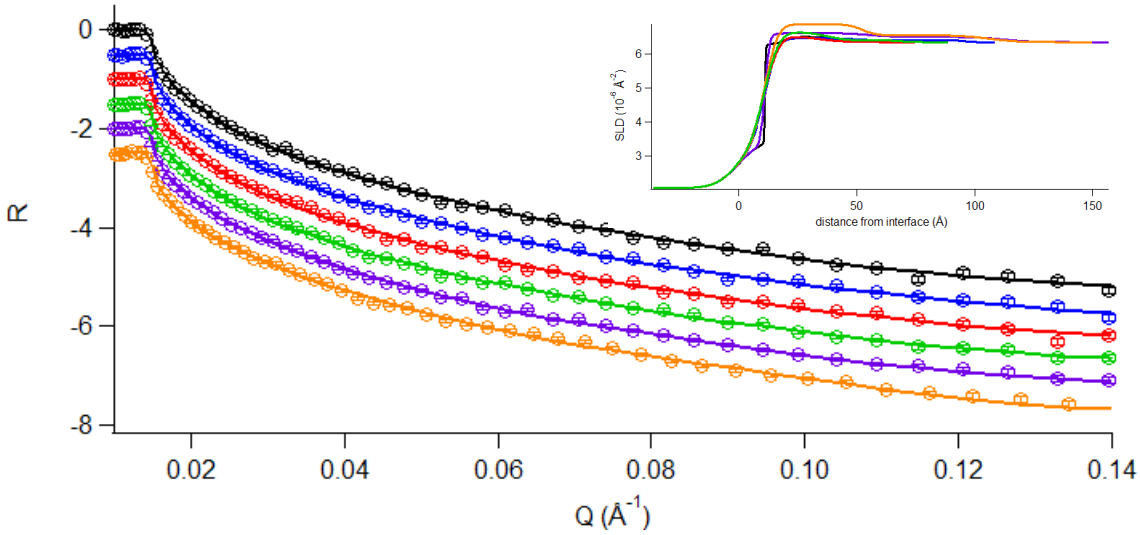


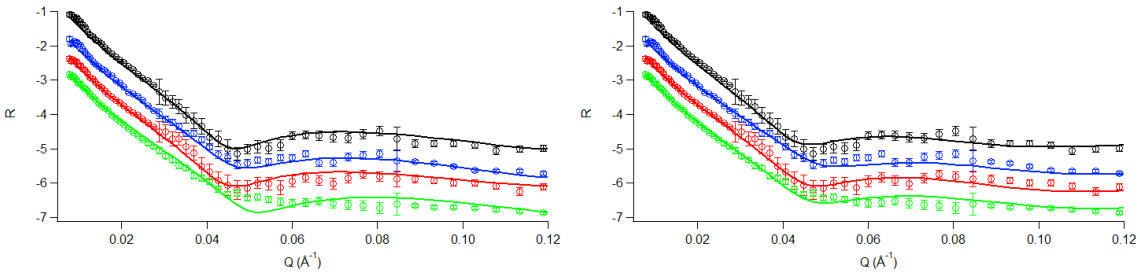
Figure B.12: Reflectivity profiles and fits showing the changes over time for adsorption of d-HSA in D_2O using a 2-layer model. The runs shown are $t_{inc} = 0$ (black), $t_{inc} = 0.75$ hrs (blue), $t_{inc} = 1.5$ hrs (red), $t_{inc} = 2.25$ hrs (green), $t_{inc} = 6$ hrs (purple) and $t_{inc} = 23$ hrs (orange) with data being offset for clarity. The inset shows the scattering length density profiles.

Appendix C

MBP neutron reflectivity data

C.1 Desorption of d-MBP

The data presented below shows the reflectivity profiles, fits and layer parameters for the desorption of d-MBP as discussed in section 3.4.4.

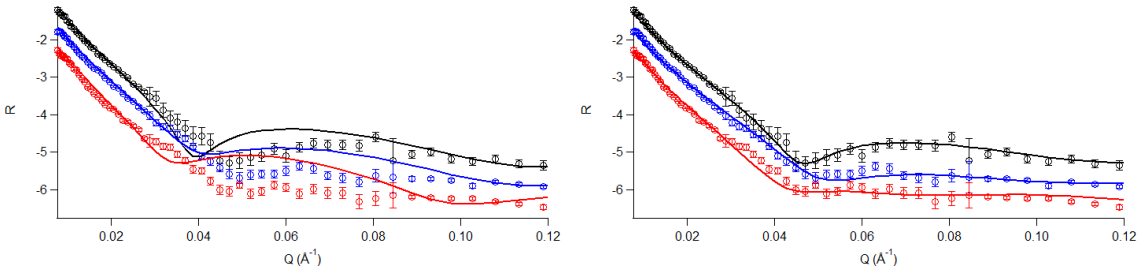


(a) (b)

Figure C.1: Reflectivity profiles and fits showing the desorption of d-MBP in H_2O with t_{inc} = 2 mins analysed using (a) a 1-layer model and (b) a 2-layer model. The runs shown are t_{ex}=0 (black), t_{ex}=1.25 hrs (blue), t_{ex}=7 hrs (red) and t_{ex}= 22 hrs (green). The layer parameters are shown in table (C.1).

t_{ex} \hrs	Layer number	Thickness \±3 Å	% Solvent ±4	Roughness			Γ \±0.2 mg m^{-2}
				ox-1	1-2	2-s	
0		73	77	5	9		2.3
1.25		73	74	4	7		2.6
7		73	77	2	9		2.3
22		65	81	4	9		1.7
0	1	43	72	2	8	6	1.6
	2	51	85				1.0
1.25	1	33	70	5	1	10	1.3
	2	51	85				1.0
7	1	37	72	1	10	7	1.4
	2	51	85				1.0
22	1	37	75	5	2	8	1.2
	2	45	85				0.9

Table C.1: Layer parameters for the 1-layer and 2-layer model of d-MBP desorption in H_2O after an incubation time of 2 minutes. Data is shown in figure (C.1).

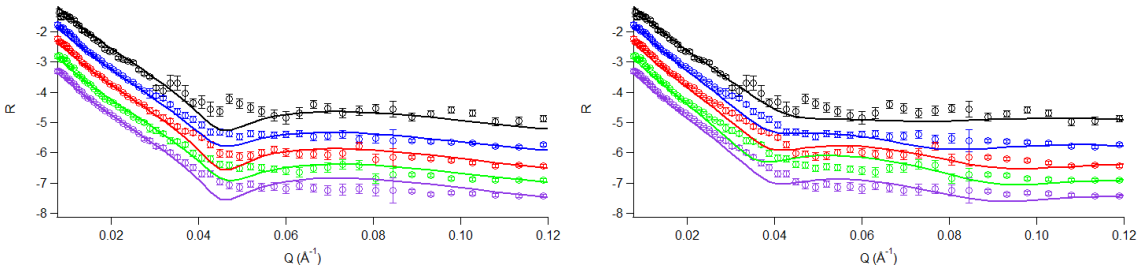


(a) (b)

Figure C.2: Reflectivity profiles and fits showing the desorption of d-MBP in H_2O with t_{inc} = 30 mins analysed using (a) a 1-layer model and (b) a 2-layer model. The runs shown are t_{ex}=0 (black), t_{ex}=1.5 hrs (blue) and t_{ex}=9 hrs (red). The layer parameters are shown in table (C.2).

t_{ex} \hrs	Layer number	Thickness \±3 Å	% Solvent ±4	Roughness			Γ \±0.2 mg m^{-2}
				ox-1	1-2	2-s	
0		82	78	5	9		2.4
1.5		83	74	3	10		2.9
9		96	74	3	8		3.3
0	1	33	63	4	2	4	1.6
	2	62	79				1.7
1.5	1	54	73	1	9	8	2.0
	2	30	89				0.4
9	1	69	71	4	10	10	2.7
	2	44	91				0.5

Table C.2: Layer parameters for the 1-layer and 2-layer model of d-MBP desorption in H_2O after an incubation time of 30 minutes. Data is shown in figure (C.2).

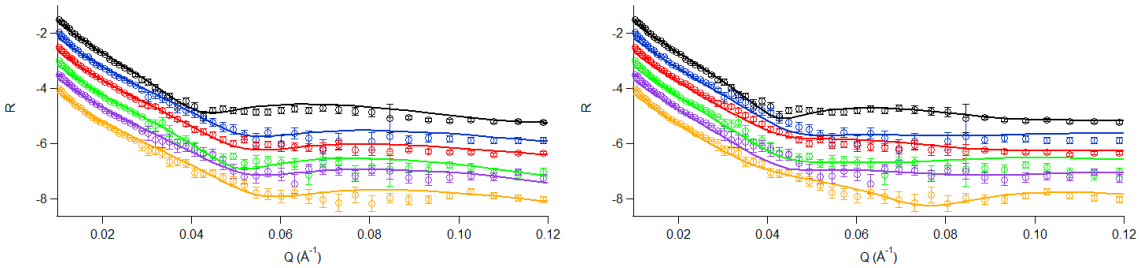


(a) (b)

Figure C.3: Reflectivity profiles and fits showing the desorption of d-MBP in H_2O with $t_{inc} = 1.5$ hrs analysed using (a) a 1-layer model and (b) a 2-layer model. The runs shown are t_{inc}=0 (black), t_{ex}=0 hrs (blue), t_{ex}=3 hrs (red), t_{ex}= 15 hrs (green) and t_{ex}= 18 hrs (purple). The layer parameters are shown in table (C.3).

t_{ex} \hrs	Layer number	Thickness \±4 Å	% Solvent ±4	Roughness			Γ \±0.2 mg m^{-2}
				ox-1	1-2	2-s	
t_{inc}=0		70	80	5	10		2.4
0		70	82	2	7		2.4
3		70	80	3	9		2.2
15		70	77	5	8		2.4
18		70	80	5	10		1.5
t_{inc}=0	1	54	70	5	10	6	2.2
	2	60	90				0.8
0	1	43	78	3	7	9	1.3
	2	52	87				0.9
3	1	45	80	4	8	7	1.2
	2	53	86				1.0
15	1	44	76	4	6	10	1.4
	2	54	87				0.9
18	1	44	76	4	5	8	1.4
	2	53	87				0.9

Table C.3: Layer parameters for the 1-layer and 2-layer model of d-MBP desorption in H_2O after an incubation time of 1.5 hours. Data is shown in figure (C.3).



(a) (b)

Figure C.4: Reflectivity profiles and fits showing the desorption of d-MBP in H_2O with t_{inc} = 4 hrs analysed using (a) a 1-layer model and (b) a 2-layer model. The runs shown are t_{inc}=0 (black), t_{inc}=2.75 hrs (blue), t_{ex}= 0 (red), t_{ex}= 2.5 hrs (green) t_{ex}= 6.5 hrs (purple) and t_{ex}=15.5 hrs (orange). The layer parameters are shown in table (C.4).

t_{ex} \hrs	Layer number	Thickness \±4 Å	% Solvent ±4	Roughness			Γ \±0.2 mg m^{-2}
				ox-1	1-2	2-s	
t_{inc}=0		78	76	5	9		2.5
t_{inc}=2.75		65	74	5	9		2.3
0		65	74	4	10		2.3
2.5		67	75	5	10		2.3
6.5		65	74	4	8		2.3
15.5		62	74	2	9		2.2
t_{inc}=0	1	39	67	1	6	8	1.7
	2	65	83				1.4
t_{inc}=2.75	1	54	75	4	8	8	1.8
	2	46	92				0.5
0	1	40	68	0	6	9	1.7
	2	63	88				1.0
2.5	1	61	70	3	9	7	2.5
	2	55	90				0.7
6.5	1	60	78	2	8	4	1.8
	2	64	93				0.6
15.5	1	60	78	3	9	7	1.8
	2	64	93				0.6

Table C.4: Layer parameters for the 1-layer and 2-layer model of d-MBP desorption in H_2O after an incubation time of 4 hours. Data is shown in figure (C.4).

C.2 Self exchange of MBP

The data presented below shows the reflectivity profiles, fits and scattering length densities for the three models discussed in section 3.4.5; a 1-layer model with $\tau = 75$ Å and 75 % solvent (figure C.5) and 2-layer models where exchange is assumed to occur only in the outer layer (figure C.6) or from both layers (figure C.7). The layer parameters for the 2-layer model are shown in table (3.26). As mentioned in section 3.4.5 it was assumed that the layer parameters (thickness and solvent percentage) were unchanged during the exchange of the proteins.

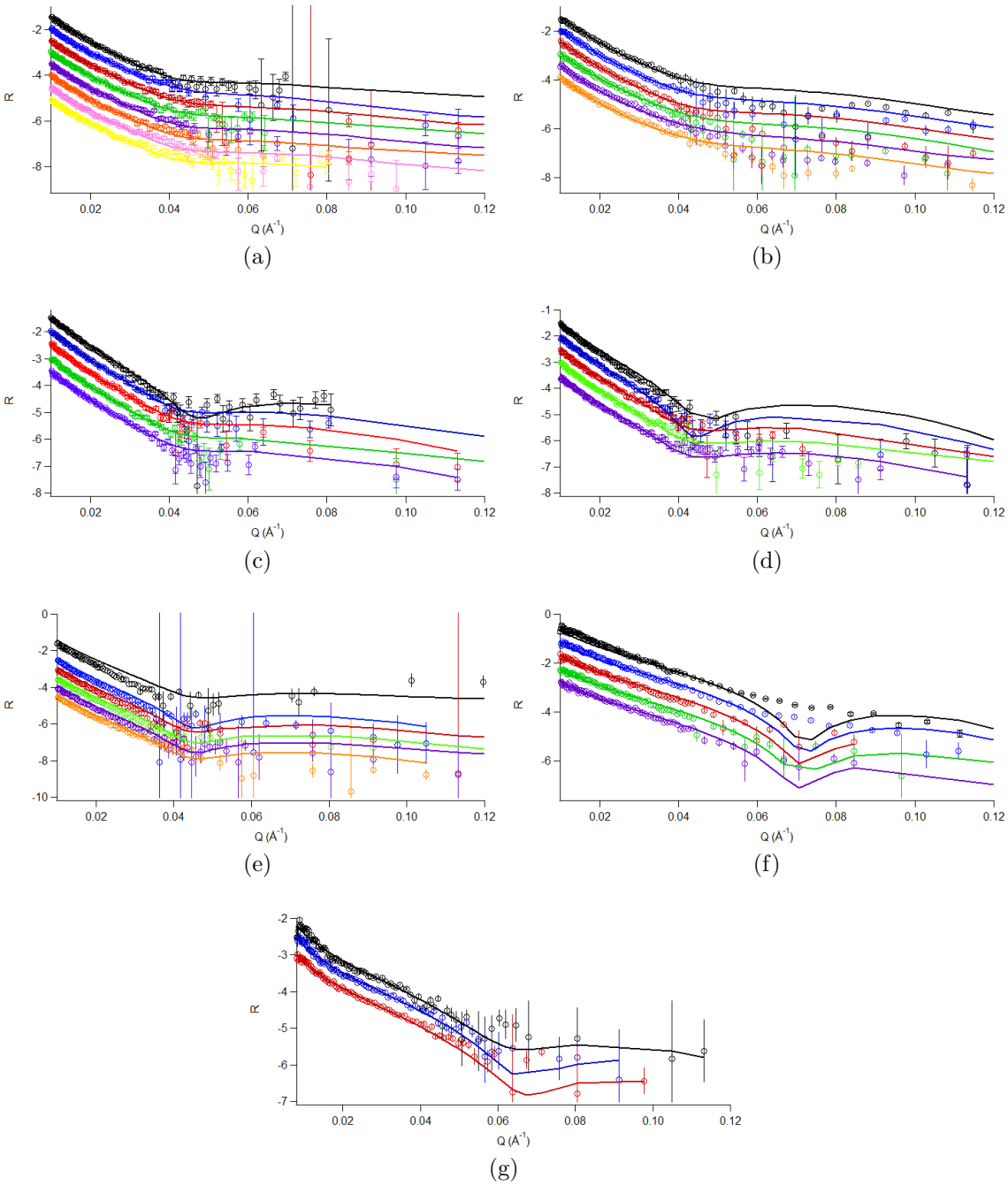


Figure C.5: Reflectivity profiles and fits for the 1-layer model of self-excahnge. Layer parameters set at τ = 75Å and solvent %=75. (a) t_{inc} = 2 min, (b) t_{inc} = 15 min, (c) t_{inc} = 30 min, (d) t_{inc} = 1.5 hrs, (e) t_{inc} = 4 hrs, (f) t_{inc} = 16 hrs (d-h) and (g) t_{inc} = 16 hrs (h-d). For t_{inc} = 2 min, 15 min and 16 hr (h-d) all runs shown are after exchange of the bulk solutions. For t_{inc} = 30 min, 1.5 hrs, 4 hrs and 16 hrs (d-h) the black data set is the final d-MBP layer beofre bulk solution exchange. Data has been offset for clarity. The values for each t_{ex} and the scattering length densities are shown in table (C.6).

t_{inc}	t_{ex} \hours	$\rho_{protein}$ $\times 10^{-6}$ Å $^{-2} \pm 0.2$	Solvent contrast
2 min	0	2.7	H_2O
2 min	1.5	2.2	H_2O
2 min	3	2.4	H_2O
2 min	6	2.4	H_2O
2 min	9	2.6	H_2O
2 min	10.5	2.5	H_2O
2 min	22.5	2.7	H_2O
2 min	30	2.9	H_2O
15 min	0	2.2	H_2O
15 min	1	2.2	H_2O
15 min	2.5	2.4	H_2O
15 min	5	1.8	H_2O
15 min	11.5	1.8	H_2O
15 min	20	1.8	H_2O
30 min	0	3.1	H_2O
30 min	1.5	2.8	H_2O
30 min	7.5	2.9	H_2O
30 min	10.5	2.9	H_2O
1.5 hours	0	4.5	H_2O
1.5 hours	1.5	3.5	H_2O
1.5 hours	4	3.5	H_2O
1.5 hours	13.5	3.6	H_2O
4 hours	0	4.5	H_2O
4 hours	1.5	4.3	H_2O
4 hours	7.5	4.3	H_2O
4 hours	10.5	4.6	H_2O
4 hours	26	4.1	H_2O
16 hours (d-h)	0	6.4	CMSi
16 hours (d-h)	3	6.2	CMSi
16 hours (d-h)	15	6.1	CMSi
16 hours (d-h)	26.5	6.0	CMSi
16 hours (h-d)	0	3.8	CMSi
16 hours (h-d)	3	4.3	CMSi
16 hours (h-d)	15	4.6	CMSi

Table C.5: The change in scattering length density of the adsorbed protein layer for the self-exchange of MBP using a fixed model of $\tau = 75$Å and solvent %=75

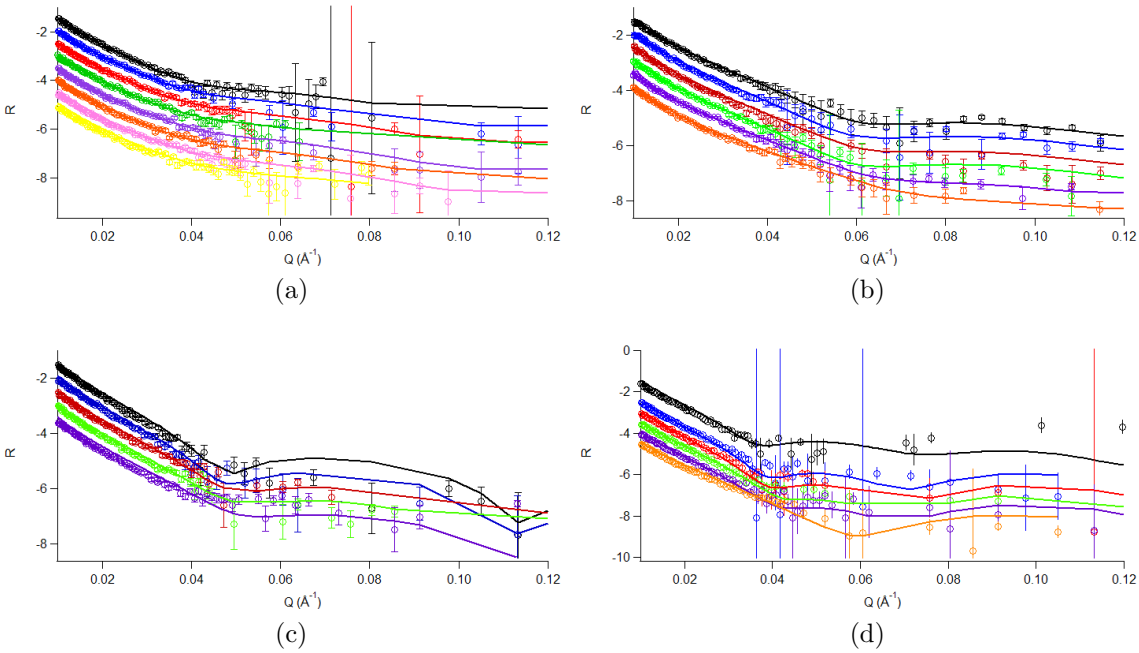


Figure C.6: Reflectivity profiles of the self-exchange of MBP over time using a 2-layer model assuming exchange is only occurring in the outer layer showing (a) t_{inc} = 2 min, (b) t_{inc} = 15 min, (c) t_{inc} = 1.5 hrs and (d) t_{inc} = 4 hrs. The top profile in (c) and (d) is the final d-MBP layer before exchange of the bulk solution. The reflectivity profiles for the other incubation times are shown in figure 3.35.

t_{inc}	t_{ex} \hours	$\rho_{protein}$ $\times 10^{-6}$ Å $^{-2} \pm 0.2$	Solvent contrast
2 min	0	2.6	H_2O
2 min	1.5	2.9	H_2O
2 min	3	2.8	H_2O
2 min	6	2.7	H_2O
2 min	9	2.7	H_2O
2 min	10.5	2.7	H_2O
2 min	22.5	2.7	H_2O
2 min	30	2.7	H_2O
15 min	0	3.0	H_2O
15 min	1	3.5	H_2O
15 min	2.5	3.6	H_2O
15 min	5	2.8	H_2O
15 min	11.5	1.9	H_2O
15 min	20	1.9	H_2O
30 min	0	4.9	H_2O
30 min	1.5	4.6	H_2O
30 min	7.5	4.7	H_2O
30 min	10.5	4.7	H_2O
1.5 hours	0	5.5	H_2O
1.5 hours	1.5	4.4	H_2O
1.5 hours	4	4.5	H_2O
1.5 hours	13.5	5.4	H_2O
4 hours	0	6.2	H_2O
4 hours	1.5	6.2	H_2O
4 hours	7.5	6.1	H_2O
4 hours	10.5	6.0	H_2O
4 hours	26	5.0	H_2O
16 hours (d-h)	0	6.2	CMSi
16 hours (d-h)	3	4.0	CMSi
16 hours (d-h)	15	3.5	CMSi
16 hours (d-h)	26.5	3.0	CMSi
16 hours (h-d)	0	6.2	CMSi
16 hours (h-d)	3	6.4	CMSi
16 hours (h-d)	15	6.4	CMSi

Table C.6: The change in scattering length density of the outer protein layer for the self-exchange of MBP using a 2-layer model and assuming all exchange occurs in the outer layer.

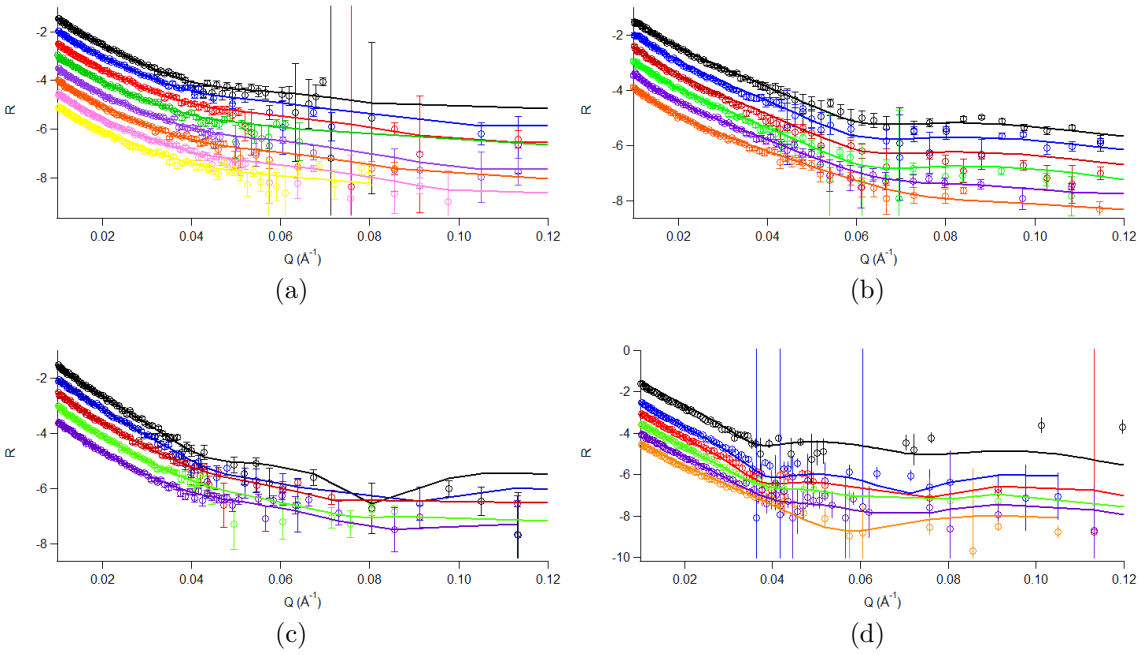


Figure C.7: Reflectivity profiles of the self-exchange of MBP over time using a 2-layer model and assuming exchange is occurring from both layers showing (a) $t_{inc} = 2$ min, (b) $t_{inc} = 15$ min, (c) $t_{inc} = 1.5$ hrs and (d) $t_{inc} = 4$ hrs. The top profile in (c) and (d) is the final d-MBP layer before exchange of the bulk solution. The reflectivity profiles for the other incubation times are shown in figure 3.35.

The table below is the scattering length data used to make the graphs in figure (3.36). Please refer to the text in section 3.4.5 for details of the models used during the analysis.

t_{inc}	t_{ex} \hours	Layer number	$\rho_{protein}$ \$\times 10^{-6}$ Å $^{-2} \pm 0.2$	Solvent contrast
2 min	0	1	4.0	H_2O
		2	3.0	
2 min	1.5	1	3.0	H_2O
		2	2.6	
2 min	3	1	3.1	H_2O
		2	2.5	
2 min	6	1	3.0	H_2O
		2	2.5	

Continued on next page

Table C.7 – continued from previous page

t_{inc}	t_{ex} \hours	Layer number	$\rho_{protein}$ $\times 10^{-6}$ Å $^{-2} \pm 0.2$	Solvent contrast
2 min	9	1	3.2	H_2O
		2	2.5	
2 min	10.5	1	3.0	H_2O
		2	2.5	
2 min	22.5	1	3.0	H_2O
		2	2.5	
2 min	30	1	3.1	H_2O
		2	1.9	
15 min	0	1	5.0	H_2O
		2	3.0	
15 min	1	1	4.3	H_2O
		2	3.0	
15 min	2.5	1	4.5	H_2O
		2	3.0	
15 min	5	1	4.5	H_2O
		2	2.5	
15 min	11.5	1	4.5	H_2O
		2	1.8	
15 min	20	1	4.5	H_2O
		2	1.8	
30 min	0	1	5.9	H_2O
		2	4.9	
30 min	1.5	1	5.8	H_2O
		2	4.4	
30 min	7.5	1	5.1	H_2O
		2	4.4	
30 min	10.5	1	5.3	H_2O
		2	4.4	

Continued on next page

Table C.7 – continued from previous page

t_{inc}	t_{ex} \hours	Layer number	$\rho_{protein}$ $\times 10^{-6}$ Å $^{-2} \pm 0.2$	Solvent contrast
1.5 hr	0	1	6.2	H_2O
		2	5.3	
1.5 hr	1.5	1	4.5	H_2O
		2	3.2	
1.5 hr	4	1	4.5	H_2O
		2	3.0	
1.5 hr	13.5	1	4.0	H_2O
		2	3.0	
4 hr	0	1	6.2	H_2O
		2	5.5	
4 hr	1.5	1	6.2	H_2O
		2	5.7	
4 hr	7.5	1	6.2	H_2O
		2	5.4	
4 hr	10.5	1	6.2	H_2O
		2	5.2	
4 hr	26	1	5.6	H_2O
		2	4.0	
16 hr (d-h)	0	1	6.2	CMSi
		2	6.4	
16 hr (d-h)	3	1	5.7	CMSi
		2	6.1	
16 hr (d-h)	15	1	5.5	CMSi
		2	6.0	
16 hr (d-h)	26.5	1	5.6	CMSi
		2	5.3	
16 hr (h-d)	0	1	4.0	CMSi
		2	4.1	

Continued on next page

Table C.7 – continued from previous page

t_{inc}	t_{ex} \hours	Layer number	$\rho_{protein}$ $\times 10^{-6}$ Å $^{-2} \pm 0.2$	Solvent contrast
16 hr (h-d)	3	1	4.7	CMSi
		2	4.4	
16 hr (h-d)	15	1	5.0	CMSi
		2	4.4	

Table C.7: The change in scattering length density of the adsorbed protein layer for the self-exchange of MBP using a 2-layer model and assuming exchange occurs in both layers.